REPLACING sp^2 HYBRIDIZED CARBON CENTERS WITH PHOSPHORUS

LUCAS C. TORRES

A DISSERTATION SUBMITTED TO
THE FACULTY OF GRADUATE STUDIES
IN PARTIAL FULFILLMENT OF THE REQUIREMENTS
FOR THE DEGREE OF
DOCTOR OF PHILOSOPHY

GRADUATE PROGRAM IN CHEMISTRY
YORK UNIVERSITY
TORONTO, ONTARIO

July 2025

Abstract

The striking parallels between the chemistry of molecular carbon and phosphorus compounds has fascinated chemists for decades and has even led to phosphorus being coined “the Carbon Copy.” A guiding tenet in organic chemistry is that carbon can be bonded to a maximum of four other atoms to satisfy the octet rule. By comparison, phosphorus, a heavier p-block element, can exist in hypervalent states and can form bonds with up to six other atoms. Apparent patterns in the bonding and reactivity of carbon and phosphorus compounds typically manifest when these elements are in lower coordination environments (bonded to few other atoms). Molecules featuring low-coordinate earth abundant p-block elements (C, P, Si, Al, etc) have generated considerable research interest as of late, with pivotal discoveries showing these systems can facilitate processes more traditionally distinctive of transition metal complexes. Such behavior includes the activation of thermodynamically strong chemical bonds, which in some cases is reversible, and the ability to directly perform catalytic transformations on organic molecules, overall pushing the needle towards more sustainable and cost-conscious chemistry. Low-coordinate phosphorus cations are one general group of compounds that show great promise in these domains.

This thesis delineates the synthesis of cations that distinctly feature a sp^2 hybridized phosphorus atom and are principally inspired from classic carbon motifs. Firstly, we explore a synthetic route to a phosphorus analog of a [3]cumulene ($R_2C=C=C=CR_2$). We found our target phospha-cumulene, also known as an allenylidene phosphonium cation, to be uniquely accessible when harnessing electron rich substituents known as N-heterocyclic imines (NHIs). The properties and reactivity of the allenylidene phosphonium cation are investigated, with one interesting reactivity pathway being a thermally reversible [2+2] cycloaddition which occurs between a P=C and C=C bond. This process is remarkable given that comparable [2+2] cycloadditions between two C=C functional groups typically requires photoexcitation. The NHI substituent platform is also used to prepare a series of phosphenium cations (the phosphorus analog of carbenes) and the reactivity of these species is subsequently disclosed.

Acknowledgments

A tremendous thank-you goes out to my supervisor, Dr. Christopher Caputo, who has been very supportive of my research and personal goals over the years. Outside of the lab, I appreciate your generally good life advice, and I have great admiration for how reliable and resourceful you are despite how many things you always have going on. Truly a master of the multitask. Importantly, I appreciate you connecting me with various collaborators throughout the years, which has allowed me to develop new perspectives, cultivate confidence, and experience life in ways I would have never imagined for myself. It will be an honour to be your first PhD graduate.

I would also like to acknowledge my committee members, Dr. Ryan Hili and Dr. Thomas Baumgartner. Thomas and his group have provided valuable insight to my research and have allowed me to broaden my knowledge through our shared group meetings over the years. I recall a meeting I had with Thomas and Chris when I was a bachelor's student, where they pitched an idea on a scrap piece of paper: new method for probing the Lewis acidity of main group compounds. This would be my first foray into inorganic chemistry and set me down the eventual path of my Graduate Studies. Thank-you for helping me find an area of chemistry I am passionate about. My gratitude also extends to my examiners, Dr. Jose Goicoechea, and Dr. Marina Freire-Gormaly. Thank you to Dr. Fabian Dielmann for welcoming me to his research group at the University of Innsbruck for a whopping 14 months. I learned an incredible amount during this time, and your expertise was critical for helping me push the boundaries of my research. I am very grateful for your mentorship, and I'm always down for a (trail) run.

Most importantly, I am grateful for the environments that both Chris and Fabian have curated in both of their respect research groups, assembling truly phenomenal groups of people. From Chris' group, particular thanks are due to the postdoc squad of Dr. Sanjay Manhas, Dr. Nico Bonnano and Dr. Avik Bhattacharjee. Collectively, the three of you taught me so much about chemistry and about the important things in life, in addition to providing endless laughs. From Fabian's group, I have immense gratitude for the friendship and help of Dr. Pawel Löwe throughout my PhD... It's crazy that we've been collaborating virtually for years at this point. It's been very nice to have someone who's extremely motivated and passionate about the chemistry of trigonal planar phosphorus cations.

From both research groups, I've made friends for life. From the Caputo lab, I have unforgettable memories with my fellow graduate students Fiona Jeeva, Taylor Cosby, and Charley Garrard. Despite living in the Alps, I've been skiing more times with the Caputo lab then with the Dielmann Group. Likewise, I had a great time with all the folks at the University Innsbruck, Franka Brylak, Dr. Tobias Bens, Markus Rödl, and Leon Schöndorf. I'll never forget when Markus and Leon drove me all the way to Munich to catch a flight on my last day in Europe. Special thanks go to my dearest friends; Maike Röthel, Jonas Franzen, Casey Lenart, Alex Sietmann, and Sven Lempereur, who have always motivated me to excel throughout my PhD and have always shown me a great time, regardless of the continent. Alex and Casey are also thanked for supporting my running journey, and I am proud to be the current head-to-head champion in marathoning between the two groups. I'd also like to give a sincere shoutout to Dr. Amir Yeganeh, my roommate during my undergraduate studies and first friend that I made through chemistry.

I appreciate the input of various talented individuals who helped me along the way, including past and present members of the Caputo, Baumgartner, and Dielmann labs. Dr. Andryj Borys, Dr. Amandeep Brar and Dr. Kevin Szkop are thanked for their input on various aspects of this thesis.

Thank you to the staff at both York University and the University of Innsbruck. Thanks to Dr. Howard Hunter for teaching me everything I currently know about NMR Spectroscopy. I'm also very grateful to the talented group of crystallographers who have provided me with stunning molecular structures over the years, Dr. Klaus Wurst, Dr. Michael Seidl, and Casey Lenart. I'd also like to thank the friends I've made over the years in the department at York, including Dr. Victor Romero Flores, Amaar Hussein, and Dr. Faizan Rasheed.

None of this would be possible without the endless support of my family; my mom, dad, and Matthew. I appreciate my close friends and sometimes travelling partners Brad Ayow, James Yantsis, Walid Nusseiri, Anthony Caruso, and Casey Lenart. Finally, thanks to my roommates and family in Innsbruck: Phine, Armin, Annika, Bella, and Nico, who kept me out of trouble and made my time in Austria a blast.

Table of Contents

Abstract ..... *ii*

Acknowledgments ..... *iii*

Table of Contents ..... *v*

List of Symbols and Abbreviations ..... *viii*

List of Tables ..... *xi*

List of Figures ..... *xii*

List of Schemes ..... *xvii*

Preface *1*

Chapter One: Electrophilic Phosphorus Compounds and Their Ties to Carbon Chemistry *4*

1.1.1 Phosphorus 4
1.1.2 Phosphorus as Lewis Bases and Acids 4
1.1.3 Why Study Electrophilic Phosphorus Compounds? 5
1.1.4 Cationic Phosphorus Lewis Acids 9
1.1.5 Phosphenium Cations $[R_2P:]^+$ 9
1.1.6 Tetracoordinate Phosphonium Cations $[PR_4]^+$ 11
1.1.7 Trigonal Planar Phosphonium Cations $[R_2P{=}E]^+$ 13
1.1.8 Phosphorandylium Dications $[PR_3]^{2+}$ 18
1.1.9 Phosphorus Analogs of Organic Molecules 19
1.1.10 Phosphorus and Nitrogen Congeners 20
1.1.11 Carbon-Phosphorus Mimicry 21

1.2 References 23

Chapter Two: En Route to a Phosphorus Analog of [3]Cumulene *28*

2.1 Introduction 29
2.1.1 Carbon Allotropes 29
2.1.2 A Brief Introduction to Cumulenes 29
2.1.3 Main-Group Cumulenes 32
2.1.4 Simple Heterocumulenes 33
2.1.5 Main Group Analogs of [3]Cumulenes 34
2.1.6 Main Group Analogs of [4]Cumulenes 39
2.1.7 Metallocumulenes and the Allenylidene Carbene 42
2.1.8 Reactivity of Metal Allenylidenes 44

2.2 Chapter Objectives: Finding a Synthetic Route to An Allenylidene Phosphonium Cation 47

2.3 Results and Discussion 49
2.3.1 Synthesis of Alkynyl Phosphines 49
2.3.2 Lewis Acids for Methoxide Abstraction 50
2.3.3 Transient Allenylidene Phosphonium Cation 52
2.3.4 Attempts to Isolate Allenylidene Phosphonium with Kinetic Stabilization 56
2.3.5 Modification of the Carbon Terminus of Alkynyl Phosphines 59

2.3.6 Alkyne Activation by Boranes 61
2.4 Conclusion and Outlook 63
2.5 Experimental Procedures 64
2.6 References 87
Chapter Three: Isolation, Characterization and Reactivity of an Allenylidene Phosphonium Cation 94
3.1 Introduction 95
3.1.1 N-Heterocyclic Carbenoid Derived Substituents 95
3.1.2 Trigonal Planar Phosphorus Cations Stabilized by NHIs 96
3.2 Chapter Objectives: Leveraging NHIs to Isolate Allenylidene Phosphonium 100
3.3 Results and Discussion 101
3.3.1 Synthesis of an Allenylidene Phosphonium Cation 101
3.3.2 Electronic Structure of Allenylidene Phosphonium Cation $[3\text{-}2]^+$, ... 108
3.3.3 Assessment of the Lewis Acidity of Allenylidene Phosphonium Cation $[3\text{-}2]^+$ 111
3.3.4 Stability of Allenylidene Phosphonium salt $[3\text{-}2][B(OC_6F_5)_4]$ 114
3.3.5 Cycloadditions with Allenylidene Phosphonium 118
3.4 Conclusion and Outlook 122
3.4.1 Heterocyclic Synthesis 122
3.4.2 Derivatization 125
3.5 Experimental 127
3.6 References 150
Chapter Four: Synthesis, Characterization and Reactivity of Alkyl-Imino-Phosphenium Cations. 157
4.1 Introduction 158
4.1.1 Ambiphilic Main Group Carbenoids 158
4.1.2 Reactivity of Phosphenium Cations 158
4.2. Chapter Objectives: N-Heterocyclic Imine Substituted Phosphenium Cations 162
4.3 Results and Discussion 165
4.3.1 Synthesis of Electrophilic NHI-substituted Phosphenium Cations 165
4.3.2 Electronic Structure of Acyclic Alkyl-Imino Phosphenium Cations 168
4.3.3 Electrophilicity of Acyclic Alkyl-Imino Phosphenium Cations 170
4.3.4 Probing the Ambiphilic Character of Acyclic Alkyl-Imino Phosphenium Cations 171
4.3.5 Oxidative Addition of O-H and N-H compounds 172
4.3.6 Attempted Carbenoid Homologation Reaction 177
4.4 Conclusions and Outlook 178
4.4.1 Attempted H_2 Activation 179
4.4.2 Electronics of Phosphenium Cation Analogs 182
4.4.3 Future Directions 183
4.5 Experimental Procedures 185

4.6.1 References 219
Chapter Five *225*
5.1 Conclusions 225
5.2 Compiled List of References 227

List of Symbols and Abbreviations

Å	Angstrom
Ad	Adamantyl
a.u.	Arbitrary Unit
CAAC	Cyclic Alkyl Imino Carbene
Cp	Cyclopentadienyl
Cy	Cyclohexyl
°	Degrees
°C	Degrees Celsius
Δ	Heating
ΔG	Free energy
ΔH	Enthalpy
δ	Chemical Shift
δ+	Partial Positive Charge
δ–	Partial Negative Charge
DART	Direct analysis in real time
DMAP	4-Dimethylaminopyridine
DFT	Density Functional Theory
ε	Molar Extinction Coefficient
Equiv.	Equivalents
eV	Electron-Volt
ESI	Electrospray Ionization
FlA	Fluoride Ion Affinity
FLP	Frustrated Lewis Pair
FMO	Frontier Molecular Orbital
h	Hours
HOMO	Highest Occupied Molecular Orbital
Hz	Hertz
^{i}Pr	Isopropyl
^{i}PrMgCl	Isopropylmagnesium chloride

IR	Infrared
J (coupling)	Coupling constant
kJ mol^{-1}	Kilojoule per mol
kcal mol^{-1}	Kilocalorie per mol
KHMDS	Potassium bis(trimethylsilyl)amide
LUMO	Lowest Unoccupied Molecular Orbital
λ	Wavelength
MBO	Mayer Bond Order
MS	Mass Spectrometry
Mes	2,4,6-$Me_3C_6H_2$
Mes*	2,4,6-*t*$Bu_3C_6H_2$
m/z	Mass to charge ratio
nBu	n-butyl
nBuLi	n-butyl lithium
NBO	Natural Bond Orbital
NHBO	N-heterocyclic boryloxy
NHC	N-Heterocyclic carbene
NHP	N-Heterocyclic phosphenium
NHCP	N-heterocyclic carbene phosphinidine
NHE	N-heterocyclic carbenoid
NHI	N-heterocyclic imine
NIAd	1,3-di-adamantylimidazolin-2-imine
NIDipp	1,3-bis(diisopropylphenyl)imidazolin-2-imine
NsIDipp	1,3-bis(diisopropylphenyl)imidazolidine-2-imine
NsI^{t}Bu	1,3-di-tertbutyimidazolidine-2-imine
NI(Me)*i*Pr	1,3-di-isopropyl-4,5-dimethylimidazolin-2-imine
NI(Benz)*i*Pr	1,3-di-isopropylbenzimidazolin-2-imine
Ph	Phenyl
π	Pi

PES	Potential Energy Surface
PCM	Polarizable Continuum Model
Pn	Pnictogen
ppm	Parts per million
r.t.	Room temperature
sBu	sec-butyl
σ	Sigma
SCXRD	Single Crystal X-ray Diffraction
SMD	Solvation Model based on Density
T	Temperature
THF	Tetrahydrofuran
TPPC	Trigonal planar phosphonium cation
^{t}Bu	*tert*-butyl
Ter	2,6-diphenylbenzene
UV-vis	Ultraviolet-visible
VSEPR	Valence shell electron pair repulsion
VT	Variable temperature
V	Unit cell volume
WBI	Wiberg Bond Index
1,2-DFB	1,2-difluorobenzene

List of Tables

Chapter 2

Table 2-1: Crystal structure refinement data for **2-2**[a] and **2-3**[a]. 84
Table 2-2: Crystal structure refinement data for **2-3**[Fl] and **2-3**[Sub] 85

Chapter 3

Table 3-1: Crystal structure refinement data **3-1**[a], **3-1**[b], and [**3-2**][$B(OC_6F_5)_4$]. 147
Table 3-2: Crystal structure refinement data [**3-2**[cyclo]][$B(OC_6F_5)_4$] and [**3-2•DMAP**][$B(OC_6F_5)_4$]. 148

Chapter 4

Table 4-1: Crystal structure refinement data [**4-2**[a]][$AlCl_4$], [**4-3**][$B(C_6F_5)_4$], and **4-1**[a]. 216
Table 4-2: Crystal structure refinement data **4-1**[c] and **4-1**[d]. 217

List of Figures

Preface

Figure P-1: Isodiagonal relationship in the early s- and p-block. 1

Chapter 2

Figure 2-1: Solid-state structure of **2-2^{a}**. Thermal ellipsoids are shown at 50% probability. For clarity, hydrogen atoms are omitted and the phenyl groups are shown in wireframe. 49
Figure 2-2: Side-on (left) and front-on (right) view of the solid-state structure of **2-3^{a}**. Thermal ellipsoids are shown at 50% probability. For clarity, hydrogen atoms are omitted, and the phenyl and perfluorophenyl groups are shown in wireframe. 52
Figure 2-3: HOMO and LUMO depictions of tetraphenyl allenylidene phosphonium cation at the BP86-D3/def2SVP level of theory, in the gas phase. 55
Figure 2-4: Solid-state structures of **2-3^{Fl}** and **2-3^{Sub}**. Thermal ellipsoids are shown at 50% probability. For clarity, hydrogen atoms are omitted, and the phenyl and perfluorophenyl groups are shown in wireframe. 60
Figure 2-5: Molecular connectivity of **2-2^{Me}•B(C_6F_5)$_3$.** Atoms and bonds are represented with ball and stick modelling. 61
Figure 2-6:^{1}H NMR spectrum showing the P-B adduct of **2-2^{a}** and B(C_6F_5)$_3$ as the predominant species in solution at room temperature (300 MHz, C_6D_6) 73
Figure 2-7:^{31}P{^{1}H} NMR spectrum showing the diagnostic resonance (δ_P = 3.7 ppm) of the P-B adduct of **2-2^{a}** and B(C_6F_5)$_3$ as the predominant species in solution at room temperature (121 MHz, C_6D_6). 74
Figure 2-8:Stacked ^{1}H NMR spectra. The top is a reference spectrum of **2-2^{a}.** The bottom is a spectrum produced from an aliquot of the reaction between **2-2^{a}** and Me_3SiOTf outlined by the above conditions. The doublet splitting peak in the upfield region of the bottom spectra (denoted with the red marker) suggests the formation of a methoxy phosphonium cation. 75
Figure 2-9: Stacked ^{1}H/^{31}P HMBC spectra (400 MHz /162 MHz) of **2-2^{a}** and the reaction between **2-2^{a}** and Me_3SiOTf**,** further suggesting the proposed phosphonium silyl cation depicted. 76

Chapter 3

Figure 3-1:Solid-state structure of **3-1**[a]. thermal ellipsoids are shown at 50 % probability. For clarity, hydrogen atoms are omitted. The Dipp groups and fluorenyl motifs are shown in wireframe. Selected atomic distances [Å] and angles [°]: P–C1 1.810(3), P–N1 1.673(2), P–N4 1.689(2), C1–C2 1.217(4), C2–C3 1.484(4), C3–O 1.436(4), N1–P–C1 104.75(12), N4–P–C1 96.23(12), N1–P–N4 96.75(11)..... 102

Figure 3-2: Bis(imino)alkynyl phosphines **3-1**[a] and **3-1**[b] with accompanying solid-state structures. Hydrogen atoms are omitted for clarity and the fluorenyl motifs are shown in wireframe. Carbon atoms of Dipp (orange) and *t*Bu (blue) are depicted in the space filling model (spheres corresponding to their 1.7-fold Van der Waals radius). Ellipsoids are drawn at 50 % probability. 103

Figure 3-3: Solid-state structure of [**3-2**][$B(OC_6F_5)_4$]. In all cases, thermal ellipsoids are shown at 50 % probability. For clarity, hydrogen atoms are omitted. The Dipp groups and fluorenyl motifs are shown in wireframe. Selected atomic distances [Å] and angles [°]: [**3-2**][$B(OC_6F_5)_4$]: P–C1 1.624(4), C1–C2 1.252(5), C2–C3 1.332(5), P–N1 1.560(3), P–N4 1.557(3), P–C1–C2 170.3(4), C1–C2–C3 179.3(4), N1–P–N4 112.55(15), N1–P–C1 123.78(17), N4–P–C1 123.37(17), C2–C3–C4 125.3(4), C2–C3–C5 127.7(3), C4–C3–C5 106.5. 105

Figure 3-4: Side on (left) and end-on (centre) perspectives of [**3-2**]$^+$, with the [$B(OC_6F_5)_4$]$^-$anion omitted. Alternate Lewis structure depiction of [**3-2**]$^+$ (right). 106

Figure 3-5: Experimental (black, 5E-5 M in CH_2Cl_2) and simulated (red, using SMD for CH_2Cl_2) UV-vis spectra of [**3-2**]$^+$. 108

Figure 3-6: Selected molecular orbitals of [**3-2**]$^+$ calculated at B3LYP-D3BJ/def2-TZVP level of theory, isovalue = 0.02 109

Figure 3-7: Calculated Mayer Bond Order analysis, Hirshfeld charges, and electrostatic potential map for [**3-2**]$^+$ at B3LYP-D3BJ/def2-TZVP level of theory. 110

Figure 3-8: Molecular structure of [**3-2•DMAP**]$^+$ with the [$B(OC_6F_5)_4$]$^-$ anion excluded. Thermal ellipsoids are shown at 50 % probability. For clarity, hydrogen atoms are omitted. The Dipp groups and fluorenyl motif are shown in wireframe. Selected atomic distances [Å] and angles [°]: P–C1

1.677(3). C1–C2 1.227(4), C2–C3 1.385(4), P–N1 1.561(3), P–N4 1.567 (2), P–N7 1.787(2), P–C1–C2 166.2(3). 114

Figure 3-9:Molecular structure of [**3-2^{cyclo}**]$^{+}$ with the [B(OC$_6$F$_5$)$_4$]$^{-}$ anion excluded. Thermal ellipsoids are shown at 50 % probability. For clarity, hydrogen atoms are omitted except for one on C8. The Dipp groups and fluorenyl motif are shown in wireframe. Selected atomic distances [Å] and angles [°]: P–N1 1.604(2), P–N4 1.5573(19), P–C1 1.817(2), P–C7 1.834(2), C1–C8 1.555(3), C1–C2 1.295(3), C2–C3 1.318(3), C6–C7 1.517(3), C7–C8 1.563(3), C8–C9 1.497(3), C9–C10 1.317(3), C10–C11 1.469(3), C6–C11 1.347(3), N1–P–N4 115.74(10), N1–P–C1 118.06(11), N4–P–C1 114.05(11), N1–P–C7 112.38(10), N4–P–C7 112.64(11), C1–C2–C3 171.8(3). 118

Figure 3-10: Cyclic voltammetry experiment of [**3-2**$^{+}$][B(OC$_6$F$_5$)$_4$] in 1,2-DFB (scan rate 100 mV/s, supporting electrolyte 0.1 M N^{n}Bu$_4$PF$_6$, potential versus Ag/AgCl, scanned from -1.9 V to 1.9 V (3 sweeps). 131

Figure 3-11: Stacked ^{31}P{^{1}H} NMR spectra monitoring the conversion of [**3-2^{cyclo}**][B(OC$_6$F$_5$)$_4$] to [**3-2•DMAP**][B(OC$_6$F$_5$)$_4$] in 1,2-DFB. 138

Figure 3-12: Stacked ^{1}H NMR spectra, the top trace corresponds to an isolated sample of [**3-2^{cyclo}**][B(OC$_6$F$_5$)$_4$] in ACN-d$_3$, the bottom trace corresponds to experiment 1.3. Following the reaction of [**3-2^{cyclo}**][B(OC$_6$F$_5$)$_4$] with DMAP, 1,2-DFB was removed under reduced pressure and the residue was directly dissolved in acetonitrile-d$_3$. The ‡'s reflects the ^{1}H NMR resonances of excess DMAP. 138

Figure 3-13: ^{1}H NMR spectra of a solution state sample of [**3-2^{cyclo}**][B(OC$_6$F$_5$)$_4$] in CD$_2$Cl$_2$ before and after exposure to air for up to 16 hours. 140

Figure 3-14: ^{19}F{^{1}H} NMR spectra of a solution state sample of [**3-2^{cyclo}**][B(OC$_6$F$_5$)$_4$] in CD$_2$Cl$_2$ before and after exposure to air for up to 16 hours. 141

Figure 3-15: ^{31}P{^{1}H} NMR spectra of a solution state sample of [**3-2^{cyclo}**][B(OC$_6$F$_5$)$_4$] in CD$_2$Cl$_2$ before and after exposure to air for up to 16 hours. 141

Figure 3-16: ^{31}P{^{1}H} NMR spectrum following the addition of Et$_3$PO to [**3-2**][B(OC$_6$F$_5$)$_4$] in CD$_2$Cl$_2$. 142

Figure 3-17: ^{1}H NMR spectrum of **[3-5]**$^{+}$in CD$_3$CN. 143

Figure 3-18: Stacked ^{31}P NMR spectra (121 MHz) monitoring the conversion of [**3-2**]$^{+}$ to [**3-5**]$^{+}$. 144

Chapter 4

Figure 4-1: Solid-state structures of **4-1^{a}** (left) **4-1^{c}** (middle), and **4-1^{d}** (right). Hydrogen atoms are omitted for clarity. Ellipsoids are drawn at 50% probability. NHI bound Dipp, *tert*-butyl, and adamantyl groups are shown in wireframe. For each phosphine, one enantiomer is shown. 166

Figure 4-2: Solid-state structure of phosphino-phosphenium salt [**4-3**][$B(C_6F_5)_4$]. Hydrogen atoms and the [$B(C_6F_5)_4$] anion are omitted for clarity. Ellipsoids are drawn at 50% probability. NHI bound Dipp groups are shown in wireframe. Selected bond length [Å] [**4-3**]$^{+}$; P1–P2 2.288(1). 167

Figure 4-3: Solid-state structure of [**4-2^{a}**][$AlCl_4$] from different perspectives. The depiction on the right excludes the anion for clarity. Additionally, hydrogen atoms are omitted and the Dipp substituents are shown in wireframe for clarity. Ellipsoids are drawn at 50% probability. Selected bond lengths [Å] and angles [°]: [**4-2^{a}**]: P–N1 1.575(8), N1–C1 1.359(1), P–C2 1.827(9), C2–P–N1 103.5(4), P–N1–C1 128.1(6)..... 168

Figure 4-4: Selected molecular orbitals of [**4-2^{a}**]$^{+}$ (HOMO and LUMO) at the B3LYP-D3BJ/def2-TZVP level of theory (top), isovalue = 0.02. 169

Figure 4-5: Calculated Mayer bond order analysis, as well as NBO and Hirshfeld Charges of [**4-2^{a}**]$^{+}$. 170

Figure 4-6: Comparison of FMO energies calculated at the B3LYP-D3BJ/def2-TZVP level of theory between alkyl-iminophosphenium cations [**4-2^{a}**]$^{+}$, [**4-2^{b}**]$^{+}$, [**4-2^{c}**]$^{+}$ and [**4-2^{d}**]$^{+}$. 182

Figure 4-7: Stacked $^{31}P\{^{1}H\}$ NMR spectra of phosphenium cations [**4-2^{b}**]$^{+}$ and [**4-2^{c}**]$^{+}$. 193

Figure 4-8: $^{31}P\{^{1}H\}$ NMR (162 MHz, 296 K) spectrum of the Gutmann-Beckett test for [**4-2^{a}**].$^{+}$ The asterisk denotes an unknown impurity..... 195

Figure 4-9: $^{31}P\{^{1}H\}$ NMR spectrum and ^{31}P NMR spectrum (zoom in) of the reaction of [**4-2^{a}**]$^{+}$ and phenol, in 1,2-DFB..... 202

Figure 4-10: Stacked $^{1}H\{^{31}P\}$ NMR spectrum and ^{1}H NMR spectrum of the reaction of [**4-2^{a}**]$^{+}$ and phenol. After removing the reaction solvent (1,2-DFB) and washing with pentanes, the remaining residue was dissolved in CD_3CN and analyzed. The purple markers indicate the proton directly bound to phosphorus which collapses to a singlet upon decoupling. The red marker corresponds to the ^{t}Bu protons. The proton represented by the purple marker and protons represented by the red marker integrate in a 1:9 ratio. 203

Figure 4-11: $^{31}P\{^{1}H\}$ spectrum and ^{31}P NMR spectrum (zoom in) in $CDCl_3$. Zoom in shows the most prominent peak. 204
Figure 4-12: $^{31}P\{^{1}H\}$ NMR (121 MHz) spectrum and ^{31}P NMR spectrum (zoom in) in $CDCl_3$ for the reaction of [**4-2^{a}**]$^{+}$ and *N,N*-methylphenyl amine. 209
Figure 4-13: Stacked $^{1}H\{^{31}P\}$ NMR (300 MHz) spectrum (top) and ^{1}H NMR spectrum (bottom) of the reaction of [**4-2^{a}**]$^{+}$ and *N,N*-methylphenyl amine. After removing the reaction solvent (1,2-DFB) and washing with pentanes, the remaining residue was dissolved in $CDCl_3$ and analyzed. The purple markers indicate the proton directly bound to phosphorus which collapses to a singlet upon decoupling. Only one resonance for the split P-H doublet can be identified in the ^{1}H NMR spectrum. The red marker corresponds to the *t*Bu protons. The green protons represent the N-methyl group. The proton represented by the purple marker, and protons represented by the green and red markers integrate in a 1:3: 9 ratio. 210
Figure 4-14:^{1}H NMR (300 MHz) spectrum in CD_2Cl_2 of the reaction between phosphenium cation [**4-2^{a}**]$^{+}$ and cyclohexyl isocyanide. 211
Figure 4-15: ^{31}P NMR (121 MHz) spectrum in CD_2Cl_2 of the reaction between phosphenium cation [**4-2^{a}**]$^{+}$ and cyclohexyl isocyanide. 212
Figure 4-16: Stacked $^{31}P\{^{1}H\}$ NMR spectrum (top) and ^{31}P NMR spectrum (middle) of an aliquot of the reaction of [**4-2^{a}**]$^{+}$ with ammonia borane in 1,2-DFB. The bottom ^{31}P NMR spectrum (red) of the secondary phosphine prepared from **4-1^{a}** and N-Selectride ®, in C_6D_6. 213

List of Schemes

Preface

Scheme P-1: Cited examples illustrating the phosphorus-carbon analogy. 2

Chapter 1

Scheme 1-1: General utilization of trichlorophosphine as an electrophile in the preparation of various classes of phosphorus compounds. The first Wittig reaction, π-bond metathesis of methylenetriphenylphosphorane and benzophenone. 5
Scheme 1-2: First intramolecular and intermolecular FLP activations of H_2. First hydrogenation using an FLP catalyst. 6
Scheme 1-3: Stable NHCs, and alkyl amino carbenes. H_2 and NH_3 activation by alkyl amino carbenes. Homologation of CO and isonitriles by alkyl-amino carbenes. 7
Scheme 1-4: Comparison between a generic bimolecular FLP system and Singlet Carbene. 8
Scheme 1-5: Structure and LUMO generalization of phosphenium cations. 9
Scheme 1-6: Select examples of early phosphenium cations. 10
Scheme 1-7: Select examples of oxidative addition occurring at phosphenium centers. 11
Scheme 1-8: Structure and LUMO generalization of phosphonium cations. 11
Scheme 1-9: Select examples of recent electrophilic phosphonium cations. 12
Scheme 1-10: Catalytic hydrodefluorination with [**1-O**]+. 13
Scheme 1-11: Generalized acceptor orbital depiction of TPPCs and their possible reactivity pathways deterring their isolation. 14
Scheme 1-12: Select examples of methylene phosphonium cations. 15
Scheme 1-13: Selenophosphonium [**1-T**]$^+$ and iminophosphonium [**1-U**]$^+$, with various canonical forms drawn to illustrate electron delocalization. 16
Scheme 1-14: (left) Methylene phosphonium [**1-S(b)**]$^+$ and 1,3-dimethylbutadiene Diels-Alder reaction. (right) Electrocyclization of methylene phosphonium [**1-X**]+ to phosphete [**1-X^{cyclo}**]$^+$. 16
Scheme 1-15: Cycloaddition chemistry of chalcogenophosphonium cations [**1-V**]$^+$/[**1-W**]$^+$. $[BArF_{24}]^-$ anions are excluded from the scheme for clarity. 17
Scheme 1-16: π-Bond metathesis of carbonyls and thiophosphonium cation [**1-W**]$^+$. 18

Scheme 1-17: (top) LUMO generalization of phosphorandylium dications. (bottom) Reactivity of the phosphorandylium dication [**1-AD**]$^{2+}$. 19
Scheme 1-18: Example of coordination chemistry with ^{t}Bu-C≡P. Cycloaddition reactions with ^{t}Bu-C≡P. 21
Scheme 1-19: Isolobal relationship between (left) alkynes and phosphaalkynes, (right) alkenes and phosphaalkenes. Isolobal species are denoted with a double ended arrow stylized with an orbital. 22
Scheme 1-20: Isolobal and isoelectronic relationship between classic carbon compounds and prominent classes of phosphorus (di)cations. 22

Chapter 2

Scheme 2-1: Simplified structures of various carbon allotropes. 29
Scheme 2-2: Comparison of an odd cumulene (top) and an even cumulene (bottom). 30
Scheme 2-3: The first cumulene **2-C** and its solid-state photodimerization to (**2-C**)$_2$. 31
Scheme 2-4: Derivatives of [3]cumulenes. 31
Scheme 2-5: CAAC-terminated [3]cumulene **2-D** and radical cation [**2-D**]$^{\bullet+}$ and dication [**2-D**]$^{2+}$. 32
Scheme 2-6: Different Lewis structures for carbon suboxide C_3O_2. 33
Scheme 2-7: Various heterocumulenes with cumulene and carbone-like canonical forms. 34
Scheme 2-8: Phosphacumulene Lewis structure representations **2-J^{a}** and **2-J^{b}**. 35
Scheme 2-9: Asymmetric cumulene synthesis with ylides **2-K**. 35
Scheme 2-10: Additional phosphacumulene ylides. 36
Scheme 2-11: Boryl-amino-acetylenes **2-L** and **2-M**. 37
Scheme 2-12: Cyclodimerization of **2-N**→(**2-N**)$_2$. 38
Scheme 2-13: Diboryne **2-O** and diboracumulene **2-P.** 38
Scheme 2-14: Boryne **2-Q^{a}** and its cumulene canonical form **2-Q^{b}**. 39
Scheme 2-15: Doubly oxidized carbene and it's canonical forms, including cumulene [**2-R^{d}**]$^{2+}$. 40
Scheme 2-16: Inorganic cumulenes [**2-T**]$^{-}$ and [**2-U**]$^{-}$. 41
Scheme 2-17: Borylimide transfer from [K][**2-T**] to heteroallenes. 42

Scheme 2-18: General structures for methylene, vinylidene, and allenylidene carbenes, as well as metal allenylidene complexes. 43
Scheme 2-19: Early methods for the synthesis of metal allenylidenes. 43
Scheme 2-20: General electronic structure and reactivity patterns of mid-late transition metal allenylidene complexes. 44
Scheme 2-21: Select examples of metal allenylidene complexes engaging in cycloaddition chemistry. 45
Scheme 2-22: Simplified mechanism for the catalytic functionalization of propargylic alcohols *via* a ruthenium-allenylidene intermediate. 46
Scheme 2-23: (top) Isolobal and isoelectronic relationship between $R_2C{=}E$ compounds and TPPCs. (bottom) The analogy extrapolated to [3]cumulene and allenylidene phosphonium, with structural comparison to metal allenylidenes. 47
Scheme 2-24: Widenhoefer's Lewis acid mediated approach to cationic gold allenylidenes. 48
Scheme 2-25: Synthesis of tetraphenyl alkynylphosphine **2-2^{a}**. 49
Scheme 2-26: Formation of Lewis adduct [**2-2^{a}•CPh$_3$**][$B(C_6F_5)_4$]. 50
Scheme 2-27: Formation of Lewis adduct **2-2^{a}•B(C_6F_5)$_3$**, and the conversion of **2-2^{a}** to **2-3^{a}** at higher temperatures. 51
Scheme 2-28: Proposed formation of **2-3^{a}**, by generation of an allenylidene phosphonium **2-2$^{a'}$** and phosphacumulene **2-2$^{a''}$** ylide intermediate. 53
Scheme 2-29: Free energy profile of the reaction of $B(C_6F_5)_3$ with phosphine **2-2^{a}** at the BP86-D3/def2SVP level of theory, in the gas phase. Energies are reported relative to the starting materials. Free energies and enthalpies (in parentheses) are given in kcal mol^{-1}. 54
Scheme 2-30: Two Lewis structures describing the target cation, phosphanyl-alkynyl carbenium and allenylidene phosphonium. 56
Scheme 2-31: (top) Formation of **2-3^{b}** from **2-2^{b}** and $B(C_6F_5)_3$. (bottom) Formation of phosphine-phosphonium salt [**2-4**]+ from phosphine **2-2^{c}** and $B(C_6F_5)_3$ 57
Scheme 2-32: (top) Selected terphenyl stabilized phosphorus multiple bond compounds. (bottom) Attempted phosphenium cation synthesis by Beckmann, and subsequent isomerization by electrophilic activation of an adjacent arene. 58
Scheme 2-33: Formation of **2-3^{Fl}**, **2-3^{Sub}** and **2-2^{Me}•B(C_6F_5)$_3$**. 60
Scheme 2-34: Terminal alkyne activation by $B(C_6F_5)_3$ in a 1,1-carboboration reaction. 61

Scheme 2-35: Selected alkyne activations to afford P/B compounds. 62

Chapter 3

Scheme 3-1: General NHE=Y substituent framework with selected examples. 95
Scheme 3-2: Neutral vs ylide canonical forms for **3-A**, and the ylidic forms for **3-B** and **3-D**. .. 96
Scheme 3-3: Synthesis of the first NHI substituted phosphine **3-E** by Me_3SiCl elimination. Phosphinyl radical **3-F** and phosphinonitrene **3-G**. 97
Scheme 3-4: Trigonal planar phosphonium cations stabilized by NHIs. 97
Scheme 3-5: Phosphorandylium dications stabilized by NHIs. 98
Scheme 3-6: Bis(imino)oxophosphonium [**3-I**]$^+$, versus (imino)(olefin)oxophosphonium [**3-M**]$^+$. 99
Scheme 3-7: Generation of an alkynyl phosphine **3-O**, by salt metathesis with ethynyl magnesium chloride and phosphenium chloride [**3-N**][Cl]. Subsequent alkylation and deprotonation of phosphine **3-O** to give phosphonioacetylide **3-P**. 100
Scheme 3-8: Synthesis of bis(imino)alkynyl phosphine **3-1^a**..... 101
Scheme 3-9: Synthesis of allenylidene phosphonium salt [**3-2**][$B(OC_6F_5)_4$]..... 104
Scheme 3-10: Comparison of the solid-state bond lengths of phosphine **3-1^a**, allenylidene phosphonium [**3-2**]$^+$, methylene phosphonium [**3-K^{NIDipp}**]$^+$ and fluorenylidene cumulene **3-Q.** 107
Scheme 3-11: Depiction of relative charges for **3-R**, [**3-T**]$^-$, and [**3-2**]$^+$. 111
Scheme 3-12: Comparison of literature gas-phase FIA values (kJ/mol) for monocationic and dicationic phosphorus super Lewis Acids. 112
Scheme 3-13: Analogous reaction of methylene phosphonium and allenylidene phosphonium cations with triethyl phosphine oxide. 113
Scheme 3-14: Synthesis of [**3-2•DMAP**]$^+$. 114
Scheme 3-15: Hydrolysis of [**3-2**]$^+$ to [**3-2•H_2O**]$^+$. The photographs show the gradual transformation of [**3-2**]$^+$ to [**3-2•H_2O**]$^+$ in the solid state, and the resulting connectivity depiction which was obtained by diffraction of hydrolyzed crystals. 115

Scheme 3-16: Stacked ^{1}H NMR (300 MHz) spectra of [**3-2•H$_2$O**][B(OC$_6$F$_5$)$_4$] acquired at different temperatures in CD_2Cl_2. Note that the allenic proton peak designated by the blue circle overlaps with the residual solvent for the acquisitions at 248 K and 238 K. 116
Scheme 3-17: Isomerization of [**3-2**]$^+$ to [**3-2^{cyclo}**]$^+$. [B(OC$_6$F$_5$)$_4$]$^-$ excluded from the scheme.. 117
Scheme 3-18: Energy profile (free energy in red, enthalpy in blue) of the reaction path [**3-2**]$^+_{model}$→TS1→[**3-2^{cyclo}**]$^+_{model}$ determined at B3LYP(D3-BJ)/def2-TZVP in CH_2Cl_2 (SMD solvation model)..... 119
Scheme 3-19: Reversible cycloadditions between main-group multiple bonds and arenes..... 120
Scheme 3-21: Doxsee's nitrile addition to titanium alkylidene complex to initially give an azametallocyclobutene, followed by a subsequent ring expansion with a second nitrile (Cp = cyclopentadienyl). Reaction of allenylidene phosphonium with acetonitrile, and its subsequent expansion to the cationic diazaphosphinine [**3-5**]$^+$. 124
Scheme 3-22: Our initially targeted allenylidene phosphonium cation [**3-2^b**]$^+$, which should be a superior candidate for pursuing cycloaddition chemistry. 125

Chapter 4

Scheme 4-1: Select examples of oxidative additions across phosphenium cations. 159
Scheme 4-2: Oxidative additions with phosphenium dications. Anions excluded from the products for clarity. 160
Scheme 4-3: Selected examples of bond activation by geometrically constrained phosphorus compounds. 161
Scheme 4-4: Intermolecular dearomatization of benzene by an NHI substituted acyclic silylene. 162
Scheme 4-5: Proposed keteniminyl phosphonium cation by Sanchez and Majoral. Other main-group carbenoid homologations with either carbon monoxide or isocyanides..... 163
Scheme 4-6: Synthesis of alkyl-imino chlorophosphines **4-1^a** to **4-1^d**, and their phosphenium [B(C$_6$F$_5$)$_4$] salts [**4-2^a**]$^+$ to [**4-2^d**]$^+$..... 165
Scheme 4-7: Reaction of [**4-2^a**][B(C$_6$F$_5$)$_4$] with DMAP and Et$_3$PO. 170
Scheme 4-8: Gutmann-Beckett acceptor numbers of selected phosphenium cations, and other NHI substituted phosphorus (di)cations..... 171

Scheme 4-9: Cycloadditions with phosphenium salt [**4-2^{a}**][$B(C_6F_5)_4$] and unsaturated substrates. 172
Scheme 4-10: Divergent reaction pathways for the activation of O-H compounds by [**4-2^{a}**]$^{+}$.. 173
Scheme 4-11: Activation of alcohols by a C_s symmetric phosphorous triamide **4-H.** 174
Scheme 4-12: Simplified reaction pathways for alcohol activation by phosphenium [**4-2^{a}**]$^{+}$. A) Single site activation of alcohols by [**4-2^{a}**]$^{+}$. B) Substituent assisted O-H activation by [**4-2^{a}**]$^{+}$. 175
Scheme 4-13: Reactions of [**4-2^{a}**]$^{+}$ with aromatic amines..... 177
Scheme 4-14: Speculative products resulting from the reaction of phosphenium cation [**4-2^{a}**][$B(C_6F_5)_4$] and cyclohexyl isocyanide..... 178
Scheme 4-15: Selected examples of H_2 activated main group centers. Alkene hydrogenation directly from dihydrogen using a geometrically constrained phosphenium cation. 180
Scheme 4- 16: Reaction of phosphenium cation [**4-2^{a}**]$^{+}$ with ammonia borane, generating a mixture of secondary phosphine **4-13** and dihydrophosphonium cation [**4-14**]$^{+}$. Independent synthesis of **4-13** from N-Selectride® and chlorophosphine **4-1^{a}**. 181
Scheme 4-17: The only H atom substituted dicoordinate carbenoid, a monosubstituted carbene stabilized by extreme steric bulk. Proposed H-substituted phosphenium cation based on an NHI. 184

Preface

Group and period organization of the periodic table provides a framework for making at-a-glance assumptions about how any given element may be similar or different to its respective neighbours.[1,2] Its predictive power extends to how chemists can anticipate the properties of a series of compounds that share near identical composition and only differ by substitution of a single key element. The most obvious trends are manifested in congeners derived from vertically positions elements that share the same valence electron configuration. An example being trivalent organopnictogens like amines (NR_3), phosphines (PR_3), arsines (AsR_3), stibines (SbR_3), and bismuthines (BiR_3), which are all noted for having a characteristic non-bonding pair of electrons, implicating these molecules as being Lewis basic in some capacity.[3,4] Trends in congeners across periods are not always apparent given that in many instances, compounds of a series will not have the same valence electron configuration. Second-period hydrides for instance, borane (B_nH_{3n}), methane (CH_4) and ammonia (NH_3), share little in common with respect to their reactivity.[1] Isodiagonality refers to anomalous trends in physical properties, bonding, or reactivity which occur between compounds derived from two diagonally positioned elements in the periodic table.[5-7] Pairs of elements that are isodiagonal are said to be in a diagonal relationship. The existence of diagonal relationships is documented to coincide with the conception of the modern periodic table in the mid 1800s, with contributors Mendeléev and Newlands both reportedly describing similarities between several element pairings, including the p-block pair of boron and silicon.[7,8] Concerning compounds with covalent bonds, isodiagonality is thought to largely be a consequence of electronegativity, the property which governs an elements' ability to release or accept electrons. [7-11] A widely discussed diagonal pair amongst the main-group elements is that of phosphorus and carbon [12-14] (Figure P-1).

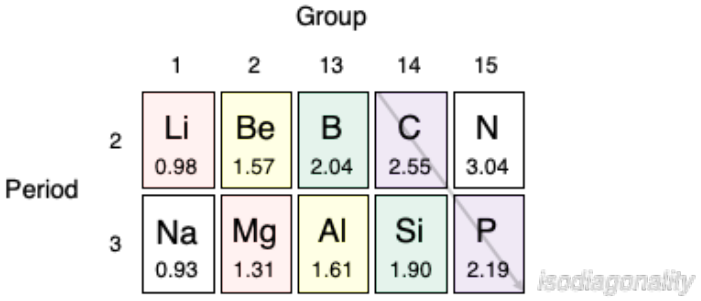

Figure P-1: Isodiagonal relationship in the early s- and p-block.

Nixon, Dillon and Mathey famously coined phosphorus as the "Carbon Copy" during the rapid expansion of phosphaorganic chemistry in the mid-late 1900s, and the moniker references similarities in the behavior of low-coordinate phosphorus and carbon compounds. The conceptual basis for why such similarities exist is largely attributed to their closely approximate electronegativities (C 2.55 and P 2.19).[12-14] The implication of this is that phosphorus is often capable of "mimicking" or playing the role of carbon when introduced to compounds in its place (Scheme P-1). [15-22] Such replacement of carbon for phosphorus is not without consequence, and doing so often comes with altered physical and chemical properties. An excerpt from Phosphorus: the Carbon Copy (1998) concerning the outlook of this area reads: "The fate of 'phosphaorganic' chemistry will be intimately linked to the discovery of new applications." [12] While the pursuit of such phosphorus compounds is primarily driven by fundamental interest and to overcome a synthetic challenge, their proliferation into applied research fields is becoming more common.

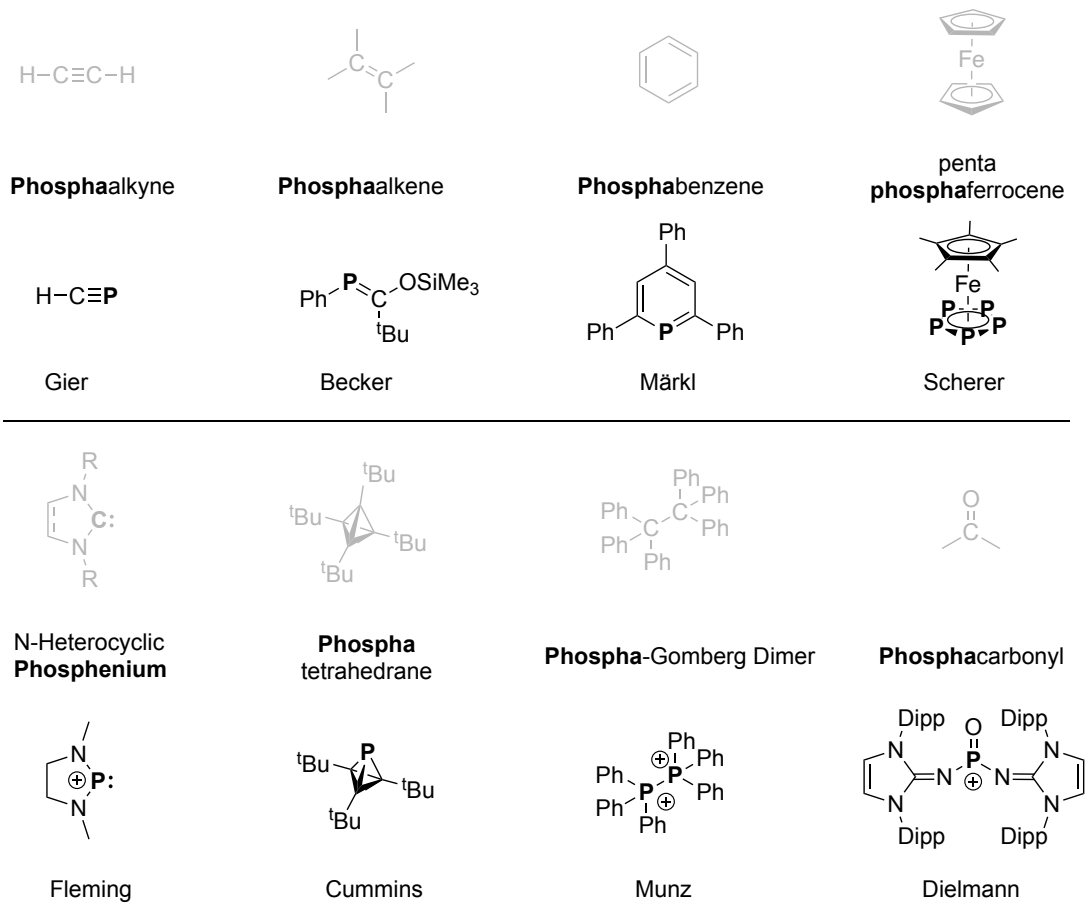

Scheme P-1: Cited examples illustrating the phosphorus-carbon analogy. [15-22]

References

1. N. N. Greenword, A. Earnshaw, Chemistry of The Elements. *Elsevier*, **2012**.
2. D. Mendeleev. *Z. Chem.* **1869**, *12*, 405-406.
3. J. M. Lipshultz, G. Li, A. T. Radosevich, *J. Am. Chem. Soc.* **2021**, *143*, 1699–1721.
4. A. Kuczkowski, S. Schulz, M. Nieger, P. R. Schreiner, *Organometallics* **2002**, *21*, 1408–1419.
5. R. L. Rich, *J. Chem. Educ.* **1986**, *63*, 828–829.
6. C. H. Cartledge, *J. Am. Chem. Soc.* **1928**, *50*, 2863-2872.
7. G. Rayner-Canham, *Found. Chem.* **2011**, *13*, 121–129.
8. A. J. Ihde, The Development of Modern Chemistry. *Dover*. **1984**
9. A. Paparo, C. D. Smith, C. Jones, C. *Angew. Chem. Int. Ed.* **2019**, *58*, 11459–11463.
10. S. Wang, J. D. Sears, C. E. Moore, A. L. Rheingold, M. L. Niedig, J. S. Figueroa, *Science.* **2022**, *375*, 1393–1397.
11. K. M. Marczenko, J. A. Zurakowski, K. L. Bamford, J. W. M. MacMillan, S. S. Chitnis, *Angew. Chem. Int. Ed.* **2019**, *58*, 18096–18101.
12. K. B. Dillon, F. Mathey, J. F. Nixon, *Phosphorus: The Carbon Copy. From Organophosphorus To Phospha-Organic Chemistry*; John Wiley & Sons: **1998**.
13. F. Mathey, *Acc. Chem. Res.* **1992**, *25*, 90–96.
14. F. Mathey, *Angew. Chem. Int. Ed.* **2003**, *42*, 1578–1604.
15. T. E. Gier, *J. Am. Chem. Soc.* **1961**, *83*, 1769–1770.
16. G. Becker, *Z. Anorg. Allg. Chemie* **1976**, *423*, 242–254.
17. G. Märkl, *Angew. Chem.* **1966**, *78*, 907–908.
18. O. J. Scherer, T. Brück, *Angew. Chem. Int. Ed.* **1987**, *26*, 59.
19. S. Fleming, M. K. Lupton, K. Jekot, *Inorg. Chem.* **1972**, *11,* 2534–2540.
20. M. Y. Riu, R. L. Jones, W. J. Transue, P. Müller, C. C. Cummins, *Sci. Adv.* **2020**, *6*, eaaz3168.
21. F. Dankert, S. P. Muhm, C. Nandi, S. Danés, S. Mullassery, P. Herbeck-Engel, B. Morgenstern, R. Weiss, P. Salvador, D. Munz, *J. Am. Chem. Soc.* **2025**. *147*, 15369-15376.
22. M. A. Wünsche, T. Witteler, F. Dielmann, *Angew. Chem. Int. Ed.* **2018**, *57*, 7234–7239.

Chapter One: Electrophilic Phosphorus Compounds and Their Ties to Carbon Chemistry

1.1.1 Phosphorus

As one of six essential elements for life, phosphorus is critical for energy transfer in biological systems and is a necessary component of genetic information.[1,2] Despite its prevalence in organisms and moderate crustal abundance, phosphorus is never encountered in any of its allotropic elemental forms (white, red, violet and black).[3,4] White phosphorus (P_4), the first discovered and synthesized allotrope,[5] is the main source of phosphorus feeding the production of a considerable amount of P containing chemicals, which includes pharmaceuticals, and flame retardants among other value-added products.[6,7,8] While an indispensable feedstock, P_4 is also a potent poison and pyrophoric material, properties which have led to its controversial use in warfare.[5] The dichotomy of phosphorus being an element simultaneously associated with life and death, serves as an allegory for the varied and often opposing properties that molecular phosphorus compounds can exhibit.

1.1.2 Phosphorus as Lewis Bases and Acids

Phosphines (formerly phosphanes, PR_3) are perhaps the most recognizable class of phosphorus compounds, best known for their nucleophilic character which is enabled through a lone pair of electrons.[9,10,11] The properties of phosphines have been delineated by decades of intense research given their use as ancillary ligands in transition-metal complexes.[12,13] As various chemical industries have integrated transition-metal-promoted transformations in their production processes, pursuit of new phosphines was, for a long time, and still is, a fruitful endeavor.[14,15,16] By comparison, studies dedicated to the electrophilic properties of phosphorus compounds represent a smaller fraction of reported molecular phosphorus research.[9,17,18,19] The electrophilicity of phosphorus is perhaps most famously exploited in synthetic chemistry to facilitate Wittig reactions. The Lewis acidity of methylene phosphoranes (phosphonium ylide, **1-A**) enables [2+2] cycloaddition with carbonyls (Scheme 1-1).[20,21] Subsequent cycloreversion liberates an alkene and an innocuous by-product, triphenylphosphine oxide, overall making the Wittig-type reaction an extremely powerful synthetic tool for academics and industrial chemists alike (Scheme 1-1). Another ubiquitously employed phosphorus synthon, trichlorophosphine, is

also electrophilic and permits access to a considerable number of organophosphorus compounds through functionalization with nucleophiles (Scheme 1-1).[6,8]

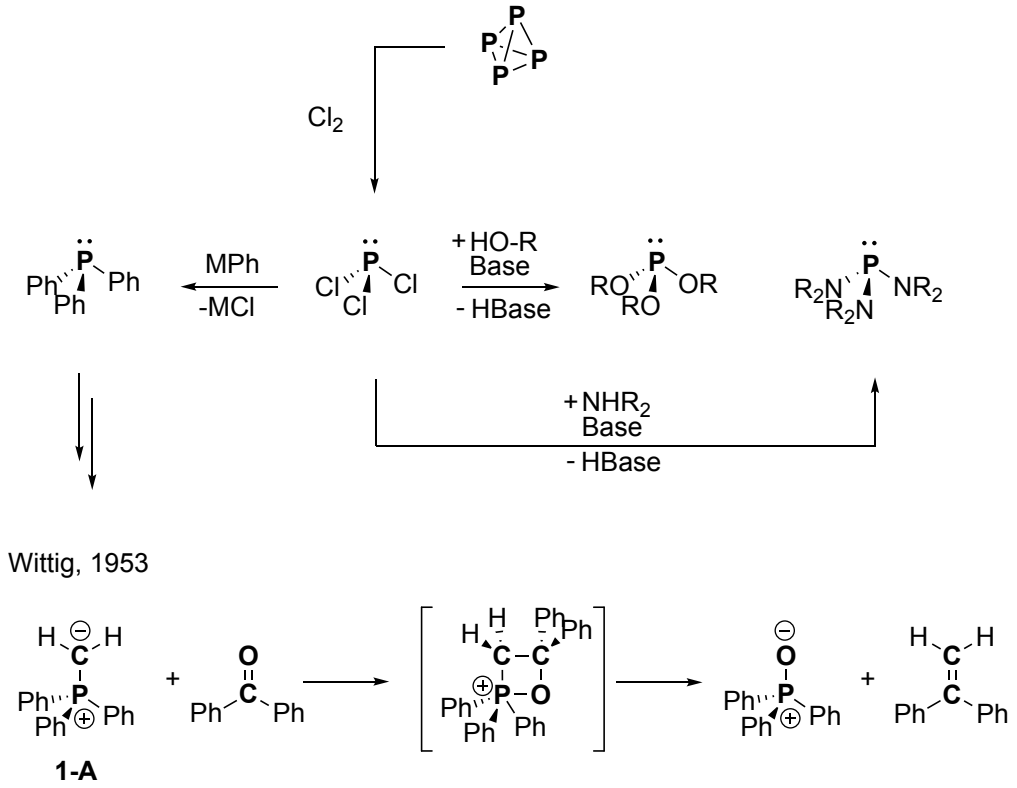

Scheme 1-1: General utilization of trichlorophosphine as an electrophile in the preparation of various classes of phosphorus compounds. The first Wittig reaction, π-bond metathesis of methylenetriphenylphosphorane and benzophenone.

1.1.3 Why Study Electrophilic Phosphorus Compounds?

Bond Activations by Main Group Systems: Frustrated Lewis Pairs and Lewis Acid Catalysis

Beyond synthetic organic chemistry, interest in electrophilic phosphorus species has increased tremendously in light of the discovery of main-group-facilitated small molecule and bond activation.[22,23,24] The activation of thermodynamically strong bonds in small molecules (H_2, CO, CO_2 or N_2) or functional groups (C–F or C–H) has historically been a hallmark of transition metal chemistry. At the time of its discovery in 2006, the reversible activation of hydrogen by a phosphino-borane $Mes_2P(C_6F_4)B(C_6F_5)_2$ **1-B** represented a new paradigm for p-block chemistry (Scheme 1-2).[25] The system debuted by the Stephan group is an intramolecularly linked Lewis

basic phosphine and Lewis acidic borane, which in concert activate H_2, giving $Mes_2P(H)(C_6F_4)(H)B(C_6F_5)_2$ **1-B•H₂**. Steric encumbrance of both the phosphine and borane component preclude the formation of acid-base adducts that would otherwise be detrimental to substrate activation. This concept can be applied to design both intramolecular and intermolecular combinations of sterically encumbered acid and base moieties, collectively known as a "frustrated Lewis pairs." (FLPs) (Scheme 1-2). Remarkably, a subsequent study by the same group would show their initial system **1-B** could add H_2 to a substrates (imines), in effect demonstrating metal-free catalytic hydrogenation.[26] Now twenty years later, FLPs have been found capable of activating numerous small molecule, and used as catalysts for various transformation, topics which have been reviewed extensively.[27,28,29]

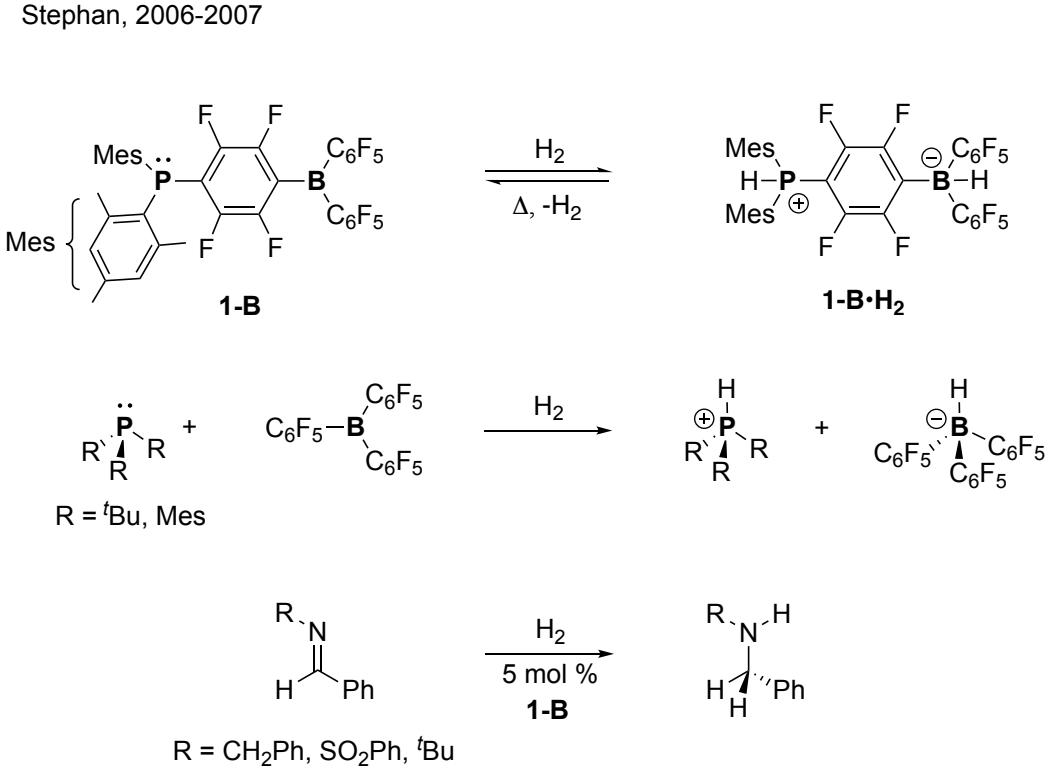

Scheme 1-2: First intramolecular and intermolecular FLP activations of H_2. First hydrogenation using an FLP catalyst.

Most pertinent to this thesis, the advent of FLP chemistry triggered an academic arms race to discover new acid and base components that would provide viable FLP combinations, leading to the isolation of countless discrete Lewis acidic phosphorus species. (to be discussed in Sections

1.6-1.9). Beyond FLPs, phosphorus Lewis acids themselves have been employed in various catalytic reactions, including but not limited to hydrodefluorinations of C–F bonds,[30,31] hydrogenations of unsaturated motifs like alkenes [32] and imines [33], hydrosilylation of alkenes and alkynes, [34] as well and Diels-Alder and Nazarov cycloadditions.[35,36]

Bond Activations by Main Group Systems: Carbenes

Roughly coinciding with the discovery of FLPs, Bertrand showed that carbenes, two-coordinate carbon-centered compounds possessing just six valence electrons, were capable of addition of H_2 and NH_3 (Scheme 1-3).[37] Activation occurs with an increase in the oxidation state of carbon from C^{II} to C^{IV}, mimicking oxidative addition transformations which are common for transition metal complexes. Activation was achieved specifically by acyclic (**1-D**) [38] and cyclic variants of alkyl-amino-carbenes (**1-E**).[39] The latter cyclic versions, abbreviated as CAACs, can be viewed as an evolution of the stable N-heterocyclic carbenes (NHCs, **1-C**) introduced by Arduengo.[40]

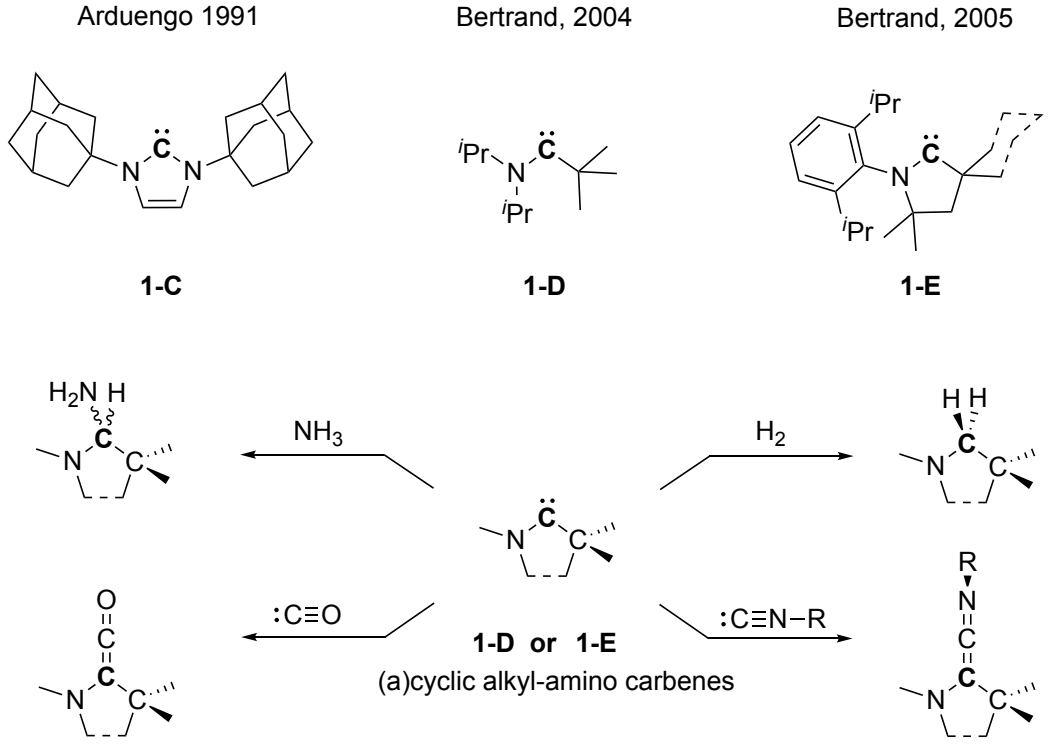

Scheme 1-3: Stable NHCs, and alkyl amino carbenes. H_2 and NH_3 activation by alkyl amino carbenes. Homologation of CO and isonitriles by alkyl-amino carbenes.

CAACs and NHCs are both singlet carbenes, which have an electronic configuration represented by a filled σ orbital and orthogonal empty *p* orbital.[41,42] In some respects, singlet carbenes are similar to FLPs, except in the former the Lewis base (donor) and Lewis acid (acceptor) is situated on a single site, rendering them ambiphilic. Analogous to a bimolecular FLP system, quenching of reactive moieties is circumvented with steric encumbrance (Scheme 1-4).

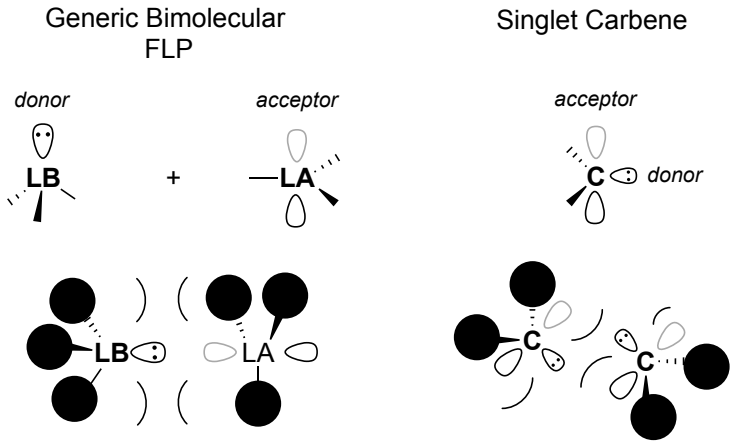

Scheme 1-4: Comparison between a generic bimolecular FLP system and Singlet Carbene.

Where FLP reactivity can be tuned by choosing the acids and bases of varying strength, [28] the acidity (lowest occupied molecular orbital, LUMO) and basicity (highest occupied molecular orbital, HOMO) of stable cyclic carbenes like CAACs and NHCs are also modular, and can be altered by differing the carbene ring size and with substituent effects.[43,44] The major distinction between CAACs and NHCs is their adjacent stabilizing atoms. NHCs see two adjacent nitrogen atoms, which thermodynamically stabilize the LUMO (mitigate acidity) of the carbene by π-electron donation. Given the high electronegativity of nitrogen, these atoms also stabilize the carbene HOMO (mitigate basicity) by an electron withdrawing effect.[43] By forgoing one adjacent nitrogen atom for a carbon atom, CAACs are simultaneously more basic and more acidic. [39] The pronounced ambiphilicity of CAACs enables the aforementioned activation of H_2 and NH_3 that is not possible with NHCs. Their higher acidity is also known to uniquely facilitate capture of neutral nucleophiles like carbon monoxide [45] or isonitriles [46], which results in the formation of ketenes and ketenimines (Scheme 1-3). Bertrand's study galvanized exploration into new carbenes amenable for bond activation. Additionally, main group analogs of carbenes ($R_2E:^n$, E = p-block element, n = charge) with the same frontier molecular orbital (FMO) arrangement, such as

silylenes, aluminylenes, and borylenes, among others, have been perused for similar applications.[47,48] This interest extends towards electrophilic phosphenium cations, the earliest known isolable carbene analogs, pre-dating the isolation of carbenes themselves by at least 15 years (to be discussed in Section 1.5).[18]

1.1.4 Cationic Phosphorus Lewis Acids

While neutral phosphorus compounds like phosphines (PR_3) and phosphonium ylides demonstrably show electrophilic behavior (Scheme 1-1), positively charged phosphorus species tend to exhibit more pronounced Lewis acid character, which can be exploited towards more challenging bond activations. Broadly, cationic phosphorus Lewis acids encompass several classes of compounds that can be delineated based on their oxidation state, coordination environment and charge number (singly or doubly charged).

1.1.5 Phosphenium Cations $[R_2P:]^+$

The aforementioned phosphenium cations $[R_2P:]^+$ are dicoordinate P(III) compounds, and are acceptors through an empty *p* orbital (Scheme 1-5).[18] Since their initial isolation in 1964 by Dimroth and Hoffman [**1-F**] $^+$, numerous cyclic and acyclic variants of phosphenium cations have been reported (Scheme 1-6).[49] Like carbenes, the thermodynamic stability of phosphenium cations is enhanced using either π-donating heteroatoms or by extensive π-delocalization. Due to electrostatic repulsion, dimerization is typically not a concern, but rather steric encumbrance can be leveraged to deter unwanted interactions with anions.

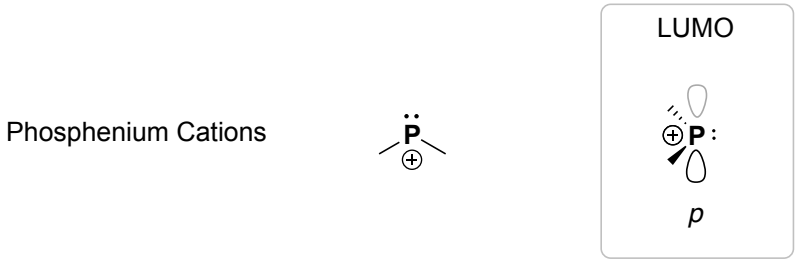

Scheme 1-5: Structure and LUMO generalization of phosphenium cations.

Many early phosphenium cations adopt the same general substituent arrangement, at least one adjacent amino group, and either a second adjacent amino group or a bulky alkyl or silyl group, though there are exceptions.[18] The bis(ferrocenium) phosphenium cation [**1-J**]$^+$ is one such

anomaly that deviates from this general structure and is stabilized by intramolecular Fe-P interactions.[50,51] First described in 1972 by Fleming [52] and subsequently investigated by several groups in the last few decades, N-heterocyclic phosphenium cations (NHPs, [**1-G**]$^+$) are species which can be viewed as analogous to NHCs **1-C**.[53,54] As ancillary ligands for transition metal complexes, NHCs have strong σ-donor and weak π-acceptor properties. By comparison, NHPs have the opposite electronic situation and are described as weak σ-donors and strong π-acceptors. Outside the coordination sphere of metals, stable phosphenium cations are generally strongly electrophilic and weakly nucleophilic species.

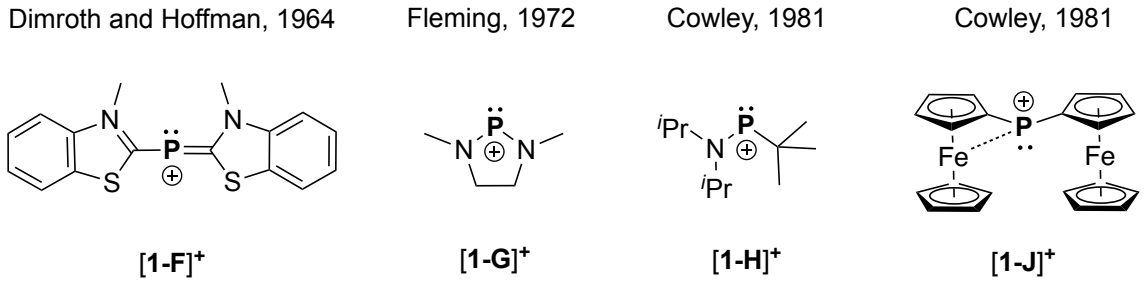

Scheme 1-6: Select examples of early phosphenium cations.

The ambiphilic character and coordinatively unsaturated nature of phosphenium cations makes them intriguing species to study on account of their potential to activate bonds by oxidative addition. In 1982, Cowley found serendipitously that a bis(amino)-phosphenium cation [**1-K**]$^+$ could activate aromatic C–H bonds of a stannocene or plumbocene (Scheme 1-7).[55] The same group also showed alkyl C–H bond activation was possible, albeit as an intramolecular rearrangement product of a cyclopentadiene substituted phosphenium cation [**1-L**]$^+$.[56] Alternatively, oxidative addition can occur across groups of unsaturation. One example that illustrates this was provided by Baxter and SooHoo who showed that bis(amino)-phosphenium [**1-K**]$^+$ can react in [4+1] cycloaddition with 1,3-butadienes to give phospholenium salts.[57] Such "metallomimetic" (transition metal-like) behavior of phosphenium cations is a topic of considerable interest at the moment, which will be discussed more thoroughly in Chapter 4.

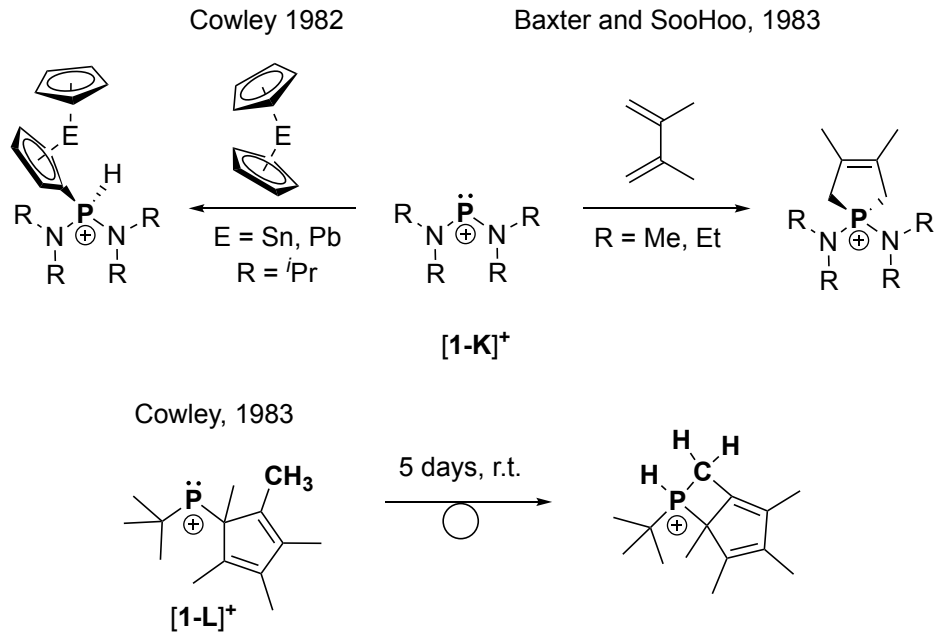

Scheme 1-7: Select examples of oxidative addition occurring at phosphenium centers.

1.1.6 Tetracoordinate Phosphonium Cations $[PR_4]^+$

Another common class of phosphorus Lewis acids are tetra-coordinate P(V) phosphonium salts $[PR_4]^+$ that are electron acceptors *via* low lying P–R σ* orbitals (Scheme 1-8).[58] Unlike phosphenium cations, the saturated coordination environment of $[PR_4]^+$ salts means their isolation rarely necessitates kinetic stabilization by steric protection or thermodynamic taming by π-electron rich substituents.

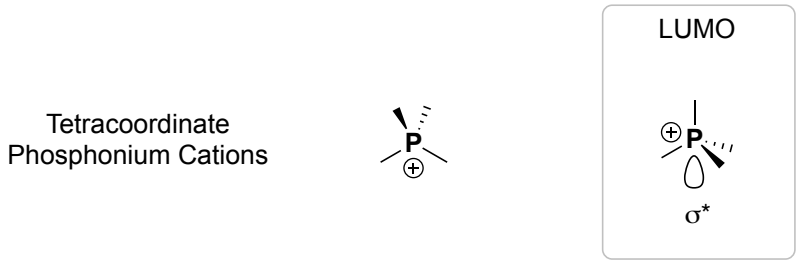

Scheme 1-8: Structure and LUMO generalization of phosphonium cations.

Despite their simplicity, tetraalkyl, tetraaryl or mixed alkyl/aryl phosphonium salts are mildly acidic and have shown useful in some catalytic bond forming reactions, namely additions to carbonyls.[59,60] Chiral phosphonium salts are also known to facilitate asymmetric organic

transformations. [61,62] With respect to enhancing the acceptor properties of phosphonium salts, several strategies have been introduced recently which will be briefly summarized. As the most accessible σ* orbitals of $[PR_4]^+$ salts are in direct opposition to the most electron withdrawing substituents, substitution with more electronegative elements is an intuitive approach to make phosphorus more electrophilic. In 2006, Terada and Kouchi prepared phosphonium cation [**1-M**]$^+$ derived from a single catechol group which exhibit Lewis acidity on account of phosphorus bonding with electronegative oxygen atoms (Scheme 1-9).[36] Substituting phosphorus with fluorine, the most electronegative element, was shown by Stephan and co-workers to afford $[PR_4]^+$ salts like [**1-O**]$^+$ with extreme electrophilicity. [30] The Stephan group also showed that rather than electronegative elements or electron withdrawing groups, positively charged substituents as seen in [**1-P**]$^+$ can be employed with similar outcomes.[63] In 2021, Greb and Stephan found that bis-catecholo-phosphonium salts [**1-Q**]$^+$ were fiercely electrophilic species on account of geometric constraints imposed by using two bidentate substituents.[64] Greb and Stephan's work aligns with a broader topic in main group chemistry where alterations in the nucleophilicity or electrophilicity of p-block element centers is induced by deforming them with restrictive substituent platforms. [19,65]

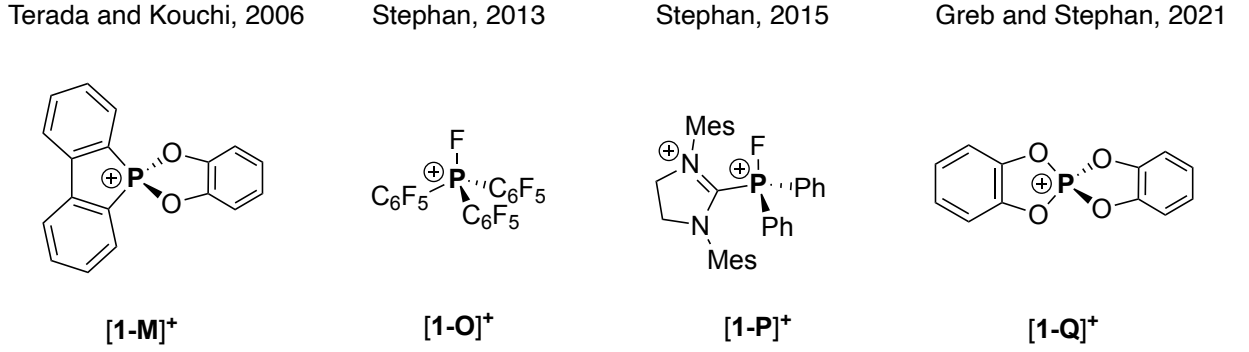

Scheme 1-9: Select examples of recent electrophilic phosphonium cations.

One application of strongly electrophilic phosphonium chemistry is their ability to facilitate heterolytic cleavage of thermodynamically strong bonds. As a result of stoichiometric anion abstractions by phosphonium cations, neutral pentacoordinate phosphoranes (PR_5) are produced. Catalytic processes can be designed by judiciously introducing reaction components that regenerate electrophilic phosphonium cations from their respective phosphoranes. An example

which illustrates this is the hydrodefluorination of fluoroalkanes using [**1-O**]$^+$.[30] [**1-O**]$^+$ facilitates C–F bond activation while a sacrificial hydrosilane source is essential for hydride delivery to the substrate and subsequent phosphonium regeneration.

Stephan, 2013

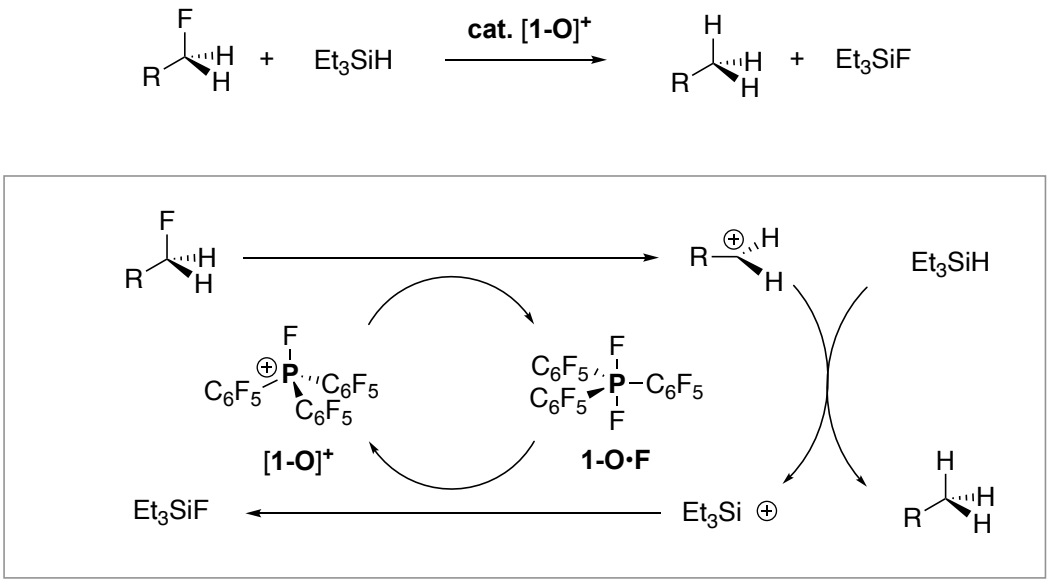

Scheme 1-10: Catalytic hydrodefluorination with [**1-O**]+.

1.1.7 Trigonal Planar Phosphonium Cations $[R_2P{=}E]^+$

Trigonal-planar phosphonium cations (TPPCs) $[R_2P{=}E]^+$ are an intriguing yet under-explored class of phosphorus(V) Lewis acids.[17] The compound class has enormous chemical diversity as different heteroelements (E) or bonding motifs can be attached to phosphorus. Phosphorus-heteroelement multiple bonding gives TPPCs their electrophilic properties, manifested in the form of low-lying acceptor orbitals of π^* character at P (Scheme 1-11).[66,67] Several inherent properties of TPPCs have made their isolation a rarity since their initial discovery by Bertrand in 1989. Firstly, on account of their positively charged phosphorus atom, TPPCs feature significantly polarized phosphorus-heteroelement bonds ($P^{\delta+}$– $E^{\delta-}$) rendering them prone to spontaneous head-to-tail dimerization.[66,68] Secondly, the Lewis acid character of $[R_2P{=}E]^+$ salts has been shown to cause recombination or unwanted coordination of their counteranions, resulting in the formation of neutral tetra-coordinate phosphoryl species.[69] Thirdly, the presence of Lewis bases in the

preparation of TPPCs is also extremely problematic, as sequestration of donor molecules results in a loss of planarity at phosphorus. Lewis base adducts of TPPCs $[R_2(LB)P{=}E]^+$ are often sought to prove the intermediacy of a TPPC when they are otherwise not isolable, [70,71] however, their properties more or less resemble those of phosphonium $[PR_4]^+$ or phosphonium ylide species.

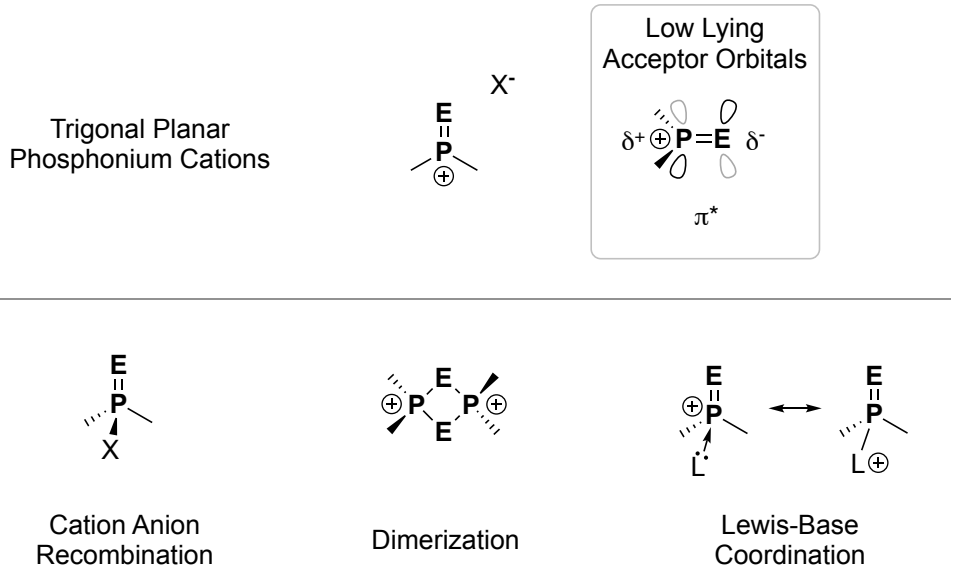

Scheme 1-11: Generalized acceptor orbital depiction of TPPCs and their possible reactivity pathways deterring their isolation.

Despite these deterrents, several strategies have prevailed to isolate TPPCs. As the chemistry of TPPCs has only been reviewed once and it was over 25 years ago, major breakthroughs and pertinent developments will be briefly summarized here.[17] Incidentally, in 1989 Bertrand's group utilized the first ever stable carbene, a phosphinosilylcarbene,[72] to also isolate the first TPPC, a methylene phosphonium $[R_2P{=}CR_2]^+$, [**1-R**]$^+$ (Scheme 1-12).[73] The stability of Bertrand's system is attributed to two key structural details; 1) Similar to phosphenium cations $[R_2P{:}]^+$, π-electron donating substituents can be used to temper Lewis acidity of the phosphorus center. Diisopropylamino (^{i}Pr$_2$N–) substituents at phosphorus accomplish this. 2) Kinetic stability is maximized through steric encumbrance with bulky groups at both ends of the P=C bond. Subsequent work from Grützmacher showed that methylene phosphonium cations can be stabilized through steric encumbrance alone, supporting cation [**1-S**]$^+$ with ^{t}Bu groups at phosphorus, and with at least one trimethylsilyl (Me_3Si–) group at carbon.[74]

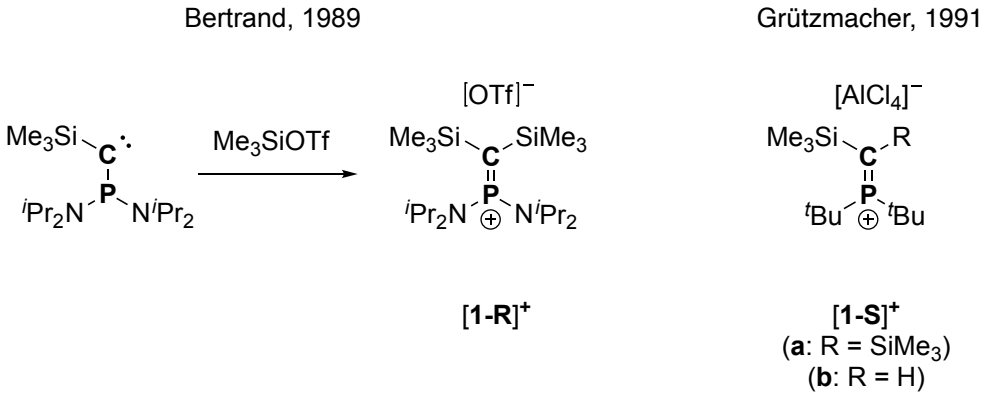

Scheme 1-12: Select examples of methylene phosphonium cations.

TPPCs featuring more electronegative elements $[R_2P{=}E]^+$ (E = N–R, O, S, Se) are especially challenging to access as such compounds have even more exaggerated $P^{\delta+}$– $E^{\delta-}$ bond polarities, furthering their propensity towards dimerization. Moreover, a strictly steric approach to their isolation is not intuitive, especially in the case of chalcogen-derived TPPCs $[R_2P{=}Ch]^+$, where substitution can only occur at one end of the phosphorus-heteroelement bond. Instead, phosphorus is substituted with potent π-donating bulky groups, but not conventional amine-derived groups. Rather, ylidic substituents which are highly efficient at dispersing and delocalizing charge over numerous atoms. In 1992, Schmidpeter would first demonstrate this by preparing a selenophosphonium $[R_2P{=}Se]^+$ [**1-T**]$^+$, exploiting triphenylyphosphoranylidene substituents $Ph_3P{=}(Ph)C–$.[75] Several canonical forms illustrate the extensive delocalizing properties of $Ph_3P{=}$(Ph)C– substituents in Scheme 1-13. In 2013, Bertrand's group prepared iminophosphonium cations $[R_2P{=}N–R]^+$ utilizing N-heterocyclic imine (NHI) substituents ([**1-U**]$^+$).[76] NHIs are also ylidic in nature and highly efficient at delocalizing π-electron density. With respect to kinetic stabilization, NHIs used in TPPCs are tailored to have a steric profile which can project and "wrap around" the P=E bond.[77] Adopting Bertrand's molecular design, Dielmann also prepared oxo- and thio-phosphonium cations [**1-V**]$^+$/[**1-W**]$^+$ $[R_2P{=}O]^+$/$[R_2P{=}S]^+$,[66,67] as well as terminal methylene phosphonium cations $[R_2P{=}CH_2]^+$.[78] More in depth discussion about the unique attributes of NHIs which make them amenable for the isolation of TPPC will be explored in detail in Chapter 3.

Schmidpeter, 1992

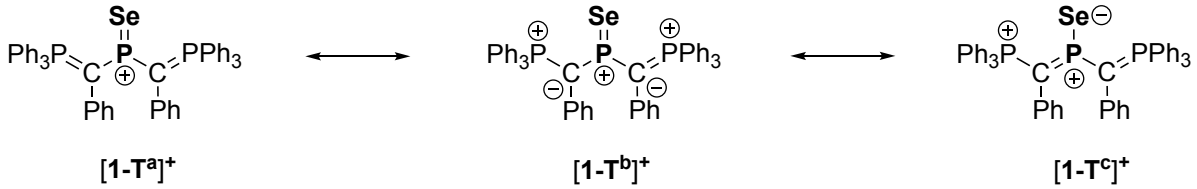

Bertrand, 2013

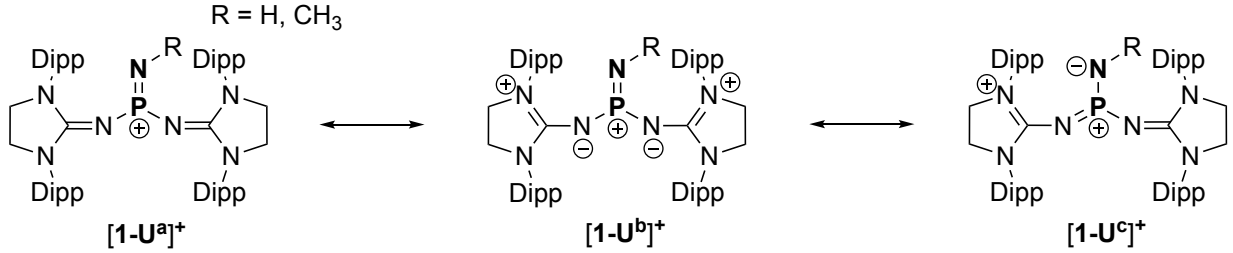

Scheme 1-13: Selenophosphonium [**1-T**]$^+$ and iminophosphonium [**1-U**]$^+$, with various canonical forms drawn to illustrate electron delocalization.

A distinctive property of TPPCs is their facile reactivity with unsaturated substrates. This is partially due to their polar P–E bonds that allow for cycloadditions to occur without a catalyst or photoexcitation. Grützmacher first hinted at this reactivity by showing that methylene phosphonium cation [**1-S(b)**]$^+$ and 1,3-dimethylbutadiene combine in a [4+2] Diels-Alder cycloaddition (Scheme 1-14).[74] Remarkably, the Grützmacher group also showed that transient methylene phosphonium species [^{t}Bu$_2$P=C(Ar)(TMS)]$^+$ [**1-X**]$^+$ are in an equilibrium with benzannulated phosphete salts [**1-X^{cyclo}**]$^+$ *via* an intramolecular electrocyclization reaction.[79]

Grützmacher, 1993

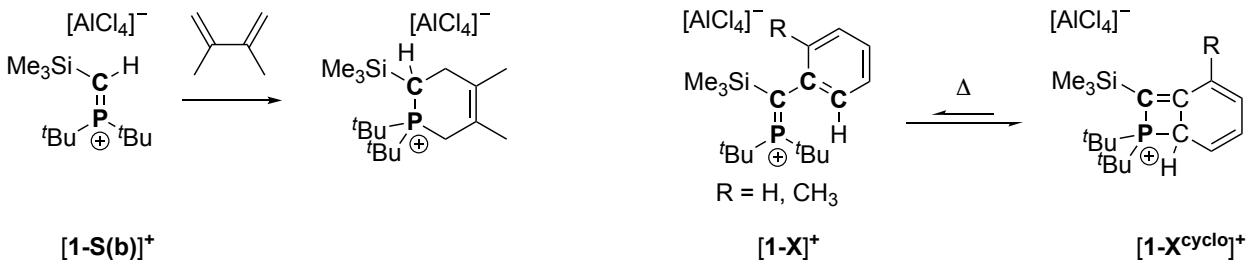

Scheme 1-14: (left) Methylene phosphonium [**1-S**(**b**)]$^+$ and 1,3-dimethylbutadiene Diels-Alder reaction. (right) Electrocyclization of methylene phosphonium [**1-X**]+ to phosphete [**1-X^{cyclo}**]$^+$.

Electrocyclic ring closing of [**1-X**]$^+$ to [**1-X^{cyclo}**]$^+$ is favorable on account of phosphorus adopting a higher coordination environment. On the contrary, the barrier to electrocyclic ring opening is likely minimal as it simultaneously relieves ring strain and results in rearomatization. More recently, Dielmann and co-workers documented [2+2] cycloadditions of oxo- and thio-phosphonium cations [**1-V**]$^+$/[**1-W**]$^+$ with terminal alkynes as a means of preparing chalcogenophosphete cations [**1-Y**]$^+$/[**1-Z**]$^+$ (Scheme 1-15).[80,81] Under thermally pressing conditions [**1-Y**]$^+$/[**1-Z**]$^+$ "open" to 1-phospha-3-chalcogenobutadienes [**1-Y^{open}**]$^+$/[**1-Z^{open}**]$^+$ by electrocyclic ring opening. Analogous to carbon butadienes, the phosphorus analog [**1-Y^{open}**]$^+$/[**1-Z^{open}**]$^+$ can participate in Diels-Alder cycloaddition reactions. The introduction of a dienophile, like acetonitrile or benzophenone, was found to afford for 6-membered cationic phosphorus heterocycles ([**1-AA**]$^+$, [**1-AB**]$^+$ and [**1-AC**]$^+$).[82] Remarkably, from chalcogenophosphonium cations [**1-V**]$^+$/[**1-W**]$^+$ to the heterocycles [**1-AA**]$^+$/[**1-AB**]$^+$, the entire process is reversible.

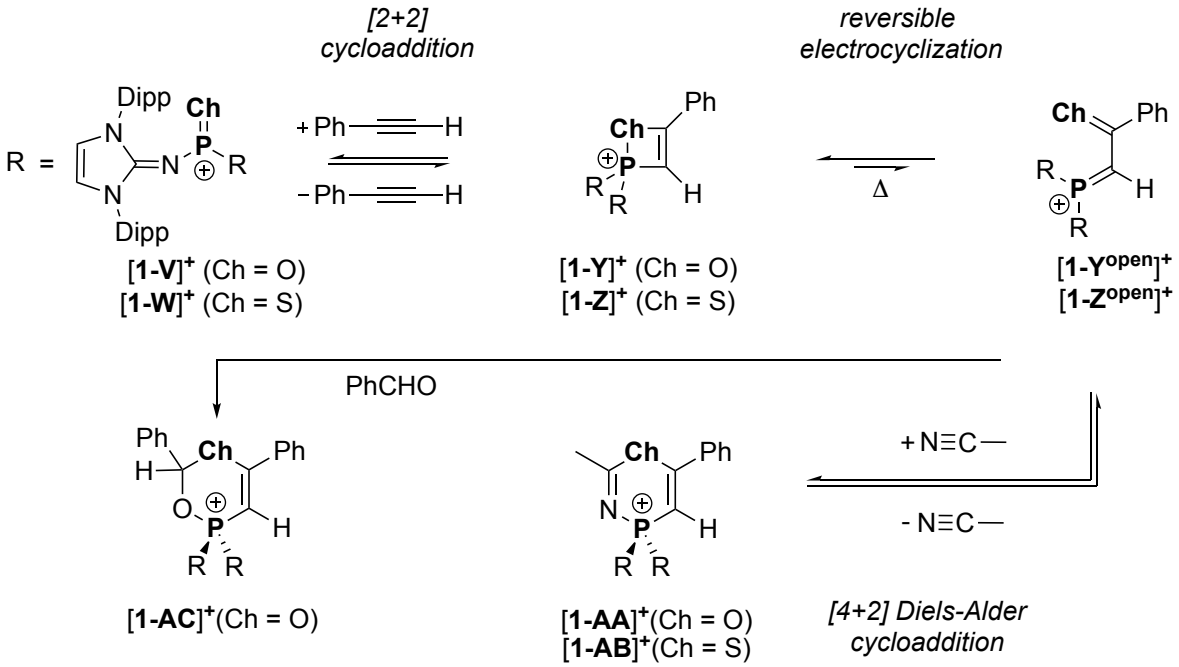

Scheme 1-15: Cycloaddition chemistry of chalcogenophosphonium cations [**1-V**]$^+$/[**1-W**]$^+$. [$BArF_{24}$]$^-$ anions are excluded from the scheme for clarity.

Thiophosphonium cation [**1-W**]$^+$ was shown in a subsequent study by Dielmann to be competent towards π-bond metathesis reactions.[67] Specifically, [**1-W**]$^+$ can readily transfer its sulfur atom to convert ketones and aldehydes to their respective thiocarbonyls (Scheme 1-16).

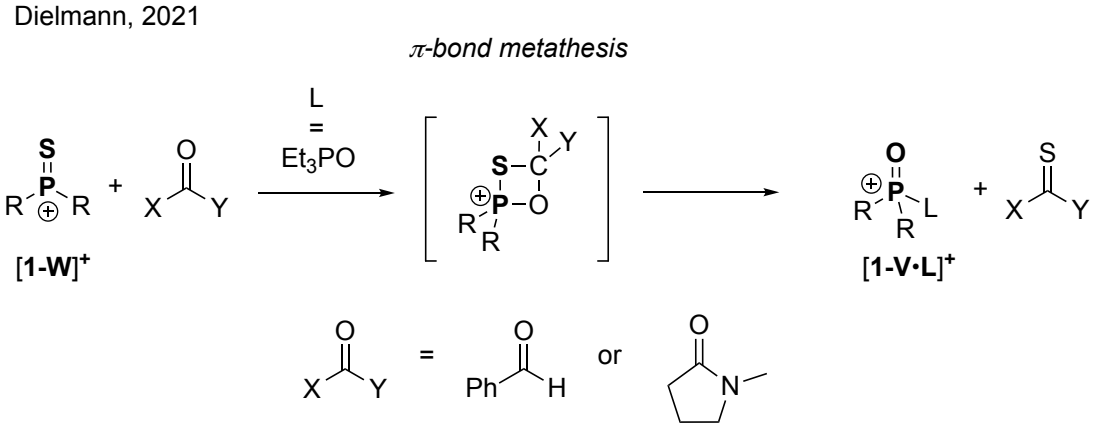

Scheme 1-16: π-Bond metathesis of carbonyls and thiophosphonium cation [**1-W**]$^+$.

1.1.8 Phosphorandylium Dications [PR_3]$^{2+}$

Phosphorandylium dications are also trigonal planar phosphorus species, but are doubly charged, thus have the formula representation [R_3P]$^{2+}$. Phosphorandylium dications derive their Lewis acidity from a vacant *p* orbital, analogous to the prototypical borane Lewis acids that are ubiquitous in both organic and inorganic synthesis (Scheme 1-17).[83] The entire compound class is represented by just two examples, both delineated by Dielmann and co-workers in 2019. Like the TPPCs reported by the same group, NHI substituents are employed to tame these aggressively electrophilic species. So far, the electrophilicity of phosphorandylium dication [**1-AD**]$^{2+}$ has been shown to react with strong bonds (C–F, C–Cl and Si–Cl) in stoichiometric reactions. Interestingly, the latent basicity of the NHI substituents of [**1-AD**]$^{2+}$ can result in co-operative activations of certain substrates (Me_3SiCl and α,α,α-trifluorotoluene), where fragments of the substrate add across a P–N bond. Since their seminal report, no subsequent chemistry on [**1-AD**]$^{2+}$ or any other phosphorandylium ion has been published, so their applications in Lewis acid catalysis, FLP chemistry, or bond activation is largely unknown.

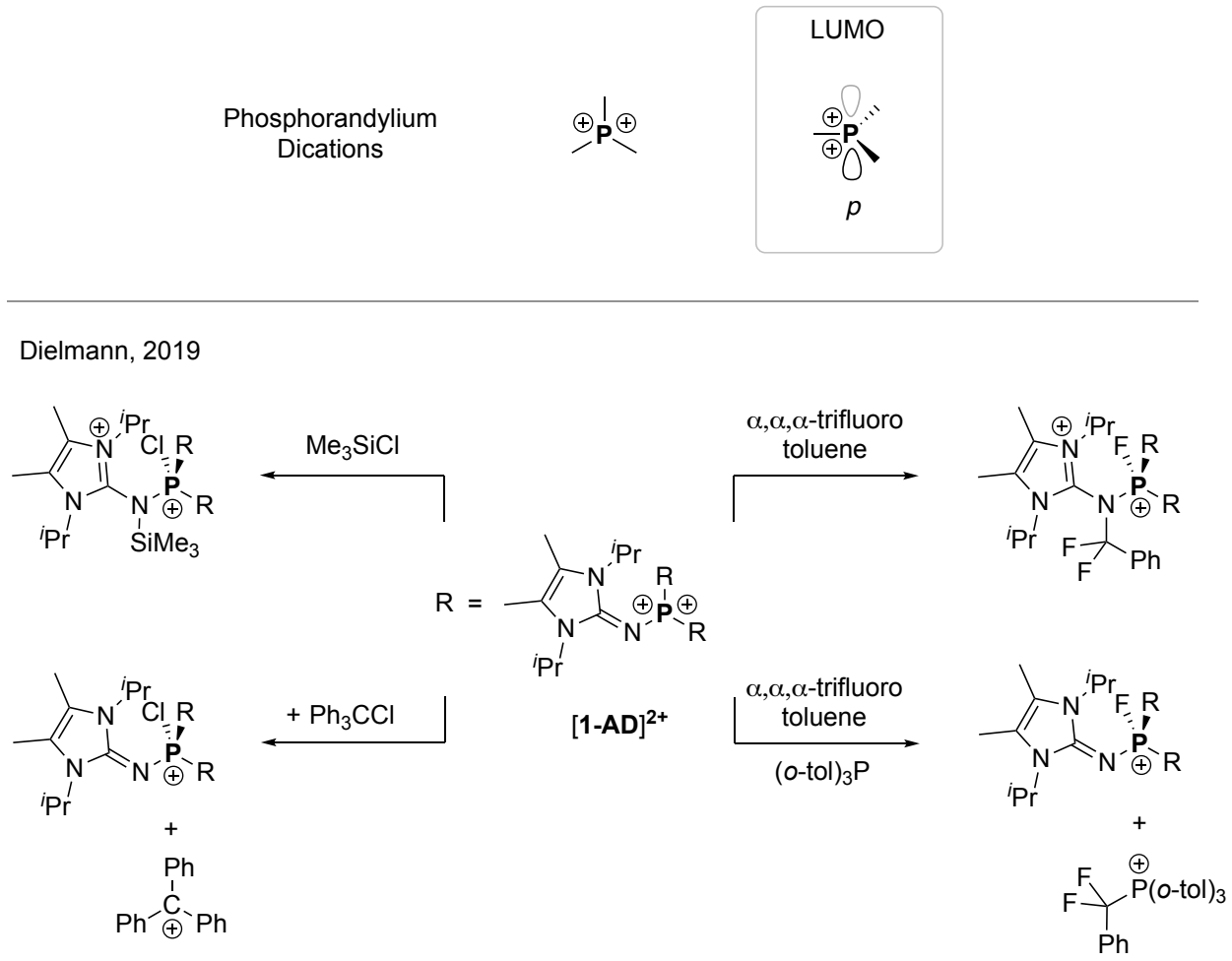

Scheme 1-17: (top) LUMO generalization of phosphorandylium dications. (bottom) Reactivity of the phosphorandylium dication [**1-AD**]$^{2+}$.

1.1.9 Phosphorus Analogs of Organic Molecules

A subset of the main-group community aspires to the synthesis of heteroelement containing analogs of common organic molecules.[48,84,85,86] Such pursuits are often done merely out of fundamental curiosity or for sake of conquering a challenge, however, serendipitous applications are often found during or after the discovery process. The overwhelming majority of modern chemical literature concerns carbon-based molecules and imagination is seemingly the limit to the sophistication, variety, and application of carbon compounds. Among the p-block, phosphorus occupies a privileged position, as it not only belongs to the same group as nitrogen but is also carbon's isodiagonal partner (see Preface). Simply put, novel compounds can be produced

whereby in some instances phosphorus replaces nitrogen, and in other cases phosphorus replaces carbon. Overall, this provides the most extensive library of organic molecules which can serve as direct inspiration for new phosphorus containing compounds.

1.1.10 Phosphorus and Nitrogen Congeners

Understanding the relationship between phosphorus and nitrogen congeners is somewhat intuitive, given that they belong to the same group of the periodic table and share common oxidation states (I, III and V). This suggests that any given pair of P and N analogs will share the same overall molecular charge and the pnictogen atom will occupy the same coordination environment. Major distinctions in the bonding and subsequent reactivity of N and P congeners can be attributed to the larger covalent radii of phosphorus, as well as its larger outer atomic orbitals which are generally more reluctant to undergo mixing (hybridization).[87,88] The former allows phosphorus to adopt penta- and hexa-coordinate bonding environments, where nitrogen cannot. The larger and more diffuse orbitals of phosphorus, especially in comparison to second-row elements like C, N and O, results in reduced P–E (E = N, C, O) π-bonding interactions. These weaker π-bonds translate to P–E multiple bond compounds, like phosphaalkenes ($R–P=CR_2$), being very reactive and having a high propensity to oligomerize or participate in cycloaddition chemistry.[89] Aside from size, Pauling electronegativity distinguishes nitrogen (3.0) and phosphorus (2.2) derived organic compounds, impacting the polarities of bonds, especially with respect to carbon (2.5) (the values provided reflect the overall element electronegativity, and it should be considered that orbital hybridization affects the electronegativity of atoms in molecules).[90] Generally, C–P bonds are comparably less polar than C–N bonds, and have an inversed electron distribution ($C^{\delta-}–P^{\delta+}$ vs $C^{\delta+}–N^{\delta-}$).[89]

The isolation of phosphalkynes (R–C≡P), the heavier congeners of nitriles (R–C≡N), presents a major milestone in P/N congener chemistry and main group multiple bond chemistry. Becker's stable phosphalkyne derivative, achieved by introduction of a sterically bulky tert-butyl (^{t}Bu) group, was ground-breaking at the time and would highlight the importance of steric factors in supporting heavy-element-to-carbon bonding.[91] The stability of ^{t}Bu–C≡P starkly contrasts the parent phosphalkyne H–C≡P which had been characterized by Gier twenty years prior but could only be handled under cryogenic conditions.[92] While not necessarily pertinent to the work of this

thesis, P/N congener chemistry continues to be an expansive research area with tremendous development in the chemistry of phospholes (pyrrole analogs),[93,94] phosphinines (pyridine analogs), [95] the phosphaethylnolate [O–C≡P]$^-$ anion (cyanate analog),[96] and the cyaphide [C≡P]$^-$ anion (cyanide analog).[97]

1.1.11 Carbon-Phosphorus Mimicry

A remarkable discovery with respect to low coordinate phosphorus chemistry came in 1981, when Nixon and co-workers would show that as ligands for transition metals, phosphaalkynes R–C≡P demonstrably prefer η^2 side on coordination through π-donor interactions, in opposition to nitriles which prefer end on η^1 coordination through their nitrogen lone pair (Scheme 1-18). [98,99] Complementary to Nixon's work, studies by Regitz in subsequent years demonstrated that phosphalkynes participate in cycloaddition chemistry, like [4+2] Diels-Alder reactions [100] and azide-alkyne coupling, [101] drawing more apparent similarities to the reactivity of organic alkynes.

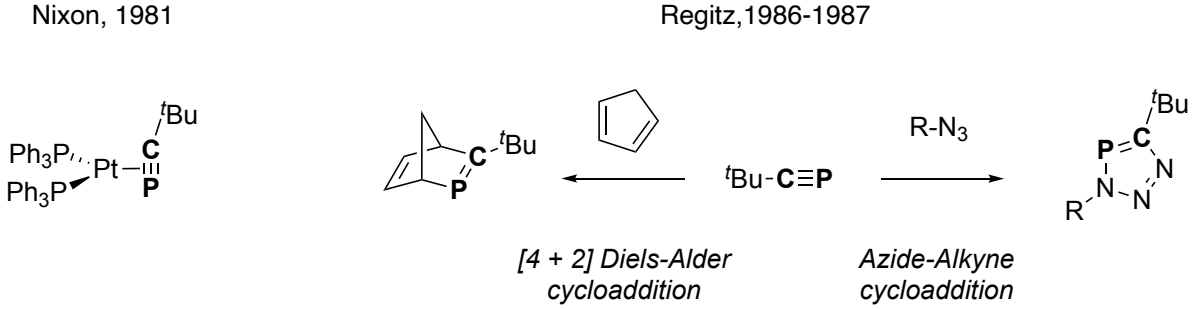

Scheme 1-18: Example of coordination chemistry with ^{t}Bu–C≡P. Cycloaddition reactions with ^{t}Bu–C≡P.

In 1981 Roald Hofmann and Kenichi Fukui were awarded the Nobel Prize in Chemistry for studies on the bonding and reactivity of related molecular fragments, which was further refined into the isolobal principle.[102] Conceptually, the principle compares compounds by their FMO symmetries — the shape and approximate energy of their HOMOs and LUMOs. Despite differences in atom connectivity, phosphaalkynes and alkynes are isolobally analogous species, predicated experimentally by similar reactivity patterns that suggest that both species have FMOs of π/π^* orbital character (Scheme 1-19). More broadly, the isolobal principle allows for countless parallels to be drawn between carbon compounds and phosphorus compounds even in cases where there are

obvious structural differences. Another isolobal relationship which is a cornerstone of phosphorus chemistry is between alkenes and phosphalkenes. [103]

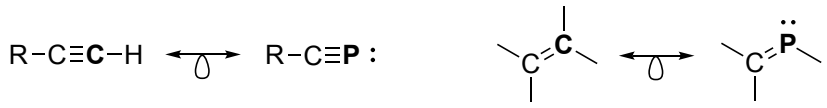

Scheme 1-19: Isolobal relationship between (left) alkynes and phosphaalkynes, (right) alkenes and phosphaalkenes. Isolobal species are denoted with a double ended arrow stylized with an orbital.

Against the backdrop of the isolobal analogy, phosphorus cations become even more fascinating chemical species. The major classes of phosphorus (di)cations (phospheniums, phosphoniums, TPPCs and phosphorandyliums) are all inherently related to carbon compounds (Scheme 1-20). Their relationship can be described as one that is both isolobal and valence isoelectronic (share the same atom connectivity and coordination environments), representing closely approximate analogs of each another. With this perspective, the principles governing stability, isolation strategies, and trends in reactivity observed for cationic phosphorus compounds can provide valuable insights into carbon chemistry, and *vice versa*. Additionally, this frame of reference can provide inspiration for new phosphorus cations derivative of common carbon compounds.

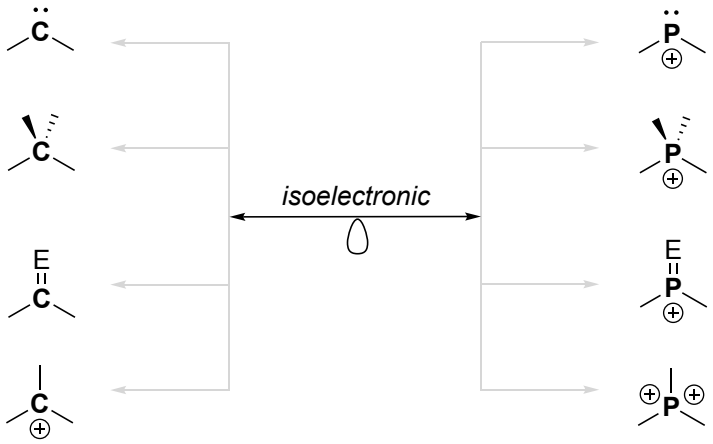

Scheme 1-20: Isolobal and isoelectronic relationship between classic carbon compounds and prominent classes of phosphorus (di)cations.

1.2 References

1. W. Schipper, *Eur. J. Inorg. Chem.* **2014**, 1567–1571.
2. K. A. Remick, J. D Helmann, *Adv. Microb. Physiol.* **2023**, *82*, 1–127.
3. F. Bachhuber, J. Von Appen, R. Dronskowski, P. Schmidt, T. Nilges, A. Pfitzner, R. Weihrich, *Angew. Chem. Int. Ed.* **2014**, *53*, 11629–11633.
4. X. Ye, M. Qi, M. Chen, L. Zhang, J. Zhang, *Adv. Mater. Interfaces* **2023**, *10*, 2201941.
5. J. Emslie, The 13th Element: The Sordid Tale of Murder, Fire, and Phosphorus, *Turner Publishing Company.* **2002**.
6, M. Donath, K. Schwedtmann, T. Schneider, F. Hennersdorf, A. Bauzá, A. Frontera, J. J. Weigand, *Nat. Chem.* **2022**, *14*, 384–391.
7. H. Grützmacher, *Nat. Chem.* **2022**, *14*, 361–364.
8. M. B. Geeson, C. C. Cummins, *ACS Cent. Sci.* **2020**, *6*, 848–860.
9. J. M. Bayne, D. W. Stephan, *Chem. Soc. Rev.* **2016**, *45*, 765–774.
10. J. M. Lipshultz, G. Li, A. T. Radosevich, *J. Am. Chem. Soc.* **2021**, *143*, 1699–1721.
11. H. Guo, Y. C. Fan, Z. Sun, Y. Wu, O. Kwon, *Chem. Rev.* **2018**, *118*, 10049–10293.
12. M. A. Wünsche, P. Mehlmann, T. Witteler, F. Buß, P. Rathmann, F. Dielmann, *Angew. Chem. Int. Ed.* **2015**, *54*, 11857–11860.
13. J. A. Gillespie, E. Zuidema, P. W. N. M. van Leeuwen, P. C. J. Kamer, Phosphorus (III) Ligands in Homogeneous Catalysis: Design and Synthesis (Eds.: P. C. J. Kamer, and P. W. N. M. van Leeuwen), John Wiley & Sons, Ltd, **2012**, 1-22
14. H. Shet, U. Parmar, S. Bhilare, A. R. Kapdi, *Org. Chem. Front.* **2021**, *8*, 1599–1656.
15. D. S. Surry, S. L. Buchwald, *Chem. Sci.* **2011**, *2*, 27–50.
16. A. L. Clevenger, R. M. Stolley, J. Aderibigbe, J. Louie, *Chem. Rev.* **2020**, *120*, 6124–6196.
17. O. Guerret, G. Bertrand, *Acc. Chem. Res.* **1997**, *30*, 486–493.
18. A. H. Cowley, R. A. Kemp, *Chem. Rev.* **1985**, *85*, 367–382.
19. D. Bawari, D. Toami, R. Dobrovetsky, *Chem. Commun.* **2025**, *61*, 5871–5882.
20 G. Wittig, G. Geissler, G. *Justus Liebigs Ann. Chem.* **1953**, *580*, 44–57.
21. P. A. Byrne, D. G. Gilheany, *Chem. Soc. Rev.* **2013**, *42*, 6670–6696.

22. R. L. Melen, *Science.* **2019**, *363*, 479–484.

23. P. P. Power, *Nature.* **2010**, *463*, 171–177.

24. D. W. Stephan, *J. Am. Chem. Soc.* **2015**, *137*, 10018–10032.

25. G. C. Welch, R. R. San Juan, J. D. Masuda, D. W. Stephan, *Science.* **2006**, *314*, 1124–1126.

26. P. A. Chase, G. C. Welch, T. Jurca, D. W. Stephan, *Angew. Chem. Int. Ed.* **2007**, *46*, 8050–8053.

27. J. Lam, K. M. Szkop, E. Mosaferi, D. W. Stephan, *Chem. Soc. Rev.* **2019**, *48*, 3592–3612.

28. J. Paradies, *Angew. Chem. Int. Ed.* **2014**, *53*, 3552–3557.

29. D. W. Stephan, G. Erker, *Angew. Chem. Int. Ed*. **2015**, *54*, 6400–6441.

30. C. B. Caputo, L. J. Hounjet, R. Dobrovetsky, D. W. Stephan, *Science*. **2013**, *341*, 1374–1377.

31 J. M. Bayne, D. W. Stephan, *Chem. Eur. J.* **2019**, *25*, 9350–9357.

32. D. Bawari, D. Toami, K. Jaiswal, R. Dobrovetsky, *Nat. Chem.* **2024**, *16*, 1261–1266.

33. T. Lundrigan, E. N. Welsh, T. Hynes, C. H. Tien, M. R. Adams, K. R. Roy, K. N. Robertson, A. W. H. Speed, *J. Am. Chem. Soc.* **2019**, *141*, 14083–14088.

34. M. Pérez, L. J. Hounjet, C. B. Caputo, R. Dobrovetsky, D. W. Stephan, *J. Am. Chem. Soc.* **2013**, *135*, 18308–18310.

35. M. Vogler, L. Süsse, J. H. W. Lafortune, D. W. Stephan, M. Oestreich, *Organometallics.* **2018**, *37*, 3303–3313.

36. M. Terada, M. Kouchi, *Tetrahedron.* **2006**, *62*, 401–409.

37. G. D. Frey, V. Lavallo, B. Donnadieu, W. W. Schoeller, G. Bertrand, *Science.* **2007**, *316*, 439–441.

38. V. Lavallo, J. Mafhouz, Y. Canac, B. Donnadieu, W. W. Schoeller, G. Bertrand, *J. Am. Chem. Soc.* **2004**, *126*, 8670–8671.

39. V. Lavallo, Y. Canac, C. Präsang, B. Donnadieu, G. Bertrand, *Angew. Chem. Int. Ed.* **2005**, *44*, 5705–5709.

40. A. J. Arduengo, R. L. Harlow, M. Kline, *J. Am. Chem. Soc.* **1991**, *113*, 361-363.

41. J. Vignolle, X. Cattoën, D. Bourissou, *Chem. Rev.* **2009**, *109*, 3333–3384.

42. M. Melaimi, M. Soleilhavoup, G. Bertrand, *Angew. Chem. Int. Ed*. **2010**, *49*, 8810–8849.

43. D. Bourissou, O. Guerret, F. P. Gabbaï, G. Bertrand, *Chem. Rev.* **2000**, *100*, 39–91.

44. S. K. Kushvaha, A. Mishra, H. W. Roesky, K. C. Mondal, *Chem. Asian J.* **2022**, *17*, e202101301.

45. V. Lavallo, Y. Canac, B. Donnadieu, W. W. Schoeller, G. Bertrand, *Angew. Chem. Int. Ed*. **2006**, *45*, 3488–3491.

46. F. Vermersch, V. T. Wang, M. Abdellaoui, R. Jazzar, G. Bertrand, *Chem. Sci.* **2024**, *15*, 3707–3710.

47. T. Chu, G. I. Nikonov, *Chem. Rev.* **2018**, *118*, 3608–3680.

48. M. He, C. Hu, R. Wei, X. F. Wang, L. L. Liu, *Chem. Soc. Rev.* **2024**, *53*, 3896–3951.

49. K. Dimroth and P. Hoffmann, *Angew. Chem. Int. Ed*. **1964**, *3*, 384

50. S. G. Baxter, R. L. Collins, A. H. Cowley, S. F. Sena, *J. Am. Chem. Soc*. **1981**, *103*, 714–715.

51. M. Olaru, A. Mischin, L. A. Malaspina, S. Mebs, J. Beckmann, *Angew. Chem. Int. Ed*. **2020**, *59*, 1581–1584.

52. S. Fleming, M. K. Lupton, K. Jekot, *Inorg. Chem.* **1972**, *11,* 2534–2540.

53. L. Rosenberg, *Coord. Chem. Rev.* **2012**, *256*, 606–626.

54. D. Gudat, A. Haghverdi, H. Hupfer, M. Nieger, *Chem. Eur. J.* **2000**, *6*, 3414–3425.

55. A. H. Cowley, R. A. Kemp, C. A. Stewart, *J. Am. Chem. Soc*. **1982**, *104*, 3239–3240.

56. S. K. Mehrotra, A. H. Cowley, *J. Am. Chem. Soc*. **1983**, *105*, 2074–2075.

57. C. K. SooHoo, S. G. Baxter, *J. Am. Chem. Soc.* **1983**, *105*, 7443-7444.

58. K. C. K. Swamy, N. S. Kumar, *Acc*. *Chem*. *Res*. **2006**, *39*, 324–333.

59. T. Mukaiyama, S. Matsui, K. Kashiwagi, *Chem. Lett.* **1989**, *18*, 993– 996,

60. R. Córdoba, J. Plumet, *Tetrahedron Lett.* **2003**, *44*, 6157– 6159.

61. C.-L. Zhu, F. -G. Zhang, W. Meng, J. Nie, D. Cahard, J. -A. Ma, *Angew. Chem. Int. Ed.* **2011**, *50*, 5869–5872.

62. J. P. Tan, K. Li, B. Shen, C. Zhuang, Z. Liu, K. Xiao, P. Yu, B. Yi, X. Ren, T. Wang, *Nat. Commun.* **2022**, *13*.

63. M. H. Holthausen, M. Mehta, D. W. Stephan, *Angew. Chem. Int. Ed.* **2014**, *53*, 6538–6541.

64. D. Roth, J. Stirn, D. W. Stephan, L. Greb, *J. Am. Chem. Soc.* **2021**, *143*, 15845–15851.

65. T. J. Hannah, S. S. Chitnis, *Chem. Soc. Rev.* **2023**, *53*, 764–792.

66. M. A. Wünsche, T. Witteler, F. Dielmann, *Angew. Chem. Int. Ed.* **2018**, *57*, 7234–7239.

67. P. Löwe, T. Witteler, F. Dielmann, *Chem. Commun.* **2021**, *57*, 5043–5046.

68. N. Burford, R. E. V. H. Spence, R. D. Rogers, Preparation, *J. Am. Chem. Soc.* **1989**, *111*, 5006–5008.

69. N. Burford, R. E. V. H. Spence, J. F. Richardson, *J. Chem. Soc. Dalton. Trans.* **1991**, 1615-1619.

70. A. D. Hendsbee, N. A. Giffin, Y. Zhang, C. C. Pye, J. D. Masuda, *Angew. Chem. Int. Ed.* **2012**, *51*, 10836–10840.

71. K. Huynh, A. J. Lough, M. A. M. Forgeron, M. Bendle, A. P. Soto, R. E. Wasylishen, I. Manners, *J. Am. Chem. Soc.* **2009**, *131*, 7905–7916.

72. A. Igau, H. Grützmacher, A. Baceiredo, G. Bertrand, *J. Am. Chem. Soc*. **1988**, *110*, 6463-6466.

73. A. Igau, A. Baceiredo, H. Grützmacher, H. Pritzkow, G. Bertrand, *J. Am. Chem. Soc.* **1989**, *111*, 6853–6854.

74. H. Grützmacher, H. Pritzkow, *Angew. Chem. Int. Ed.* **1991**, *30*, 709–710.

75. A. Schmidpeter, G. Jochem, K. Karaghiosoff, C. Robl, *Angew. Chem. Int. Ed.* **1992**, *31*, 1350–1352.

76. F. Dielmann, C. E. Moore, A. L. Rheingold, G. Bertrand, *J. Am. Chem. Soc.* **2013**, *135*, 14071–14703.

77. T. Ochiai, D. Franz, S. Inoue, *Chem. Soc. Rev.* **2016**, *45*, 6327–6344.

78. P. Löwe, M. A. Wünsche, F. R. S. Purtscher, J. Gamper, T. S. Hofer, L. F. B. Wilm, M. B. Röthel, F. Dielmann, *Chem. Sci.* **2023**, *14*, 7928–7935.

79. U. Heim, H. Pritzkow, U. Fleischer, H. Grützmacher, *Angew. Chem. Int. Ed*. **1993**, *32*, 1359–1361

80. P. Löwe, M. Feldt, M. A. Wünsche, L. F. B. Wilm, F. Dielmann, *J. Am. Chem. Soc.* **2020**, *142*, 9818–9826.

81. P. Löwe, M. Feldt, M. B. Röthel, L. F. B. Wilm, F. Dielmann, *Inorg. Chem.* **2021**, *60*, 14509–14514.

82. P. Löwe, dissertation, Westfälische Wilhelms-Universität Münster, **2022**.

83. P. Mehlmann, T. Witteler, L. F. B. Wilm, F. Dielmann, *Nat. Chem.* **2019**, *11*, 1139–1143.

84. Y. K. Loh, S. Aldridge, *Angew. Chem. Int. Ed.* **2021***, 60,* 8626 –8648

85 P. P. Power, *Organometallics.* **2020**, *39*, 4127–4138.

86. C. Weetman, *Chem. Eur. J.* **2021**, *27*, 1941–1954.

87. W. Kutzelnigg, *Angew. Chem. Int. Ed.* **1984**, *23*, 272–295.

88. K. B. Dillon, F. Mathey, J. F. Nixon, *Phosphorus: The Carbon Copy. From Organophosphorus To Phospha-Organic Chemistry*; John Wiley & Sons. **1998**.

89. F. Mathey, *Acc. Chem. Res.* **1992**, *25*, 90–96.

90. H. A. Bent. *J. Chem. Educ.* **1960**, 37, 616–624.

91. G. Becker, G. Gresser, W. Uhl, *Z. Naturforsch B.* **1981**, *36*, 16–19.

92. T. E. Gier, *J. Am. Chem. Soc.* **1961**, *83*, 1769–1770.

93. M. P. Duffy, W. Delaunay, P. A. Bouit, M. Hissler, *Chem. Soc. Rev.* **2016**, *45*, 5296–5310.

94. N. Asok, J. R. Gaffen, T. Baumgartner, *Acc. Chem. Res.* **2023**, *56*, 536–547.

95. C. Müller, L. E. E. Broeckx, I. De Krom, J. J. M. Weemers, *Eur. J. Inorg. Chem.* **2013**, 187–202.

96. J. M. Goicoechea, H. Grützmacher, *Angew. Chem. Int. Ed.* **2018**, *57*, 16968–16994.

97. T. Görlich, P. Coburger, E. S. Yang, J. M. Goicoechea, H. Grützmacher, C. Müller, C. *Angew. Chem. Int. Ed.* **2023**, *62*, e202217749.

98. J. C. T. R. Burckett-St. Laurent, P. B. Hitchcock, H. W. Kroto, F. Nixon, *J. Chem. Soc., Chem. Commun.* **1981**, 1141–1143.

99. J. F. Nixon, *Endeavour.* **1991**, *15*, 49–57.

100. W. Rösch, M. Regitz, *Z. Naturforsch B*. **1987**, *41*, 931-934.

101. W. Rösch, T. Facklam, M. Regitz, *Tetrahedron.* **1987**, *43*, 3247–3256.

102. R. Hoffman, *Angew. Chem. Int. Ed.* **1982**, *27*, 711–800.

103. F. Mathey, *Angew. Chem. Int. Ed.* **2003**, *42*, 1578–1604.

Chapter Two: En Route to a Phosphorus Analog of [3]Cumulene

Some of the content in this chapter has been published:

1. L. C. Torres, R. Dobrovetsky, C. B. Caputo, *Chem. Commun*. **2021**, 57, 8272-8275

2. L. C. Torres, A. Brar, J. LeBlanc, C. B. Ameyaw, C. B. Caputo, *Z. Anorg. Allg. Chem.* **2023**, 649, e202200383.

The content presented herein has been reproduced with explicit permission granted by Wiley and the Royal Society of Chemistry. Amandeep Brar and Clive Ameyaw contributed to the synthesis of additional compounds that are not featured in this thesis but are featured in publication 2. Computations were performed by Roman Dobrovetsky. SCXRD data collection and solving was performed by Jesse LeBlanc and Christopher Caputo. Christopher Caputo made contributions to the writing and editing of the manuscripts. I am grateful for the opportunity to work alongside them. Additional supporting information, including interpretation of NMR spectra, is available online.

2.1 Introduction

2.1.1 Carbon Allotropes

Like phosphorus, elemental carbon exists as several allotropes, each with distinct chemical and physical properties.[1,2] Diamond and graphite are natural allotropes that are essential to various industrial and commercial sectors of our global economy (Scheme 2-1). Within recent decades there has been substantial research on alternative carbon allotropes, such as nanotubes and fullerenes**,** exploring their fundamental properties and applications across electronic, medicinal, and energy domains, among others. Linear carbon is a theoretical allotrope characterized by an infinite arrangement of *sp*-hybridized carbon atoms and has garnered interest from scientists due to its potential as a conductive "molecular wire" material.[3,4,5,6] Structurally, linear carbon could feature carbon atoms connected *via* alternating single and triple bonds $(-C\equiv C-)_\infty$ (alpha-carbyne) or with consecutive double bonds $(=C=C=)_\infty$ (beta-carbyne). To date, either form of carbyne has yet to be successfully synthesized or definitively characterized.

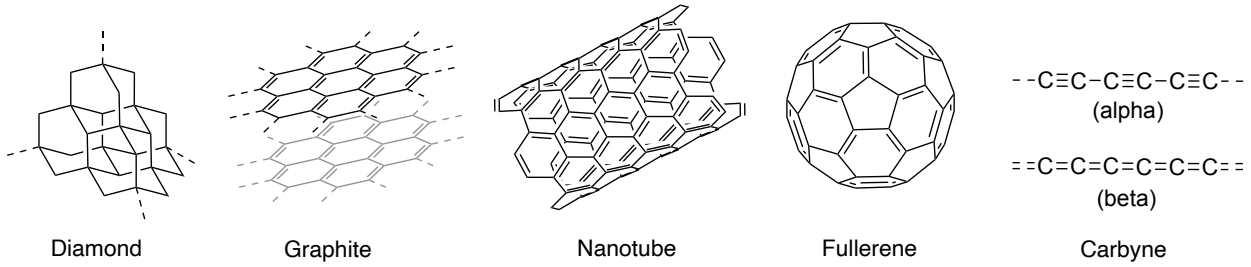

Scheme 2-1: Simplified structures of various carbon allotropes.

2.1.2 A Brief Introduction to Cumulenes

[*n*]Cumulenes are small linear carbon compounds with continuous double bonds (n = # of double bonds), resembling fragments of beta-carbyne.[6,7,8] Their study has been a concern of physical chemists, suggesting their use as models for understanding the potential properties of carbyne. [*n*]Cumulenes are also molecules of great interest to synthetic chemists as their π-electron rich framework offers a wealth of potential transformations.[9] Irrespective of length, all [n]cumulenes are terminated with sp^2 carbon atoms. Major structural and electronic distinctions become apparent when cumulenic chains feature either an odd (n = 3,5,7…) or even (n = 4,6…) number of double bonds. [7,8,10,11] Odd cumulenes like [3]cumulene **2-A** have two non-degenerate orthogonal π-

systems where the substituents on the terminal sp^2 carbons are mutually co-planar (Scheme 2-2). One π-system conjugates the entire length of the molecule and facilitates π-interactions with the end groups, while a second, lower energy π-system conjugates internal *sp-sp* carbon π-bonds. Even cumulenes, like [4]cumulene **2-B**, are axially twisted molecules with their terminal end group substituents lying perpendicular. The orthogonal π-systems are degenerate, and there are minimal conjugative interactions between each individual set of end groups. In either case, the capping end groups can be modified to tailor the electronics, photophysical properties and stability of the cumulene system.

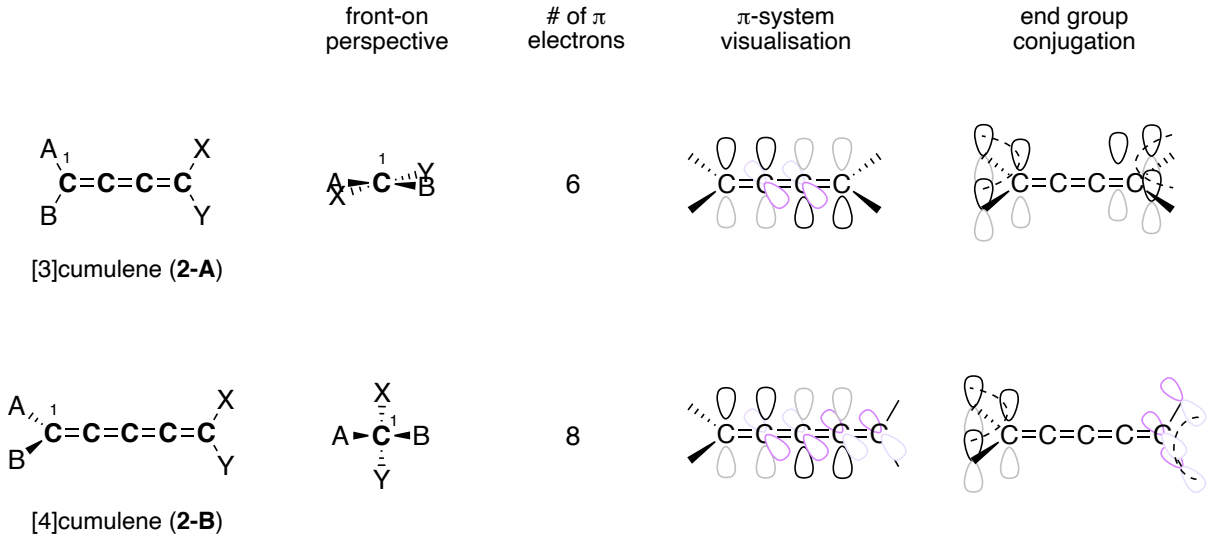

Scheme 2-2: Comparison of an odd cumulene (top) and an even cumulene (bottom).

[3]Cumulenes, the earliest reported [n]cumulenes, are significantly more prevalent than longer homologues due to the increased instability and synthetic challenges associated with higher cumulenes. [7,8] First discovered in 1921 by Brand and coworkers, 1,1,4,4-tetraphenylbutatriene "[3]Ph" **2-C** is the ancestor of cumulenic compounds.[12] Remarkably, this π-electron-rich system was later found to undergo solid-state photo-induced dimerization *via* an intermolecular [2+2] cycloaddition of the terminal C–C bonds, giving (**2-C**)$_2$ (Scheme 2-3).[13]

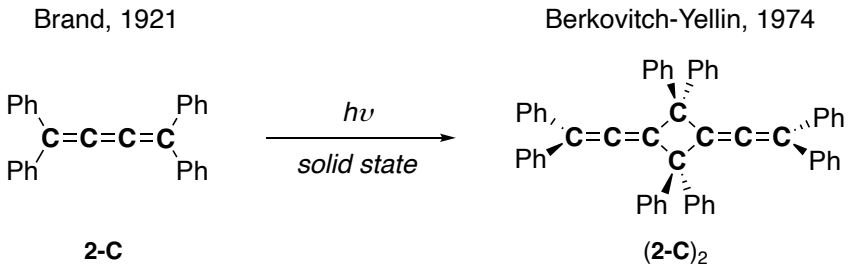

Scheme 2-3: The first cumulene **2-C** and its solid-state photodimerization to (**2-C**)$_2$.

Following Brand's initial report, [3]cumulenes featuring diverse substituents, including halogens,[14] alkyls,[15] aryls,[16] ferrocenes,[17] and N-heterocycles[18] have been reported thereafter, delineating the impact of terminal substitution (cited examples correspond to structures in Scheme 2-4). Generally, the largest contributor to cumulene stability is steric hinderance, with bulky groups deterring undesirable dimer- and oligomer-ization reactions.[7,8,19] The effect of electronic tuning through π-conjugative effects is largely manifested in the absorption properties and solid-state structures of [3]cumulenes. Absorption spectra of [3]cumulenes typically feature a maximum absorption (λ_{max}) between 300-400 nm corresponding to a HOMO → LUMO transition, which shifts to lower energy when π-conjugating substituents like arenes are present. Furthermore, π-conjugation influences structural bond lengths. When delocalization of π-electron density into substituents is possible, elongated (reduction in bond order) of the terminal double bonds is observed.

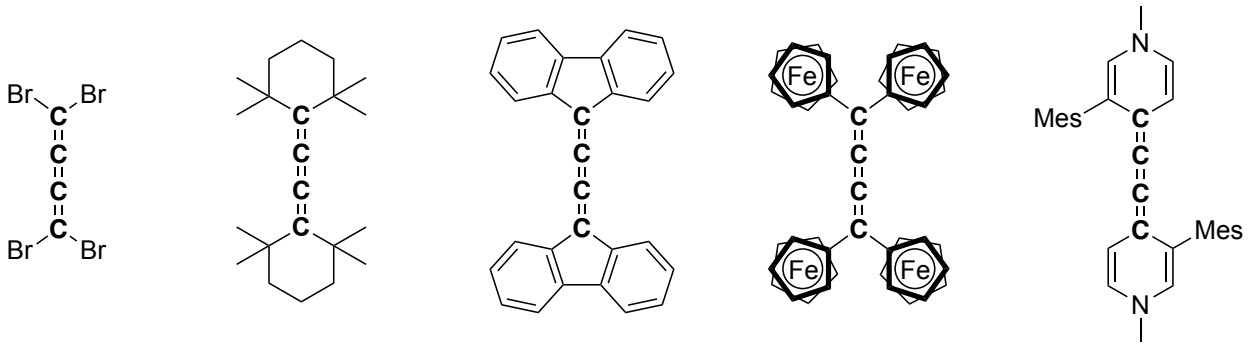

Scheme 2-4: Derivatives of [3]cumulenes.

The redox properties of [3]cumulenes are also tunable with substituent effects. Bertrand and Roesky independently showed that a [3]cumulene system **2-D** terminated with CAACs is also stable in electron-deficient states. Compound **2-D** can be oxidized by a single electron to a [3]cumulene radical cation [**2-D**]$^{\bullet+}$, or doubly oxidized to a [3]cumulene dication [**2-D**]$^{2+}$ (Scheme

2-5).[20,21] Lastly, terminal substitution of cumulenes has distinct impacts on reactivity pathways; however, this aspect will be discussed when appropriate in this thesis.

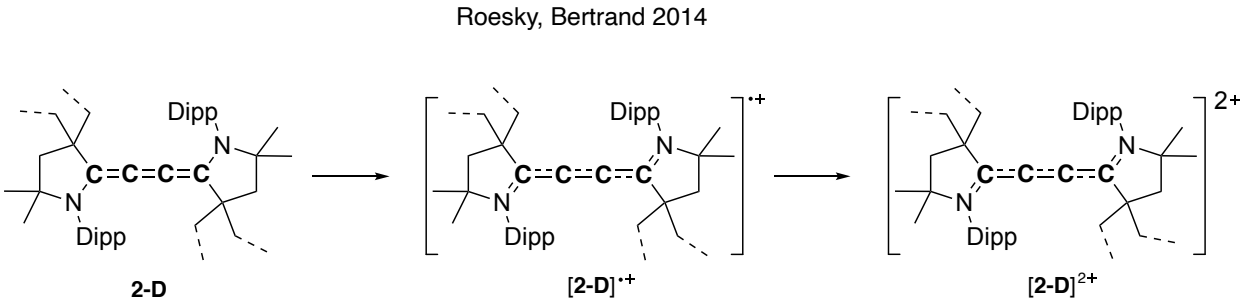

Scheme 2-5: CAAC-terminated [3]cumulene **2-D** and radical cation [**2-D**]$^{\bullet+}$ and dication [**2-D**]$^{2+}$.

2.1.3 Main-Group Cumulenes

Broadly speaking, the stabilization of p-block elements in low-coordination environments requires judicious substituent choice, where an appropriate balance of electronic and steric properties must be struck.[22,23] Innovations in substituent design coupled with the insight of the isolobal analogy, has allowed chemists to uncover p-block analogs of various classic carbon containing motifs. Among them, main group carbenes (R_2E:),[24] carbonyls (R_2E=O),[25] imines (R_2E=NR),[26,27] alkenes (R_2E=ER_2),[28,29] and alkynes (RE≡ER)[30] have been subject to intense investigation in recent decades. One area of development in synthesis pertains to the preparation of main group cumulenes; cumulene compounds featuring *sp* or sp^2 hybridized p-block atoms in lieu of carbon. Compared to a traditional carbon cumulene which features non-polar C–C bonds, the introduction of one or more p-block elements to a cumulene results in structures with polarized heteroatomic bonds. Moreover, the displacement of carbon with main-group elements can also introduce formal charges to cumulene systems. Thus, the polarity that arises in these systems often renders their π-bonds highly reactive towards (cyclo)addition reactions. From a fundamental perspective, main group cumulenes exhibit exceptionally unique electronic properties, which can be delineated through spectroscopic and computational studies. Cumulated motifs can also be strategically integrated into main-group systems as a design element, providing additional stability to highly reactive functional groups *via* delocalization. A representative set of main-group cumulenes will be discussed in this thesis, and are generally organized into three categories of compounds: i)

simple heterocumulenes, ii) analogs of [3]cumulenes, and iii) analogs of [4]cumulenes. Allenes (less commonly referred to as [2]cumulenes) will not be discussed.

2.1.4 Simple Heterocumulenes

Simple heterocumulenes are cumulene compounds comprised almost entirely of second row elements and are unique in the aspect that their isolation does not require stabilization through substituent effects. In 1873, Brodie encountered carbon suboxide (C_3O_2) by exposing carbon monoxide to electric current.[31] Diels and Wolf would later propose the connectivity of C_3O_2 to be O=C=C=C=O **2-E^a**, representing the first example of a heterocumulene and even pre-dating the discovery of carbon cumulenes by at least a decade (Scheme 2-6).[32,33] The cumulene bonding description for C_3O_2 was met with skepticism after Jensen showed experimentally that in the gas phase C_3O_2 exhibits a non-linear structure, bent about the central carbon atom by approximately 24° (∠C–C–C 156°),[34] findings that were subsequently corroborated *in silico*.[35] This would eventually lead to a revised bonding model, suggesting C_3O_2 to have the character of a carbone (OC→C←CO) where the central carbon atom is dicoordinate and has two sets of lone pairs **2-E^b**.[36] In 2000, Seppelt would provide crystallographic evidence showing a nearly linear structure for C_3O_2 in the solid state.[37] A third charge separated Lewis structure **2-E^c** would also be considered and investigated computationally by Frenking. [36]

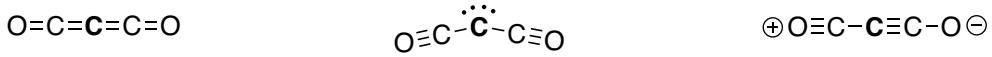

2-E^a **2-E^b** **2-E^c**

Scheme 2-6: Different Lewis structures for carbon suboxide C_3O_2.

Since the isolation of C_3O_2, several other isoelectronic 5-atomic heterocumulenes have been prepared, which includes the synthesis of carboisocyanate cation $[OCNCO]^+$ [**2-F**]$^+$,[38] and anions cyanoketenate $[NCCCO]^-$ [**2-G**]$^-$,[39,40] cyanothioketenyl $[NCCCS]^-$ [**2-H**]$^-$,[41] and cyanodiazomethanide $[NCCNN]^-$ [**2-I**]$^-$ (Scheme 2-7). Like C_3O_2, their bonding description as cumulene species are subject to debate considering [**2-F**]$^+$ and [**2-I**]$^-$ are considerably bent in the solid state. [**2-G**]$^-$ can adopt a linear or bent structure depending on the nature of the counter cation. Interestingly, for the analogs cyano-derived series of valence-isoelectronic anions ([**2-G**]$^-$, [**2-H**]$^-$

and [**2-I**]$^-$) Gessner and Frenking suggest that a dative bonding model [NC→C←L]$^-$ best describes these compounds, and can be used to rationalize trends in their linearity. [41] When considering N_2, CO, and CS as ligands (L) bound to the central carbon, they can be ranked by their π-acceptor character as follows N_2<CO<CS. Computations produce a structure for the free anion [NCCCS]$^-$ [**2-H**]$^-$which is linear, while simulated structures for [NCCCO]$^-$ [**2-G**]$^-$and [NCCNN]$^-$ [**2-I**]$^-$ are more bent (carbone like) as π-acceptor strength of the ligand diminishes. Taken together, the use of π-accepting groups should be considered when targeting a cumulene species. While [**2-G**]$^-$ is stable indefinity, [**2-F**]$^+$, [**2-I**]$^-$, and [**2-H**]$^-$ are all metastable species that degrade by dimer- or oligomerization. Nonetheless, their isolation is remarkable and the (meta)stability of these compounds could be attributed to a combination of resonance and electrostatic repulsion. Electrostatic repulsion is thought to be a deterrent towards oligomerization reactions in other p-block unsaturated anions. [42]

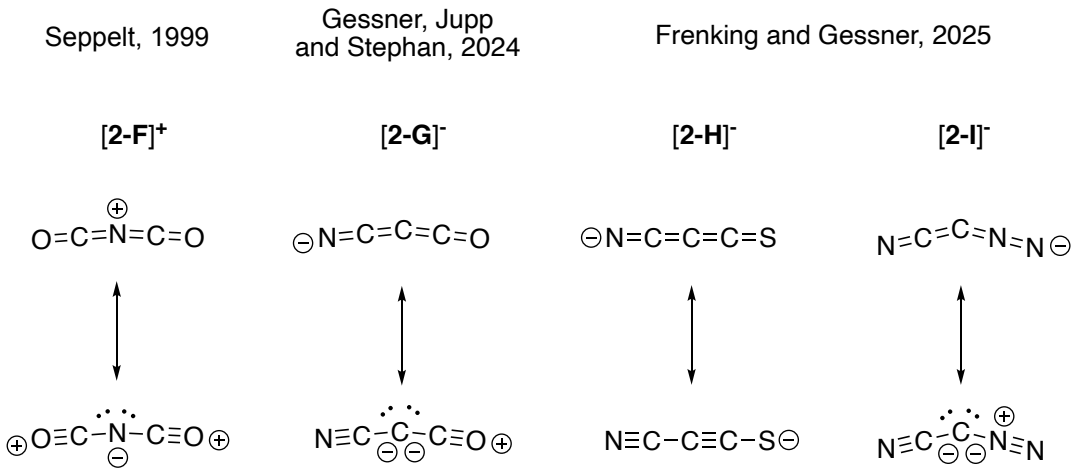

Scheme 2-7: Various heterocumulenes with cumulene and carbone-like canonical forms.

2.1.5 Main Group Analogs of [3]Cumulenes

Birum and Matthews' investigations into phosphacumulenes $R_3P{=}C{=}C{=}E$ (E = O, S, NR)[43,44,45] **2-J** can be considered the earliest aspiration towards p-block inspired [3]cumulenes. Contrary to their nomenclature, phosphacumulenes vaguely resemble the electronic structure of [3]cumulenes and are best represented by a Lewis structure which illustrates ylidic character ($P^{\delta+}$– $C^{\delta-}$) **2-J^b**. (Scheme 2-8).

Birum and Matthews, 1966

2-J[a] **2-J[b]**

Scheme 2-8: Phosphacumulene Lewis structure representations **2-J[a]** and **2-J[b]**.

The ylidic form of **2-J** rationalizes the considerably bent structure of phosphacumulenes. The P center is disconnected from the π-system of the cumulated component, though there is some partial double bond character between C1 and P due to C:→P donation into the P-Ph σ* orbitals, and as well as Coloumbic interactions between the charged $P^{(+)}$ and $C^{(-)}$ centers.[46,47] In 1977, Bestmann reviewed the chemistry of phosphacumulenes, showcasing them as ylide reagents in Wittig type transformations. [48] The author also highlighted that these species are reaction partners towards [2+2], [2+3], and [2+4] cycloaddition reactions, combining with electron deficient unsaturated substrates about the C1–C2 π-bond. Ironically, Bestmann's group showed that a variation of phosphacumulenes that have the formula $R_3P{=}C{=}C{=}CR_2$ **2-K,** can be employed as ylides to synthesize carbon [3]cumulenes *via* transfer of the $C{=}C{=}CR_2$ unit, which is particularly useful for preparing asymmetric cumulene compounds (Scheme 2-9).[49]

Bestmann, 1970

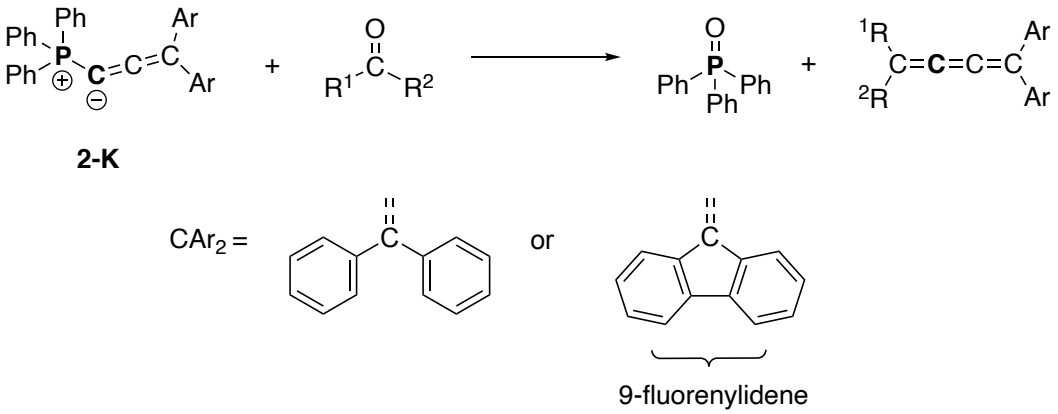

2-K

Scheme 2-9: Asymmetric cumulene synthesis with ylides **2-K**.

Since their discovery 60 years ago, phosphacumulenes have seen greater adoption in organic synthesis, with "Bestmann's ylide" $Ph_3P{=}C{=}C{=}O$ now being a commercially available reagent.[48,50,51] Although outside the scope of this thesis due to being poor representations of true cumulene systems, other phosphacumulene species have seen enormous development in recent years, with some recommended contributions coming from the groups of Gessner,[52] Hansmann, [53] and Liu.[54,55] (Scheme 2-10).

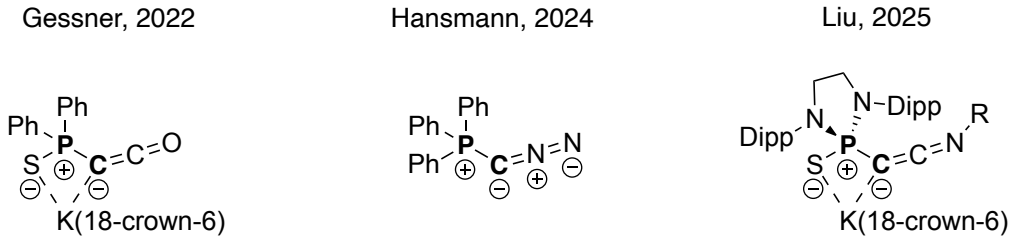

Scheme 2-10: Additional phosphacumulene ylides.

More closely resembling the electronic structure of [3]cumulenes, Nöth prepared boryl-amino-acetylenes ($R_2N{-}C{\equiv}C{-}BR_2$) **2-L**, which were anticipated to have cumulenic character on account of push-pull (N:→B) interactions [56] (Scheme 2-11). Unfortunately, the exact structure of these compounds could not be delineated crystallographically by the authors. Yamashita and colleagues would later report a derivative compound $(Et_2)_2N{-}C{\equiv}C{-}BMes_2$ **2-M**, where boron would be supported by kinetically stabilizing mesityl substituents.[57] Compound **2-M** was found to feature a trigonal planar boron atom (sum of bond angles 360°), and a nearly planar nitrogen atom (sum of bond angles 357°), while also adopting mutually co-planar terminal substituents. N–C and B–C bond distances for **2-M** lie between reported single and double bond distances for each respective bond unit, while the C–C distance is between reported $C_{sp}{-}C_{sp}$ double and triple bonds. Computational support for **2-M** would also indicate partial double bond character for N–C and B–C and partial triple bond character for C–C, delineating a structural description of **2-M** which is somewhere between two canonical forms, an alkyne **2-M^a** and butatriene **2-M^b**. Collectively, these reports illustrate one viable strategy towards preparing main-group cumulene analogs, which is to exploit isoelectronic relationships between smaller unsaturated bonding units and apply them

to extended π-systems. In their specific case, **2-L** and **2-M** can be viewed as foundationally predicated on the isoelectronic relationship between B=N and C=C bonding units.[58]

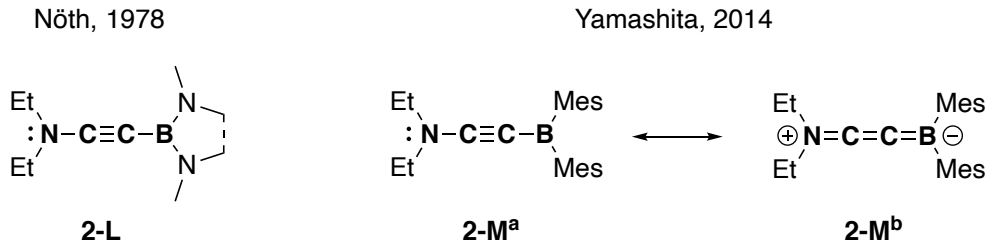

Scheme 2-11: Boryl-amino-acetylenes **2-L** and **2-M**.

Subsequently, the Yamashita group attempted to expand the scope of boryl-amino-acetylene species, investigating derivatives with diminished steric demand at boron.[59] Interestingly, *in situ* generation of either $Et_2N–C{\equiv}C–BR_2$ **2-N(a)** (BR_2 = 9-borabicyclononyl) **2-N(b)** (BR_2 = BPh_2) gave mixtures of the target compounds and [2+2] cyclodimerization products **3-N**$_2$ (Scheme 2-12). Dimerization occurs across the B–C bond and is reminiscent of the photodimerization of tetraphenylbutatriene **2-C**→(**2-C**)$_2$ except **2-N**→(**2-N**)$_2$ is thermally driven and reversible. DFT analysis suggested that the dimerization process **2-N**→(**2-N**)$_2$ for both derivatives (**2-N(a)** and **2-N(b)**) is nearly thermoneutral and highlights a key difference between all carbon and heteroatomic cumulenes. Given the $B^{\delta+}$– $C^{\delta-}$ bond polarization of **2-N,** dimerization is proposed to initially occur by nucleophilic attack of a carbon atom of one molecule of **2-N** to the boron atom of another molecule of **2-N**. The cyclization of **2-N**→(**2-N**)$_2$ thus occurs in two consecutive C–B bond forming events, allowing for a [2+2] cycloaddition to occur thermally, circumventing a concerted [2+2] cycloaddition, which would be a symmetry forbidden process.

Yamashita, 2017

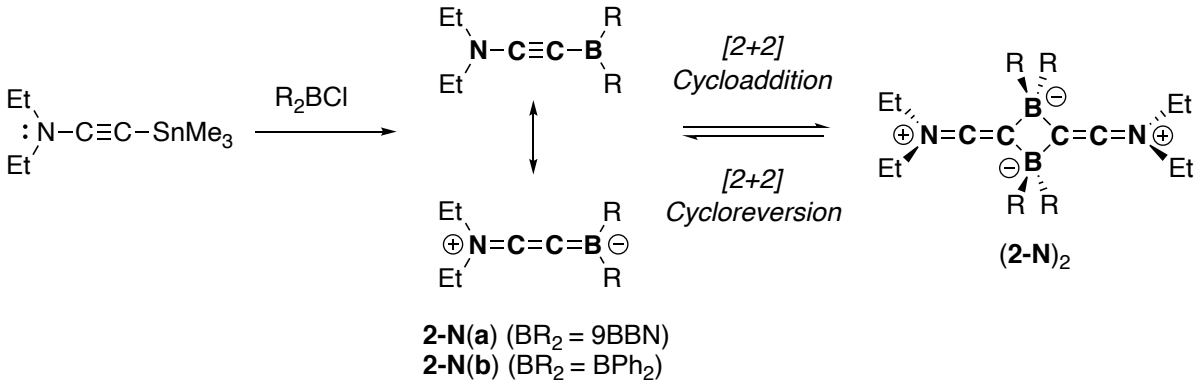

2-N(**a**) (BR_2 = 9BBN)
2-N(**b**) (BR_2 = BPh_2)

Scheme 2-12: Cyclodimerization of **2-N**→(**2-N**)$_2$.

Braunschweig and co-workers have also made considerable progress in main-group cumulene synthesis. In 2014, the group prepared R–B≡B–R **2-O**, an isoelectronic diboron analog of an alkyne R–C≡C–R that is stabilized by two bulky NHC substituents (Scheme 2-13).[60] Remarkably, by instead approaching the synthesis of diboryne with CAAC substituents, the structure of the resulting diboryne **2-P** more closely approaches that of a cumulene.[61] The strong π-accepting properties of CAACs [62] give **2-P** an extensively delocalized π-system, with multiple-bond character across the C–B–B–C framework. Fascinatingly, diboracumulene **2-P** only possesses 4 electrons in its π system, making it valence isoelectronic to the aforementioned [3]cumulene dication $[(CAAC)_2C_2]^{2+}$ [**2-D**]$^{2+}$.[20,21] Braunschweig's work would show that π-accepting motifs like CAACs can be strategically leveraged to approach cumulenic main group species.

Braunschweig, 2012

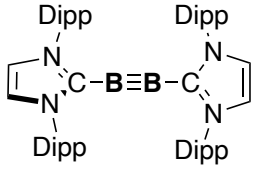

2-O

Braunschweig, 2014

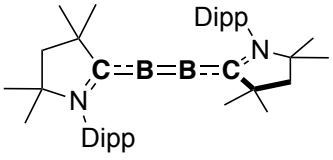

2-P

Scheme 2-13: Diboryne **2-O** and diboracumulene **2-P.**

The same group would later report the first neutral boryne R^1–B≡C–R (CAAC^{Me})–B≡C=(–(SiMe$_3$)(Mes*) (Mes* = 2,4,6-tri-tert-butylphenyl) **2-Q** (Scheme 2-14).[63] Despite its categorization as a main-group alkyne, crystallographic parameters of **2-Q** reveal many similarities to [3]cumulenes, including a mostly linear structure and mutually co-planar terminal substituents. DFT analysis suggests that **2-Q** has considerably multiple bond character across the C–B–C–N unit, with the terminal C–B and C–N bonds having double bond character, while the central B–C approaches triple bond character. UV-vis spectroscopy revealed electronic similarities to [3]cumulenes, with **2-Q** showing a λ_{max} at 418 nm, corresponding to a π→π* transition. Overall, **2-Q** can be viewed as partially between boryne **2-Q^a** and cumulene **2-Q^b** canonical forms, with its stability not only attributed to the use of bulky groups, but also on account of extensive delocalization of the B≡C π-system with the terminal amine and CAAC substituents.

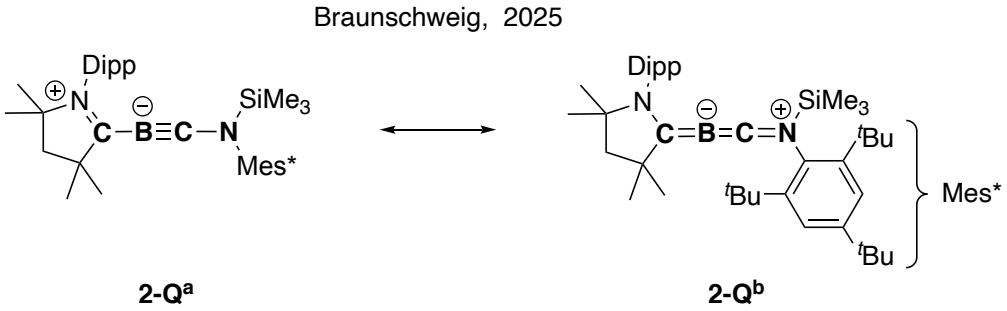

Scheme 2-14: Boryne **2-Q^a** and its cumulene canonical form **2-Q^b**.

2.1.6 Main Group Analogs of [4]Cumulenes

Tremendous progress in the development of carbene chemistry (R_2C:) has generated interest in related carbon species like carbene radical cations $(R_2C)^{\bullet+}$ and dications $(R_2C)^{2+}$.[64] In 2023, Loh and Bertrand reported the isolation of the first carbene dication [**2-R**]$^{2+}$, a breakthrough achievement considering that such a species is presumed to be very electrophilic.[65] To subdue its reactivity, electron-rich CAAC-derived imine substituents were employed. Fascinatingly, in the solid state, [**2-R**]$^{2+}$ adopts the structure of a [4]cumulene (R_2C=N=C=N=CR_2), albeit with an unusual zigzag distortion (Scheme 2-15). [**2-R**]$^{2+}$ can be represented by several canonical forms, although crystallographic and computation data suggests that the carbon and nitrogen containing

cumulene [**2-R^{d}**]$^{2+}$ is the most accurate bonding description. Like boryne **2-Q**, [**2-R**]$^{2+}$ is another highly reactive main-group species that is tamed by being embedded within a cumulenic system.

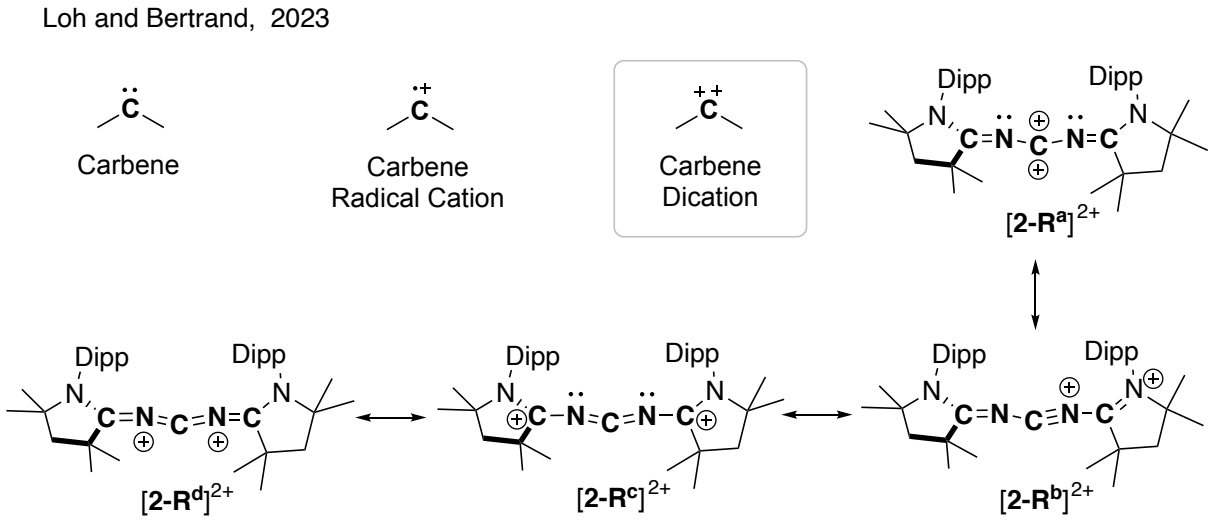

Scheme 2-15: Doubly oxidized carbene and it's canonical forms, including cumulene [**2-R^{d}**]$^{2+}$.

In 2024, Goicoechea and Aldridge reported the synthesis of the first cumulene entirely composed of inorganic elements (Scheme 2-16). [66] The two anionic [4]cumulene analogs [**2-T**]$^{-}$ and [**2-U**]$^{-}$ replace every sequential C=C bonding unit with an isoelectronic B=N unit, resulting in compounds with B–N–B–N–B chains. [**2-T**]$^{-}$ was isolated as a potassium salt [K][**2-T**] and with the cationic component sequestered [K(18-crown-6)][**2-T**]. Interestingly, irrespective of the cation, [**2-T**] has a considerable trans-bent geometry. Such bent geometries have been computationally predicted for even cumulenes systems terminated with weakly π-accepting substituents like NHCs.[10,11] The authors found that the addition of the electrophilic borane $B(C_6F_5)_3$ to [K][**2-T**] gave a new salt, where the anionic component [**2-U**]$^{-}$ is a completely linear cumulene system. Linearity is attributed to complexation of borane to the terminal boryl heterocycles of the cumulene, enhancing their π acceptor properties.

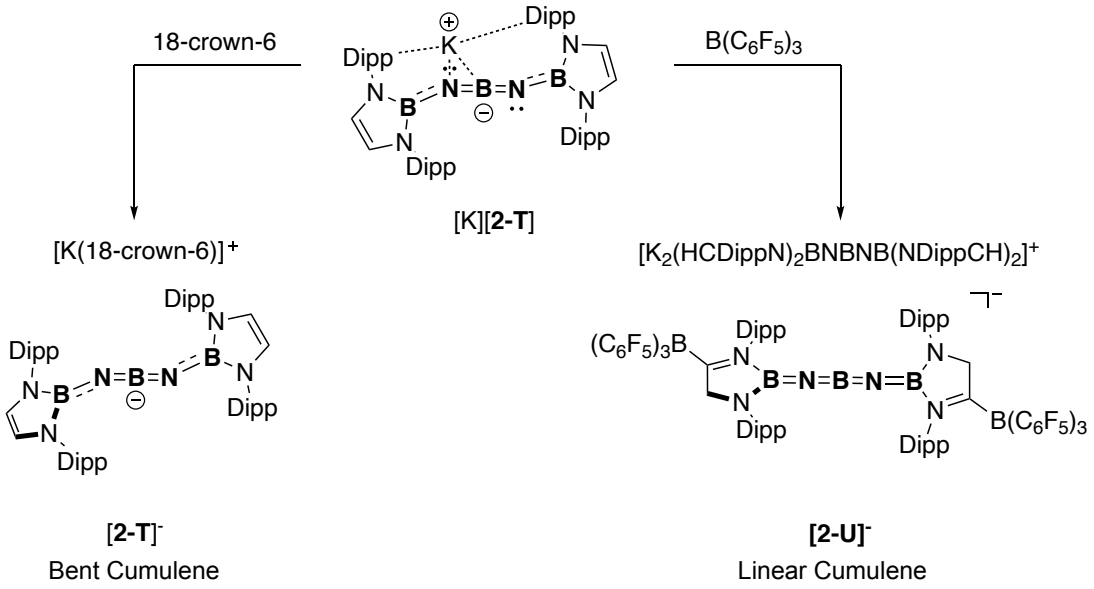

Scheme 2-16: Inorganic cumulenes [**2-T**]$^-$ and [**2-U**]$^-$.

On account of the intrinsic polarity of B–N bonds within the B–N–B–N–B chain, [K][**2-T**] was found to facilitate a range of reactions.[67] Heteroallenes like CO_2, CS_2, R–P–CO (R = $(H_2CDippN)_2P$) combine with [K][**2-T**] by reacting along one of the internal N–B bonds, providing synthetic access to new inorganic chains *via* π-bond metathesis of a borylimide group (Scheme 2-17). The composition of the by-products formed in these reactions was unclear but suggested by the authors to be cyclic potassium metaborate aggregates $[KBO_2]_3$, at least in cases where [K][**2-T**] combines with oxygenated heteroallenes.

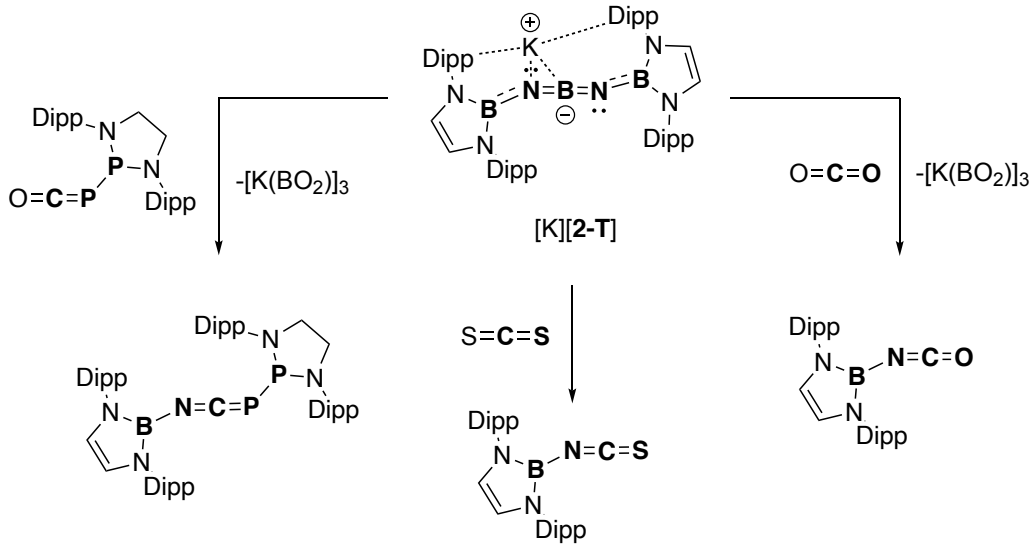

Scheme 2-17: Borylimide transfer from [K][**2-T**] to heteroallenes.

2.1.7 Metallocumulenes and the Allenylidene Carbene

Metallocumulenes, as the name suggest, are cumulene compounds which are associated with metal centers. Most commonly they take the form of a carbon cumulene where one terminal sp^2 C atom is replaced with a metal complex, giving the bonding description $[L_xM=C=(C)_y=CR_2]^n$ (y = repeating C units, n = charge).[68,69] Metallocumulenes have been prepared up to 8-atomic systems (y =5), but by far the most common are 4-atom species $[L_xM=C=C=CR_2]^n$, colloquially known as allenylidenes complexes (Scheme 2-18). The term allenylidene refers to the unsaturated carbene species $:C=C=CR_2$, which like vinylidene $:C=CR_2$ and methylene $:CR_2$ carbenes, are more stable in coordination complexes. In addition to the cumulated canonical form $[L_xM=C=C=CR_2]^n$, allenylidenes are often represented with charge-separated Lewis structures to rationalize their reactivity patterns. Free allenylidenes $:C=C=CR_2$ are unknown entities and thus the formation of most metal allenylidene complexes requires the cumulated unit be generated within the coordination sphere of a metal.[70] This was first shown in 1976 by independent reports from the groups of Fischer [71] and Berke [72] (debuted in the same issue of *Angewandte Chemie*). Fischer's synthesis to neutral group 6 allenylidenes occurs by Lewis acid-mediated EtOH elimination from chromium or tungsten amino-vinylcarbene complexes (Scheme 2-19).

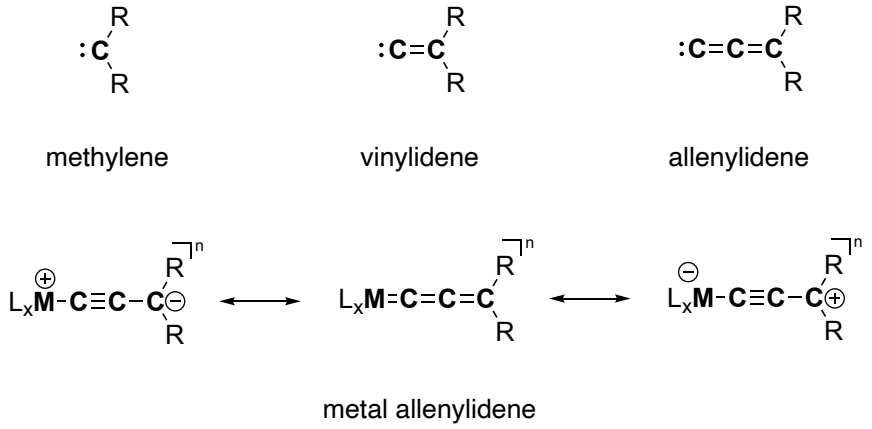

Scheme 2-18: General structures for methylene, vinylidene, and allenylidene carbenes, as well as metal allenylidene complexes.

Berke employed a η^2-methylpropiolate manganese precursor, which was transformed to the allenylidene complex by treatment with *t*BuLi and HCl. Selegue's group then introduced a method that cleverly utilizes commercial propyn-1-ols to produce ruthenium(II) acetylides, which affects the formation of allenylidene complexes upon dehydration.[73]

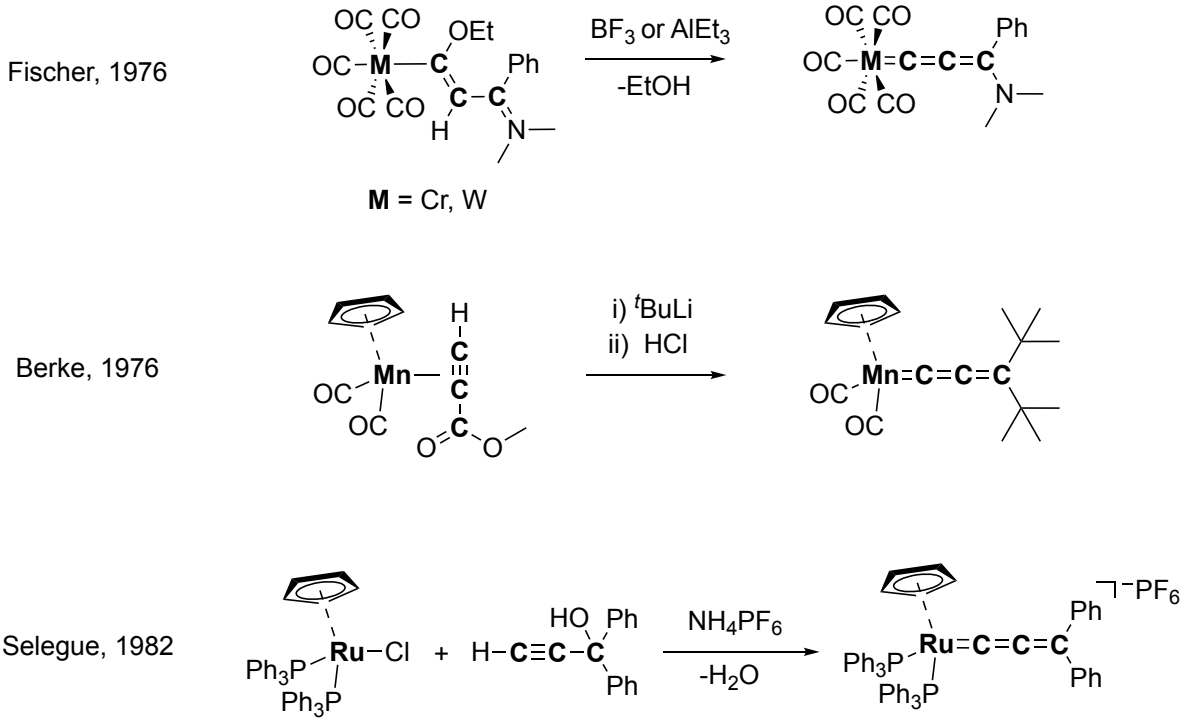

Scheme 2-19: Early methods for the synthesis of metal allenylidenes.

Following these seminal discoveries, allenylidene complexes have been synthesized for a range of transition metals, including group 4 (titanium and zirconium), 7 (manganese and rhenium), 8 (iron, ruthenium, and osmium), 9 (rhodium and iridium), and 10 (palladium), the chemistry of which has been reviewed by Bruce,[68] as well as Cadierno and Gimeno.[69] More recently allenylidene complexes have been expanded to include group 11 (silver[70] and gold[74,75,76,77]) and f-block (uranium[78] and thorium[79]) species.

2.1.8 Reactivity of Metal Allenylidenes

The vast majority of described allenylidene complexes in literature are derived from mid-to-late transition metals. The reactivity of such complexes has been generalized in existing reviews and is understood as follows: the alpha and gamma carbon (C_α and C_γ) atoms of the allenylidene fragment exhibit electrophilic character, while the beta carbon (C_β) has nucleophilic character.[68,69,80] (Scheme 2-20) Accordingly, the addition of nucleophiles to metal allenylidenes generally occurs at either C_α or C_γ, with the regioselectivity of the reaction outcome dependant on the specific metal atom, ligand environment, steric and electronic properties of the allenylidene, and the nature of the nucleophile employed (hard vs soft). By comparison, electrophiles add to the C_β. Substrates containing heteroelement-hydrogen bonds (N–H, O–H) are known to react along one of the unsaturated bonds.

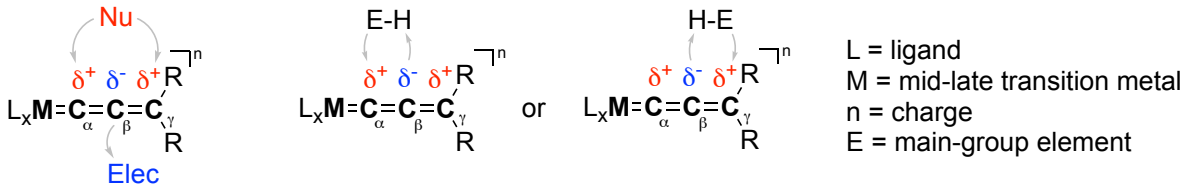

Scheme 2-20: General electronic structure and reactivity patterns of mid-late transition metal allenylidene complexes.

Intriguingly, the bond polarity that manifests along the cumulenic chain of allenylidenes renders them reactive towards cycloadditions, which can occur across either of the three unsaturated bonds ($M{=}C_\alpha$, $C_\alpha{=}C_\beta$, $C_\beta{=}C_\gamma$). [68,69,80] In this aspect, allenylidene complexes are platforms to construct structurally diverse scaffolds. Illustrative examples for the diversity of cycloaddition chemistry with metal-allenylidenes are described in Scheme 2-21. The neutral rhodium allenylidene **2-V**

prepared by Werner and co-workers reacts with terminal alkynes to form π-allyl complexes **2-W**, showcasing an initial [2+2] cycloaddition of the Rh=C_α bond and a C=C bond.[81] Diez et al. synthesized the cationic ruthenium allenylidene [**2-X**]$^+$ featuring a phosphine ligand with a pendant allyl group.[82] The allyl group was subsequently shown to undergo a [2+2] cycloaddition with the C_α=C_β allenylidene bond furnishing [**2-Y**]$^+$. Esteruelas demonstrated that the C_β=C_γ bond of allenylidenes can also engage in cycloaddition chemistry, with ruthenium allenylidene [**2-Z**]$^+$ shown to provide [**2-AA**]$^+$ by a Diels-Alder reaction with a butadiene. [83]

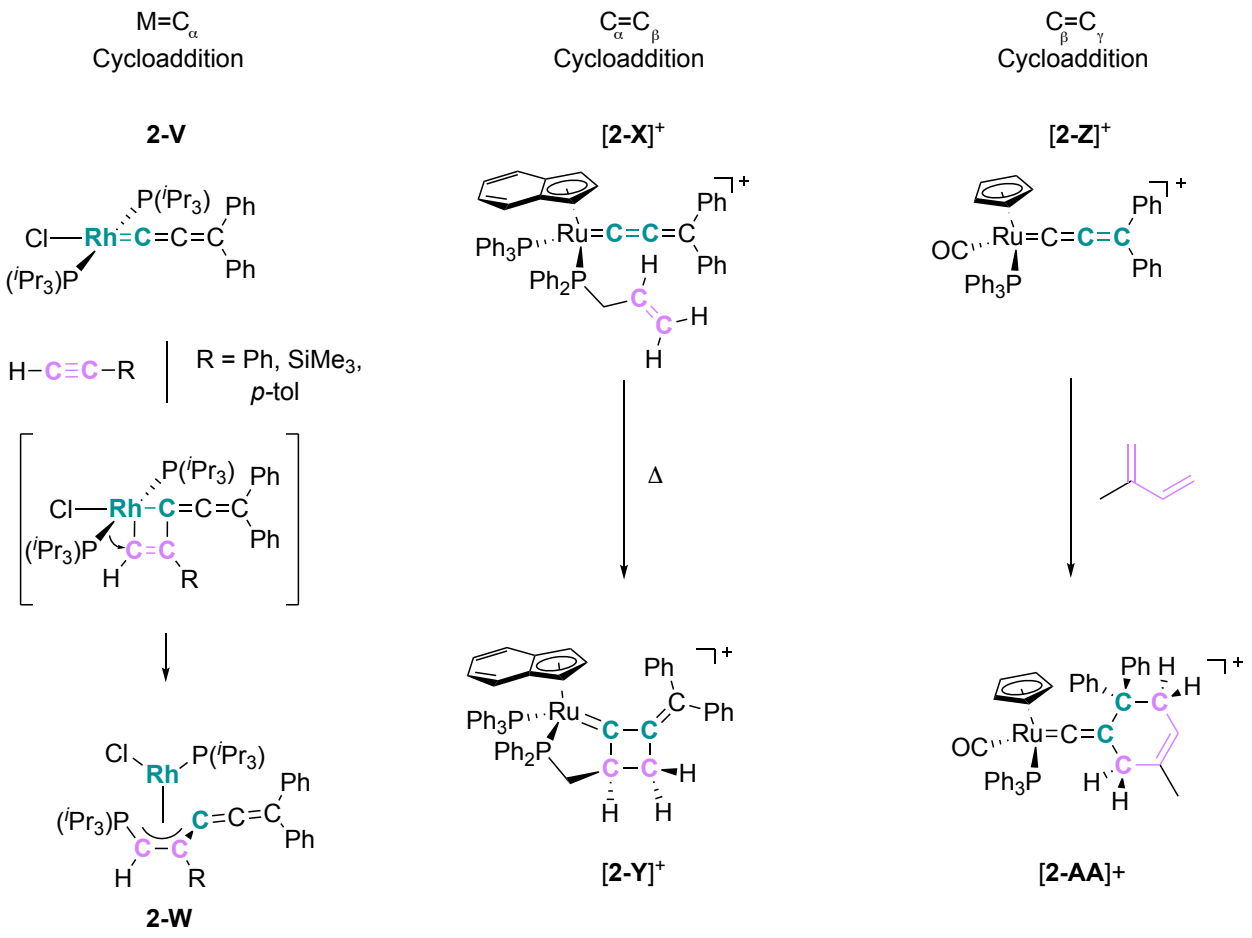

Scheme 2-21: Select examples of metal allenylidene complexes engaging in cycloaddition chemistry.

In recent decades, various synthetic methods have been developed around intercepting catalytically generated metal allenylidene intermediates.[69,80] Historically, the largest focus in this area is the functionalization of propargylic substrates through ruthenium catalysis. As shown previously in Scheme 2-19, propargylic alcohols and ruthenium chloride precursors readily form

Ru-allenylidenes under mild conditions.[73] Subsequently, carbon or heteroatom-centered nucleophiles can be coupled to electrophilic Ru-allenylidenes species, affording structurally modified alkynes (Scheme 2-22). [80,84,85] A breadth of nucleophiles have been investigated, and this general reaction principle has been applied to include intramolecular variants, as well as stereoselective transformations. Catalytic functionalization of propargylic substrates *via* the formation of Cu-allenylidene [86,87] and Au-allenylidene [88,89,90] intermediates are also burgeoning research areas but their discussion is beyond the scope of this thesis.

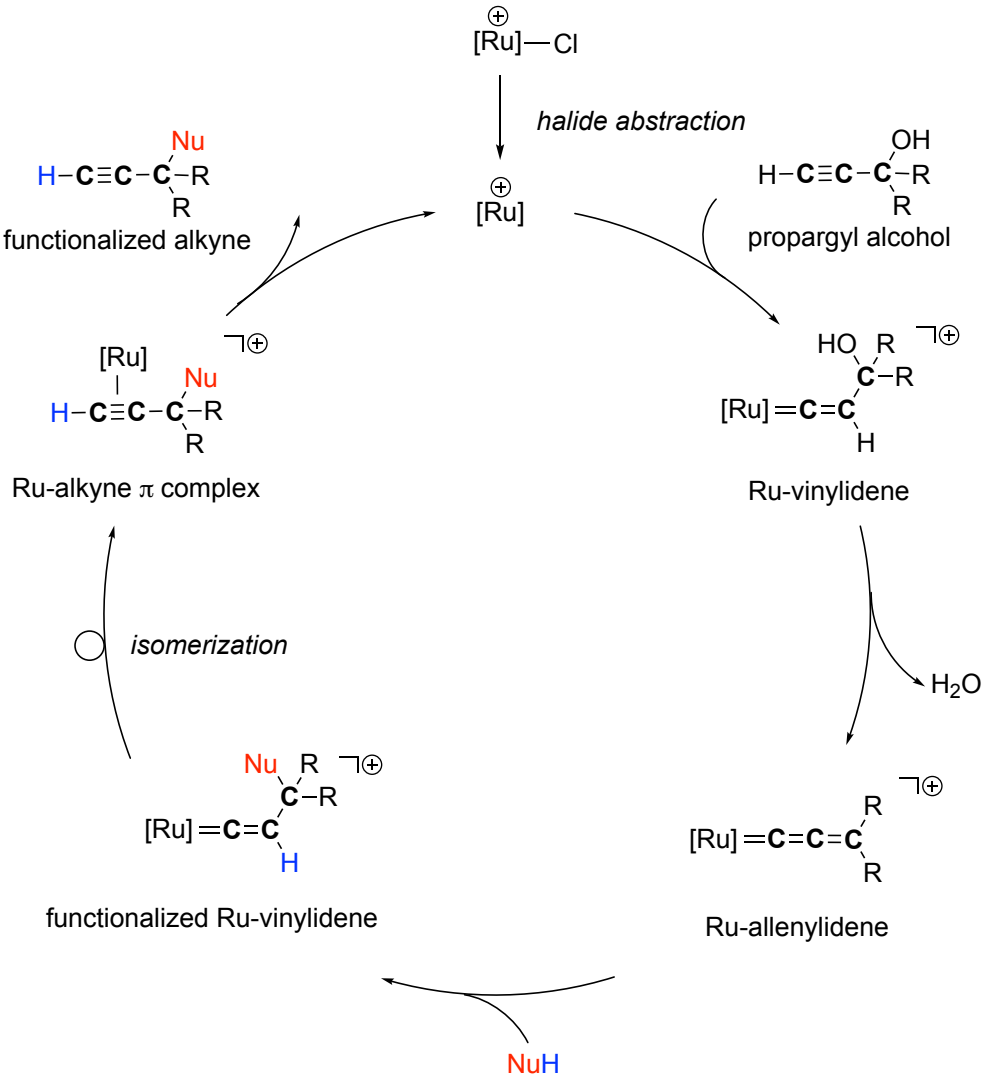

Scheme 2-22: Simplified mechanism for the catalytic functionalization of propargylic alcohols *via* a ruthenium-allenylidene intermediate.

2.2 Chapter Objectives: Finding a Synthetic Route to An Allenylidene Phosphonium Cation

With significant progress being made in the isolation of heterocumulene compounds, coupled with ongoing efforts to uncover parallels between the chemistries of phosphorus and carbon, our research aspired towards the synthesis of novel phosphorus containing cumulenes. Our primary synthetic target was allenylidene phosphonium $[R_2P{=}C{=}C{=}CR_2]^+$, conceived as an isoelectronic analog of [3]cumulene $[R_2C{=}C{=}C{=}CR_2]$ (Scheme 2-23). The structural and electronic comparison between allenylidene phosphonium and [3]cumulene is predicated on the established isolobal analogy between TPPCs $[R_2P{=}E]^+$ and unsaturated carbon compounds $(R_2C{=}E)$.[91,92,93] Importantly, unlike phosphacumulene ylides **2-J^b**, the coordinatively unsaturated P atom of $[R_2P{=}C{=}C{=}CR_2]^+$ would be electronically integrated into the cumulene π-system. If isolable, allenylidene phosphonium would be expected to behave as a strong electrophile like other TPPCs.[26,94] As a cumulene analog, such a species would be interesting to explore in cycloaddition chemistry. Lastly, while chemists have managed to prepare isoelectronic cumulene analogs based on various main group elements (mainly N and B), such compounds exclude heavy elements, thus an allenylidene phosphonium would be unique in this aspect. Since the isolobal substitution of phosphorus occurs in place of a terminal cumulene carbon atom, the proposed cation could draw some fundamentally interesting comparisons to metal allenylidene complexes.

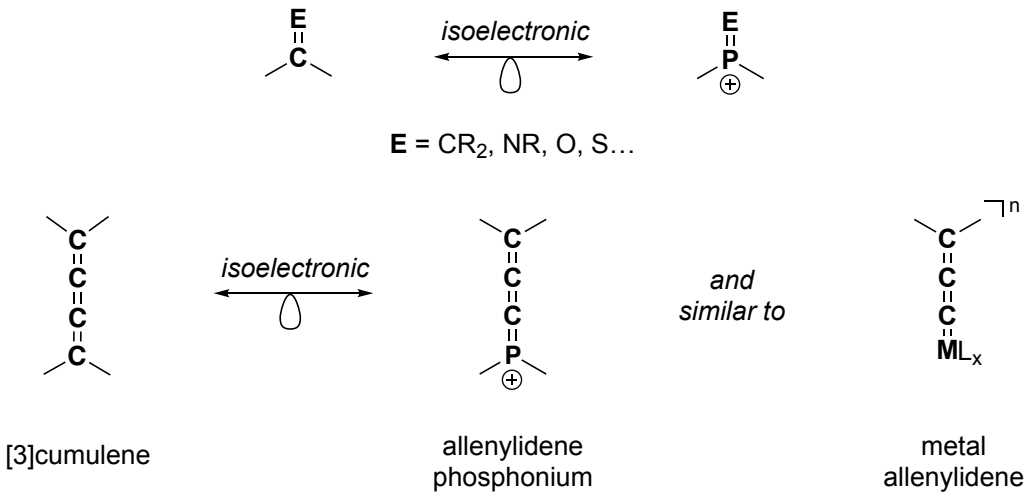

Scheme 2-23: (top) Isolobal and isoelectronic relationship between $R_2C{=}E$ compounds and TPPCs. (bottom) The analogy extrapolated to [3]cumulene and allenylidene phosphonium, with structural comparison to metal allenylidenes.

Paying direct homage to Brand's first cumulene **2-C**, we wanted to begin our investigations by attempting to prepare the tetraphenyl allenylidene phosphonium cation $[Ph_2P{=}C{=}C{=}CPh_2]^+$. Though the isolation of TPPCs without sterically demanding or π-electron donating substituents is virtually unprecedented, our rationale posited that charge dispersion through cumulenic delocalization, in conjunction with Coulombic repulsion, might provide sufficient stabilization for the target cation. To approach the synthesis of $[Ph_2P{=}C{=}C{=}CPh_2]^+$, we were inspired by work by Widenhoefer's group, who reported a novel synthesis of cationic (allenylidene)carbene gold complexes from acetylide precursors *via* a Lewis acid-mediated methoxide (CH_3O^-) abstraction strategy (Scheme 2-24).[76] The preparation of metal allenylidenes typically uses or generates protic acids or strong bases however, Widenhoefer's method obfuscates this by instead opting to employ a mild Lewis acid, (Me_3SiOTf). Conveniently, this protocol introduces a weakly coordinating anion (triflate) and produces an innocuous by-product (Me_3SiOMe). Thus, the method is appealing for the preparation of cationic allenylidene species that are expected to be electrophilic, oxophilic, moisture sensitive, and (or) prone to degradation by Brønsted acids and bases.[79] This led us to implore whether CH_3O^- abstraction of an alkynyl phosphine of the form $Ph_2P{-}C{\equiv}C{-}C(OCH_3)Ph_2$, could provide viable entry to allenylidene phosphonium.

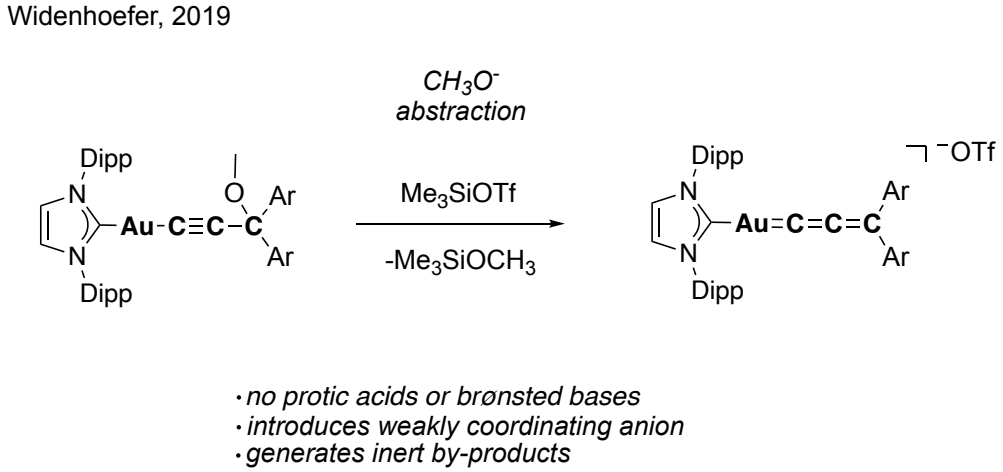

Scheme 2-24: Widenhoefer's Lewis acid mediated approach to cationic gold allenylidenes.

2.3 Results and Discussion

2.3.1 Synthesis of Alkynyl Phosphines

Inspired by Widenhoefer's approach, tetraphenyl alkynylphosphine **2-2[a]** was synthesized in moderate yield (60 %) by deprotonation of **2-1[Ph]** with *n*-BuLi, followed by subsequent treatment with chlorodiphenylphosphine ($ClPPh_2$) (Scheme 2-25). P–C bond formation was confirmed by ^{31}P NMR spectroscopy of **2-2[a]** which shows a resonance at δ = -34.0 ppm.

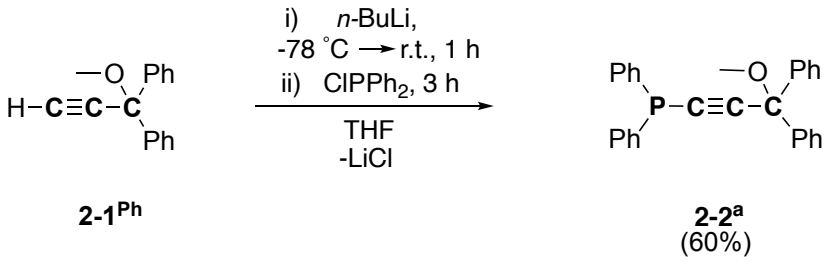

Scheme 2-25: Synthesis of tetraphenyl alkynylphosphine **2-2[a]**.

Compound **2-2[a]** can be handled briefly in atmospheric conditions and was crystalized in bulk by cooling a hot saturated ethanol solution. The solid-state structure was determined by a SCXRD study, which showed a minimally encumbered phosphorus atom in a pyramidalized geometry (sum bond angles around phosphorus ~ 303°) (Figure 2-1).

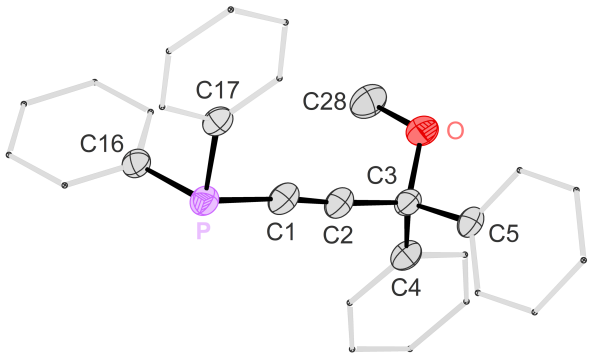

Figure 2-1: Solid-state structure of **2-2[a]**. Thermal ellipsoids are shown at 50% probability. For clarity, hydrogen atoms are omitted and the phenyl groups are shown in wireframe.

2.3.2 Lewis Acids for Methoxide Abstraction

With phosphine **2-2^{a}** in hand, CH_3O^- abstraction was pursued with various Lewis acids. Firstly, $[Ph_3C][B(C_6F_5)_4]$ gave the P:→C Lewis adduct $[\mathbf{2\text{-}2^{a}{\bullet}CPh_3}]^+$ paired with $[B(C_6F_5)_4]$ as the anion, as suggested by ^{11}B, ^{13}C, ^{19}F, and ^{31}P NMR spectroscopic methods (Scheme 2-26).[95] The formation of compound $[\mathbf{2\text{-}2^{a}{\bullet}CPh_3}]^+$ indicated an obstacle to overcome in our approach, which is that the basicity of the phosphorus lone pair can sequester the Lewis acid reagent.

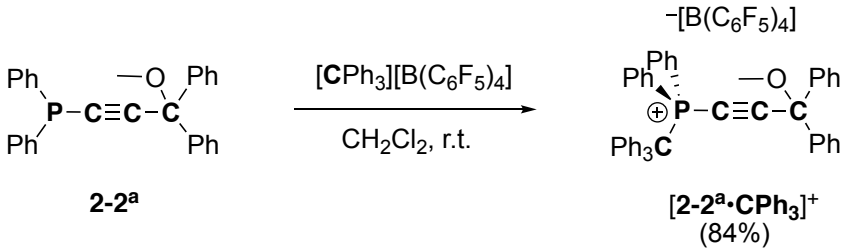

Scheme 2-26: Formation of Lewis adduct $[\mathbf{2\text{-}2^{a}{\bullet}CPh_3}][B(C_6F_5)_4]$.

To mitigate the generation of an acid-base adduct like $[\mathbf{2\text{-}2^{a}{\bullet}CPh_3}]^+$, we opted to employ more traditionally oxophilic Lewis acids. In this respect, the perfluorinated triaryl borane $B(C_6F_5)_3$, which is documented to facilitate heterolytic C–O bond scissions, was investigated.[96] Addition of $B(C_6F_5)_3$ to **2-2^{a}** initially lead to the formation of **2-2^{a}•B(C$_6$F$_5$)$_3$**, evidenced by *in situ* NMR spectroscopic experiments (Scheme 2-27). The formation **2-2^{a}•B(C$_6$F$_5$)$_3$** was supported by $^{31}P\{^1H\}$ NMR spectroscopy, which showed complete consumption of **2-2^{a}** and the formation of a major species in solution (*ca.* 94%), with a broadened singlet centered at δ = +3.7 ppm. The corresponding ^1H NMR spectrum retained many of the resonance features of **2-2^{a}**, including the diagnostic singlet corresponding to the methyl ether group. Heating a benzene solution of **2-2^{a}•B(C$_6$F$_5$)$_3$** to 60 °C resulted in quantitative conversion to a new product **2-3^{a}**, supported by the observation of a $^{31}P\{^1H\}$ NMR resonance at δ = 67.0 ppm, shifted to downfield frequencies relative to phosphine **2-2^{a}** (δ = -34.0 ppm). The corresponding ^1H NMR spectrum showed a doublet resonance at δ = 2.93 ppm ($^3J_{PH}$ = 11.4 Hz), which collapsed to a singlet upon ^{31}P decoupling. The $^{11}B\{^1H\}$ NMR spectrum showed a sharp signal which was observed at δ = −13.6 ppm, while the $^{19}F\{^1H\}$ NMR spectrum had a set of signals at δ = -129.6 ppm . -159.7 ppm, and -165.1 ppm. The $^{13}C\{^1H\}$ NMR spectrum showed a resonance at δ = 214 ppm, which is in the typical range for an *sp*-hybridized allenic carbon atom. Collectively, the data suggested the product to be a geminally substituted phosphonium-borato-allene **2-3^{a}**.

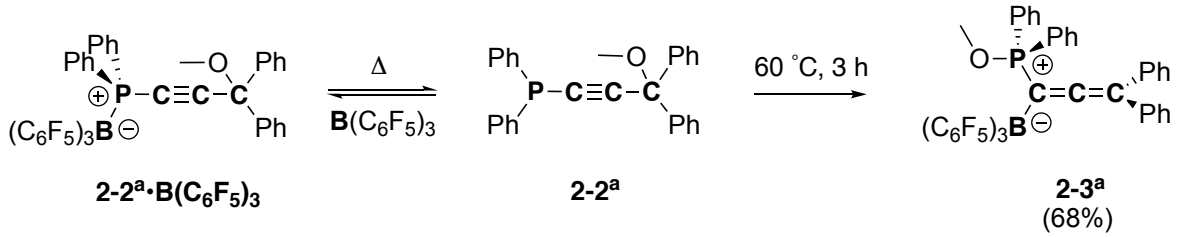

Scheme 2-27: Formation of Lewis adduct **2-2^{a}•B(C_6F_5)$_3$**, and the conversion of **2-2^{a}** to **2-3^{a}** at higher temperatures.

The prerequisite to heat a solution of **2-2^{a}•B(C_6F_5)$_3$** to facilitate this conversion suggested that **2-2^{a}•B(C_6F_5)$_3$** and its Lewis pair constituents (phosphine **2-2^{a}** and B(C_6F_5)$_3$) are in a temperature dependent equilibrium. At room temperature, conversion of **2-2^{a}** to **2-3^{a}** occurs, but on the timescale of weeks. Lastly, CH_3O^- abstraction was attempted with Me_3SiOTf, but was found to result in the formation of a cationic analog of allene **2-3^{a}**, where a neutral trimethylsilyl group is found in-place of the anionic borate center. The reaction was found to be poorly reproducible, therefore the isolation and characterization of this compound was not extensively pursued.

A SCXRD study provided unambiguous identification for allene **2-3^{a}** (Figure 2-2). The allene fragment of **2-3^{a}** is almost completely linear (C1–C2–C3 of 176.0 (2)°). The P–C1 bond distance of **2-3^{a}** is 1.780(2) Å, longer with respect to the P–C1 bond of **2-2^{a}** 1.762(2) Å. Elongation of the C1–C2 bond is observed upon zwitterion formation from 1.210(3) Å to 1.311(2) Å, in agreement with an overall decreased bond order from a triple bond (**2-2^{a}**) to a double bond (**2-3^{a}**). Contraction of the C2–C3 bond was observed from 1.476(3) Å in **2-2^{a}** to 1.317(2) Å in **2-3^{a}**. The bond angles around both terminal allene carbons (C1 and C3) are nearly trigonal planar (totalling 359.0(3)° and 360° respectively). The substituents around C1 and C3 are mutually orthogonal, consistent with an allene system. Lastly, both phosphorus and boron are in tetracoordinate bonding environments.

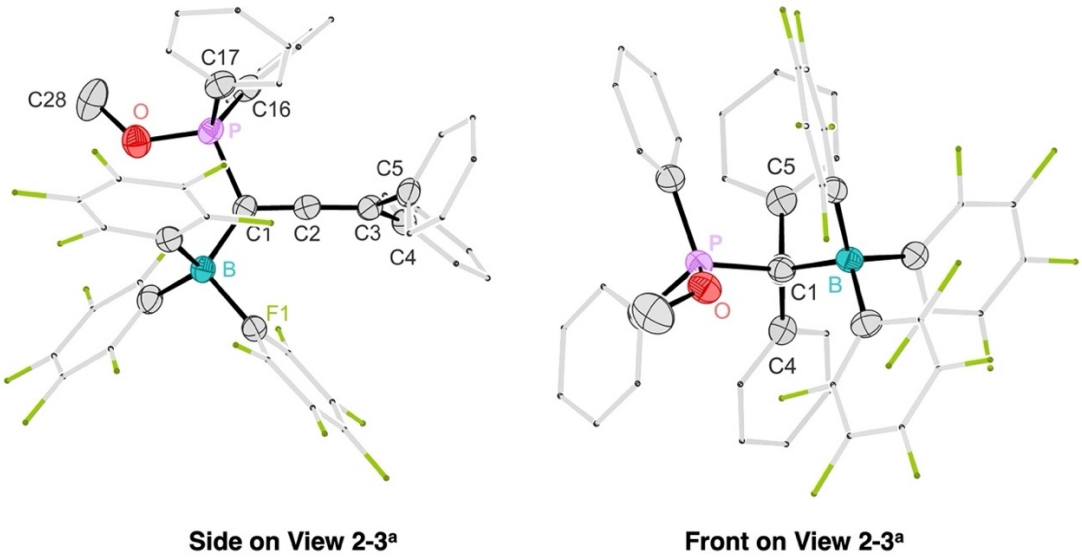

Figure 2-2: Side-on (left) and front-on (right) view of the solid-state structure of **2-3ª**. Thermal ellipsoids are shown at 50% probability. For clarity, hydrogen atoms are omitted, and the phenyl and perfluorophenyl groups are shown in wireframe.

2.3.3 Transient Allenylidene Phosphonium Cation

Concerning the formation of **2-3ª** from $B(C_6F_5)_3$ and phosphine **2-2ª**, the reaction was proposed to be initiated by CH_3O^- abstraction, initially generating an ion pair of the target allenylidene phosphonium cation $[Ph_2P{=}C{=}C{=}CPh_2]^+$ [**2-2ª'**]$^+$ and borate anion $[H_3CO{-}B(C_6F_5)_3]^-$ (Scheme 2-28). The presumed high electrophilicity of [**2-2ª'**]$^+$ is thought to result in recombination with its anionic component $[CH_3O{-}B(C_6F_5)_3]^-$ by transfer of the methoxide group. This results in the formation of a neutral phosphacumulene ylide **2-2ª''.** Ylide **2-2ª''** reacts with $B(C_6F_5)_3$ to give allene **2-3ª**. The composition of **2-3ª** resembles a P/B zwitterion previously reported by Krempner, prepared by combination of phosphoranylideneketene (Ph_3PCCO) and $B(C_6F_5)_3$.[97]

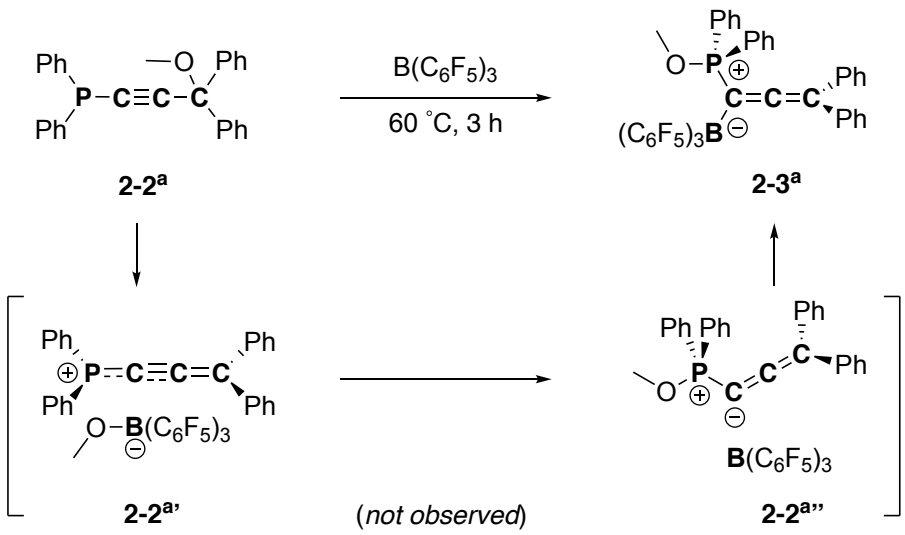

Scheme 2-28: Proposed formation of **2-3**[a], by generation of an allenylidene phosphonium **2-2**[a]**'** and phosphacumulene **2-2**[a]**''** ylide intermediate.

Quantum chemical calculations were performed at the BP86-D3/def2SVP level of theory in the gas phase to supplement the proposed reaction cascade (Scheme 2-29).[98,99,100] DFT showed that the formation of adduct **2-2**[a]**•B(C$_6$F$_5$)$_3$** (pathway A) is kinetically favored, and its formation is considerably more exergonic than methoxide abstraction (pathway B). Methoxide abstraction of **2-2**[a] by B(C$_6$F$_5$)$_3$ to the transient allenylidene phosphonium **I2** is very exergonic (ΔG = -13.59 kcal mol^{-1}) and highly exothermic (ΔH = -30.91 kcal mol^{-1}). From allenylidene phosphonium **I2**, P–O bond formation by CH_3O^- transfer from [CH$_3$O–B(C$_6$F$_5$)$_3$]$^-$ proceeds initially by a barrierless process to **I3**. From **I3**, the formation of phosphacumulene ylide **I4 and** regeneration of free B(C$_6$F$_5$)$_3$ is both endergonic (ΔG = +5.84 kcal mol^{-1}) and endothermic (ΔH = +7.44 kcal mol^{-1}). The last step of this process, sequestration of B(C$_6$F$_5$)$_3$ by ylide **I4 to afford 2-3**[a] is highly exergonic (ΔG = -38.14 kcal mol^{-1}). Overall, the formation of **2-3**[a] from **2-2**[a] and B(C$_6$F$_5$)$_3$ is very exergonic and exothermic (ΔG_{rxn} = -46.48 kcal mol^{-1} and ΔH_{rxn} = -65.12 kcal mol^{-1}). Nonetheless, heating is required to disrupt adduct **2-2**[a]**•B(C$_6$F$_5$)$_3$**, such that the reaction can proceed *via* pathway B. This hints at the possibility of leveraging steric encumbrance as a means of obfuscating the formation of Lewis adducts, either by employing bulkier phosphines (*vide infra*) or bulkier Lewis acids.

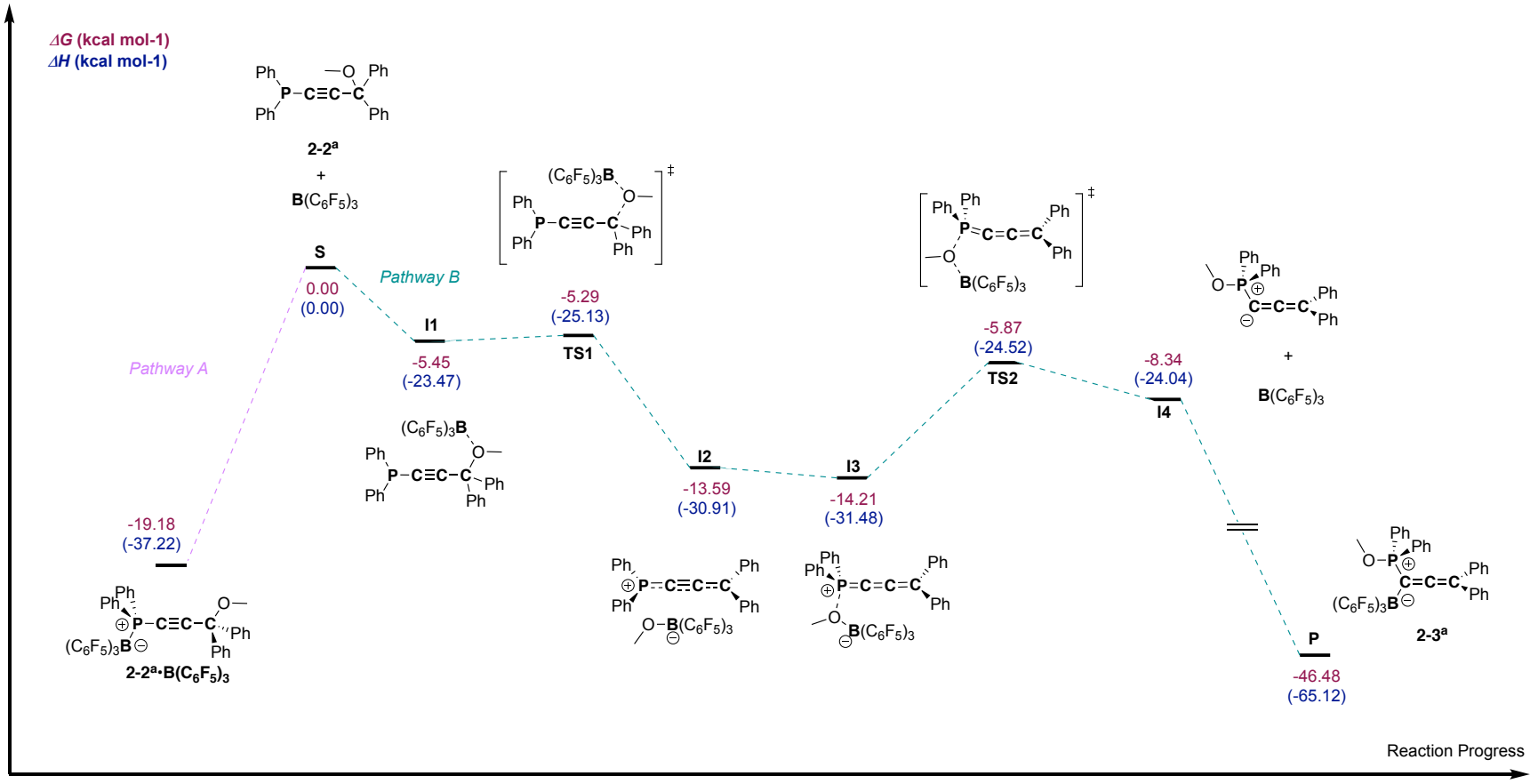

Scheme 2-29: Free energy profile of the reaction of $B(C_6F_5)_3$ with phosphine **2-2ª** at the BP86-D3/def2SVP level of theory, in the gas phase. Energies are reported relative to the starting materials. Free energies and enthalpies (in parentheses) are given in kcal mol^{-1}.

.

Ultimately, mechanistic insight from the transformation of **2-2ª** to **2-3ª** reveals two key deterrents in the way of isolating allenylidene phosphonium: 1) Phenyl substituents at phosphorus are clearly not suitable, unable to impart the necessary kinetic or thermodynamic stabilization to affect the target and 2) while $B(C_6F_5)_3$ performs methoxide abstraction as intended, the anion $[CH_3O–B(C_6F_5)_3]^-$ which is generated is not inert towards subsequent chemistries.

Despite not being isolable, the structural parameters of tetraphenyl allenylidene phosphonium ([**2-2ª'**]$^+$ **or I2**) were produced in the gas phase at the BP86-D3/def2SVP level of theory (Figure 2-3). The computed structure has a short P–C1 bond length (1.732 Å) compared to the experimentally observed bond length for phosphine **2-2ª** (1.762(2) Å). The C1–C2 bond length increases from 1.198(3) Å in **2-2ª** to 1.248 Å in **I2**, while a contraction in bond length is noted for C2–C3, from 1.481(3) Å in **2-2ª** to 1.388 Å in **I2**. Notably, when compared to the experimental parameters of previously reported methylene phosphonium cations $[R_2P{=}CR_2]^+$ (P–C bond lengths range from 1.62 Å –1.68Å), [101.102,103,104] the predicted P–C1 bond length is considerably longer. Moreover, while the terminal carbon center (C3) of **I2** is planarized, the P center is pyramidalized. FMO depictions of **I2** show that a significant contribution to the HOMO comes from an orbital at phosphorus with lone pair character, with minor contributions from π-bonding orbitals between P–C1 and C2–C3. In the LUMO depiction, a *p* orbital at C3 is prominent, with minor contributions at C1 and P likely reflecting π* antibonding combinations. Collectively, the structure of **I2** produced by theory is best described as a hybrid of two Lewis structure representations, an allenylidene phosphonium and a phosphanyl-alkynyl-carbenium (Scheme 2-30).

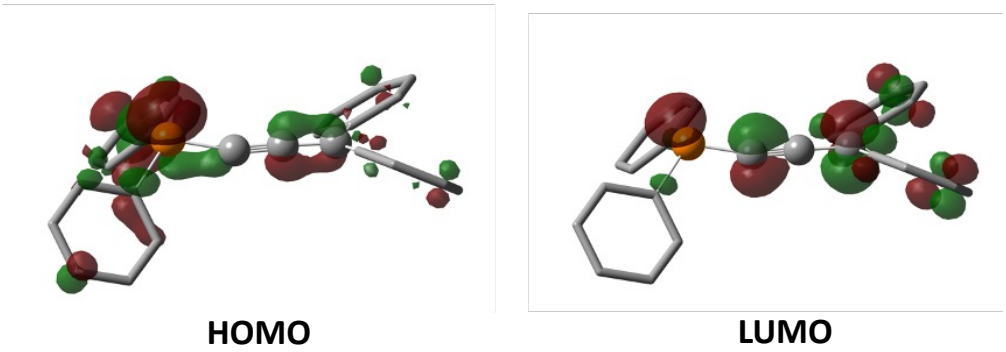

Figure 2-3: HOMO and LUMO depictions of tetraphenyl allenylidene phosphonium cation at the BP86-D3/def2SVP level of theory, in the gas phase.

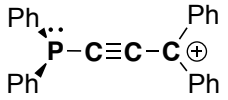

phosphanyl-alkynyl carbenium

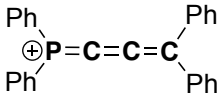

allenylidene phosphonium

Scheme 2-30: Two Lewis structures describing the target cation, phosphanyl-alkynyl carbenium and allenylidene phosphonium.

2.3.4 Attempts to Isolate Allenylidene Phosphonium with Kinetic Stabilization

We then turned our attention to the preparation of phosphines with increased steric bulk at phosphorus in efforts to improve the kinetic stability of the target cation. Phosphine derivatives $R_2P–C{\equiv}C–C(OCH_3)Ph_2$ **2-2^{b}** (R = Cy) and **2-2^{c}** (R = Mes) were prepared according to the same procedure used for **2-2^{a}**. The analogous allene **2-3^{b}** was prepared from **2-2^{b}** and $B(C_6F_5)_3$ in similar yield (Scheme 2-31). Notably, this reaction proceeded to completion at room temperature within 12 hours, in stark contrast to room temperature reactions of **2-2^{a}** and $B(C_6F_5)_3$ which took several weeks to reach full conversion. The observed difference in qualitative reaction rates could indicate an association between the steric accessibility of the phosphorus lone pair and the efficiency of the phosphine-to-allene rearrangement, with larger substituents (Cy > Ph) at phosphorus likely minimizing unwanted acid-base interactions. In agreement, Lewis adduct formation of di(cyclohexyl)alkynylphosphine **2-2^{b}** and $B(C_6F_5)_3$ could not even be observed by NMR spectroscopy. In contrast to **2-2^{a}** and **2-2^{b}**, the reaction between phosphine **2-2^{c}** and $B(C_6F_5)_3$ occurred with very poor selectivity. Addition of $B(C_6F_5)_3$ to **2-2^{c}** at room temperature immediately produced a dark green colored solution, which was discerned as a complex mixture by heteronuclear NMR spectroscopy. We then thought that performing the reaction in a hydrocarbon solvent like pentane or hexane would allow for the precipitation and subsequent characterization of any cationic intermediates produced in the reaction. Accordingly, the same reaction in pentane led to the instantaneous precipitation of a light green solid. Reconstitution in benzene-d_6 allowed for spectroscopic analysis and revealed the formation of a single new product, evidenced by a pair of doublets in the $^{31}P\ \{^{1}H\}$ NMR spectrum at δ = -5.4 and -18.7 ppm, sharing identical coupling constants ($^{1}J_{PP}$ = 211 Hz), and integrating in a ratio of 1 : 1. The large coupling constant and doublet splitting pattern indicated the formation of a new species with two chemically distinct phosphorus

environments connected through a single bond. A ^{11}B {^{1}H} NMR signal at δ = -1.7 ppm suggested the formation of the tetracoordinate borate counter anion $[H_3CO–B(C_6F_5)_3]^-$. Notable features of the ^{1}H NMR spectrum included two resonances for the $–OCH_3$ functionality, one singlet at δ = 2.75 ppm, and a second broad singlet at δ = 3.55 ppm, which integrate equally. Based on the above spectroscopic features, we assigned this product to be the phosphine-phosphonium cation [**2-4**]$^+$ (Scheme 2-31).

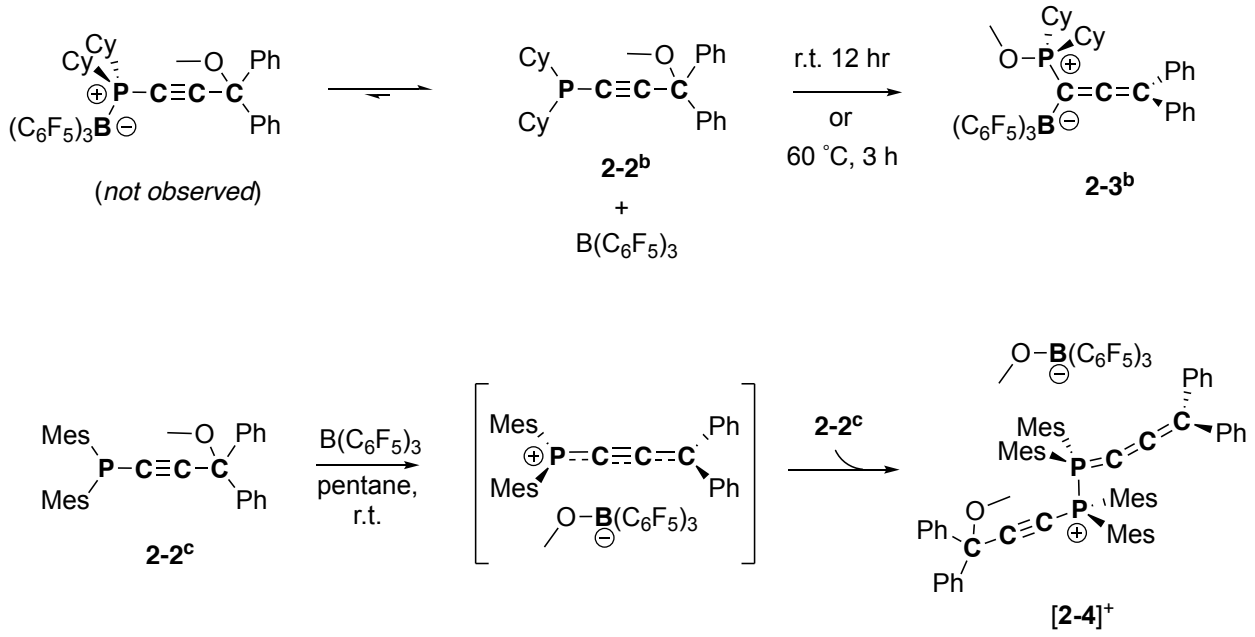

Scheme 2-31: (top) Formation of **2-3^b** from **2-2^b** and $B(C_6F_5)_3$. (bottom) Formation of phosphine-phosphonium salt [**2-4**]+ from phosphine **2-2^c** and $B(C_6F_5)_3$.

This assignment was further confirmed *via* detailed ^{13}C and two-dimensional NMR spectroscopic analysis, as well as mass spectrometry. Unfortunately [**2-4**]$^+$ was observed to decompose slowly in solution (~90–95% remaining after 2 days), which precluded its crystallization and thus an unambiguous identification with a SCXRD study. In the absence of solid-state data, DFT at BP86-D3/def2SVP level of theory was used to support the identification of [**2-4**]$^+$. Simulated ^{31}P NMR shifts for [**2-4**]$^+$ closely agree with the experimental data.[105] DFT also showed that the formation of [**2-4**]$^+$ from **2-2^c** and $B(C_6F_5)_3$ is favorable (ΔG_{rxn} = -17.52 kcal mol^{-1} and ΔH_{rxn} = -36.12 kcal mol^{-1}). Phosphine-phosphonium [**2-4**]$^+$ can be understood as a donor-acceptor complex of phosphine **2-2^c** and a transiently formed allenylidene phosphonium cation. The formation of [**2-4**]$^+$ provides experimental evidence for allenylidene phosphonium $[R_2P=C=C=CR_2]^+$ as an

intermediate in the conversion of alkynyl phosphines **2-2** to allenes **2-3**. Lastly, in an effort to halt the formation of dimeric species like [**2-4**]$^+$, we looked to further increase the steric demand at phosphorus and opted to employ *meta*-terphenyl (Ter) substituents. Ter substituents are particularly effective for isolating low coordinate main group systems because of their encapsulating "pocket-" or "umbrella-" like steric profile.[106] Such extreme sterics have been leveraged to access numerous neutral phosphorus-main group element double bond compounds, among them phosphatrielenes like phosphaborenes (RP=B-R),[107] phosphaalenes (RP=Al-R),[108] phosphagallenes (RP=Ga-R), and phosphaindenes (RP=In-R)[109], however they have yet to be successfully employed for the isolation of low coordinate phosphorus cations (Scheme 2-32). Beckmann previously attempted to produce phosphenium cations based on two permethylated Ter substituents [$^{C_6Me_6}Ter_2P]^+$ but found that these species isomerize by electrophilic activation of one of the flanking arene substituents.[110]

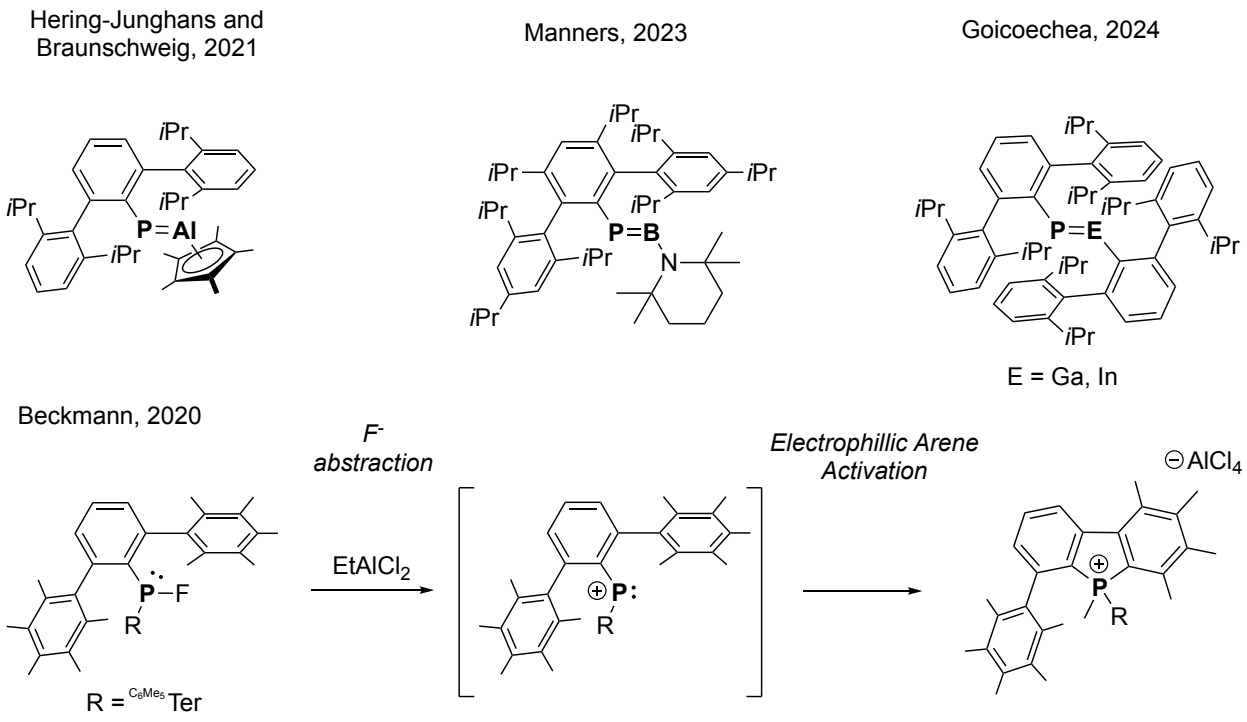

Scheme 2-32: (top) Selected terphenyl stabilized phosphorus multiple bond compounds. (bottom) Attempted phosphenium cation synthesis by Beckmann, and subsequent isomerization by electrophilic activation of an adjacent arene.

Nonetheless we prepared the parent $^{H}Ter_2PCl$, where each terphenyl substituent is unsubstituted. Unfortunately, in our hands, alkynyl phosphines could not be produced from $^{H}Ter_2PCl$. Alkynylation of $^{H}Ter_2PCl$ with lithium or magnesium acetylides of **2-1^{Ph}**, even under forcing conditions, was not observed. While the steric profile of the Ter class of substituents may be appealing for the isolation of allenylidene phosphonium, extreme encumbrance of the phosphorus atom in chlorophosphine $^{H}Ter_2PCl$ was ultimately a deterrent in the context of our synthetic approach.

2.3.5 Modification of the Carbon Terminus of Alkynyl Phosphines

The successful isolation of an allenylidene phosphonium cation clearly requires significant changes to the substituents bound to phosphorus. However, we still wanted to obtain some insights into what role the substituents at the carbon terminus play in facilitating the transformation of alkynyl phosphines **2-2** to their corresponding allenes **2-3**, and whether they would have any discernible influence on stabilizing the target cation.

To crudely probe this, an analogous series of phosphines $Ph_2P{-}C{\equiv}C{-}C(OCH_3)R_2$ was prepared, which included **2-2^{Fl}** (CR_2 = 9-fluorenylidene) **2-2^{Sub}** (CR_2 = 5-dibenzo-cyclohepteneylidene) and **2-2^{Me}** (R = methyl). **2-2^{Fl}** and **2-2^{Sub}** both retain the π-conjugating arene substituents of the parent phosphine **2-2**, but here we opted to fuse these groups together. For **2-2^{Me}**, substituents with π-conjugative influences were completely forgone. Perhaps unsurprisingly, **2-2^{Fl}** and **2-2^{Sub}** react with $B(C_6F_5)_3$ with the same selectivity as **2-2,** providing allenes **2-3^{Fl}** and **2-3^{Sub}**, respectively. **2-3^{Fl}** and **2-3^{Sub}** were characterized by heteronuclear NMR spectroscopy, mass spectrometry and SCXRD (Figure 2-4). By comparison, combining **2-2^{Me}** and $B(C_6F_5)_3$ exclusively produced a phosphine borane adduct, **2-2^{Me}•B(C_6F_5)$_3$**. A single crystal of **2-2^{Me}•B(C_6F_5)$_3$** was subject to an SCXRD study, and although the data was of poor quality, the connectivity of **2-2^{Me}•B(C_6F_5)$_3$** could be confirmed, providing irrefutable evidence that borane coordination at phosphorus is a competing process to methoxide abstraction (Scheme 2-33). Interestingly, heating **2-2^{Me}•B(C_6F_5)$_3$** for prolonged periods of time did not provide any evidence for conversion to an allene product. We can speculate that aryl groups may play a role in facilitating heterolytic bond cleavage of the methoxide group, presumably in stabilizing the formation of the carbenium center which is generated in the transition state.

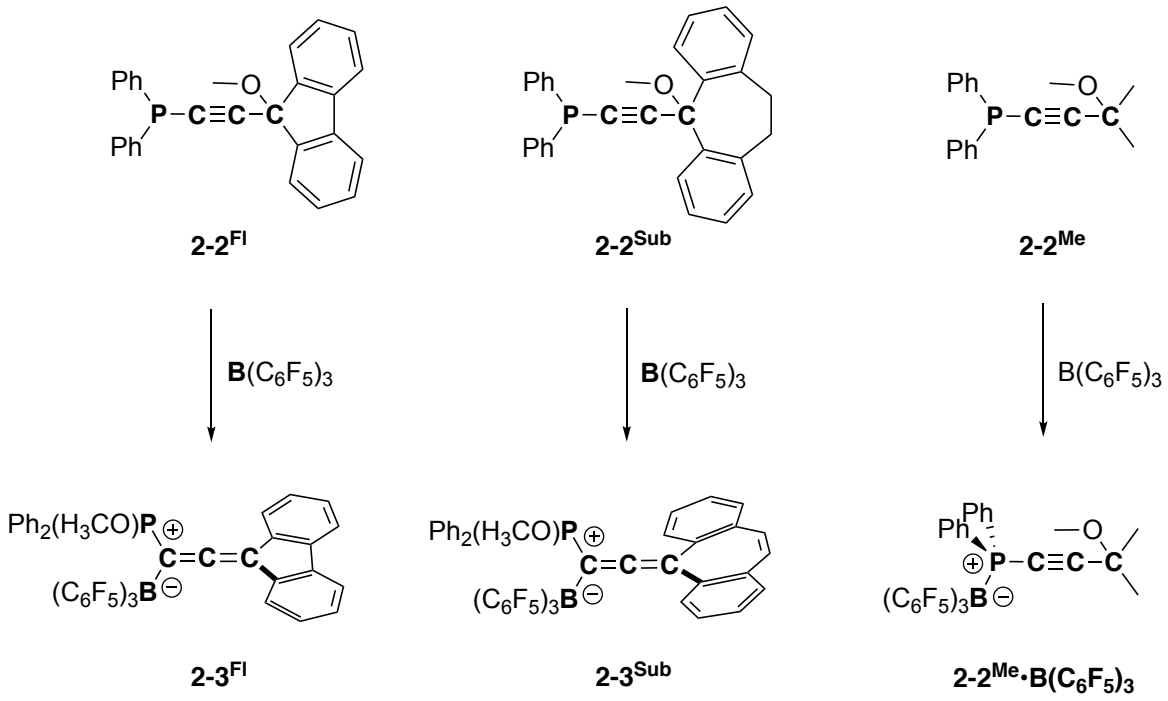

Scheme 2-33: Formation of **2-3^{Fl}**, **2-3^{Sub}** and **2-2^{Me}•B(C$_6$F$_5$)$_3$**.

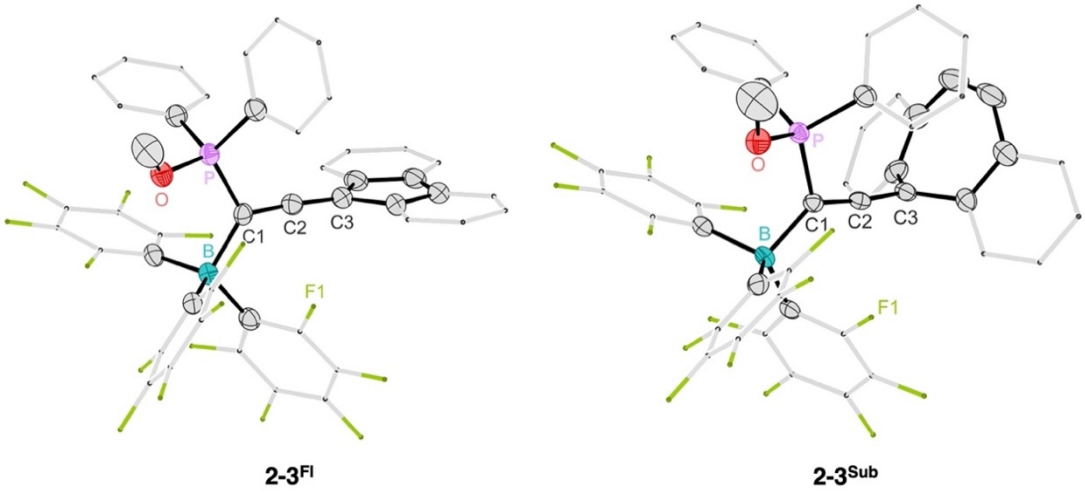

Figure 2-4: Solid-state structures of **2-3^{Fl}** and **2-3^{Sub}**. Thermal ellipsoids are shown at 50% probability. For clarity, hydrogen atoms are omitted, and the phenyl and perfluorophenyl groups are shown in wireframe.

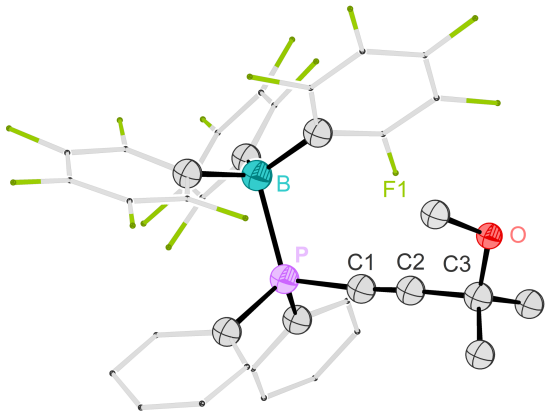

Figure 2-5: Molecular connectivity of **2-2^{Me}•B(C_6F_5)$_3$.** Atoms and bonds are represented with ball and stick modelling.

2.3.6 Alkyne Activation by Boranes

The activation of alkynes by Lewis acidic boranes has relevance to both organic and main-group synthesis, particularly because B(C_6F_5)$_3$ and similar analogs are staple reagents in many Lewis acid mediated transformations and are common components of FLPs. Terminal alkynes typically combine with B(C_6F_5)$_3$ or other acidic boranes to afford alkenyl boranes *via* 1,1-carboboration (Scheme 2-34).[111,112] This process has recently been mechanistically probed by Duarte, Cowley, and Thomas, showing that the reaction proceeds by a σ-bond forming event between one of the alkyne carbon atoms and the borane, initially giving an intermediate zwitterionic alkenyl borate species.[113] Isomerization by a subsequent hydride and aryl shift then gives the resulting alkenyl boranes. Alternatively, the zwitterionic intermediate can be chemically trapped with a Lewis base.

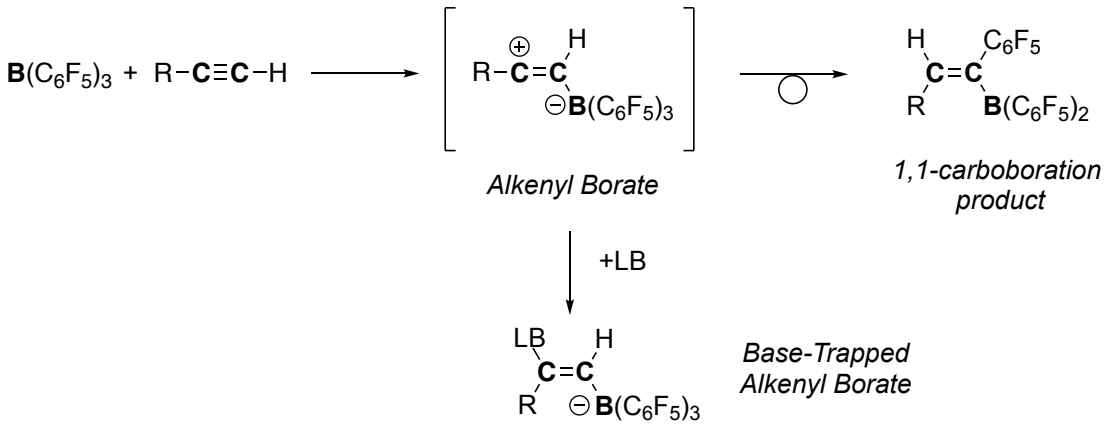

Scheme 2-34: Terminal alkyne activation by B(C_6F_5)$_3$ in a 1,1-carboboration reaction.

The initial formation of a σ-adduct explains the outcome of many intermolecular and intramolecular reactions involving alkynes (terminal and internal) and Lewis acidic boranes. For example, when studying the activation of alkynes by FLPs, the Stephan group showed that a combination of triaryl phosphines and $B(C_6F_5)_3$ affords 1,2-substituted P/B alkenes. The 1-2 addition pattern of the alkene implies the reaction involves a zwitterionic alkenyl borate intermediate (Scheme 2-35).[114] Yamaguchi's phosphonium-borate bridged stilbenes are formed by exploiting the same principle, albeit in an intramolecular fashion.[115] Lastly and perhaps most relevant to our current study, Erker and co-workers showed that alkynyl phosphines $Ar_2P–C\equiv C–R$ (Ar = Ph or Mes, R = Ph) and $B(C_6F_5)_3$ combine to give phosphine-borane-substituted alkenes.[116] Here, the alkyne component simply reacts with $B(C_6F_5)_3$ by typical 1,1-carboboration. The structural differences between Erker's phosphines, and our alkynyl phosphines **2-2** gives divergent reactivity pathways with $B(C_6F_5)_3$. Methoxide abstraction of phosphines **2-2** by $B(C_6F_5)_3$ completely circumvents carboboration chemistry, which permits access to new structural motifs.

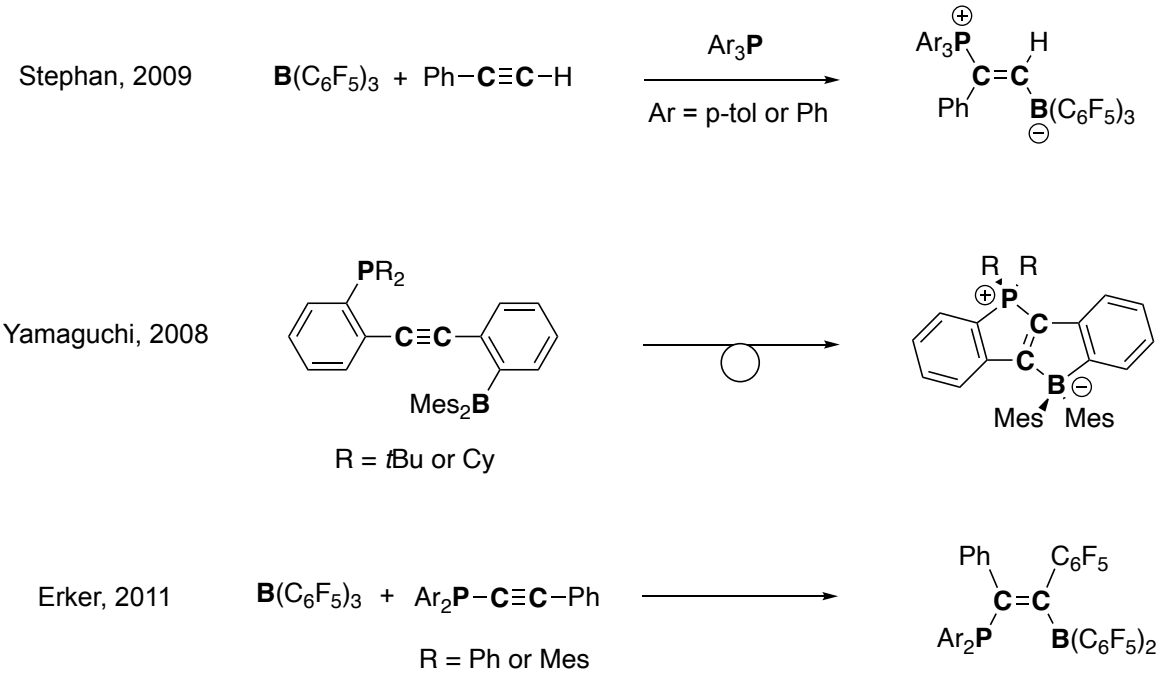

Scheme 2-35: Selected alkyne activations to afford P/B compounds.

2.4 Conclusion and Outlook

Here, a synthetic strategy was devised to approach the isolation of allenylidene phosphonium cations. Serendipitously, alkynyl phosphines **2-2**, with the general formulation $R_2P{-}C{\equiv}C{-}C(OCH_3)R_2$, were found to yield geminally substituted phosphonium borato-allenes **2-3** in the presence of $B(C_6F_5)_3$. Although the target compound, $[Ph_2P{=}C{=}C{=}CPh_2]^+$, was not isolable *via* our proposed route, the intermediacy of unsaturated three-coordinate phosphonium salts could be validated with both experimental and computational studies. Interestingly, quantum chemical analysis of $[Ph_2P{=}C{=}C{=}CPh_2]^+$ suggests that the structure is represented as somewhere between a phosphine stabilized carbocation and a phosphorus centered cation. Ultimately, this chapter serves as foundational groundwork that would inform the successful isolation of an allenylidene phosphonium species, which will be discussed in Chapter 3.

2.5 Experimental Procedures

2.5.1 General Remarks: All manipulations were performed under an inert atmosphere of dry argon or nitrogen, employing standard Schlenk and glovebox techniques. Dry and oxygen-free solvents were utilized, which were obtained from a solvent purification system and then stored over molecular sieves. All glassware was oven-dried at 150 °C. ^{1}H, ^{11}B, ^{13}C, ^{19}F, and ^{31}P nuclear magnetic resonance (NMR) spectra were recorded on Bruker Neo 700 MHz, Bruker AVANCE (IV) Neo 400 MHz, Bruker ARX 300 MHz spectrometers, at the NMR facilities at York University. Chemical shifts are given in parts per million (ppm) relative to $SiMe_4$ (^{1}H, ^{13}C), BF_3•Et_2O (^{11}B, ^{19}F), and 85% H_3PO_4 (^{31}P) and they were referenced to the residual solvent signals (CD_2Cl_2: ^{1}H δ_H =5.32, ^{13}C δ_C = 54.00; C_6D_6: ^{1}H δ_H = 7.16, ^{13}C δ_C = 128.06; CD_3CN: δ_H =1.94, ^{13}C δ_C = 118.26; $CDCl_3$: δ_H =7.26, ^{13}C δ_C = 77.16;) or internally by the instrument after locking and shimming to the deuterated solvent (^{11}B, ^{19}F, ^{31}P). Coupling constants are reported in Hertz (Hz) and NMR multiplicities are abbreviated as follows: s = singlet, d = doublet, t = triplet, q = quartet, p = pentet, sext = sextet, sept = septet, m = multiplet, br = broad signal. Elemental analysis was performed by using Vario EL Cube Elemental Analyzer and the best obtainable data has been presented. Mass spectrometry data was provided from the AIMS Mass Spectrometry Laboratory at the University of Toronto. Samples were run in DART positive ion mode, utilizing an AccuTOF 4G instrument.

2.5.2 Reagents and Handling: All compounds were purchased from commercial sources (Sigma Aldrich, Alfa Aesar, Tokyo Chemical Industry, Oakwood chemicals) and used as received, with the exception of $ClPPh_2$ which was purified by vacuum distillation immediately before use. **2-1**^{Fl}, **2-1**^{Sub}, and **2-1**^{Me} are literature reported compounds which were prepared by adapting previous methods.

Additional Supplementary Information for this chapter is available online:
https://pubs.rsc.org/en/content/articlelanding/2021/cc/d1cc03249f#!divCitation
https://onlinelibrary.wiley.com/doi/10.1002/zaac.202200383

2.5.3 General Procedure for the preparation of Alkynyl Phosphines (A).

Terminal alkynes (1.00 equiv) were dissolved in THF (5-10 mL/ mmol) and cooled to -78°C. A slight excess of ***n*-BuLi** (1.6M in hexanes, 1.05 – 1.15 equiv) was then added dropwise , and the mixture was immediately allowed to warm to 25 °C and subsequently stirred for 1 hour. The reaction mixture was cooled back down to -78 °C prior to the dropwise addition of chloro diaryl or dialkyl phosphine **ClR_2P** (1.05 equiv). Reaction mixtures were gradually left to warm to room temperature for a minimum of 3 hours. In all cases, the volatiles were removed *in vacuo*, and the resulting residues were extracted with diethyl ether. The phosphines were all relatively robust to air and moisture, so an aqueous wash was performed to ensure the removal of Li salts. After which, they were purified by column chromatography.

2.5.4 General Procedure for the preparation of Allenes (B)

Phosphines 2-2 were combined with an equimolar amount of $B(C_6F_5)_3$. For each reaction, the specific solvent that was used is noted, but generally, the rearrangement occurs with the same selectivity in arene solvents (C_6H_6, toluene), or halogenated solvents (CH_2Cl_2, $CHCl_3$). Temperature conditions are delineated for each transformation. In all cases, during isolation of allenes **2-3**, the product was washed with a generous amount of pentane.

2.5.5 Preparation of Alkynyl phosphine 2-2[a]

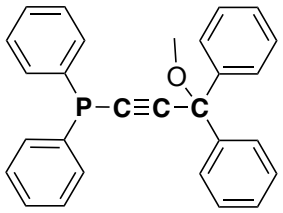

Following general procedure **A**, **2-1**^{Ph} (256 mg, 1.15 mmol, 1.00 equiv), n-BuLi (0.75 mL, 1.6M in hexanes, 1.2 mmol, 1.05 equiv) and PPh_2Cl (267 mg, 217 uL, 1.2 mmol, 1.05 equiv) were used to prepare **2-2**[a]. The residue was then purified by flash chromatography (eluting with 5% EtOAc, 95% hexanes). Subsequently, recrystallization from hot ethanol and drying afforded the title compound as a white powder.

Yield: 267 mg (0.66 mmol, 60%)

^{1}H NMR ($CDCl_3$, 300 MHz, 300 K): δ (ppm) = 7.68 – 7.49 (m, 8H, aromatic C-H), 7.36 – 7.27 (m, 12H, aromatic C-H), 3.41 (s, 3H, OCH_3).

$^{13}C\{^{1}H\}$ NMR ($CDCl_3$, 101 MHz, 301K): δ (ppm) = 143.1 (s, CPh_2: *ipso*), 136.3 (d, $^{1}J_{CP}$ = 6.5 Hz, PPh_2: *ipso*), 132.7 (d, $^{2}J_{CP}$ = 21 Hz, PPh_2: *ortho*), 129.2 (s, PPh_2 :*para*), 128.8 (d, $^{3}J_{CP}$ = 7.6 Hz, PPh_2: *meta*), 128.4, 127.9, and 126.9 (s, aryl carbons of CPh_2), 107.8 (s, P-C≡*C*), 87.1 (d, $^{1}J_{CP}$ = 11.9 Hz, P-*C*≡C), 81.9 (s, *C*Ph_2), 53.0 (s, O*C*H_3).

^{31}P NMR ($CDCl_3$, 162 MHz, 301K) δ (ppm) = -34.0 (p, *J* = 8.7 Hz).

DART-HRMS: *m/z* calculated for $\{M+H]^+$: 407.1559. Found: 407.1568

2.5.6 Preparation of Alkynyl phosphine 2-2^{b}

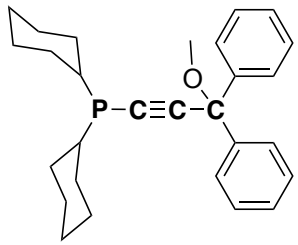

Following general procedure **A**, **2-1^{Ph}** (400 mg, 1.8 mmol, 1.00 equiv), n-BuLi (1.3 mL, 1.6M in hexanes, 2.07 mmol, 1.15 equiv) and PCy_2Cl (441 mg, 418 uL, 1.9 mmol, 1.05 equiv) were used to prepare **2-2^{b}**. The title compound was purified on silica gel eluting with 100% hexanes, affording an orange oil after removing solvent.

Yield: 565 mg (1.35 mmol, 75%)

^{1}H NMR ($CDCl_3$, 400 MHz, 299 K): δ (ppm) = 7.58 – 7.54 (m, 4H, CPh_2 C-H), 7.34 – 7.28 (m, 4H, CPh_2 C-H), 7.24 – 7.22 (m, 2H, CPh_2 C-H), 3.37 (s, 3H, OCH_3), 1.92 (d, $^{3}J_{HH}$ = 12.9 Hz, 2H, PCy_2 C-H) 1.77 (br, 8H, PCy_2 C-H), 1.68 (d, $^{3}J_{HH}$ = 12.9 Hz, 2H, PCy_2 C-H), 1.44 – 1.11 (m, 10H).

^{13}C{^{1}H} NMR ($CDCl_3$, 101 MHz, 299K): δ (ppm) = 143.5 (s, CPh_2: *ipso*), 128.2, 127.7, and 126.9 (s, aryl carbons of CPh_2), 105.1 (d, $^{1}J_{CP}$ = 6.5 Hz P-C≡*C*), 88.1 (d, $^{1}J_{CP}$ = 27.2 Hz, P-*C*≡C), 81.8 (s, *C*Ph_2), 52.8 (s, O*C*H_3). 33.1 (d, J_{CP} = 8 Hz, PCy_2), 30.2 (d, J_{CP} = 17.4 Hz, PCy_2), 29.6 (d, J_{CP} = 4.5 Hz, PCy_2), 27.2 (d, J_{CP} = 13.9 Hz, PCy_2), 27.1 (d, J_{CP} = 6.9 Hz, PCy_2). 26.5 (PCy_2).

^{31}P{^{1}H} NMR ($CDCl_3$, 162 MHz, 299 K): δ (ppm) = 21.9.

DART-HRMS: *m/z* calculated for {M+H]$^{+}$: 419.2498. Found: 419.2505

2.5.7 Preparation of Alkynyl phosphine 2-2^{c}

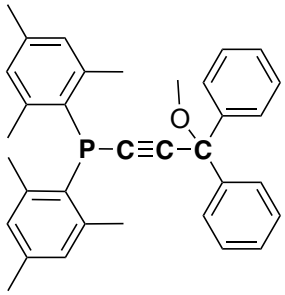

Following general procedure A, **2-1^{Ph}** (0.511 mg, 2.3 mmol, 1.00 equiv), n-BuLi (1.65 mL, 1.6M in hexanes, 2.64 mmol, 1.15 equiv) and $PMes_2Cl$ (735 mg, 2.41 mmol, 1.05 equiv) were used to prepare **2-2^{c}**. The title compound was purified on silica gel eluting with hexanes. The residue was washed with cold ethanol and dried to yield a white solid.

Yield: 335 mg, (0.68, 30%)

^{1}H NMR ($CDCl_3$, 300 MHz, 291 K): δ (ppm) = 7.37 (m, 4H, aromatic C-H), 7.23 (m, 6H, aromatic C-H), 6.79 (d, $^{4}J_{HP}$ = 3.3 Hz, 4H, Mes-CH), 3.24 (s, 3H, OCH_3), 2.34 (s, 12H, Mes-CH_3 : *ortho*), 2.25 (s, 6H, Mes-CH_3 :*para*).

$^{13}C\{^{1}H\}$ NMR (CDCl3, 101 MHz, 301K): δ (ppm) = 143.2 (s, CPh_2: *ipso*), 141.8 (d, $^{1}J_{CP}$ = 15.6 Hz, $PMes_2$:*ipso*), 138.4 ($PMes_2$:*para*), 130.0 ($PMes_2$:*meta*), 129.9 ($PMes_2$:*ortho*), 128.2, 127.6, and 126.9 (s, aryl carbons of CPh_2), 106.7 (d, $^{2}J_{CP}$ = 5.7 Hz P-C≡*C*), 88.8 (d, $^{1}J_{CP}$ = 12.7 Hz, P-*C*≡C), 81.8 (s, *C*Ph_2), 52.8 (s, O*C*H_3), 23.1 (d, $^{3}J_{CP}$ = 5.7 Hz, Mes-*C*H_3 :*ortho*), 21.0 (Mes-CH_3 :*para*).

^{31}P NMR ($CDCl_3$, 121 MHz, 291 K) δ (ppm) = -57.9.

DART-HRMS: *m/z* calculated for $\{M+H]^+$: 491.2498. Found: 491.2504

2.5.8 Preparation of Alkynyl phosphine 2-2^{Fl}

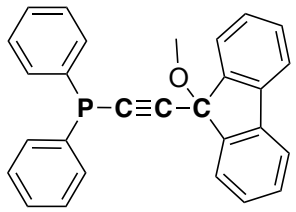

Following general procedure A, **2-1^{Fl}** (315 mg, 1.42 mmol, 1.00 equiv), n-BuLi (0.94 mL, 1.6M in hexanes, 1.5 mmol, 1.05 equiv) and PPh_2Cl (331 mg, 269 uL, 1.5 mmol, 1.05 equiv) were used to prepare **2-2^{Fl}**. The title compound was purified on silica gel eluting with 5% EtOAc, 95% hexanes, yielding an off-white solid.

Yield: 180 mg (0.44 mmol, 31%)

^{1}H NMR (CD_2Cl_2, 300 MHz, 298 K): δ (ppm) = 7.69 (t, *J* = 7.8 Hz, 4H, aromatic C-H), 7.54 (m, 4H, aromatic C-H), 7.45 (dt, *J* = 7.8 Hz, *J* = 1.3 Hz, 2H, aromatic C-H), 7.35 (dt, *J* = 7.5 Hz, *J* = 1.3 Hz, 2H, aromatic C-H), 7.34 (m, 6H), 3.17 (s, 3H, OC*H*$_3$).

^{13}C{^{1}H} NMR (CD_2Cl_2, 101 MHz, 299K): δ (ppm) = 144.3 (aromatic C-H), 140.5 (aromatic C-H), 136.5 (d, $^1J_{CP}$ = 6.5 Hz PPh_2: *ipso*), 132.8 (d, $^2J_{CP}$ = 21 Hz, PPh_2: *ortho*), 130.3 (aromatic C-H), 129.5 (aromatic C-H), 129.0 (d, $^3J_{CP}$ = 7.5 Hz, PPh_2: *meta*), 128.7 (aromatic C-H), 125.4 (aromatic C-H), 120.7 (aromatic C-H), 107.7 (s, P-C≡*C*), 81.4 (d , $^1J_{CP}$ = 11.3 Hz, P-*C*≡C), 81.1 (s, *C*Ar$_2$), 52.3 (O*C*H$_3$).

^{31}P NMR (CD_2Cl_2, 121 MHz, 298K) δ (ppm) = -34.4 (p, $^3J_{HP}$ = 8.6 Hz).

DART-HRMS: *m/z* calculated for {M+H]$^+$: 405.14079. Found: 45.14078

2.5.9 Preparation of 2-2^{Sub}

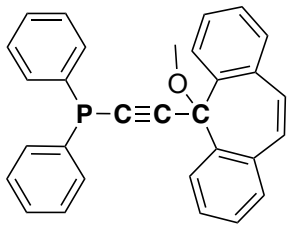

Following general procedure A, **2-1^{sub}** (1.51 g, 6.1 mmol, 1.00 equiv), n-BuLi (4.0 mL, 1.6M in hexanes, 6.4 mmol, 1.05 equiv) and PPh_2Cl (1.41 g, 1.15 mL, 6.4 mmol, 1.05 equiv) were used to prepare **2-2^{Sub}**. After volatiles were removed by vacuum, the residue was extracted with CH_2Cl_2 and washed with water. The title compound was purified on silica gel eluting with 5% diethyl ether, 95% hexanes, yielding a light green powder.

Yield: 1.1 g (2.5 mmol, 40%)

^{1}H NMR ($CDCl_3$, 300 MHz, 298 K): δ (ppm) = 8.27–8.00 (br, 2H, aromatic C-H), 7.86 – 7.69 (br, 4H, aromatic C-H), 7.46 – 7.28 (m, 12H aromatic, C-H), 7.09 (s, 2H), 3.97 -2.80 (br, OCH_3). Spectrum of **2-2^{Sub}** exhibits considerable broadening of the aromatic C-H and aliphatic -OCH3 signal associated with the dibenzo[a,d]cycloheptene or "Sub" group.

^{13}C{^{1}H} NMR ($CDCl_3$, 101 MHz, 298K): δ (ppm) = 136.6 (aromatic C-H), 136.1 (d, $^1J_{CP}$ = 6.3 Hz PPh_2: *ipso*), 133.6, 132.9 (d, $^1J_{CP}$ = 21 Hz, PPh_2: *ortho*), 130.9 (aromatic C-H), 129.6 (aromatic C-H), 128.9 (d, $^3J_{CP}$ = 7.4 Hz, PPh_2: *meta*), 128.2 (aromatic C-H), 127.8 (aromatic C-H), 106.6, 89.9, 83.3, 77.3, 52.7 (O*C*H_3).

^{31}P NMR ($CDCl_3$, 121 MHz, 298K) δ (ppm) = -33.9.

DART-HRMS: *m/z* calculated for $\{M+H]^+$: 431.15510. Found: 431.15514

2.5.10 Preparation of 2-2^{Me}

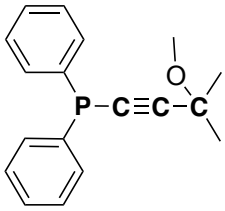

2-2^{Me} was prepared by a modified procedure where alkyne **2-1^{Me}** was first deprotonated with *i*PrMgCl, and the magnesium acetylide [ClMg][2-1^{Me}] was isolated. [ClMg][2-1^{Me}] (848 mg, 1.6 mmol, 1 equiv) was dissolved in THF and cooled to -78°C. Then PPh_2Cl (353 mg, 287 uL, 1.6 mmol, 1.05 equiv) was added in a single portion. The volatiles were removed in vacuo and the residues taken up in CH_2Cl_2, then filtered through an alumina pad on fritted glass. The title compound was isolated as a yellow/orange oil.

Yield: 343 mg (1.6 mmol, 75%)

^{1}H NMR (C_6D_6, 400 MHz, 298 K): δ (ppm) = 7.74-7.68 (m, 4H, aromatic C-H), 7.09-7.03 (m, 4H, aromatic C-H), 7.04-6.98 (m, 2H, aromatic C-H), 3.28 (s, 3H, OCH_3), 1.39 (s, 6H, C(CH_3)$_2$.

^{13}C{^{1}H} NMR (C_6D_6, 176 MHz, 299K): δ (ppm) = 137.2 (d, $^1J_{CP}$ = 7.1 Hz PPh_2: *ipso*), 132.9 (d, $^2J_{CP}$ = 21 Hz, PPh_2: *ortho*), 129.2, 128.9 (d, $^3J_{PC}$ = PPh_2: *meta*), 111.6 (s, P-C≡*C*), 81.4 (d , $^1J_{CP}$ = 9.7 Hz, P-*C*≡C), 71.4 (*C*Me_2) 51.8 (O*C*H_3), 28.3 (C*Me*$_2$)

^{31}P NMR ($CDCl_3$, 121 MHz, 301K) δ (ppm) = -34.3 (p, $^3J_{HP}$ = 8.6 Hz).

DART-HRMS: *m/z* calculated for {M+H]$^+$: 283.1252 Found: 283.1250

2.5.11 Preparation of Allene phosphine 2-3[a]

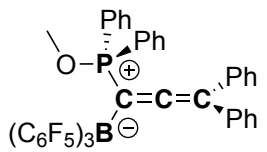

An equimolar amount of **2-2[a]** (8.13 mg, 0.02 mmol) and $B(C_6F_5)_3$ (10.23 mg, 0.02 mmol) were dissolved in deuterated benzene (600 uL) and the solution was transferred to an NMR tube equipped with a Teflon tap. The solution was heated to 60 °C, with 31P NMR indicating complete conversion after 3 hours.

Alternatively, **2-2a** (81.3 mg, 0.02 mmol) and $B(C_6F_5)_3$ (100.3 mg, 0.02 mmol) were dissolved in benzene (3 mL) and heated to 60 °C for 8 hours. Solvent was removed in vacuo and the residue was washed with a generous amount of pentane. Drying again affording the title compound as a bright yellow/green solid.

Yield: 123.4 mg (0.13 mmol, 68%)

^{1}H NMR (C_6D_6, 300 MHz, 290 K) δ (ppm) = 7.03 (m, 9H), 6.98-6.90 (m, 5H), 6.91-6.82 (m, 2H), 6.72 (td, 4H, $^{3}J_{HH}$ = 7.7 Hz), 2.93 (d, $^{3}J_{PH}$ = 11.4 Hz, 3H).

^{11}B{^{1}H} NMR (C_6D_6, 96 Hz, 291 K) δ (ppm) = -13.6.

^{13}C{^{1}H} NMR partial (101 MHz, C_6D_6, 300K) δ (ppm) = 214.0 (s, C2 allene), 149.1 (dm, $^{1}J_{CF}$ = 240 Hz, -$B(C_6F_5)_3$, (o-F)), 139.6 (dm, $^{1}J_{CF}$ = 244 Hz, -$B(C_6F_5)_3$, (p-F)), 137.2 (dm, $^{1}J_{CF}$ = 238 Hz, -$B(C_6F_5)_3$, (m-F)), 136.4 (d, $^{4}J_{PC}$ = 3.0 Hz, $P(C_6H_5)_2$ (p-C)), 134.6 (d, $^{1}J_{PC}$ = 10 Hz, C1 allene), 132.3 (d, $^{2}J_{PC}$ = 10.8 Hz, $P(C_6H_5)_2$ (o-C)), 129.1 (d, $^{3}J_{PC}$ = 12.8 Hz, $P(C_6H_5)_2$ (m-C)), 128.9 (d, *J* = 5 Hz), 128.9, 122.9 (d, $^{1}J_{PC}$ = 99 Hz, $P(C_6H_5)_2$ (ipso-C)), 110.3 (d, $^{3}J_{PC}$ = 24.2 Hz, C3 allene), 57.6 (d, $^{2}J_{PC}$ = 11.1 Hz, P-OCH_3).

^{19}F{^{1}H} (C_6D_6, 282 MHz, 291 K) δ (ppm) = -129.6 (s, br, 6F (*o*-F)), -159.7 (t, J = 21 Hz, 3F (*p*-F)), -165.1 (m, 6F (*m*-F).

^{31}P{1H} NMR (C_6D_6, 121 MHz, 291K) δ (ppm) = 67.0.
EA: Calculated (%): C, 60.16; H, 2.52. Found (%): C, 59.58; H, 3.19 (averaged over four samples).

2.5.12 Room temperature reactivity study of 2-2[a] with $B(C_6F_5)_3$.

Under the same conditions as the NMR scale preparation of **2-3[a]**, (Section 2.5.11) but the reaction was monitored at room temperature after addition. The predominant species in solution is a P-B Lewis pair, with minimal conversion to allene **2-3[a]** after 3 hours.

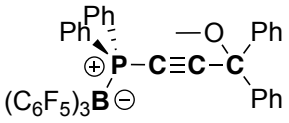

2-2[a]·B(C_6F_5)$_3$

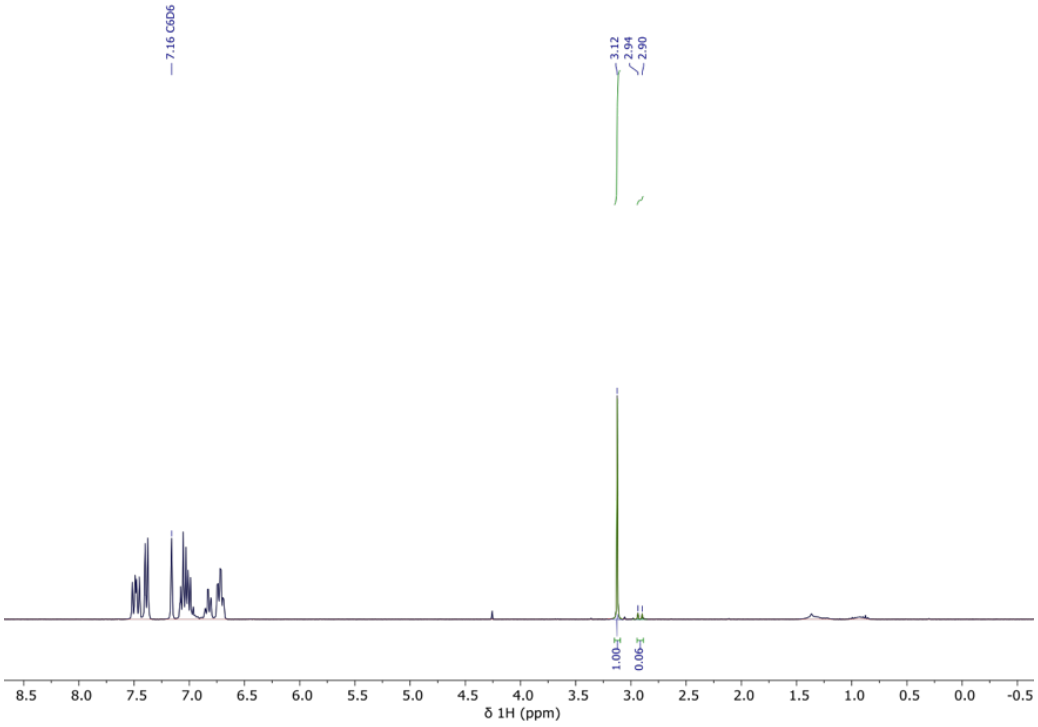

Figure 2-6:^{1}H NMR spectrum showing the P–B adduct of **2-2[a]** and $B(C_6F_5)_3$ as the predominant species in solution at room temperature (300 MHz, C_6D_6)

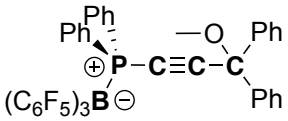

2-2^{a}•B(C_6F_5)$_3$

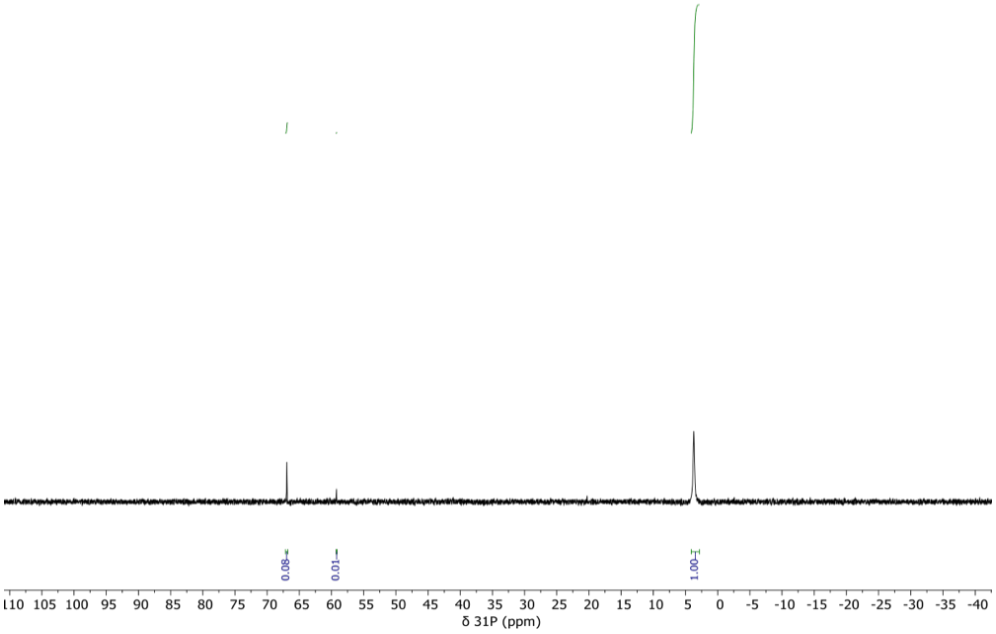

Figure 2-7:$^{31}P\{^{1}H\}$ NMR spectrum showing the diagnostic resonance (δ_P = 3.7 ppm) of the P–B adduct of **2-2^{a}** and $B(C_6F_5)_3$ as the predominant species in solution at room temperature (121 MHz, C_6D_6).

2.5.12 Reactivity of 2-2[a] with Me_3SiOTf

A chloroform-*d* solution of **2-2[a]** (0.02 mmol, 8.1 mg) was added *via* syringe to a chloroform-*d* solution of Me_3SiOTf (0.03 mmol, 1.5 equiv) at -94°C, in the absence of light. The reaction mixture was allowed to warm to room temperature and stir, resulting in a gradual color change to bright yellow-green. An aliquot was taken for NMR analysis after 2 hours. ^{1}H and ^{31}P $\{^{1}H\}$ NMR are consistent with the formation of a methoxy phosphonium cation. The cationic species drawn remains elusive in our experimentation and the synthesis could never be replicated.

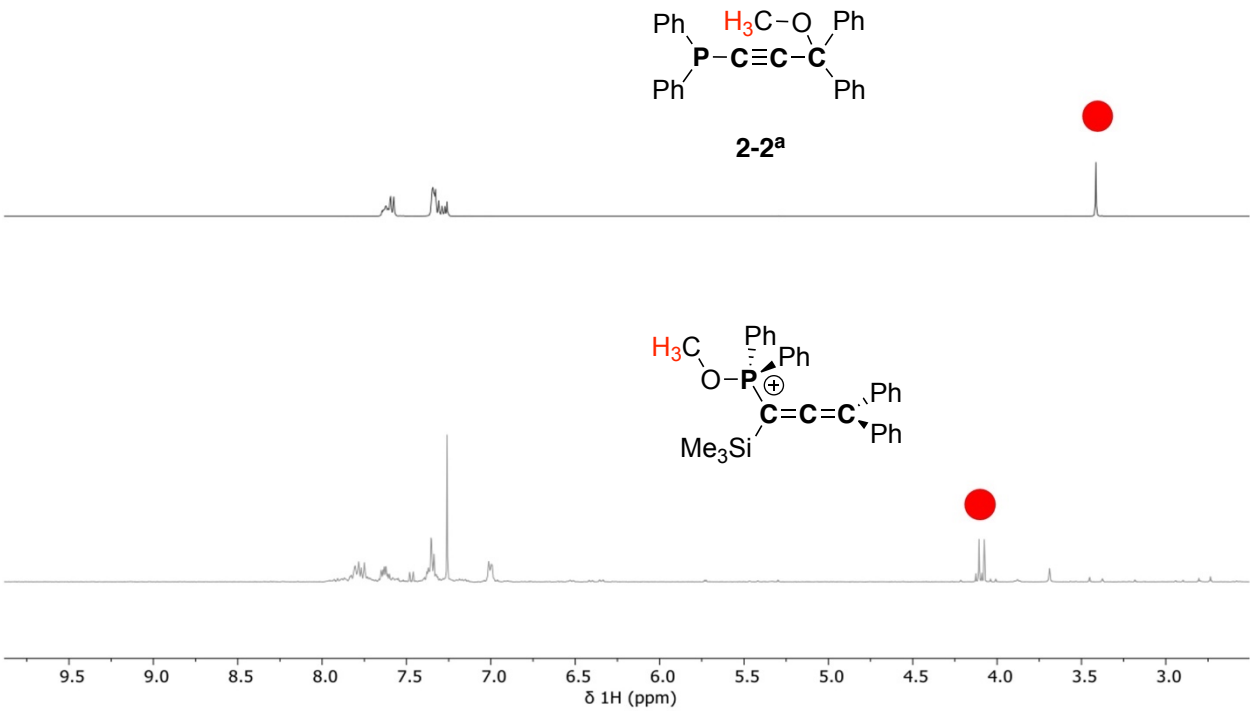

Figure 2-8:Stacked ^{1}H NMR spectra. The top is a reference spectrum of **2-2[a].** The bottom is a spectrum produced from an aliquot of the reaction between **2-2[a]** and Me_3SiOTf outlined by the above conditions. The doublet splitting peak in the upfield region of the bottom spectra (denoted with the red marker) suggests the formation of a methoxy phosphonium cation.

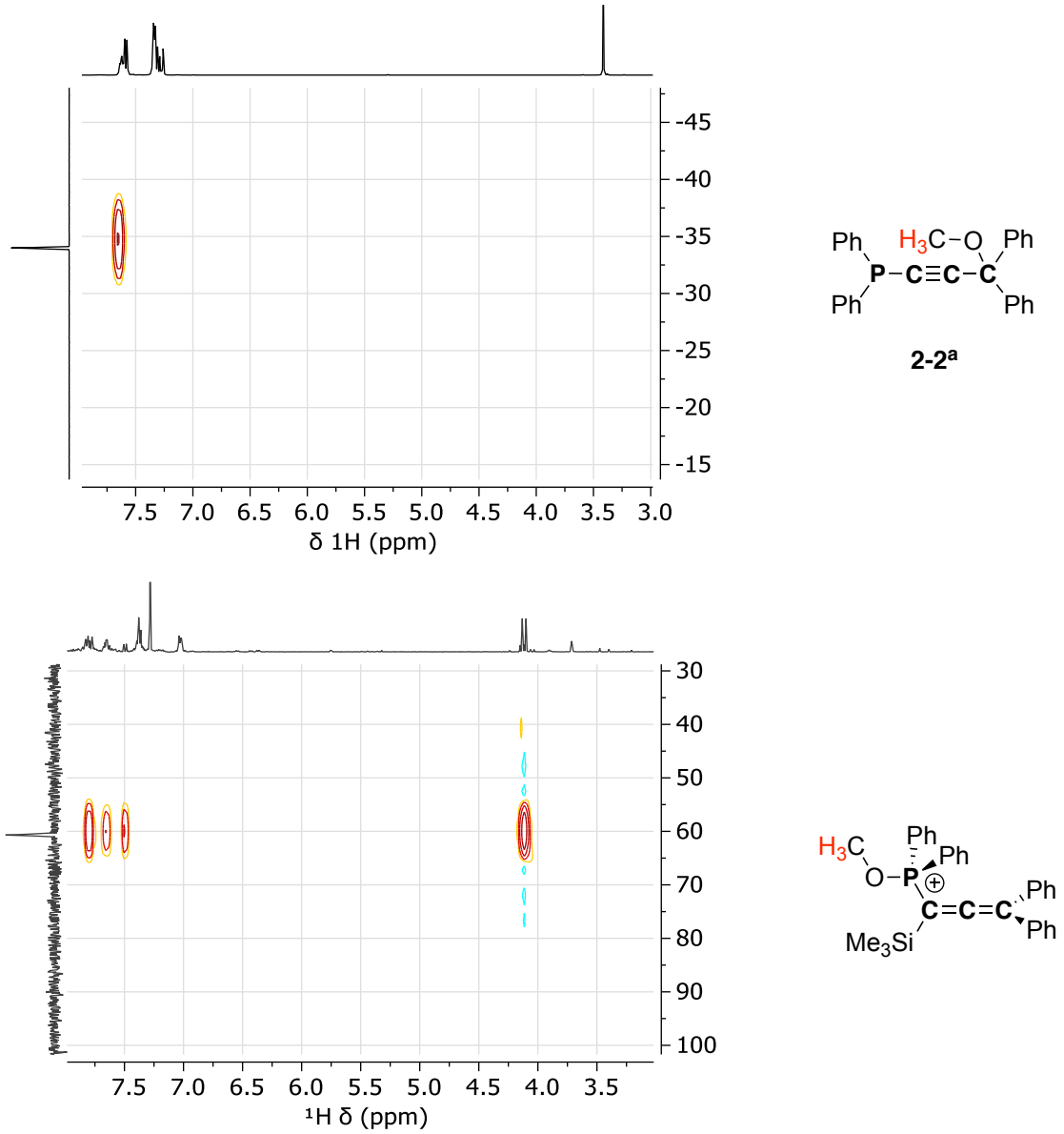

Figure 2-9: Stacked $^{1}H/^{31}P$ HMBC spectra (400 MHz /162 MHz) of **2-2**[a] and the reaction between **2-2**[a] and Me_3SiOTf**,** further suggesting the proposed phosphonium silyl cation depicted.

2.5.13 Preparation of Allene phosphine 2-3[b]

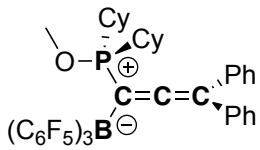

2-2[b] (41.9 mg, 0.1 mmol) and $B(C_6F_5)_3$ (51.2 mg, 0.1 mmol) were dissolved in benzene (3 mL) and heated to 60 °C for 3 hours. Solvent was removed in vacuo and the residue was washed with a generous amount of pentane. Drying again affording the title compound as a yellow/orange solid.

Yield: 59.0 mg (0.063 mmol, 63%)

^{1}H NMR (CD_2Cl_2, 300 MHz, 298 K) δ (ppm) = 7.49-7.16 (m, 6H), 7.01 (d, J = 7.3 Hz, 4H), 3.37 (d, $^3J_{PH}$ = 10.2 Hz, 3H), 2.23-1.93 (br, 3H), 1.89-1.52 (br, 10 H), 1.47-1.23 (br, 5H), 1.19-1.03 (br, 4H), 0.99-0.79 (m, 3H). aliphatic protons corresponding to the -Cy substituents integrate higher than expected due to a pentane contaminant that could not be removed from the sample even with extended time under vacuum.

^{11}B{^{1}H} NMR (C_6D_6, 96 Hz, 293 K) δ (ppm) = -13.4.

^{13}C{^{1}H} NMR partial (C_6D_6, 101 MHz, 301K) δ (ppm) = 212.9 (s, C2 allene), 149.1 (dm, $^1J_{CF}$ = 241 Hz, -$B(C_6F_5)_3$, (o-F)), 139.8 (dm, $^1J_{CF}$ = 236 Hz, -$B(C_6F_5)_3$, (p-F)), 137.4 (dm, $^1J_{CF}$ = 236 Hz, -$B(C_6F_5)_3$, (m-F)), 134.8 (d, $^1J_{PC}$ = 8.1 Hz, $P(C_6H_5)_2$ (p-C)), 128.9 (d, J = 5 Hz), 128.8, 108.9 (d, $^3J_{PC}$ = 20 Hz, C3 allene), 55.3 (d, $^2J_{PC}$ = 10.1 Hz, P-OCH3), P-*Cy* carbons: 38.4 (d, J = 50.5 Hz), several overlapping peaks from 27.2-26.7, 25.6.

^{19}F{^{1}H} (C_6D_6, 282 MHz, 293 K) δ (ppm) = -128.7 (br, 6F (*o*-F)), -159.0 (t, J = 21 Hz, 3F (*p*-F)), -164.9 (br, 6F (*m*-F).

^{31}P{^{1}H} NMR (C_6D_6, 121 MHz, 293K) δ (ppm) = 82.8

EA: Calculated (%): C, 59.37; H, 3.79. Found (%): C, 58.58; H, 3.27.

2.5.14 Preparation of Dimer [2-4]$^{+}$

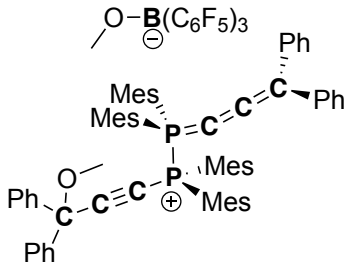

2-2^{c} (9.8 mg, 0.02 mmol) was dissolved in a minimal amount of pentane, added to an equimolar amount of $B(C_6F_5)_3$, and subsequently allowed to stir for 30 minutes. A pale light green solid proceeded to crash out of solution, was washed with pentane repeatedly, dried briefly in vacuo, and reconstituted in deuterated benzene for NMR analysis.

^{1}H NMR (C_6D_6, 400 MHz, 303 K) δ (ppm) = 7.12–7.02 (m, 12 H, Ph-H), 6.95 (t, J = 7.7 Hz, 4H, Ph-H), 6.63 (d, $^{4}J_{PH}$ = 5.6 Hz, 4H, Mes-H) 6.60 (d, $^{4}J_{PH}$ = 3.5 Hz, 4H, Mes-H), 6.16 (d, $^{2}J_{HH}$ = 7.8 Hz, 4H, Ph-H), 3.55 (br, 3H, CH_3O-B$(C_6F_5)_3$) 2.76 (s, 3H, CH_3O-C), 2.24 (s, 12H), 2.09 (s, 12H), 2.02 (s, 6H), 2.01 (s, 6H).

^{11}B{^{1}H} NMR (C_6D_6, 128 MHz, 303 K) δ (ppm) = -1.7 (s)

^{13}C{^{1}H} NMR Partial (C_6D_6, 176 MHz, 295 K) δ (ppm) = (dm, J_{CF} = 241 Hz, CH_3O-B(C_6F_5)$_3$, (o-F)), 137.5 (dm, J_{CF} = 250 Hz, CH_3O-B(C_6F_5)$_3$, (p-F)), 146.3 (d, J = 3.2 Hz) 143.4 (d, J = 18 Hz) 142.5 (d, J = 11.1 Hz) and 140.6, 133.3 (d, J = 12.7 Hz, P-*Mes$_2$*, (m-C)), 131.2, 131.7 (d, J = 6.8 Hz, 127.2 (s, Ph aryl carbon),121.1 (d, J = 20.4 Hz), 118.5 (d, $^{1}J_{PC}$ = 87.6 Hz, Mes_2P=*C*), 117.1 (d, J = 17.2 Hz), 93.9 (dd, $^{1}J_{PC}$ = Hz 87.2, $^{2}J_{PC}$ = Hz 64.7, Mes_2P-*C*≡C), 82.7 (d, $^{3}J_{PC}$ = 2.8 Hz, CH_3O-*C*RPh_2), 74.8 (d, J_{PC} = 167 Hz) *53.1 (s, *C*H_3O-B$(C_6F_5)_3$, *53.1 (s, *C*H_3O-C) *signals partially overlapped, 23.9 (s) 23.6 (d, $^{3}J_{PC}$ = 15.1 Hz) and 20.7 (s) P-*Mes$_2$* methyl carbons.
meta-carbon and *ipso*-carbon of the CH_3O-B(C_6F_5)$_3$ counteranion are not observed.

^{19}F{^{1}H} NMR (C_6D_6, 282 MHz, 296 K) δ (ppm) = -133.7 (d, $^{3}J_{FF}$ = 23.9 Hz, 6F, (*o*-F)), -162.3 (s, br, 3F (*p*-F)), -166.5 (s, br, 6F (*m*-F).
*spectra displays significant broadening of the *para*-F resonance

^{31}P{^{1}H} NMR (C_6D_6, 162 MHz, 303 K) δ (ppm) = -5.3 ($^{1}J_{PP}$ = 211 Hz) -18.7 ($^{1}J_{PP}$ = 211 Hz) ppm.
ESI-HRMS: m/z calculated for $(M+2H)^{2+}$, $[C_{67}H_{68}OP_2]^{2+}$:475.2367, m/z Found: 475.2400

2.5.15 Preparation of Phosphine 2-2[a] trityl adduct [2-2[a]•CPh_3]$^+$

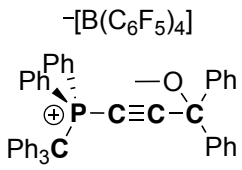

2-2[a] (12.19 mg, 0.03 mmol) and $[CPh_3][B(C_6F_5)_4]$ (27.67 mg, 0.03 mmol) were dissolved in CH_2Cl_2 and stirred for 16 h at room temperature. Solvent was removed *in vacuo.* Crude material was rinsed with pentane, yielding a green solid.

Yield: 33.7 mg (0.025 mmol, 84% yield).

^{1}H NMR (CD_3CN, 400 MHz, 297 K) δ (ppm) = 7.76 (t, $^3J_{HH}$ = 7.8 Hz, 2H), 7.53 (t, $^3J_{HH}$ = 7.8 Hz, 3H), 7.48 (dd, $^3J_{HH}$ = 8 Hz, $^4J_{PH}$ = 4 Hz, 4H) 7.42-7.34 (m, 12H), 7.34-7.26 (m, 2H), 7.26-7.12 (m, 12H), 3.24 (s, 3H).

^{11}B{^{1}H} NMR (128 MHz, C_6D_6, 297 K) δ (ppm) = -15.9.

^{13}C{^{1}H} NMR partial ($CDCl_3$, 176 MHz, 298 K) δ (ppm) =148.3 (dm, $^1J_{CF}$ = 242 Hz, B(C_6F_5)$_4$ (o-C)), 139.5 (-C(OCH$_3$)(C_6H_5)$_2$ (ipso-C)), 138.3 (dm, $^1J_{CF}$ = 244 Hz, B(C_6F_5)$_4$ (p-C)), 136.4 (dm, $^1J_{CF}$ =242 = Hz, B(C_6F_5)$_4$ (m-C)), 135.8 (d, $^3J_{PC}$ = 3.2 (CPh_3, ipso-C), 134.2 (d, $^2J_{PC}$ = 10 Hz, P(C_6H_5)$_2$ (o-C)), 131.4 (d, $^4J_{PC}$ = 6.8 Hz, P(C_6H_5)$_2$ (p-C)), 130.4 (d, $^3J_{PC}$ = 6.8 Hz, P(C_6H_5)$_2$ (m-C)), 129.5 (s, br (*o*, *m*, *p*-C), 129.4, 129.1, and 126.7 (s, C_{aryl} of -C(OCH$_3$)(C_6H_5)$_2$), 119.8 (d, $^1J_{PC}$ = 85 Hz, P(C_6H_5)$_2$ (ipso-C)), 119.4 (d, $^2J_{PC}$ = 17.8 Hz, P-C≡*C*) 82.5 (d, $^3J_{PC}$ = 2.5 Hz, ≡C-*C*(OCH$_3$)(C_6H_5)$_2$), 73.3 (d, $^1J_{PC}$ = 162 Hz, P-*C*≡C)) 67.8 (d, $^1J_{PC}$ = 45.1 Hz, CPh_3), 53.7 (s, -O*C*H$_3$) ppm. B(C_6F_5)$_4$ (*ipso*-C) not observed.

^{19}F{^{1}H} NMR ($CDCl_3$, 282 MHz, 298 K) δ (ppm) = -132.6 (br, 8F, (o-F)), -163.2 (t, $^3J_{F-F}$ = 21 Hz, 4F (p-F)), -166.9 (8F (m-F)).

^{31}P{^{1}H} NMR (C_6D_6, 162 MHz, 297 K) δ (ppm) = 10.7.

EA: Calculated (%): C, 64.18; H, 2.88. Found (%): C, 65.10; H, 2.51.

2.5.16 Reactivity of Phosphine 2-2^{Me,} and $B(C_6F_5)_3$ to give adduct 2-2^{Me}•$B(C_6F_5)_3$

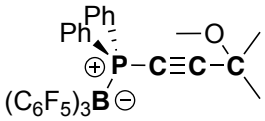

A benzene solution (2 mL) of $B(C_6F_5)_3$ (126.2 mg, 0.25 mmol) was added to a benzene (2 mL) solution of **2-2^{Me}** (69.9 mg, 0.25 mmol) at room temperature and stirred for 30 minutes. After which the solvent was removed by vacuum evaporation. The resulting solid was washed repeatedly with pentane (2 x 3 mL) and dried to afford the title compound as an off-white powder. ^{1}H and ^{31}P NMR, as well as an SCXRD study confirmed the formation of **2-2^{Me}•$B(C_6F_5)_3$**

Yield: 145.6 mg (74 %, 0.18 mmol).

^{1}H NMR ($CDCl_3$, 300 MHz, 298K) δ (ppm) = 7.51– 7.44 (m, 6H), 7.38-7.31 (m, 4H), 3.17 (s, 3H), 1.40 (s, 6H).

$^{31}P\{^{1}H\}$ NMR (C_6D_6, 121 MHz, 298K) δ (ppm) = 3.5 ppm.

2.5.17 Preparation of 2-3^{Fl}

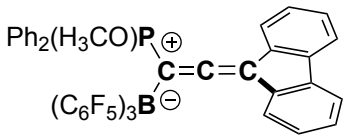

Toluene solutions of B(C6F5)3 (76 mg, 0.15 mmol, 1 equiv, 2 mL) and 2 (60 mg, 0.15 mmol, 1 equiv, 2 mL) were combined at room temperature and stirred for 30 minutes, after which the solvent was removed by vacuum evaporation. The resulting solid was washed with pentanes and dried to afford the title compound as a white powder.

Yield: 108.6 mg (0.12mmol, 80 %).

^{1}H NMR (CD_2Cl_2, 300 MHz, 298 K) δ (ppm) = 7.70– 7.60 (m, 6H), 7.54– 7.31 (m, 12H), 3.68 (d, $^{3}J_{PH}$= 11.9 Hz, 3H).

^{11}B{^{1}H} NMR ($CDCl_3$, 96 MHz, 296K) δ (ppm) = -13.3.

^{13}C{^{1}H} NMR ($CDCl_3$, 176 MHz, 296K) δ (ppm) = 210.7 (s, C2 allene), 148.3 (dm, $^{1}J_{CF}$ = 240 Hz, -B(C_6F_5)$_3$ (o-F)), 139.2 (dm, $^{1}J_{CF}$ = 251 Hz, -B(C_6F_5)$_3$ (p-F)), 138.4 (d, J_{PC} = 2.1 Hz), 136.8 (dm,$^{1}J_{CF}$ = 249 Hz, -B(C_6F_5)$_3$ (o-F)), 136.8 (d, J_{PC} = 9.6 Hz), 136.7, 135.13, 132.5 (d, J_{PC} = 8 Hz), 129.5 (d, J_{PC} = 12.7 Hz), 128.4 (d, J_{PC} = 1.7 Hz), 127.2 (d, J_{PC} = 1.6 Hz), 124.6, 122.3 (d, $^{1}J_{PC}$ = 100 Hz, P(C_6H_5)$_2$ (ipso-C)), 120.3 (s), 105.6 (d, $^{3}J_{PC}$ = 23.5 Hz, C3 allene), 57.9 (d, $^{2}J_{PC}$ = 9.8 Hz, P-OCH3),

^{19}F{^{1}H} NMR ($CDCl_3$, 282 MHz, 295K) δ (ppm) = -130.6 (br, 6F, (o-F)), -159.9 (t, $^{3}J_{FF}$ = 20.6 Hz, 3F, (p-F)), -165.3 (t, $^{3}J_{FF}$ = 17.7 Hz, 6F, (m-F)).

^{31}P{^{1}H} NMR (C_6D_6, 121 MHz, 296K) δ (ppm) = 66.3.

Elemental Analysis: Calculated %: 60.68 C, 2.31 H. Analysis Weight %: 60.58 C, 2.00 C.

2.5.18 Preparation of 2-3^{Sub}

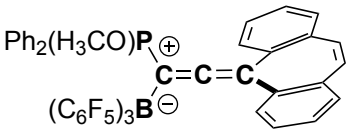

Toluene (2 mL) solutions of $B(C_6F_5)_3$ (53.6 mg, 0.105 mmol) and **2-2^{Sub}** (45 mg, 0.105 mmol) were combined at room temperature and stirred for 30 minutes, after which the solvent was removed by vacuum evaporation. The resulting solid was washed with pentanes and dried to afford the title compound as a white powder.

Yield: 45.8 mg (0.05 mmol, 49%).

^{1}H NMR ($CDCl_3$, 700 MHz, 298K) δ (ppm) = 7.53 (br, 2H), 7.45 – 7.29 (m, br, 5H) 7.17 – 6.86 (m, br, 11H) 6.10 (s, br, 2H), 3.46 (d, $^{3}J_{PH}$ = 11.7 Hz, 3H).

^{11}B{^{1}H} NMR ($CDCl_3$, 96 MHz, 296K) δ (ppm) = -14.2.

^{13}C{^{1}H} NMR Partial ($CDCl_3$, 176 MHz, 298K) δ (ppm) = 211.1 (C2 allene), 147.9 (dm, $^{1}J_{CF}$ =237 Hz), 148.3 (dm, $^{1}J_{CF}$ =236 Hz),139.1 (dm, $^{1}J_{CF}$ = 249 Hz, -B(C_6F_5)$_3$), 136.7, 134.2, 134.0 (d, *J* = 9.4 Hz), 133.7 (d, *J* = 6.4 Hz), 132.2 (br), 130.2,129.5,129.0 (d, *J* = 13.1 Hz), 128.9,128.1, 127.9 (d, *J* = 24.2Hz), 122.6 (d, *J* = 100 Hz), 110.1 (d, *J* = 23.5 Hz), 57.8 (d, $^{2}J_{PC}$ = 9.7 Hz, P-OCH_3)

^{19}F{^{1}H} NMR ($CDCl_3$, 282 MHz, 298K) δ (ppm) = -122.9 (br, o-F), -133.1 (br, o-F), -160.2 (br, p-F), -165.5 (br. m-F).

^{31}P{^{1}H} NMR ($CDCl_3$, 121 MHz, 298K) δ (ppm) = 69.4.

Elemental Analysis: Calculated %: 61.17 C, 2.46 H. Analysis Weight % 59.79 C, 2.30 H.

The “Sub” group results in broadened NMR features in the ^{1}H, ^{13}C and ^{19}F NMR spectra,

2.5.19 SCXRD Analyses

Diffraction data was collected on a Bruker APEX-II CCD diffractometer with a MoKα (λ = 0.71073) radiation source. Crystals were chosen under paratone oil and mounted to the diffractometer under a stream of N_2 and kept at 173.0 K during data collection. Using Olex2,[S1] the structure was solved with the XS structure solution program using Direct Methods and refined with the SHELXL[S2] refinement package using Least Squares minimization.

2-2^{a}: Colorless single crystals were obtained by layering a saturated solution of CH_2Cl_2 with isopropanol at room temperature.

2-3^{a}: Transparent green/yellow single crystals were obtained by layer a CH_2Cl_2 with pentane at room temperature.

2-3^{Fl}: Yellow single crystals were obtained by slow evaporation of a concentrated benzene solution

2-3^{Sub}: Colorless single crystals were obtained by slow evaporation of a concentrated benzene solution

Table 2-1: Crystal structure refinement data for **2-2**[a] and **2-3**[a].

Compound	**2-2**[a]	**2-3**[a]
CCDC	2055307	2055304
Empirical formula	$C_{28}H_{23}OP$	$C_{46}H_{23}OBF_{15}P$
Formula weight	406.46	918.42
Temperature/K	173.00K	173.00K
Crystal system	Triclinic	Orthorhombic
Space group	*P-1*	*Pbca*
a/Å	6.1570(9)	17.915 (3)
b/Å	10.7695 (15)	20.056 (4)
c/Å	17.131 (2)	22.245 (4)
a/°	79.693 (5)	90
b/°	81.084 (5)	90
g/°	88.594 (5)	90
Volume/Å^3	1104.1 (3_	7993(3)
Z	2	8
r_{calc}g/cm^3	1.223	1.527
m/mm^{-1}	0.141	0.177
F(000)	428.0	3696.0
Crystal size/mm^3	0.3 × 0.2 × 0.2	0.5 × 0.4 × 0.8
Radiation	MoK_a (l = 0.71073)	MoK_a (l = 0.71073)
2Q range for data collection/°	4.908 to 55.284	4.456 to 55.014
Index ranges	-8 ≤ h ≤ 7, -14 ≤ k ≤ 14, -22 ≤ l ≤ 22	-23 ≤ h ≤ 23, -26 ≤ k ≤ 26, -28 ≤ l ≤ 28
Reflections collected	33207	272402
Independent reflections	5069 [R_{int} = 0.0776, R_{sigma} = 0.0444]	9180 [R_{int} = 0.0716, R_{sigma} = 0.0193]
Data/restraints/parameters	5069/0/272	9180/0/578
Goodness-of-fit on F^2	1.087	1.080
Final R indexes [I>2s (I)]	R_1 = 0.0710, wR_2 = 0.1760	R_1 = 0.0416, wR_2 = 0.1070
Final R indexes [all data]	R_1 = 0.0782, wR_2 = 0.1814	R_1 = 0.0585, wR_2 = 0.1229
Largest diff. peak/hole/ eÅ^{-3}	0.45/-0.27	0.38/-0.36

Table 2-2: Crystal structure refinement data for **2-3^{Fl}** and **2-3^{Sub}**.

Compound	**2-3^{Fl}**	**2-3^{Sub}**
CCDC	2221768	2221769
Empirical formula	$C_{48}H_{23}OBF_{15}P$	$C_{42}H_{27}OBF_{15}P$
Formula weight	942.44	994.51
Temperature/K	173.00K	174.00K
Crystal system	Orthorhombic	Orthorhombic
Space group	*Pca21*	*Pbca*
a/Å	21.4649(13)	12.3754(4)
b/Å	10.0810(6)	19.9927(6)
c/Å	18.8504(9)	35.3541(13)
a/°	90	90
b/°	90	90
g/°	90	90
Volume/Å^3	4079.0(4)	8747.2(5)
Z	4	8
r_{calc}g/cm^3	1.535	1.51
m/mm^{-1}	0.175	0.168
F(000)	1896	4016
Crystal size/mm^3	0.15 × 0.15 × 0.15	0.1× 0.05 × 0.05
Radiation	MoK_a (l = 0.71073)	MoK_a (l = 0.71073)
2Q range for data collection/°	4.464 to 55.1	4.038 to 55.092
Index ranges	-27 ≤ h ≤ 27, -13 ≤ k ≤ 13, -20 ≤ l ≤ 24	-16 ≤ h ≤ 16, -24 ≤ k ≤ 25, -45 ≤ l ≤ 45
Reflections collected	52469	107072
Independent reflections	8837 [R_{int} = 0.0605, R_{sigma} = 0.0400]	10032 [R_{int} = 0.0843, R_{sigma} = 0.0405]
Data/restraints/parameters	8837/1/596	10032/0/633
Goodness-of-fit on F^2	1.06	1.053
Final R indexes [I>2s (I)]	R_1 = 0.0398, wR_2 = 0.0817	R_1 = 0.0479, wR_2 = 0.1045
Final R indexes [all data]	R_1 = 0.0602, wR_2 = 0.0904	R_1 = 0.0908, wR_2 = 0.1256
Largest diff. peak/hole/ eÅ^{-3}	0.19/-0.24	0.31/-0.29

3.5.20 Computational Details

All Density Functional Theory (DFT) calculations were performed using Gaussian 09.2 [S3] Geometry optimization of all the molecules, intermediates, and the transition state were carried out using the BP86(D3)/def2-SVP basis sets implemented in the Gaussian 09 software.[S4,S5] Thermal energy corrections were extracted from the results of frequency analysis performed at the same level of theory. Frequency analysis of all the molecules and intermediates contained no imaginary frequency showing that these are energy minima. The transition state geometries gave one imaginary frequency at expected reaction coordinates confirming that it is a first-order saddle point. NMR calculations at PBE1PBE/6-31G(d) level of theory in gas phase. The ^{31}P chemical shifts referenced to calculated H_3PO_4 at the same level of theory. [S6]

2.6 References

1. F. Ahmad, A. Mahmood, T. Muhmood, *Heteroatom-Doped Carbon Allotropes: Progress in Synthesis, Characterization and Applications.***2024***, 1*, 1-18.
2. X. Ye, M. Qi, M. Chen, L. Zhang, J. Zhang, *Adv. Mater. Interfaces.* **2023**, *10*, 2201941.
3. R. J. Lagow, J. J. Kampa, H. C. Wei, S. L. Battle, J. W. Genge, D. A. Laude, C. J. Harper, R. Bau, R. C. Stevens, J. F. Haw, E. Munson, *Science*. **1995**, *267*, 362–367.
4. R. H. Baughman, *Science.* **2006**, *312*, 1009–1010.
5. R.R. Tykwinski, *Chem. Rec.* **2015**, *15*, 1060–1074.
6. W. Xu, E. Leary, S. Hou, S. Sangtarash, M. T. González, G. Rubio-Bollinger, Q. Wu, H. Sadeghi, L. Tejerina, K. E. Christensen, N. Agraït, S. J. Higgins, C. J. Lambert, R. J. Nichols, H. L. Anderson, *Angew. Chem. Int. Ed.* **2019**, *131*, 8466–8470.
7. J. A. Januszewski, R. R. Tykwinksi, *Chem. Soc. Rev*. **2014**, *43*, 3184-3203
8. D. Wendinger, R. R. Tykwinksi, *Acc. Chem. Res*. **2017**, *50*, 1468-1479.
9. L. Leroyer, V. Maraval, R. Chauvin, *Chem. Rev.* **2012**, *112*, 1310–1343.
10 P. Pinter, D. Munz, *J. Phys. Chem. A.* **2020**, *124*, 10100–10110.
11. M. H. Garner, R. Hoffmann, S. Rettrup, G. C. Solomon, *ACS Cent. Sci.* **2018**, *4*, 688–700.
12. K. Brand, *Ber. Dtsch. Chem. Ges. B*. **1921**, *54*, 1987–2006.
13. Z. Berkovitch-Yellin, M. Lahav, L. Leiserowitz, *J. Am. Chem. Soc.* **1974**, *96*, 918–920.
14. P. H. Liu, L. Li, J. A. Webb, Y. Zhang, N. S. Goroff, Org Lett. **2004**, *6*, 2081–2083.
15. H. Irngartinger, W. Götzmann, *Angew. Chem. Int. Ed.* **1986**, *25*, 340–342.
16. E. Weber, W. Seichter, R-J. Wang, T. C. W. Mak, *Bull. Chem. Soc. Jpn.* **1991**, *64*, 659-66717.
17. B. Bildstein, M. Schweiger, H. Kopacka, K. H. Ongania, K. Wurst, *Organometallics* **1998**. *17*, 2414–2424.
18. D. Wu, Y. Li, R. Ganguly, R. Kinjo, *Chem. Commun.* **2014**, *50*, 12378–12381.

19. M. Franz, J. A. Januszewski, D. Wendinger, C. Neiss, L. D. Movsisyan, F. Hampel, H. L. Anderson, A. Görling, R. R. Tykwinski, *Angew. Chem. Int. Ed.* **2015**, *54*, 6645–6649.

20. Y. Li, K. C. Mondal, P. P. Samuel, H. Zhu, C. M. Orben, S. Panneerselvam, B. Dittrich, B. Schwederski, W. Kaim, T. Mondal, D. Koley, H. W. Roesky, *Angew. Chem. Int. Ed.* **2014**, *53*, 4168–4172.

21. L. Jin, M. Melaimi, A. Kostenko, M. Karni, Y. Apeloig, C. E. Moore, A. L. Rheingold, G. Bertrand, *Chem. Sci.* **2016**, *7*, 150–154.

22. R. L. Melen, *Science.* **2019**, *363*, 479–484.

23. P. P. Power, *Nature,* **2010**, *463*, 171–177.

24. M. He, C. Hu, R. Wei, X. F. Wang, L. L. Liu, *Chem. Soc. Rev.* **2024**, *53*, 3896–3951.

25. Y. K. Loh, S. Aldridge, *Angew. Chem. Int. Ed.* **2021***, 60 ,*8626 –8648

26. F. Dielmann, C. E. Moore, A. L. Rheingold, G. Bertrand, *J. Am. Chem. Soc.* **2013**, *135*, 14071–14703.

27. M. Fischer, M. M. D. Roy, L. L. Wales, M. A. Ellwanger, C. McManus, A. F. Roper, A. Heilmann, S. Aldridge, *Angew. Chem. Int. Ed.* **2022**, *61*, e202211616.

28. P. P. Power, *Organometallics*. **2020**, *39*, 4127–4138.

29. C. Weetman, *Chem. Eur. J.* **2021**, *27*, 1941–1954.

30. R. C. Fischer, P. P. Power, *Chem. Rev.* **2010**, *110*, 3877–3923.

31. B. C. Brodie, *Proc. Roy. Soc. (London)*. **1873***, 21*, 245–247.

32. L. H. Reyerson, K. Kobe, *Chem. Rev.* **1930**, *7*, 479–492.

33. O. Diels, B. Wolf, *Ber. Dtsch. Chem. Ges.* **1906**, *39*, 689-697.

34. P. Jensen, J. W. C. Johns, *J. Mol. Spectrosc.* **1986**, *118*, 248-266.

35. J. Koput, *Chem. Phys. Lett.* **2000**, *320*, 237.

36. R. Tonner, G. Frenking, *Chem. Eur. J.* **2008**, *14*, 3260–3272.

37. A. Ellern, T. Drews, K. Seppelt, *Z. anorg. allg. Chem.* **2001**, *627*, 73–76.

38. I. Bernhardi, T. Drews, K. Seppelt, *Angew. Chem. Int. Ed.* **1999**, *38*, 2232–2233.

39. F. Krischer, M. Jorges, T. F. Leung, H. Darmandeh, V. H. Gessner, *Angew. Chem. Int. Ed*. **2023**, *62*, e202309629.

40. T. Wang, Z. Guo, L. E. English, D. W. Stephan, A. R. Jupp, M. Xu, *Angew. Chem. Int. Ed.* **2023**, *63, e202402728*.

41. Q. Le Dé, Y. Zhang, L. Zhao, F. Krischer, K. S. Feichtner, G. Frenking, V. H. Gessner, V. H. *Angew. Chem. Int. Ed.* **2025**, *64*, e202422496.

42. J. M. Goicoechea, H. Grützmacher, *Angew. Chem. Int. Ed.* **2018**, *57*, 16968–16994.

43. C. N. Matthews, G. H. Birum, *Tetrahedron Lett.* **1966**, *7*, 5707–5710.

44. C. N. Matthews, J. S. Driscoll, H.G. Birum, *Chem. Commun.(London).* **1966**, 736–737.

45. C. N. Matthews, G. H. Birum, G. H. *Acc. Chem. Res.* **1969**, *2*, 373-379.

46. R. Bertani, M. Casarin, L. Pandolfo, *Coord. Chem. Rev.* **2003**, *236*, 15–33.

47. L. T. Scharf, V. H. Gessner, *Inorg. Chem.* **2017**, *56*, 8599–8607.

48. H. J. Bestmann, *Angew. Chem. Int. Ed*. *Engl*., **1977**, *16*, 349–364.

49. G. Schmid, H. J. Bestmann, *Tetrahedron Letters*. **1975**, *46*. 4025–4026.

50. R. Schobert, C. Hölzel, *Topics in Heterocyclic Chemistry.* **2007**, *12*, 193-218.

51. A. Brar, D. K. Unruh, N. Ling, C. Krempner, C. *Org. Lett.* **2019**, *21*, 6305–6309.

52. M. Jörges, F. Krischer, V. H. Gessner, *Science.* **2022**, *378*, 1331– 1336.

53. T. Koike, J.-K. Yu, M. M. Hansmann, *Science.* **2024***, 385*, 305–311.

54. R. Wei, X.-F. Wang, D. A. Ruiz, L. L. Liu, *Angew. Chem. Int. Ed.* **2023**, *62*, *e202219211*.

55. X.-F. Wang, R. Wei, Q. Liang, C. Hu, L. L. Liu, *Chem*. **2025**. *11*, 102444.

56. H. -O. Berger, H. Nöth, B. Wrackmeyer B. *J. Organomet. Chem.* **1978**, *145*, 17-20.

57. K. Onuma, K. Suzuki, M. Yamashita, *Chem. Lett.* **2015**, *44*, 405–407.

58. M. J. D. Bosdet, W. E. Piers, *Can. J. Chem.* **2009**, *87*, 8–29.

59. R. Kitamura, K. Suzuki, M. Yamashita, *Chem. Commun.* **2018**, *54*, 5819, 5822.

60. H. Braunschweig, R. D. Dewhurst, K. Hammond, J. Mies, K. Radacki, A. Vargas, *Science.* **2012**, *336*, 1420–1422.

61. J. Böhnke, H. Braunschweig, W. C. Ewing, C. Hörl, T. Kramer, I. Krummenacher, J. Mies, A. Vargas, *Angew. Chem. Int. Ed.* **2014**, *53*, 9082–9085.

62. V. Lavallo, Y. Canac, C. Präsang, B. Donnadieu, G. Bertrand, *Angew. Chem. Int. Ed.* **2005**, *44*, 5705–5709.

63. M. Michel, S. Kar, L. Endres, R. D. Dewhurst, B. Engels, H. Braunschweig, *Nat. Synth.* **2025**, *4*, https://doi.org/10.1038/s44160-025-00763-1.

64 A. K. Day, M. Abdellaoui, M. Soleilhavoup, G. Bertrand, *Chem Catal.* **2024**, *5*, 101159.

65. Y. K. Loh, M. Melaimi, M. Gembicky, D. Munz, G. Bertrand, *Nature.* **2023**, *623*, 66–70.

66. J. Tang, C. Hu, A. E. Crumpton, M. Dietz, D. Sarkar, L. P. Griffin, J. M. Goicoechea, S. Aldridge, *J. Am. Chem. Soc.* **2024**, *146*, 30778−30783.

67. J. Tang, C. Hu, A. E. Crumpton, L. P. Griffin, J. M. Goicoechea, S. Aldridge, *Chem. Sci.* **2024**, *16*, 2231–2237.

68. M. I. Bruce, *Chem. Rev*. **1991**, *91*, 197−257.

69. V. Cadierno, J. Gimeno, *Chem. Rev.* **2009**, *109*, 3512–3560.

70. M. Asay, B. Donnadieu, W. W. Schoeller, G. Bertrand, *Angew. Chem. Int. Ed.* **2009**, *48* 4796–4799.

71. E. O. Fischer, H. J. Kalder, A. Frank, F. H. Köhler, G. Huttner, *Angew. Chem. Int. Ed***. 1976**, *15*, 623–624.

72. H. Berke, *Angew. Chem. Int. Ed***. 1976**, *15*, 624.

73. J. P. Selegue, Organometallics. **1982**, *1,* 217–218.

74. M. H. Hansmann, F. Rominger, A. S. K. Hashmi, *Chem. Sci.* **2013**, *4*, 1552–1559.

75. L. Jin, M. Melaimi, A. Kostenko, M. Karni, Y. Apeloig, C. E. Moore, A. L. Rheingold, G. Bertrand, G. *Chem. Sci.* **2016**, *7*, 150–154.

76. N. Kim, R. A. Widenhoefer, *Angew. Chem. Int. Ed.* **2018**, *57*, 4722–4726.

77. X. S. Xiao, C. Zou, X. Guan, C. Yang, W. Lu, C. Che, *Chem. Commun.* **2016**, *52*, 4983–4986.

78. G. T. Kent, X. Yu, G. Wu, J. Autschbach, T. W. Hayton, *Chem. Sci.* **2021**, *12*, 14383–14388.

79. O. Ordoñez, X. Yu, M. A. Schuerlein, G. Wu, J. Autschbach, T. W. Hayton, *J. Am. Chem. Soc.* **2024**, *146*, 28306−28319

80. S. W. Roh, K. Choi, C. Lee, C. *Chem. Rev.* **2019**, *119*, 4293–4356.

81. H. Werner, R. Wiedemann, M. Laubender, B. Windmüller, P. Steinert, O. Gevert, J. Wolf, *J. Am. Chem. Soc.* **2002**, *124,* 6966–6980.

82. J. Díez, M. P. Gamasa, J. Gimeno, E. Lastra, A. Villar, *Organometallics* **2005**, *24*, 1410–1418.

83. M. Baya, M. L. Buil, M. A. Esteruelas, A. M. López, E. Oñate, J. Ramón Rodríguez, *Organometallics.* **2002**, *21*, 1841–1848.

84. J. Gimeno, V. Cadierno, J. Díez, S. E. García-Garrido, *Chem. Commun.* **2004**, 2716–1717.

85. Y. Nishibayashi, I. Wakiji, M. Hidai, *J. Am. Chem. Soc.* **2000**, *122*, 11019–11020.

86. R. J. Detz, M. M. E. Delville, H. Hiemstra, J. H. Maarseveen, *Angew. Chem. Int. Ed.* **2008**, *47*, 3777–3780.

87. G. Hattori, H. Matsuzawa, Y. Miyake, Y. Nishibayashi, *Angew. Chem. Int. Ed.* **2008**, *47* 3781–3783.

88. X. Sun, X. Duan, N. Zheng, W. Song, *Org. Lett.* **2023**, *25*, 2798–2805.

89. X. Duan, H. Shi, Y. Yue, W. Song, *Chem. Commun.* **2024**, *60*, 3926–3929.

90 Y. Wei, J. Jiang, Y. Jing, Z. Ke, L. Zhang, *Angew. Chem. Int. Ed.* **2024**, *136*, e202402286.

91. O. Guerret, G. Bertrand, *Acc. Chem. Res.* **1997**, *30*, 486–493.

92. P. Löwe, dissertation, Westfälische Wilhelms-Universität Münster, **2022**.

93. M. A. Wünsche, dissertation, Westfälische Wilhelms-Universität Münster, **2018**.

94. M. A. Wünsche, T. Witteler, F. Dielmann, *Angew. Chem. Int. Ed.* **2018**, *57*, 7234–7239.

95. L. Cabrera, G. C. Welch, J. D. Masuda, P. Wei, D. W. Stephan, *Inorganica Chim. Acta*

2006, *359*, 3066–3071.

96. M. H Holthausen, T. Mahdi, C. Schlepphorst, L. J. Hounjet, J. J. Weigand, D. W. Stephan, *Chem. Commun.* **2014**, *50*, 10038–10040.

97. A. Brar, D. K. Unruh, A. J. Aquino, C. Krempner, *Chem. Commun.* **2019**, *55*, 3513–3516.

98. Q.S. Li, J. Zhang, S. Zhang, *Chem. Phys. Lett.* **2005**, *404*, 100–106.

99. S. Grimme, J. Antony, S. Ehrlich, H. Krieg, *J. Chem. Phys.* **2010**, *132*, 154104.

100. F. Weigend, R. Ahlrichs, *Phys. Chem. Chem. Phys.* **2005**, *7*, 3297–3305.

101. P. Löwe, M. A. Wünsche, F. R. S. Purtscher, J. Gamper, T. S. Hofer, L. F. B. Wilm, M. B. Röthel, F. Dielmann, *Chem. Sci.* **2023**, *14*, 7928–7935.

102. H. Grützmacher, H. Pritzkow, *Angew. Chem. Int. Ed.* **1991**, *30*, 709–710.

103. A. Igau, A. Baceiredo, H. Grützmacher, H. Pritzkow, G. Bertrand, *J. Am. Chem. Soc.* **1989**, *111*, 6853–6854.

104. F. Lavigne, E. Maerten, G. Alcaraz, N. Saffon-Merceron, C. Acosta-Silva, V. Branchadell, A. Baceiredo, *J. Am. Chem. Soc.* **2010**, *132*, 8864–8865.

105. S. K. Latypov, F. M. Polyancev, D. G. Yakhvarov, O. G. Sinyashin, *Phys. Chem. Chem. Phys.* **2015**, *17*, 6976–6987.

106. J. A. C. Clyburne, N. McMullen, *Coord. Chem. Rev.* **2000**, *210*, 73–99.

107. E. LaPierre, B. O. Patrick, I. Manners, *J. Am. Chem. Soc.* **2023**, *145*, 7107–7112.

108. M. Fischer, S. Nees, T. Kupfer, J. T. H. Braunschweig, C. Hering-Junghans, *J. Am. Chem. Soc.* **2021**, *143*, 4106–4111.

109. A. García-Romero, C. Hu, M. Pink, J. M. Goicoechea, *J. Am. Chem. Soc.* **2024**. *147*, 1231-1239

110. M. Olaru, D. Duvinage, Y. Naß, L. A. Malaspina, S. Mebs, J. Beckmann, *Angew. Chem. Int. Ed.* **2020**, *59*, 14414–14417.

111. G. Kehr, G. Erker, *Chem. Commun.* **2012**, *48*, 1839–1850.

112. B. Wrackmeyer, K. Horchler, R. Boese, *Angew. Chem. Int. Ed.* **1989**, *2*, 1500–1502.

113. A. Bismuto, G. S. Nichol, F. Duarte, M. J. Cowley, S. P. Thomas, *Angew. Chem. Int. Ed.* **2020**, *59*, 12731–12735.

114. M. Dureen, D. W. Stephan, *J. Am. Chem. Soc.* **2009**, *131*, 8396–8397.

115. A. Fukazawa, H. Yamada, S. Yamaguchi, *Angew. Chem. Int. Ed.* **2008**, *47*, 5582–5585.

116. O. Ekkert, G. Kehr, R. Fröhlich, G. Erker, *J. Am. Chem. Soc.* **2011**, *133*, 4610–4616.

3.6.2 Crystallographic and Computational References

S1. O. V. Dolomanov, L. J. Bourhis, R. J. Gildea, J. A. K. Howard and H. Puschmann, *J. Appl. Crystallogr.* **2009**, 42, 339–341.

S2. G. Sheldrick GM SADABS. University of Göttingen, Göttingen **1996**.

S3. Gaussian 09, Revision D.01, M. J. Frisch, G. W. Trucks, H. B. Schlegel, G. E. Scuseria, M. A. Robb, J. R. Cheeseman, G. Scalmani, V. Barone, B. Mennucci, G. A. Petersson, H. Nakatsuji, M. Caricato, X. Li, H. P. Hratchian, A. F. Izmaylov, J. Bloino, G. Zheng, J. L. Sonnenberg, M. Hada, M. Ehara, K. Toyota, R. Fukuda, J. Hasegawa, M. Ishida, T. Nakajima, Y. Honda, O. Kitao, H. Nakai, T. Vreven, J. A. Montgomery, Jr., J. E. Peralta, F. Ogliaro, M. Bearpark, J. J. Heyd, E. Brothers, K. N. Kudin, V. N. Staroverov, T. Keith, R. Kobayashi, J. Normand, K. Raghavachari, A. Rendell, J. C. Burant, S. S. Iyengar, J. Tomasi, M. Cossi, N. Rega, J. M. Millam, M. Klene, J. E. Knox, J. B. Cross, V. Bakken, C. Adamo, J. Jaramillo, R. Gomperts, R. E. Stratmann, O. Yazyev, A. J. Austin, R. Cammi, C. Pomelli, J. W. Ochterski, R. L. Martin, K. Morokuma, V. G. Zakrzewski, G. A. Voth, P. Salvador, J. J. Dannenberg, S. Dapprich, A. D. Daniels, O. Farkas, J. B. Foresman, J. V. Ortiz, J. Cioslowski, and D. J. Fox, Gaussian, Inc., Wallingford CT, **2013**.

S4. Q. S. Li, J. Zhang, S. Zhang, Chem. Phys. Lett. **2005**, *404*, 100–106; (b) S. Grimme, J. Antony, S. Ehrlich, H. Krieg, J. Chem. Phys. **2010**, *132*, 154104.

S5. F. Weigend and R. Ahlrichs, Phys. Chem. Chem. Phys., **2005**, *7*, 3297–3305.

S6. S. K. Latypov, F. M. Polyancev, D. G. Yakhvarov, O. G. Sinyashin Phys. Chem. Chem. Phys., **2015**, *17*, 6976- 6987.

Chapter Three: Isolation, Characterization and Reactivity of an Allenylidene Phosphonium Cation

Some content in this chapter has been published:

L. C. Torres, P. Löwe, A. Bhattacharjee, M. B. Röthel, M. Seidl, J. LeBlanc, K. Wurst, F. Dielmann, C. B. Caputo, *Angew. Chem. Int. Ed.* 2025. DOI: 10.1002/anie.202502201.

 Additional supporting information is available online. Conceptualization of the project was by Christopher Caputo, Fabian Dielmann, Pawel Löwe, and the primary author. Pawel's expertise and mentorship was important to the design and execution of critical experiments. Assistance with synthetic preparation of N-heterocyclic imine precursors was provided by Maike Röthel. Computations were performed by Avik Bhattacharjee. SCXRD data collection and solving was performed by Michael Seidl, Jesse LeBlanc, and Klaus Wurst. Avik Bhattacharjee, Pawel Löwe, Fabian Dielmann and Christopher Caputo made contributions to the writing of the manuscript. Pawel Löwe adapted the article into a German version, which is also available to view on *Angewandte Chemie.* I am indebted to all my co-authors, and incredibly grateful for the opportunity to work with them, and for their contributions.

3.1 Introduction

3.1.1 N-Heterocyclic Carbenoid Derived Substituents

Recently, the framework NHE=Y (Y = p-block element, NHE = N-heterocyclic carbenoid) has emerged as a new category of substituents which are particularly effective for facilitating the isolation of low-coordinate or unsaturated main-group compounds, as well as electron deficient metal centers (Scheme 3-1). Notable examples belonging to this substituent class include the previously introduced NHI **3-A**,[1] as well as the N-heterocyclic olefin (NHO) **3-B**,[2] N-heterocyclic boryloxy (NHBO) **3-C**,[3] and N-heterocyclic carbene phosphinidine (NHCP) **3-D**.[4,5,6] From the prospective of electronics, NHE=Y analogs are π-donor substituents, which is more apparent for imino- (**3-A**), olefinic- (**3-B**), or phosphinidino- (**3-D**) groups when represented with an ylidic canonical form which places negative charge and two sets of lone pairs on the exocyclic atom (Scheme 3-2). A key characteristic of this general substituent platform is its electronic and steric modularity. Electronic properties can be fine-tuned by alteration of the heterocyclic (NHE) component. To simplify with an example, NHIs derived from electron rich unsaturated NHCs have been shown to consequently yield stronger π-donors than their saturated analogs.[7,8] In essence, the NHE=Y substituents inherit the electronic properties of its NHE component. Another advantage of the substituent design is that steric properties can be tuned by modifying the groups bound to their heterocyclic nitrogen atoms. [1] In this way, both electronics and sterics can be altered to meet the precise demands necessary to isolate a desired reactive species.

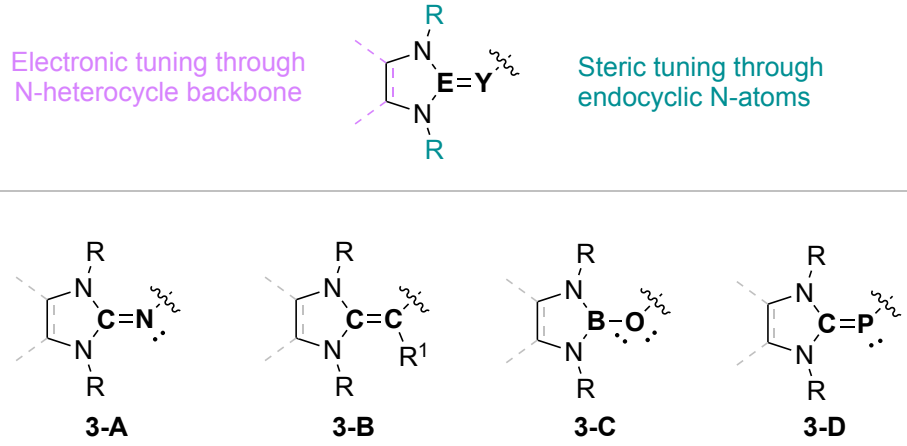

Scheme 3-1: General NHE=Y substituent framework with selected examples.

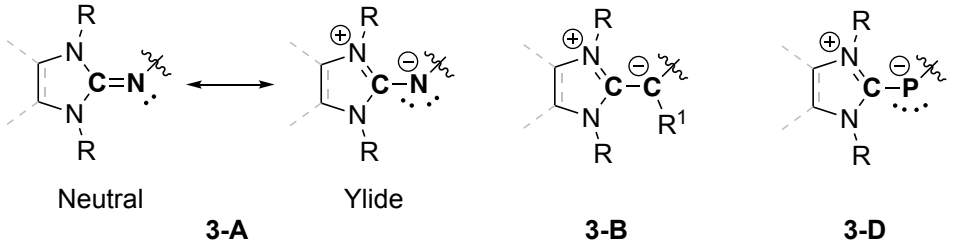

Scheme 3-2: Neutral vs ylide canonical forms for **3-A**, and the ylidic forms for **3-B** and **3-D**.

Major electronic differences exist between the **3-A** – **3-D** substituent groups, which are delineated by the nature of the exocyclic atom (Y). For example, despite being π-donors, **3-A** and **3-C** have varying degrees of σ-electron withdrawing character due to their exocyclic atom being electronegative (N and O, respectively).[3] At the time of writing this thesis, a review has been published by Zhong comparing the electronics and applications of NHIs, NHOs, and NHCPs, which can be referred to for a detailed explanation of their differences.[9]

3.1.2 Trigonal Planar Phosphorus Cations Stabilized by NHIs

The synthesis of TPPCs has benefited immensely from the advent of NHE=Y type substituents. In particular, imino groups (**3-A**) have shown to be critical for uncovering new planar cationic phosphonium species $[R_2P{=}E]^+$, enabling their preparation on scales amenable for systematic studies of their structure and reactivity. The use of NHI substituents in phosphorus chemistry dates to 1996 with seminal work from Kuhn, preparing the first NHI substituted phosphine **3-E** (Scheme 3-3). [10] The group's methodology installs the imine to the phosphorus center by an elimination reaction, thermodynamically driven by loss of Me_3SiCl. This strategy has become staple for making (NHI)-P compounds, intentionally avoiding the use of any harsh organometallic bases which can lead to undesired side reactions or introduce salt contaminants.[11] The NHI motif would reappear around 15 years later, utilized by the Bertrand group to stabilize various low-coordinate phosphorus species, including a phosphinyl radical **3-F** [12] and phosphinonitrene **3-G**,[13] both employing a bis(imine) framework. **3-F** and **3-G** leverage one of the bulkiest NHI derivatives available, the 1,3-bisdiisopropylphenylimidazolidine-2-ylidenamino (NsIDipp) group, which is used when maximal steric protection is desired.

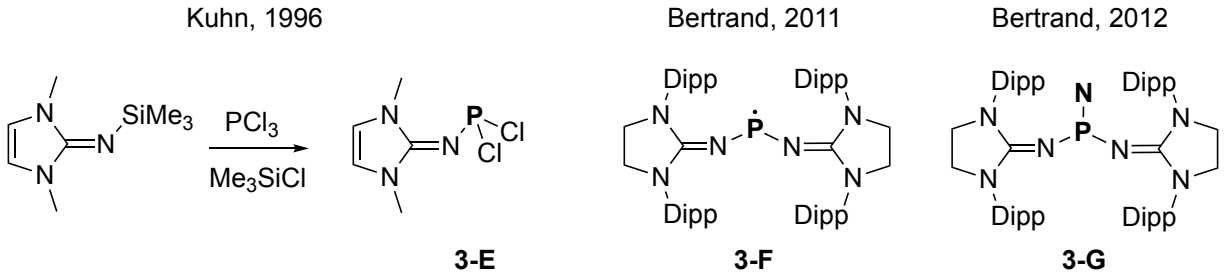

Scheme 3-3: Synthesis of the first NHI substituted phosphine **3-E** by Me_3SiCl elimination. Phosphinyl radical **3-F** and phosphinonitrene **3-G**.

NsIDipp substituents would be exploited by the same group to prepare the first iminophosphonium cations $[R_2P{=}N\text{-}R^1]^+$ [**3-H**]$^+$ (R^1 = H, CH_3) (Scheme 3-4). [14] Dielmann and co-workers would later isolate chalcogenophosphonium cations $[R_2P{=}Ch]^+$ (Ch = O; [**3-I**]$^+$ [15] Ch = S; [**3-J**]$^+$ [16]) using 1,3-bisdiisopropylphenylimidazolin-2-ylidenamino (NIDipp) substituents, a more electron rich version of NsIDipp, which is preferentially chosen for more electron deficient targets. Dielmann also debuted terminal methylene phosphonium cations $[R_2P{=}CH_2]^+$, prepared with either NIDipp ([**3-K**$^{\mathbf{NIDipp}}$]$^+$) or 1,3-ditertbutyimidazolidine-2-ylidenamino (NsI*t*Bu) substituents ([**3-K**$^{\mathbf{NsI}t\mathbf{Bu}}$]$^+$). [17] NHI substituents thermodynamically stabilize these species by functioning as intramolecular π-electron donors, which tempers the acidity of their low-lying P-centered acceptor orbitals.

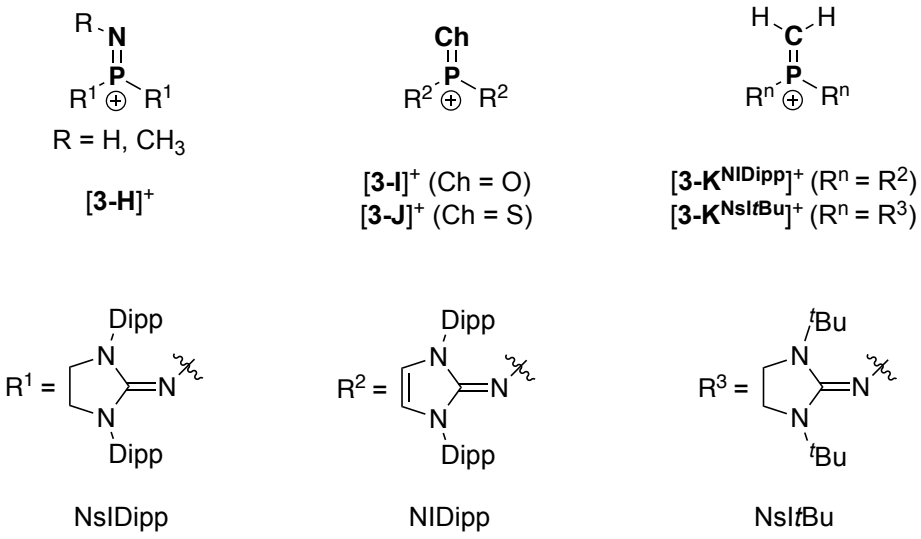

Scheme 3-4: Trigonal planar phosphonium cations stabilized by NHIs.

Similarly, planar phosphorandylium dications $[R_3P]^{2+}$ [**3-L**]$^{+}$, were also shown to be isolable with NHI substituents, including with 1,3-diisopropyl-4,5-dimethylimidazolin-2-ylidenamino (NI(Me)*i*Pr) and 1,3-diisopropylbenzimidazolin-2-imine (NI(Benz)*i*Pr) groups (Scheme 3-5).[7] As $[R_3P]^{2+}$ species are isoelectronic to tertiary carbenium cations, silylium cations, boranes, and alanes, their most obvious chemical property is their electrophilicity. In this respect, Dielmann showed that the Lewis acid character of $[R_3P]^{2+}$ species is tunable by use of different NHIs. [**3-L$^{NI(Benz)iPr)}$**]$^{2+}$, based on a more electron deficient benzannulated NHC, is consequently a stronger Lewis acid than [**3-L$^{NI(Me)iPr)}$**]$^{2+}$ derived from an electron rich methylated NHC.

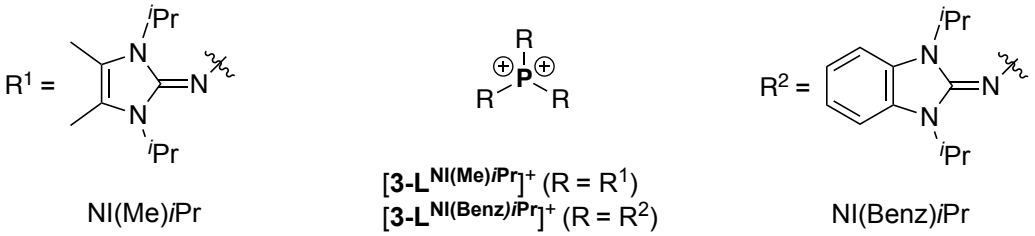

Scheme 3-5: Phosphorandylium dications stabilized by NHIs.

While the application of NHIs in TPPCs and phosphorandylium dications is now well described, olefinic substituents (**3-B**) have only been investigated sparingly. Dielmann and co-workers showed that oxophosphonium species $[R_2P{=}O]^{+}$ can not only be prepared with two NHI substituents ([**3-I**]$^{+}$), but also with a combination of NHI and NHO substituents ([**3-M**]$^{+}$) (Scheme 3-6).[15] When compared to NHIs, NHOs have weaker π-donor capacity, but simultaneously have less σ-withdrawing character as the exocyclic substituent atom (C) is less electronegative. The mixed imino-olefin-oxophosphonium salt [**3-M**]$^{+}$ was experimentally and computationally shown to be considerably less electrophilic than the bis(imino)oxophosphonium [**3-I**]$^{+}$. This suggests that when directly comparing the influence of NHIs and NHO substitution in TPPCs, NHOs can be considered superior from the perspective of providing thermodynamic stability. However, this increased stability comes along with a trade-off in that their reactivity in subsequent chemistry with unsaturated substrates or small molecules is consequently diminished, hence the infrequent use of NHOs.[18,19] A delicate balance of stability and reactivity is optimal. Along this note, when choosing an NHE=Y substituent to isolate a TPPC, the steric profile should be highly considered.

"Over protection" by using the bulkiest available substituent will be advantageous for isolation but disadvantageous when exploring subsequent chemistry.

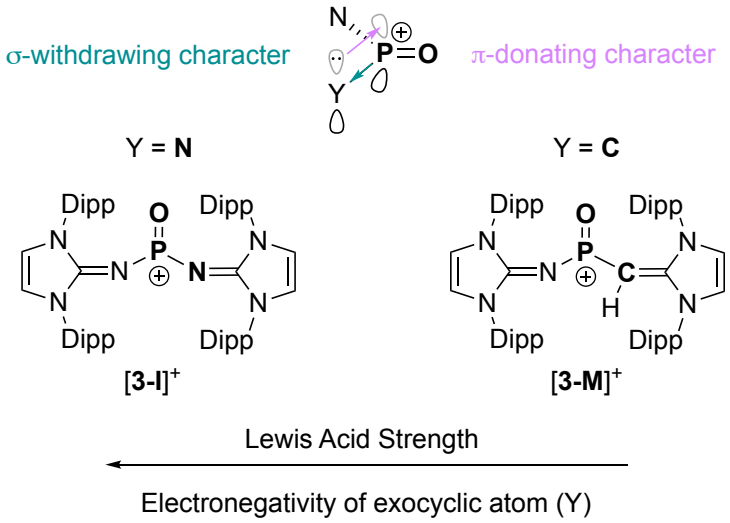

Scheme 3-6: Bis(imino)oxophosphonium [**3-I**]$^+$, versus (imino)(olefin)oxophosphonium [**3-M**]$^+$.

To date, no examples of trigonal planar phosphorus cations have been reported utilizing boryloxy **3-C** or carbene phosphinidine **3-D** substituents, as both platforms have only recently been explored in the context of supporting main group centers. The literature suggests that boryloxy- substituents (**3-C**) are better suited towards the isolation of neutral or anionic low coordinate centers that can benefit from both π-electron donation and strong σ-electron withdrawing effects.[3,20,21,22,23] Phosphinidino- (**3-A^{NHCP}**) substituents have shown useful in the isolation of heavy element (Ge, Sn, Pb etc.) main group systems, as the exocyclic P atom can more efficiently interact with its adjacent element due to a closer approximation of orbital size. [6,24,25,26] As it stands, NHIs are the *de-facto* substituent motif to affect the isolation of planarized phosphorus cations.

3.2 Chapter Objectives: Leveraging NHIs to Isolate Allenylidene Phosphonium

Ong and Frenking showed that a bis(imino)phosphenium cation [**3-N**]$^+$ derived from NIDipp groups can be functionalized with an ethynyl Grignard reagent *via* salt metathesis.[27] The *in situ* generated alkynyl phosphine **3-O** was used to prepare the first isolable phosphonioacetylide **3-P** (Scheme 3-7). We thought that in an analogous way, γ-methoxy alkynes (**2-1^{Ph}**, **2-1^{Fl}**, **2-1^{Sub}**, or **2-1^{Me}** from Chapter 2) and bis(imino)phosphenium cations like [**3-N**]$^+$ could be used to prepare bis(imino)alkynyl phosphines $R_2P–C{\equiv}C–C(OCH_3)Ar_2$ (R = NHI).[28] Given that decoration of phosphorus atoms with bulky π-donating groups has been key to the isolation of various $[R_2P{=}E]^+$ compounds, these bis(imino)alkynyl phosphines would be promising precursor candidates to affect the isolation of allenylidene phosphonium cations $[R_2P{=}C{=}C{=}CAr_2]^+$.

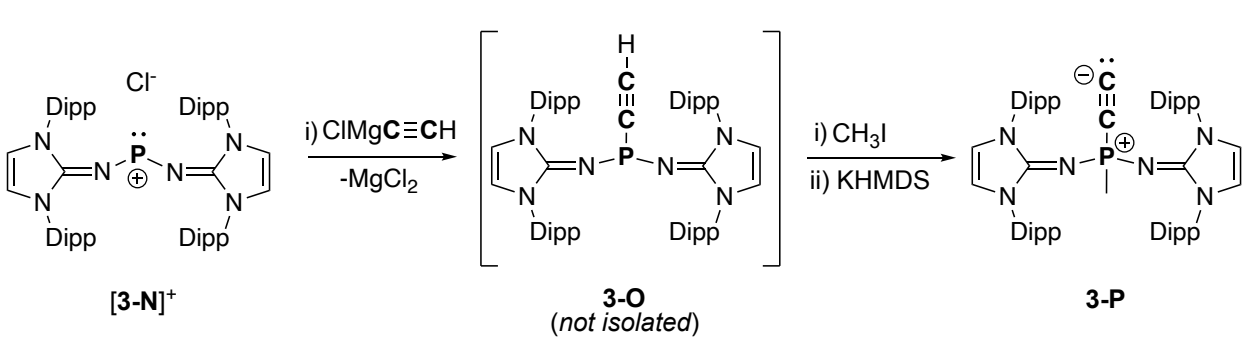

Scheme 3-7: Generation of an alkynyl phosphine **3-O**, by salt metathesis with ethynyl magnesium chloride and phosphenium chloride [**3-N**][Cl]. Subsequent alkylation and deprotonation of phosphine **3-O** to give phosphonioacetylide **3-P**.

3.3 Results and Discussion

3.3.1 Synthesis of an Allenylidene Phosphonium Cation

Bis(imino)alkynyl phosphine **3-1^{a}** based on NIDipp substituents, was targeted as a possible precursor to access the allenylidene phosphonium cation. We opted to terminate alkynyl phosphine **3-1^{a}** with a fluorenyl scaffold expecting that this motif would offer additional stabilization to the target $[R_2P{=}C{=}C{=}CAr_2]^+$ cation on account of extending the π-system. Compound **3-1^{a}** was readily prepared in a reaction of 9-ethynyl-9-methoxy-9*H*-fluorene **2-1^{Fl}** with *n*-BuLi at -78 °C, with the subsequent addition of the phosphenium chloride [**3-N**][Cl] (Scheme 3-6).[17,27] Compound **3-1^{a}** was isolated in a yield of 58 % and crystallized from a concentrated *n*-hexane solution. The phosphine shows a singlet at δ = 51.9 ppm in the ^{31}P NMR spectrum, consistent with previously reported NHI-substituted phosphines. The $^{13}C\{^1H\}$ NMR resonances corresponding to the α, β, and γ carbons of **3-1^{a}** were identified as features at δ = 94.9 ppm ($^1J_{PC}$ = 65 Hz), 92.0 ppm ($^2J_{PC}$ = 8 Hz), and 81.2 ppm ($^3J_{PC}$ = 2 Hz), respectively. Phosphine **3-1^{a}** is extremely sensitive towards moisture and oxygen. The high Lewis basicity of **3-1^{a}** results in decomposition in halogenated solvents, as well as in acetonitrile. A SCXRD study indicated that **3-1^{a}** has an expected pyramidalized geometry at the N_2PC unit (sum of angles: 298°) and exhibits a considerable degree of steric crowding around the P center (Figure 3-1). The P–C1 bond length in **3-1^{a}** is 1.810(3) Å, is in the range for a P–C single bond and consistent with other previously reported alkynyl phosphines.[28,29,30] The C1–C2 bond is 1.217(4) Å, consistent with a C–C triple bond, while the C2–C3 bond length agrees with a C*sp*–C*sp*^{3} single bond (1.484(4) Å).

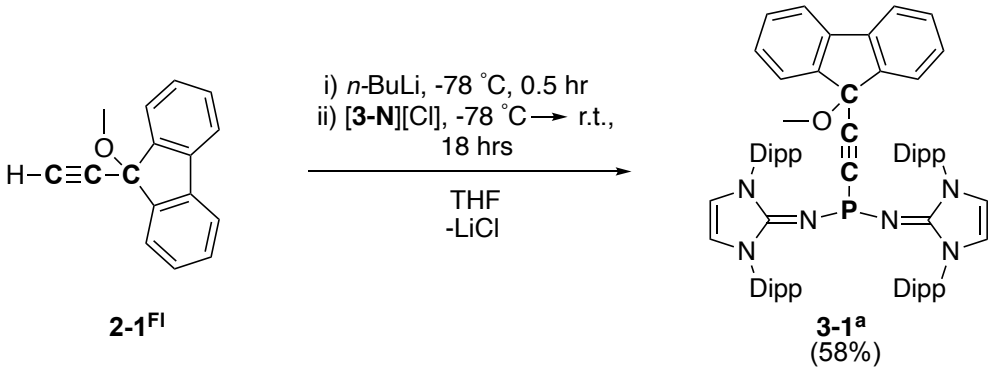

2-1^{Fl} **3-1^{a}** (58%)

Scheme 3-8: Synthesis of bis(imino)alkynyl phosphine **3-1^{a}**.

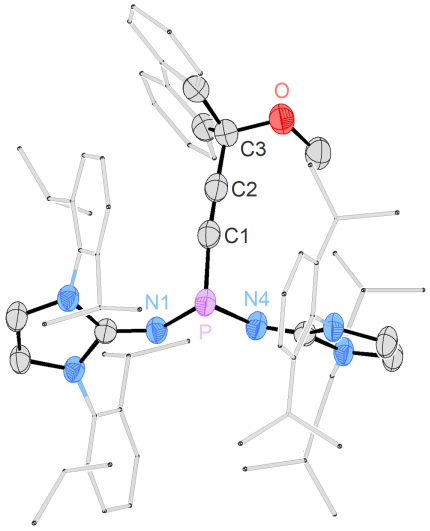

Figure 3-1: Solid-state structure of **3-1**[a]. Thermal ellipsoids are shown at 50 % probability. For clarity, hydrogen atoms are omitted. The Dipp groups and fluorenyl motifs are shown in wireframe. Selected atomic distances [Å] and angles [°]: P–C1 1.810(3), P–N1 1.673(2), P–N4 1.689(2), C1–C2 1.217(4), C2–C3 1.484(4), C3–O 1.436(4), N1–P–C1 104.75(12), N4–P–C1 96.23(12), N1–P–N4 96.75(11).

We also attempted to prepare **3-1**[b], a bis(imino)alkynyl phosphine derived from NsI^{t}Bu, a less sterically demanding and less electron rich N-heterocyclic imine substituent. The synthesis of **3-1**[b] proved to be challenging, as the phosphenium chloride reagent [(NsI^{t}Bu^2)$_2$P][Cl][31] had poor compatibility with the reaction conditions previously utilized to prepare **3-1**[a]. Addition of the *in situ* generated lithium acetylide [Li][**2-1**^{Fl}] to [(NsI^{t}Bu^2)$_2$P][Cl] would reproducibly give intense dark blue-purple reaction mixtures, potentially implicating the formation of radical species as undesired products. Potassium bis(trimethylsilyl)amide (KHMDS), sodium hydride (NaH), and isopropylmagnesium chloride (^{i}PrMgCl) were investigated as alternative bases to deprotonate **2-1**^{Fl} and affect the subsequent metathesis reaction to give **3-1**[b], with ^{i}PrMgCl providing the most promising results. Unfortunately, when using sub- or stoichiometric amounts of ^{i}PrMgCl, **3-1**[b] was always accompanied by trace alkyne **2-1**^{Fl}. When using a slight excess of ^{i}PrMgCl, the formation of **3-1**[b] was accompanied by an alkyl phosphine (NsI^{t}Bu^2)$_2$P^{i}Pr, formed by direct salt metathesis of the Grignard reagent to phosphenium chloride [(NsI^{t}Bu^2)$_2$P][Cl]. In either case, subsequent purification of **3-1**[b] *via* extraction was not successful. Crystals of **3-1**[b] were obtained from a pentane solution after extracting a crude reaction mixture of **3-1**[b], but the reaction and crystallization conditions could not be replicated on scales amenable for investigating its

subsequent reactivity. Nonetheless, solid-state structural details of **3-1^{b}** were obtained and indicate that the steric environment around the phosphorus center is considerably less crowded when compared to **3-1^{a}**, which is made evident through space fill modelling (Figure 3-2).

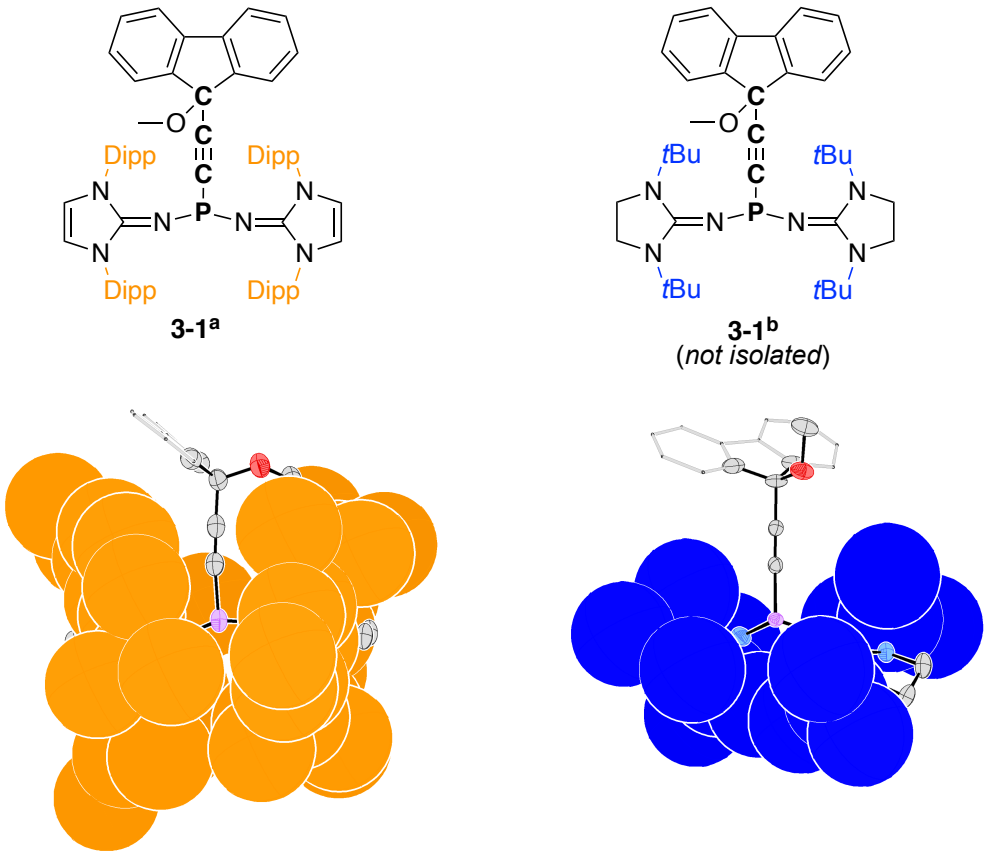

Figure 3-2: Bis(imino)alkynyl phosphines **3-1^{a}** and **3-1^{b}** with accompanying solid-state structures. Hydrogen atoms are omitted for clarity and the fluorenyl motifs are shown in wireframe. Carbon atoms of Dipp (orange) and *t*Bu (blue) are depicted in the space filling model (spheres corresponding to their 1.7-fold Van der Waals radius). Ellipsoids are drawn at 50 % probability.

The allenylidene phosphonium cation [**3-2**]$^{+}$ was prepared by CH_3O^- anion abstraction from **3-1^{a}** using the borate ester $B(OC_6F_5)_3$ (Scheme 3-7).[32] Carrying out this reaction in either pentanes or *n*-hexane instantaneously resulted in the precipitation of a bright red solid, which was subsequently characterized by multinuclear NMR spectroscopy at -20 °C (Note: low temperature characterization was undertaken as NMR experiments at room temperature suggested [**3-2**]$^{+}$ undergoes a subsequent transformation (*vide infra*)). The main feature of the NMR spectra of [**3-2**]$^{+}$ are the ^{13}C resonances corresponding to the α, β, and γ cumulene carbons, which show doublets

at $\delta = 99.1$ ppm ($^1J_{PC}$ = 263 Hz), 161.9 ppm ($^2J_{PC}$ = 34 Hz), and 94.6 ppm ($^3J_{PC}$ = 31 Hz), respectively. Compared to **3-1**^{a}, the J_{PC} coupling constants for α–γ are all roughly one order of magnitude larger, consistent with a change in oxidation state from P(III) to P(V), as well as an increase in s-orbital character of the phosphorus-carbon bond in [**3-2**]$^{+}$.

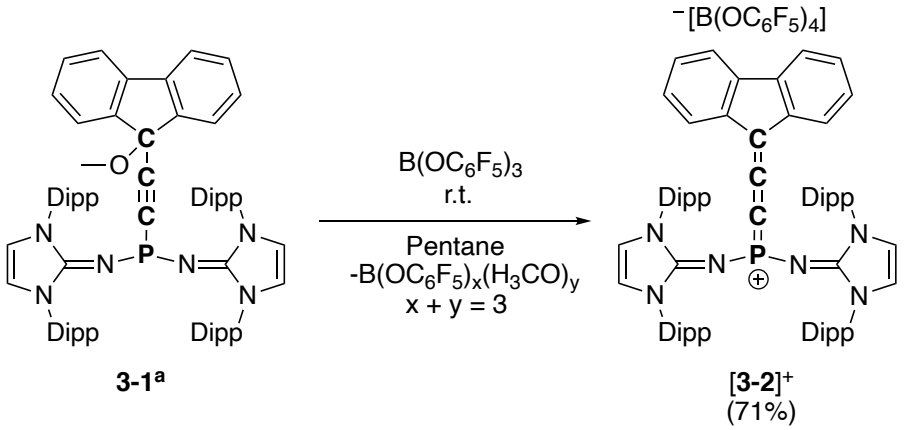

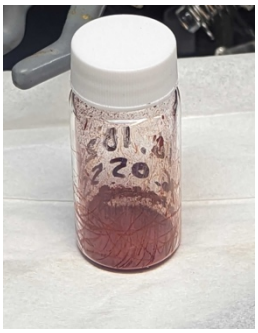

Scheme 3-9: Synthesis of allenylidene phosphonium salt [**3-2**][$B(OC_6F_5)_4$].

Despite a change in oxidation state, the ^{31}P NMR chemical shift of [**3-2**]$^{+}$ ($\delta = 43.9$ ppm) is only shifted slightly to lower frequencies relative to phosphine **3-1**^{a}.[14,16,17,33] Interestingly, heteronuclear NMR experiments suggested the identity of the anion to be $[B(OC_6F_5)_4]^-$, evidenced by a sharp signal at $\delta = 1.6$ ppm in the ^{11}B NMR spectrum, and three distinct resonances observed in the ^{19}F NMR spectrum (δ = -156.9, -167.9, and -171.2 ppm). While the reaction of **3-1**^{a} and $B(OC_6F_5)_3$ was anticipated to give [**3-2**]$^{+}$ paired with a methoxy-borate $[H_3CO–B(OC_6F_5)_3]^-$ counterion, the exclusive presence of $[B(OC_6F_5)_4]^-$ implies that substituent redistribution occurs

during the reaction, liberating neutral borate esters with the form ($B(OC_6F_5)_x(H_3CO)_y$) (x + y = 3).[34,35,36] After purification by washing with pentane or hexanes, [**3-2**][$B(OC_6F_5)_4$] was obtained in yields up to 71%. The isolation of [**2**]$^+$ was also initially attempted with other CH_3O^- abstracting agents, including TMSOTf, and $Al(C_6F_5)_3$, but such reactions either gave the target cation with poorly defined anionic components, or were unselective. $B(C_6F_5)_3$ could also cleanly afford [**3-2**]$^+$, but was accompanied by the anion [$H_3CO–B(C_6F_5)_3$]$^-$. The high symmetry of the [$B(OC_6F_5)_4$] anion provides easily interpretable heteronuclear NMR handles (^{11}B, ^{13}C and ^{19}F). Storing a CH_2Cl_2/pentane solution of [**3-2**][$B(OC_6F_5)_4$] at -40 ºC afforded crystals suitable for a SCXRD study (Figure 3-3). In the molecular structure, the phosphorus atom has a planar coordination environment (sum of angles: 360°). The formulation of the anion was confirmed to be [$B(OC_6F_5)_4$]$^-$ and is well separated from the cationic component.

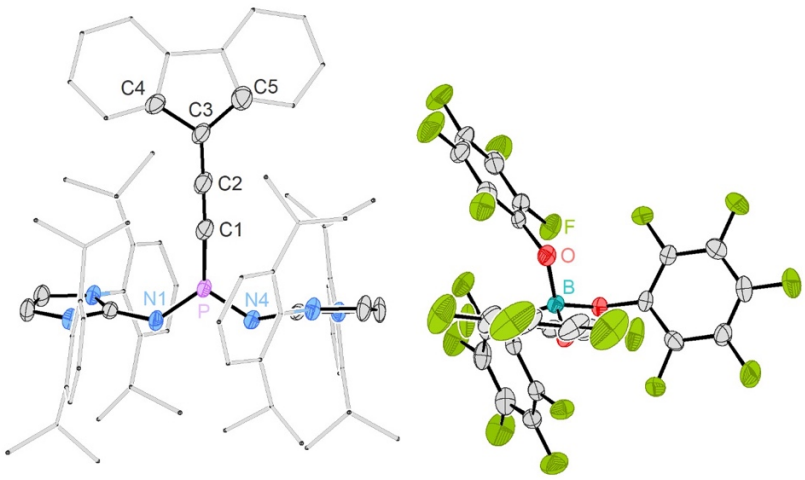

Figure 3-3: Solid-state structure of [**3-2**][$B(OC_6F_5)_4$]. In all cases, thermal ellipsoids are shown at 50 % probability. For clarity, hydrogen atoms are omitted. The Dipp groups and fluorenyl motifs are shown in wireframe. Selected atomic distances [Å] and angles [°]: [**3-2**][$B(OC_6F_5)_4$]: P–C1 1.624(4), C1–C2 1.252(5), C2–C3 1.332(5), P–N1 1.560(3), P–N4 1.557(3), P–C1–C2 170.3(4), C1–C2–C3 179.3(4), N1–P–N4 112.55(15), N1–P–C1 123.78(17), N4–P–C1 123.37(17), C2–C3–C4 125.3(4), C2–C3–C5 127.7(3), C4–C3–C5 106.5.

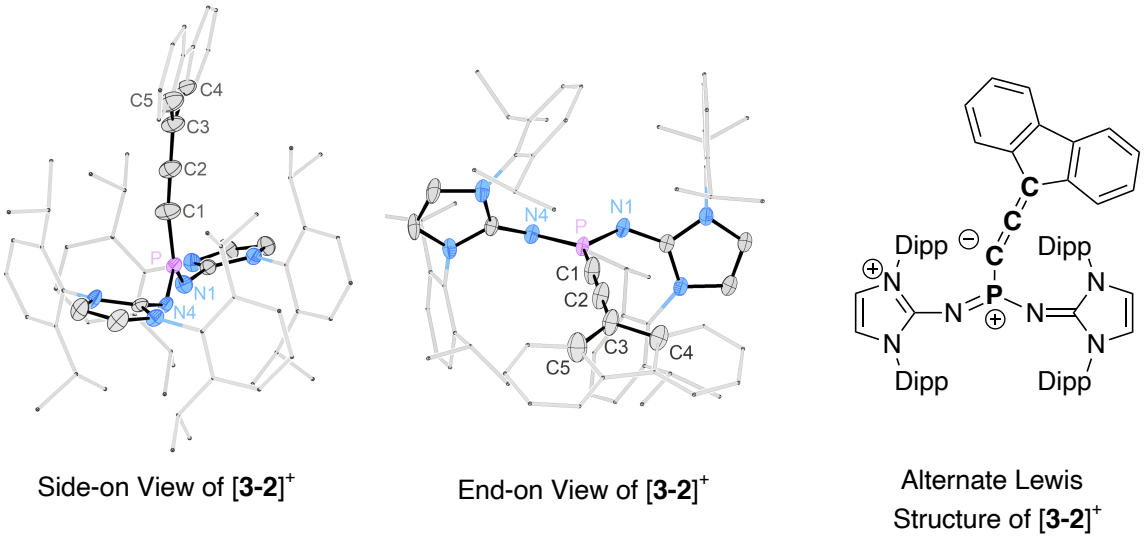

Figure 3-4: Side-on (left) and end-on (centre) perspectives of [**3-2**]$^+$, with the $[B(OC_6F_5)_4]^-$anion omitted. Alternate Lewis structure depiction of [**3-2**]$^+$ (right).

The cation [**3-2**]$^+$ deviates slightly from the ideal linearity of a [3]cumulene, with bending about the P terminus (∠P–C1–C2 angle of 170.3°), made evident in a side-on depiction (Figure 3-4). Bending of [**3-2**]$^+$ may be rationalized by representing the compound with an extreme Lewis structure representation which places a formal negative charge at C1 (Figure 3-4). As seen in the end on view, the phosphorus-bound NIDipp substituents and terminal carbon-bound aryl rings are nearly co-planar, with a measured N1–N4–C4–C5 twist angle of 7.9 °. The P–C1 bond distance of 1.624(4) Å is relatively short for a methylene phosphonium analog,[37,38,39] and comparable in length to the P–C bond of the NHI substituted terminal methylene phosphonium ions [**3-K^{NsItBu}**]$^+$ (1.621(5) Å) and [**3-K^{NIDipp}**]$^+$ (1.619(3) Å) previously prepared by Dielmann.[17] The C1–C2 distance of [**3-2**]$^+$ is 1.252(5) Å, which is short for a C–C double bond but typical for the C*sp*–C*sp* bond of [3]cumulenes.[40,41,42] The C2–C3 bond length is 1.332(5) Å which agrees with a typical terminal cumulene C*sp*–C*sp*^{2} double bond. The P–N bonds (average distance of 1.559 Å) are in the range of P–N double bonds (1.50–1.60Å), which reflects strong π-donation from the exocyclic nitrogen atom of the NHI substituents to the phosphorus atom.[14,15] Bond lengths of **3-1^a**, [**3-2**]$^+$, [**3-K^{NIDipp}**]$^+$ [17] and fluorenylidene [3]cumulene **3-Q** [42] are summarized in Scheme 3-10.

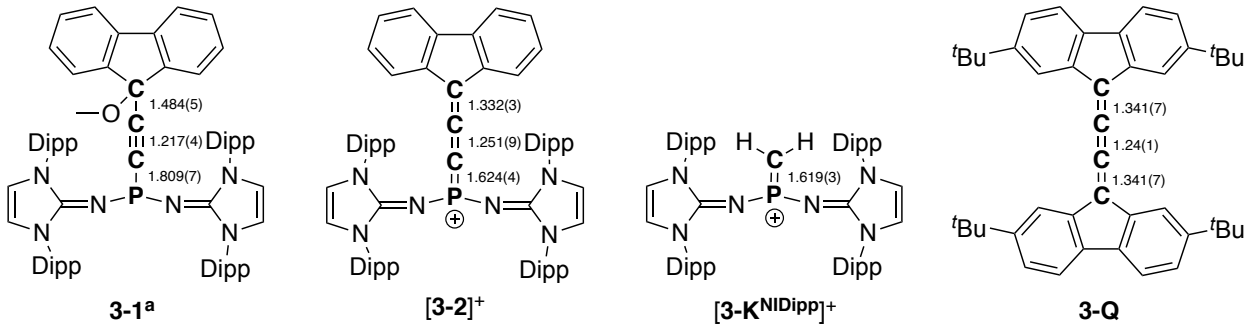

Scheme 3-10: Comparison of the solid-state bond lengths of phosphine **3-1**[a], allenylidene phosphonium [**3-2**]$^+$, methylene phosphonium [**3-K**$^{\mathbf{NIDipp}}$]$^+$ and fluorenylidene cumulene **3-Q.**

3.3.2 Electronic Structure of Allenylidene Phosphonium Cation [3-2]$^+$,

To gain insight into the electronic structure of [**3-2**]$^+$, UV-vis spectroscopy was undertaken. In CH_2Cl_2, this compound showed a high intensity band at λ = 483 nm (ε = 18500 M^{-1} cm^{-1}) and a lower intensity band at λ = 407 nm (ε = 12150 M^{-1} cm^{-1}). The λ_{max} absorption of [**3-2**]$^+$ is red-shifted relative to tetraphenylbutatriene **2-C** (λ_{max} at 420 nm).[40] TD-DFT calculations (B3LYP/6-311+G(d)) were in excellent agreement with the experimental UV-vis, simulating an absorption spectrum centered at 478 nm, corresponding to a HOMO-LUMO transition (Figure 3-5).

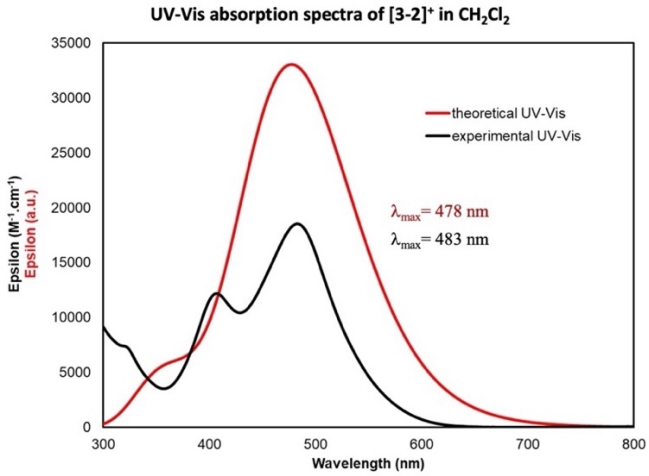

Figure 3-5: Experimental (black, 5E-5 M in CH_2Cl_2) and simulated (red, using SMD for CH_2Cl_2) UV-vis spectra of [**3-2**]$^+$.

The IR spectrum showed a distinct band at 1983 cm^{-1} for [**3-2**]$^+$ that falls between the range of C=C and C≡C bonds, suggesting this feature corresponds to the C*sp*–C*sp* bond. Computational simulation on a truncated model for [**3-2**]$^+$ produced a stretching vibration at 2085 cm^{-1} for the C*sp*–C*sp* bond, confirming our experimental assignment. The redox behavior of [3]cumulenes has been established in the literature.[13] Tykwinski and co-workers showed that a sterically encumbered tetraaryl [3]cumulene shows two reversible oxidation events, and one reversible reduction event.[43] Moreover, Bertrand and Roesky were able to chemically prepare both singly and doubly oxidized [3]cumulene species (see Section 2.1.2).[44,45] We observe at least one irreversible reduction and one irreversible oxidation event for [**3-2**]$^+$ in cyclic voltammetry at -

0.75 V and +0.62 V, respectively vs Ag/AgCl. As these features were not reversible, no attempts were made to chemically oxidize or reduce [**3-2**]$^+$.

For a more comprehensive understanding of the electronic structure of [**3-2**]$^+$, DFT calculations were performed at the B3LYP-D3BJ/def2-TZVP level of theory.[46,47,48] The optimized geometry of [**3-2**]$^+$ was found to be in excellent agreement with the solid-state structure. These calculations revealed that the HOMO encompasses the P–C1 and C2–C3 π-bonding orbitals, as well as the delocalized π-system of the fluorenylidene entity (Figure 3-6). Additionally in the HOMO, the exocyclic nitrogen atom from each NHI substituent has an orbital with *p*-type symmetry, which is directly aligned with the rest of the π-system. The HOMO-2 corresponds to the orthogonal C1–C2 π-bonding combination and to the π-system of the NHI substituents. The LUMO picture corresponds to π* orbitals along P–C1, C2–C3 and N–P bonds. C–C π* orbitals in the fluorenyl group are also represented in the LUMO depiction. The antibonding combination for C1–C2 is represented as a π* orbital in the LUMO+1 (not shown). Collectively, these contributions indicate a fully conjugated system which extends to include the substituents at the carbon and phosphorus termini. Extended conjugation in [**3-2**]$^+$ presumably gives close convergence of the HOMO and LUMO energies, indicated by a small singlet-triplet gap of 2.87 eV, which is a crude indication of facile reactivity.

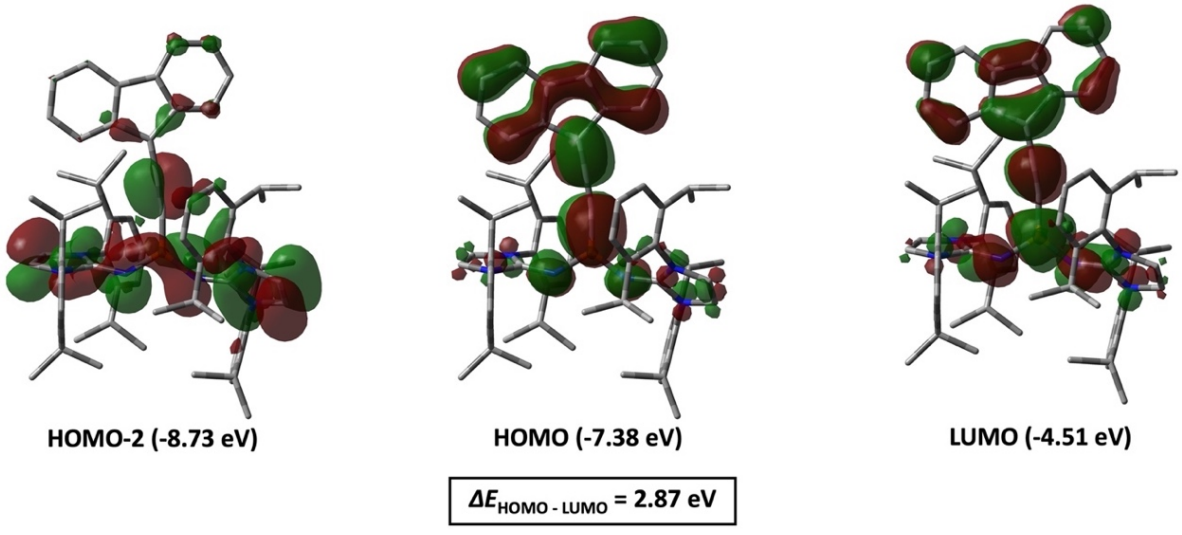

Figure 3-6: Selected molecular orbitals of [**3-2**]$^+$ calculated at B3LYP-D3BJ/def2-TZVP level of theory, isovalue = 0.02

Mayer bond orders for P–C1 (1.58), C1–C2 (2.01), and C2–C3 (1.39) indicate significant double bond character along the P–C–C–C motif, especially with respect to the C1–C2 unit. (Figure 3-7). Hirshfeld charges analyses revealed that the P atom (+0.41) is the most electrophilic site in [**3-2**]$^+$ and the α-carbon carries a negative charge (-0.15), suggesting a polarized $P^{\delta+}$–$C^{\delta-}$ bond. The β-carbon (+0.03) and γ-carbon (-0.01) are nearly neutral. The electrostatic potential map illustrates that [**3-2**]$^+$ is polarized with respect to the entire molecule, showing an electron-depleted P terminus, and an electron-rich C terminus.

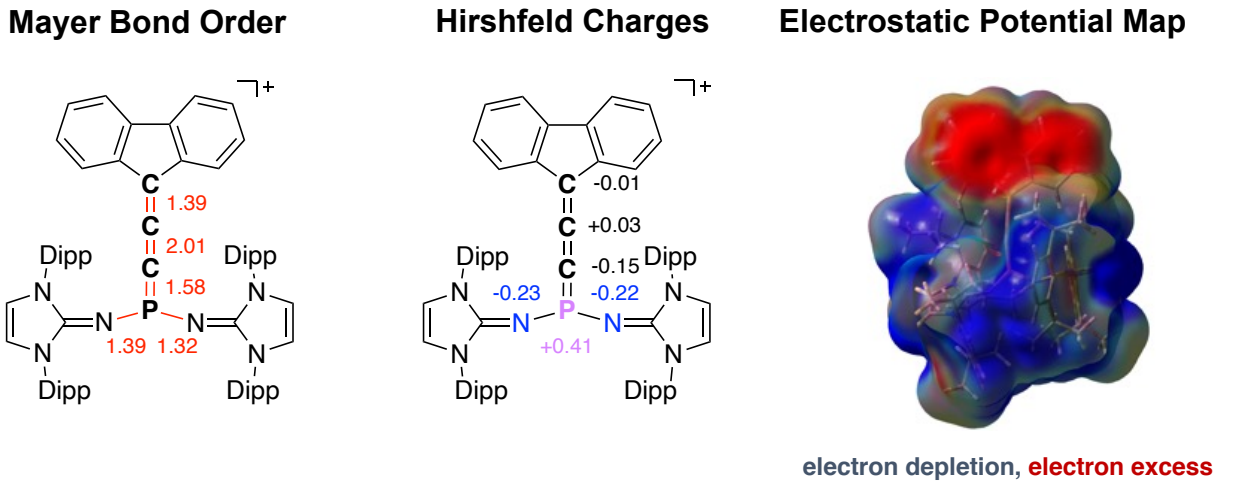

Figure 3-7: Calculated Mayer Bond Order analysis, Hirshfeld charges, and electrostatic potential map for [**3-2**]$^+$ at B3LYP-D3BJ/def2-TZVP level of theory.

The electronic structure of [**3-2**]$^+$ can draw some interesting comparisons to metal allenylidenes complexes. Almost all allenylidenes have the electronic situation illustrated with Kolobova's manganese (I) allenylidene **3-R** in Scheme 3-11.[49,50] The distribution of relative charges in **3-R** indicates the most electrophilic sites on the allenylidene ligand occur at the C1 and C3 centres, while the metal center and C2 have nucleophilic character. In 2024, Autschbach and Hayton would prepare an allenylidene based on a highly electropositive metal, thorium [**3-T**]$^-$ (Scheme 3-11).[51] In contrast to prior reported allenylidenes, [**3-T**]$^-$ was shown both experimentally and computationally to exhibit a reversed distribution of relative charges, where the metal center and C2 are electropositive, while C1 and C3 are electronegative. Remarkably, the distribution of relatively charges of [**3-2**]$^+$ resembles [**3-T**]$^-$, on account of the allenylidene being associated with a highly electron deficient cationic phosphorus center.

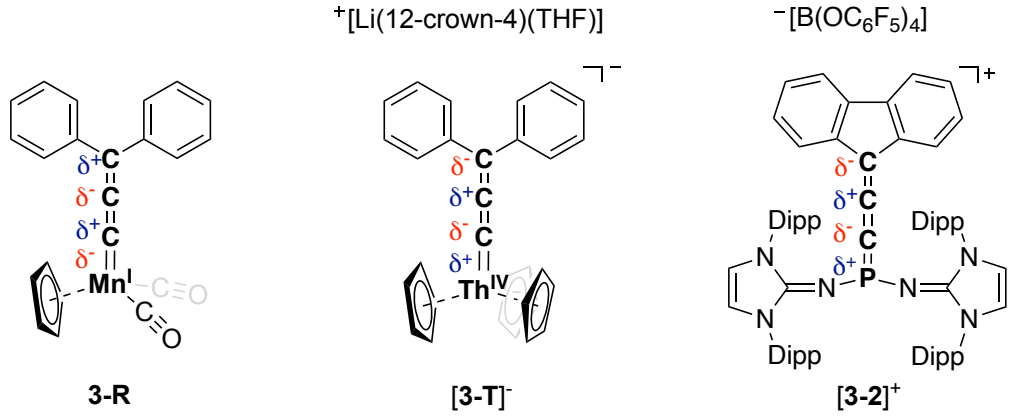

Scheme 3-11: Depiction of relative charges for **3-R**, [**3-T**]$^-$, and [**3-2**]$^+$.

3.3.3 Assessment of the Lewis Acidity of Allenylidene Phosphonium Cation [3-2]$^+$

A combination of FMO depictions, Hirshfeld charge calculations and the electrostatic potential map suggests [**3-2**]$^+$ is a potent phosphorus Lewis acid. To further evaluate this theoretically, fluoride ion affinities (FIA) were determined using Christe's method, and computed in both gas phase as well as using a polarizable continuum model for CH_2Cl_2.[52] The gas phase FIA of [**3-2**]$^+$ suggested a high degree of electrophilicity (655 kJ·mol^{-1}), exceeding that of SbF_5 (483 kJ·mol^{-1}) [15] which is typically used as the benchmark to define Lewis super-acid character (Scheme 3-12). The FIA of [**3-2**]$^+$ exceeds previously reported three-coordinate oxophosphonium cations [**3-I**]$^+$ (634 kJ·mol^{-1}) and [**3-M**]$^+$ (618 kJ·mol^{-1}) [15] but is lower than reported values for other monocationic phosphorus acids like Stephan's organofluorophosphonium $[(C_6F_5)_3PF]^+$ ([**3-U**]$^+$) FIA: 795 kJ·mol^{-1}),[53] as well as Greb's perchloro catecholato-phosphonium salt $[P(Cl_4cat)_2]^+$ ([**3-V**]$^+$) (FIA: 845 kJ·mol^{-1}).[54] Allenylidene phosphonium cation [**3-2**]$^+$ is considerably less acidic than Dielmann's phosphorandylium dication [**3-L$^{NI(Benz)iPr}$**]$^{2+}$.[7] Accounting for dampening of the FIA by CH_2Cl_2 solvation (366 kJ·mol^{-1}), [**3-2**]$^+$ is still considered a strong electrophile.

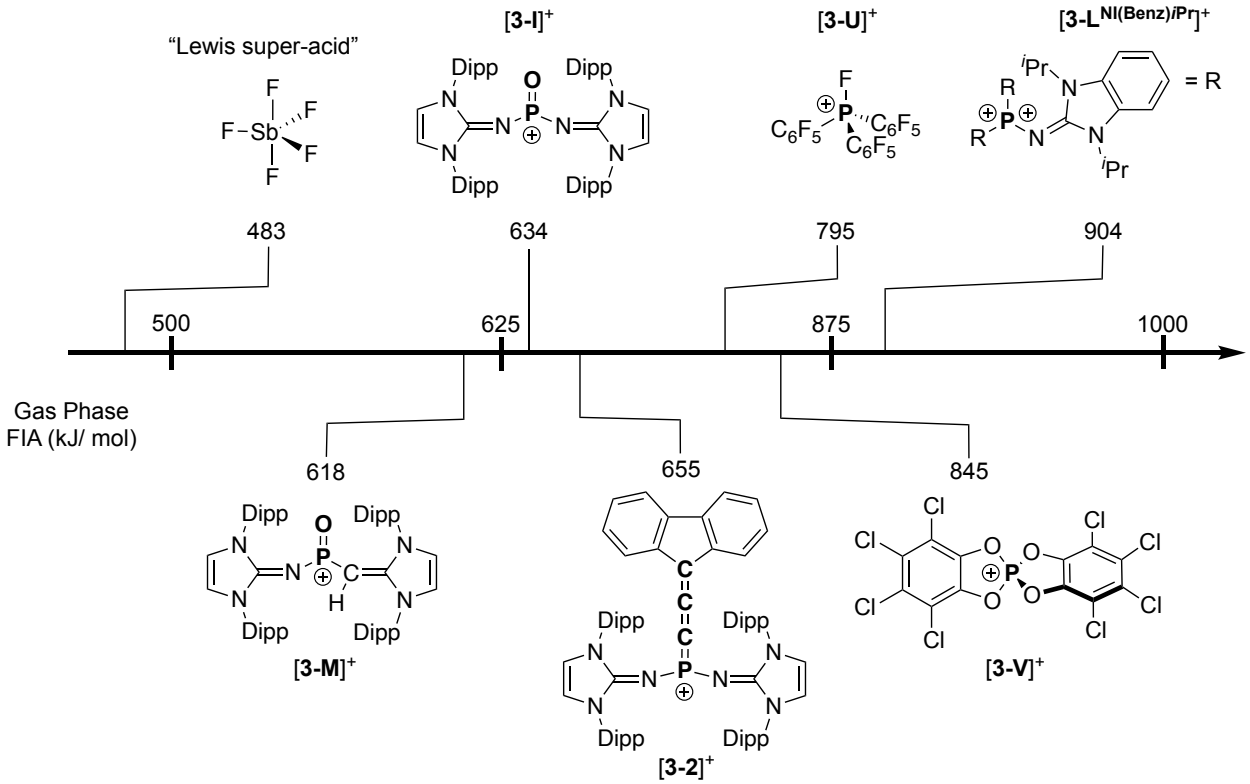

Scheme 3-12: Comparison of literature gas-phase FIA values (kJ/mol) for monocationic and dicationic phosphorus super Lewis Acids.

It was next attempted to obtain an experimental Lewis acidity measure for [**3-2**]$^+$. The typical quantitative test for assessing the Lewis acidity of main group electrophiles is the Gutmann-Beckett method.[55,56] The method uses a Lewis basic probe, triethyl phosphine oxide (Et_3PO), and evaluates the strength of its interactions with the Lewis acid analyte using ^{31}P NMR spectroscopy. Unfortunately, the ^{31}P NMR spectrum of a test between Et_3PO and [**3-2**]$^+$ in CD_2Cl_2 suggests that an unwanted reaction occurs which involves decomposition of the Et_3PO probe by P–O bond cleavage. Unpublished results in the Dielmann Group showed that methylene phosphonium cation [**3-K**]$^+$ reacts with Et_3PO in an oxygen atom transfer reaction, which initially involves a [2+2] cycloaddition (Scheme 3-13).[19] The product of the reaction is a methylene bridged phosphoryl phosphonium cation [**3-W**]$^+$. *In situ* ^{31}P NMR analysis suggests that [**3-2**]$^+$ reacts with Et_3PO to give the analogous species [**3-3**]$^+$ as the largest component of a mixture of products. Cation [**3-3**]$^+$ is evidenced by a set of doublets at $\delta = 34.8$ and -14.6 ppm ($^2J_{PP} = 29$ Hz) that is in close agreement to the spectroscopic features of Dielmann's cation [**3-W**]$^+$.

Pawel Löwe Dissertation

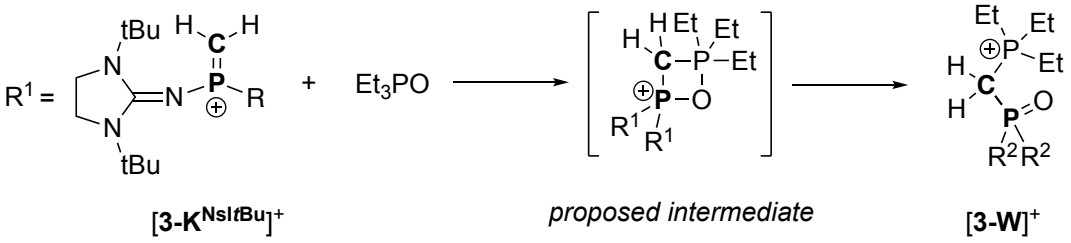

[**3-K**$^{\mathbf{NsItBu}}$]$^+$ *proposed intermediate* [**3-W**]$^+$

Present Study

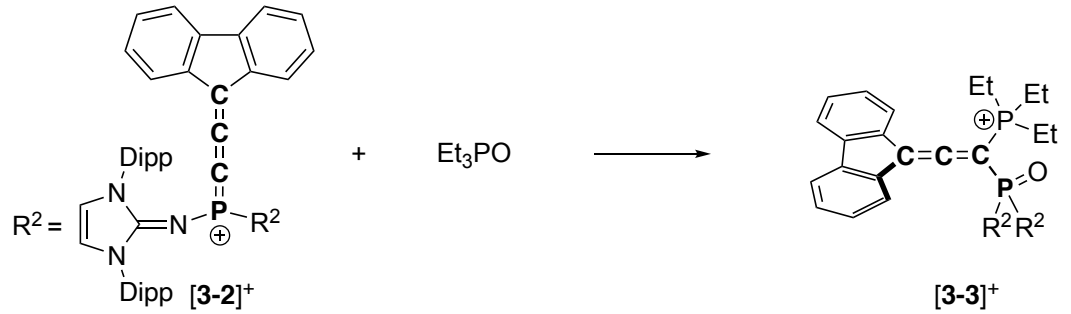

[**3-2**]$^+$ [**3-3**]$^+$
observed in situ

Scheme 3-13: Analogous reaction of methylene phosphonium and allenylidene phosphonium cations with triethyl phosphine oxide.

As an alternative for demonstrating Lewis acidic character, [**3-2**]$^+$ was treated with the Lewis base 4-dimethylaminopyridine (DMAP) (Scheme 3-14).[14,15] Combining a CH_2Cl_2 solution of [**3-2**]$^+$ with DMAP at -40 °C gave the donor-acceptor compound [**3-2•DMAP**]$^+$ which is a cationic $\sigma^4\lambda^5$ phosphacumulene with a ^{31}P NMR chemical shift of δ = 30.4 ppm ($^3J_{PH}$ = 8.2 Hz). The formation of [**3-2•DMAP**]$^+$ was supported by ^{1}H/^{31}P HMBC NMR spectroscopy which indicated coupling between the DMAP ortho protons and the ^{31}P nuclei (^{1}H δ = 7.75/^{31}P δ = 30.4, $^3J_{HP}$ = 8.2 Hz). The identity of [**3-2•DMAP**][B(OC$_6$F$_5$)$_4$] was unambiguously confirmed by a SCXRD study, revealing a tetracoordinate phosphorus center and a cumulenic fragment with a bent geometry (∠P–C1–C2 angle of 166.2(3)°) (Figure 3-8). This data differs to previously reported neutral phosphacumulene ylides **2-J** (R_3P=C=C=X; X = CR_2, O, S) which typically have considerably more bent P–C1–C2 angles.[57,58,59] For example, phosphacumulene ylide Ph_3P=C=C=CAr_2 **2-K** (CAr_2 = 9-fluorenylidene) has a P–C1–C2 angle of 136.4(2)°.[60] Compared to [**3-2**]$^+$, [**3-2•DMAP**]$^+$has a longer P–C1 bond (1.677(3) Å), but this bond length is consistent with the P–C bond of cumulated ylides.

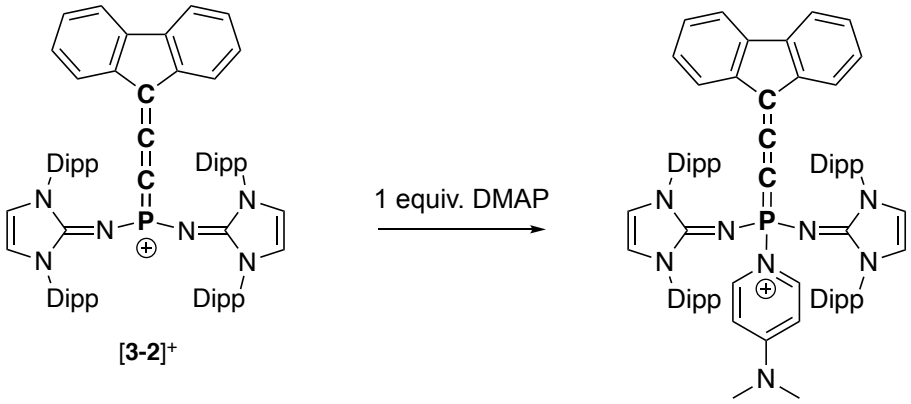

Scheme 3-14: Synthesis of [**3-2•DMAP**]$^+$.

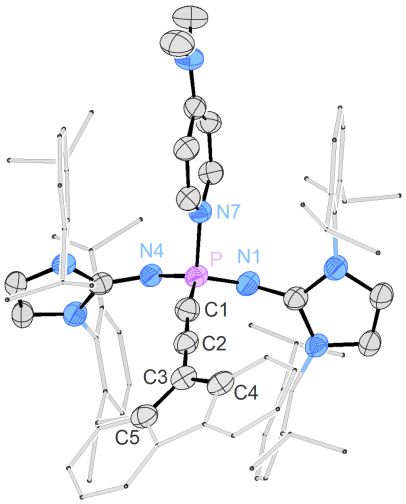

Figure 3-8: Molecular structure of [**3-2•DMAP**]$^+$ with the $[B(OC_6F_5)_4]^-$ anion excluded. Thermal ellipsoids are shown at 50 % probability. For clarity, hydrogen atoms are omitted. The Dipp groups and fluorenyl motif are shown in wireframe. Selected atomic distances [Å] and angles [°]: P–C1 1.677(3). C1–C2 1.227(4), C2–C3 1.385(4), P–N1 1.561(3), P–N4 1.567 (2), P–N7 1.787(2), P–C1–C2 166.2(3).

3.3.4 Stability of Allenylidene Phosphonium salt [3-2][B(OC$_6$F$_5$)$_4$]

Like other low-valent phosphorus cations, [**3-2**]$^+$ was expected to have poor robustness to atmospheric conditions. We found that in solution, [**3-2**]$^+$ decomposes instantaneously when exposed to air, which is indicated by dissipation of its characteristic red color. Solid samples of [**3-2**][$B(OC_6F_5)_4$] degrade more slowly upon atmospheric exposure. Remarkably, the red single crystals of [**3-2**][$B(OC_6F_5)_4$] which were used for SCXRD studies gradually changed color to yellow after brief exposure to air, but retained their crystallinity (Scheme 3-15). This allowed for a subsequent SCXRD experiment, in which the connectivity of the hydrolysis product [**3-**

2•H₂O][B(OC₆F₅)₄] could be elucidated, although the data set was poor quality. Compound [**3-2•H₂O**][B(OC₆F₅)₄] was intentionally prepared by sonicating a wet pentane suspension of [**3-2**]⁺ under an argon atmosphere. Hydrolysis of [**3-2**][B(OC₆F₅)₄] to [**3-2•H₂O**][B(OC₆F₅)₄] occurs in analogous manner to the hydrolysis of the iminophosphonium cations [**3-H**]⁺ reported by Bertrand and co-workers.[14] Heteronuclear NMR spectroscopy and HRMS confirmed the structure of [**3-2•H₂O**][B(OC₆F₅)₄]. Interestingly, [**3-2•H₂O**][B(OC₆F₅)₄] is a dynamic species in solution, evidenced by broadening of all the ^{1}H and ^{13}C NMR resonances corresponding to the N-heterocyclic imine substituents. Variable temperature (VT) NMR spectroscopy was used to identify the exocyclic guanidine proton resonance, which can be observed at temperatures below 268 K. Spectra acquired above 268 K suggest proton exchange occurs between the two imine substituents on the NMR time scale (Scheme 3-16).

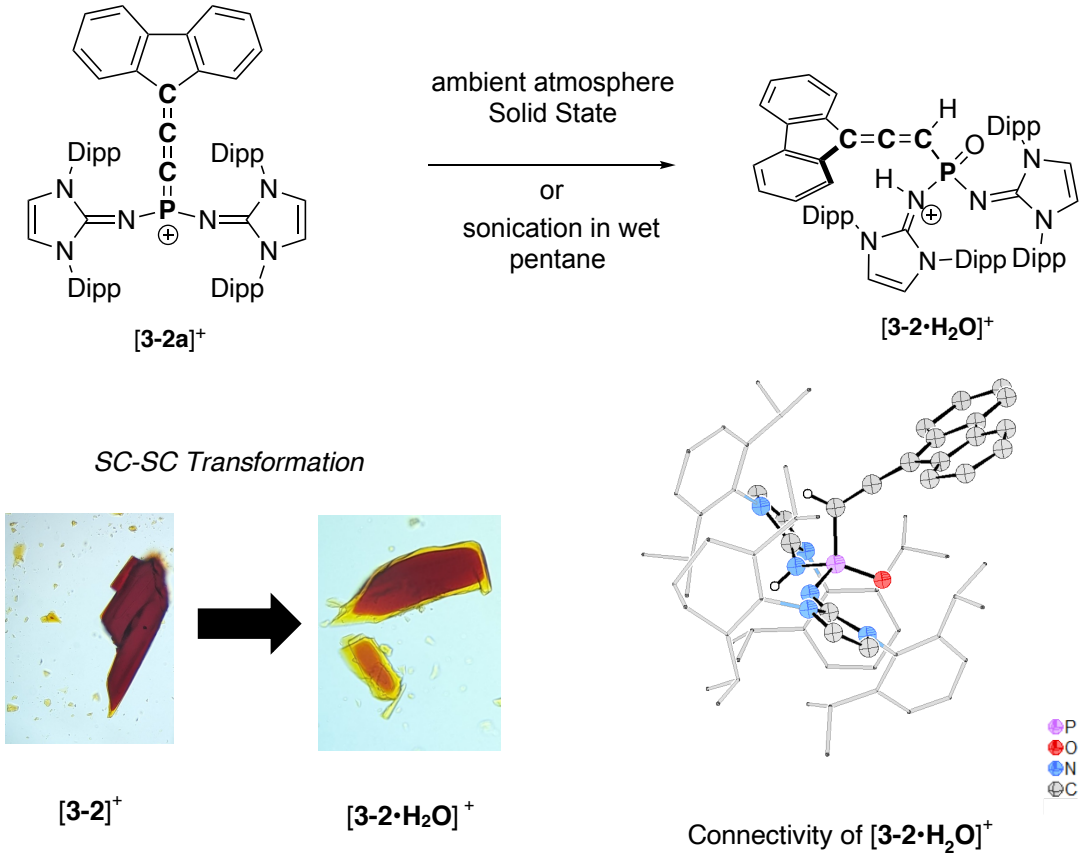

Scheme 3-15: Hydrolysis of [**3-2**]⁺ to [**3-2•H₂O**]⁺. The photographs show the gradual transformation of [**3-2**]⁺ to [**3-2•H₂O**]⁺ in the solid state, and the resulting connectivity depiction which was obtained by diffraction of hydrolyzed crystals.

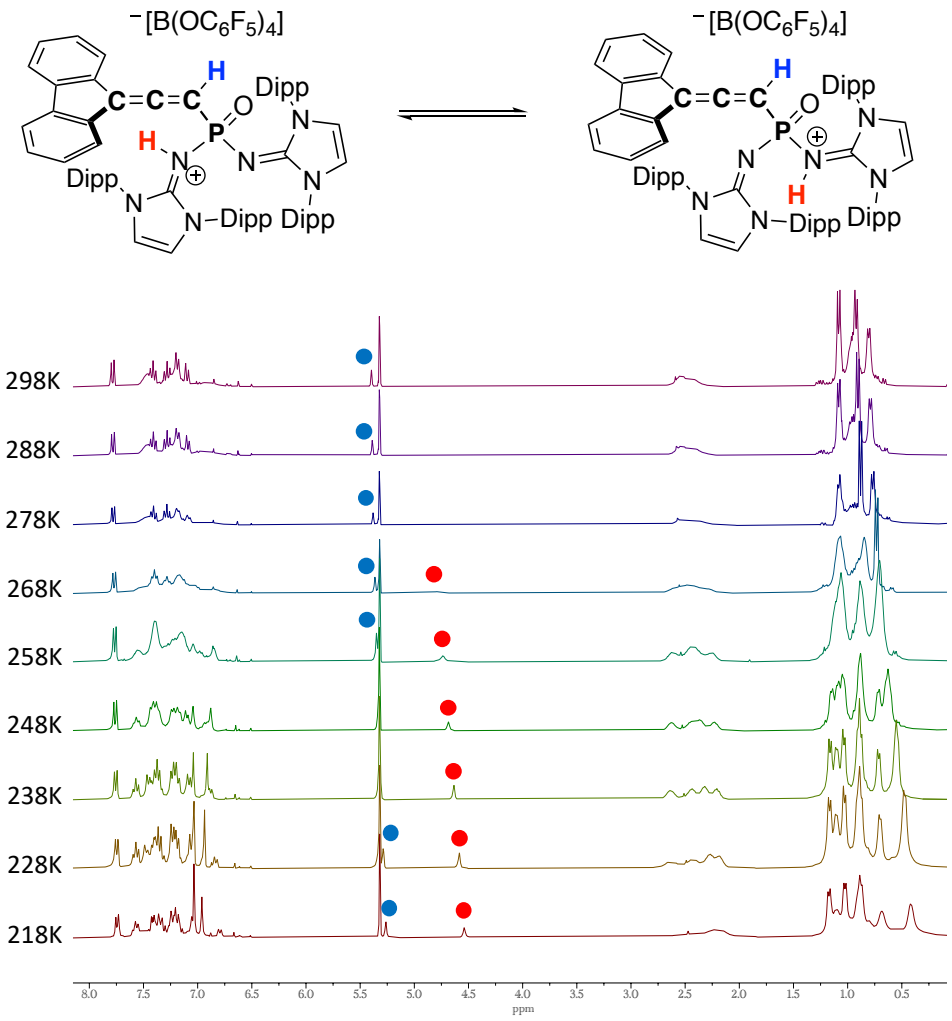

Scheme 3-16: Stacked ^{1}H NMR (300 MHz) spectra of [**3-2•H$_2$O**][B(OC$_6$F$_5$)$_4$] acquired at different temperatures in CD_2Cl_2. Note that the allenic proton peak designated by the blue circle overlaps with the residual solvent for the acquisitions at 248 K and 238 K.

The phosphonium cation [**3-2**]$^+$ showed impressive stability in the solid state, with no indication of decomposition occurring at room temperature under an inert atmosphere. However, when dissolved at room temperature in polar non-coordinating solvents, such as dichloromethane, trifluorotoluene or 1,2-difluorobenzene (1,2-DFB), [**3-2**]$^+$ slowly rearranges to a new compound, quantitatively after 5 days. This new compound exhibits a singlet resonance (δ = 16.3 ppm) in the ^{31}P NMR spectrum, and most notably, this reaction proceeds to form the same product with the exclusion of light. The corresponding ^{1}H NMR spectrum suggested a high degree of asymmetry in the product which initially precluded a structural assignment.

Gratifyingly, colorless single crystals could be obtained by slow evaporation of a CH_2Cl_2 solution at room temperature. A SCXRD study revealed the compound to be cyclic phosphonium cation [**3-2^{cyclo}**]$^+$, resulting from a [2+2] cycloaddition of the P–C1 double bond with a C–C double bond of an adjacent 2,6-diisopropylphenyl (Dipp) substituent (Scheme 3-17). The dearomatized cyclohexa-1,3-diene ring of the tetracyclic cation [**3-2^{cyclo}**]$^+$ shows two double bonds (C6–C11 1.347(3) Å, C9–C10 1.317(3) Å) and four single bonds (C6–C7 1.517(3) Å, C7–C8 1.563(3) Å, C8–C9 1.497(3) Å, C10–C11 1.469(3) Å) (Figure 3-9). The P_1C_3 ring adopts a slightly puckered butterfly shape (interior angle sum of 352°), with the bond angle at the phosphorus center being the smallest (C1–P–C7 78°). Cation [**3-2^{cyclo}**]$^+$ has an allene fragment, with the substituents at C1 and C3 placed in orthogonal planes. Additionally, [**3-2^{cyclo}**]$^+$ features ^{13}C NMR resonances characteristic of a C3 allene system, the most notable being a very deshielded doublet at 194.2 ppm ($^2J_{CP}$ = 10 Hz) corresponding to the *sp* hybridized central allene carbon.

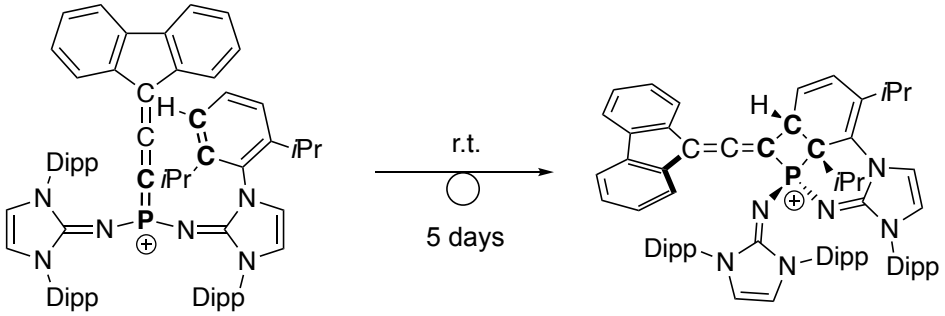

Scheme 3-17: Isomerization of [**3-2**]$^+$ to [**3-2^{cyclo}**]$^+$. $[B(OC_6F_5)_4]^-$ excluded from the scheme.

Unlike [**3-2**]$^+$, cation [**3-2^{cyclo}**]$^+$ is surprisingly tolerant to atmospheric moisture and oxygen. Solution state samples of [**3-2^{cyclo}**][$B(OC_6F_5)_4$] showed no signs of decomposition with respect to the cation component after overnight exposure to ambient conditions. On the contrary, anion decomposition was observed after several hours, with ^{19}F NMR spectra indicating the formation of several anionic borate species, as well as pentafluorophenol. While not trivial, the synthesis of [**3-2^{cyclo}**]$^+$ with a more robust weakly coordinating cation could be a promising avenue to accessing a water and air stable surrogate of [**3-2**]$^+$.

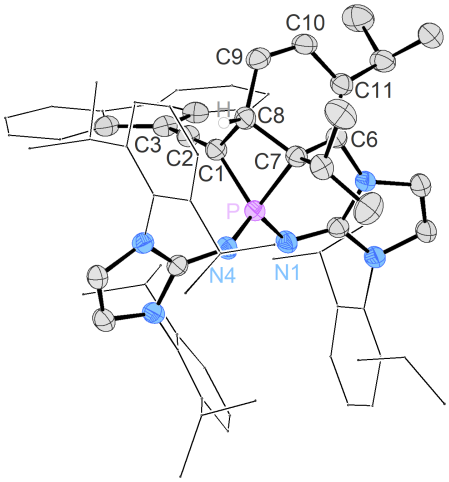

Figure 3-9: Molecular structure of [**3-2**$^{\mathbf{cyclo}}$]$^+$ with the [B(OC$_6$F$_5$)$_4$]$^-$ anion excluded. Thermal ellipsoids are shown at 50 % probability. For clarity, hydrogen atoms are omitted except for one on C8. The Dipp groups and fluorenyl motif are shown in wireframe. Selected atomic distances [Å] and angles [°]: P–N1 1.604(2), P–N4 1.5573(19), P–C1 1.817(2), P–C7 1.834(2), C1–C8 1.555(3), C1–C2 1.295(3), C2–C3 1.318(3), C6–C7 1.517(3), C7–C8 1.563(3), C8–C9 1.497(3), C9–C10 1.317(3), C10–C11 1.469(3), C6–C11 1.347(3), N1–P–N4 115.74(10), N1–P–C1 118.06(11), N4–P–C1 114.05(11), N1–P–C7 112.38(10), N4–P–C7 112.64(11), C1–C2–C3 171.8(3).

3.3.5 Cycloadditions with Allenylidene Phosphonium

The conversion of [**3-2**]$^+$ to [**3-2**$^{\mathbf{cyclo}}$]$^+$ captivated our interest given that thermal [2+2] cycloadditions are symmetry forbidden. DFT methods were employed to gain mechanistic insight into the transformation of [**3-2**]$^+$ to [**3-2**$^{\mathbf{cyclo}}$]$^+$ using the truncated model compounds [**3-2**]$^+_{\text{model}}$ and [**3-2**$^{\mathbf{cyclo}}$]$^+_{\text{model}}$ having three of their Dipp substituents replaced with methyl substituents (Scheme 3-18). Utilizing B3LYP-D3BJ/def2-TZVP level of theory [46,47,48] and employing an implicit CH_2Cl_2 solvation, the reaction coordinate suggests the transformation occurs by a concerted [2+2] cycloaddition process *via* a single transition state (TS1 $\Delta G^{\ddagger} = 131$ kJ·mol^{-1}). The isomers [**3-2**]$^+_{\text{model}}$ and [**3-2**$^{\mathbf{cyclo}}$]$^+_{\text{model}}$ have a minor energy difference, with the reaction process being slightly endergonic (ΔG =+26 kJ·mol^{-1}), but equally exothermic (ΔH = -26 kJ·mol^{-1}). For a reaction that occurs within a few days at room temperature, a slightly lower energy transition state would be expected, as well as an overall exergonic reaction landscape, however this discrepancy may be due to using truncated structures. Nevertheless, we wanted to explore whether an equilibrium between [**3-2**]$^+$and [**3-2**$^{\mathbf{cyclo}}$]$^+$ could be established at elevated temperatures. Chemical corroboration of the thermal reversibility of [**3-2**$^{\mathbf{cyclo}}$]$^+$ to [**3-2**]$^+$ was demonstrated by gently heating a sample of [**3-**

2^{cyclo}]$^{+}$ in 1,2-DFB to 60 °C, in the dark, and trapping [**3-2**]$^{+}$ with an excess of DMAP, yielding [**3-2•DMAP**][B(OC$_6$F$_5$)$_4$]. Note that DMAP does not react with [**3-2**^{cyclo}]$^{+}$ at room temperature and required prolonged heating to achieve full conversion. The driving force for cycloreversion can be rationalized by the alleviation of ring strain and rearomatization of the Dipp substituent. This compensates for the energetic penalty associated with a change in geometry about the phosphorus center from tetrahedral [**3-2**^{cyclo}]$^{+}$ to trigonal planar [**3-2**]$^{+}$.[61]

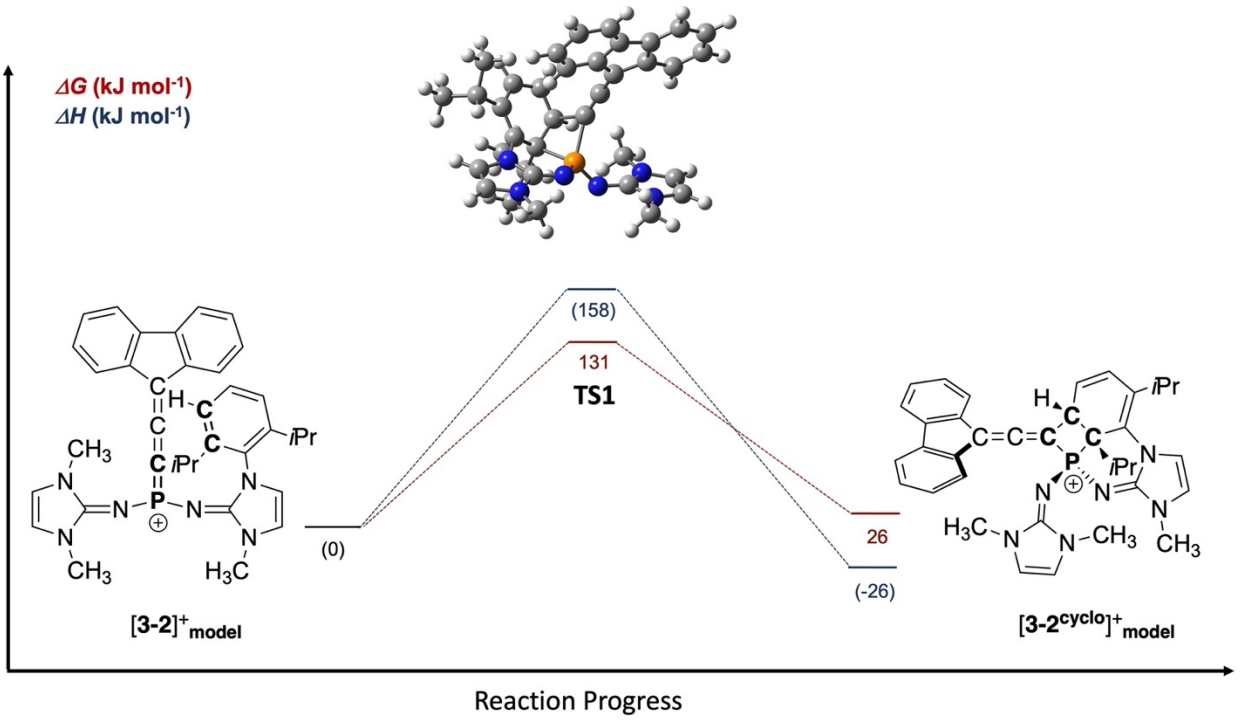

Scheme 3-18: Energy profile (free energy in red, enthalpy in blue) of the reaction path [**3-2**]$^{+}_{model}$→TS1→[**3-2**^{cyclo}]$^{+}_{model}$ determined at B3LYP(D3-BJ)/def2-TZVP in CH_2Cl_2 (SMD solvation model).

Bond activations involving arenes are of great relevance to organic chemists as they present opportunities to construct complex ring systems. For main group systems, inert arene activations are challenging and typically occur *via* a single atom insertion process, most often facilitated by an ambiphilic center such as a carbene[17,62,63] or heavier analogs, such as phosphinidines,[64,65,66] silylenes,[67,68,69,70,71,72,73] aluminylenes.[21,74] Few arene activations occur across an unsaturated main group bond, and very rarely do these processes occur reversibly (Scheme 3-19). Concerning TPPCs, only one previous study has demonstrated a reversible arene activation process. Illustrated

in Scheme 1-14 (Section 1.1.8), the Grützmacher group showed that transient methylene phosphonium species undergo electrocyclization with a flanking arene substituents to give benzannulated $\sigma^4\lambda^5$ phosphete salts.[61] Stephan and co-workers provided the first example of a reversible cycloaddition of a P–C multiple bond and an arene, a [4+2] cycloaddition which occurs between a Dipp substituent and a phosphalkene (Scheme 3-19).[75] Wesemann reported an intramolecular [2+2] cycloaddition between a germaborene ($R_2Ge{=}BR_2$) and a flanking arene group, which is photochemically initiated.[76] Despite sharing few similarities from a mechanistic perspective to the currently presented work, the process we observe is most reminiscent to recent contributions by the Bertrand group which detail the isomerization of a super nucleophilic bis(imino)carbene to a polycyclic compound *via* a reversible [3+2] cycloaddition with a proximal Dipp substituent.[77] Although unusual with arenes, such 1,3-dipolar cycloaddition reactions, as well as [4+2] cycloaddition reactions with multiple bonds are common in organic synthesis to form five- and six-membered rings, respectively.

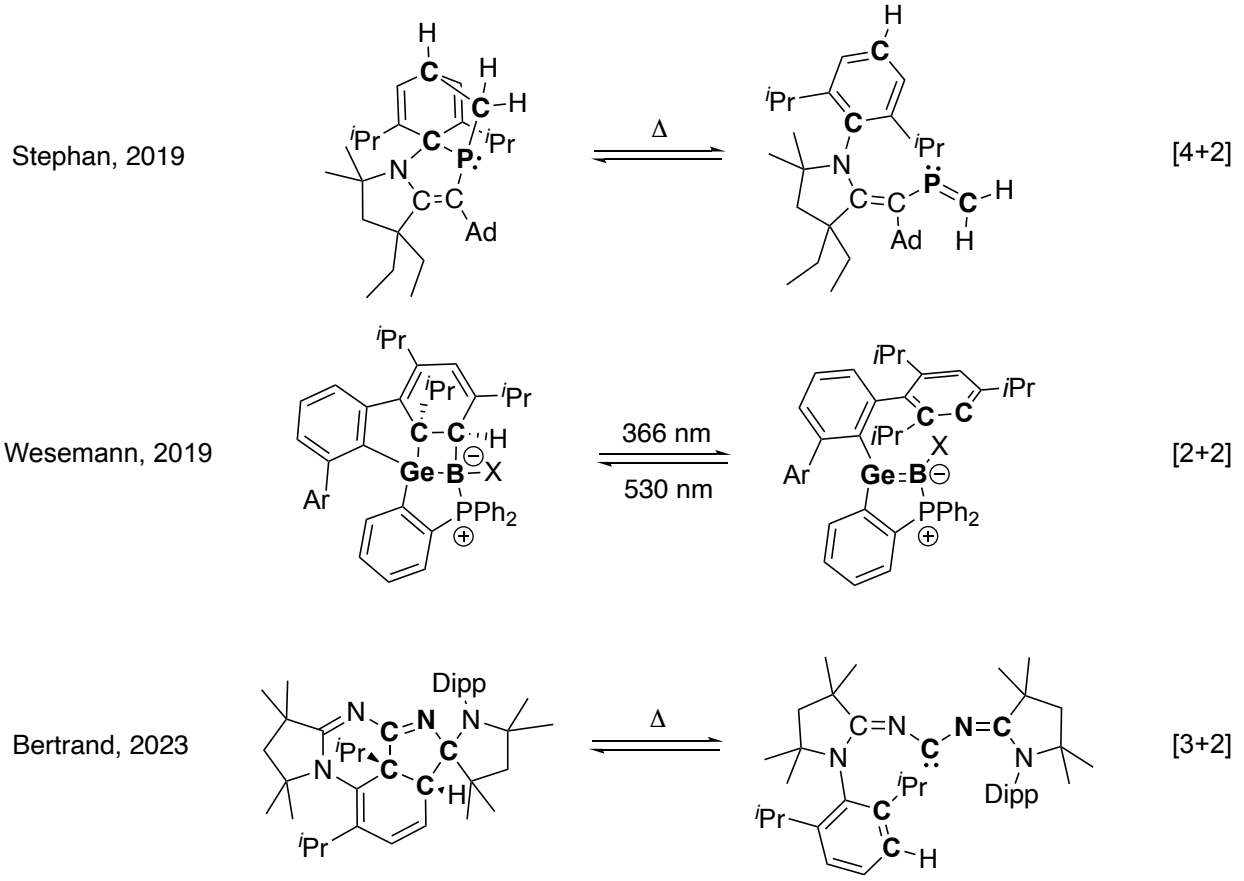

Scheme 3-19: Reversible cycloadditions between main-group multiple bonds and arenes.

Intrigued by the intramolecular cycloaddition which gives [**3-2**$^{\mathbf{cyclo}}$]$^+$ from [**3-2**]$^+$, an intermolecular cycloaddition reaction was also pursued. In the presence of acetonitrile, [**3-2**]$^+$ was found to form the cationic 1,2-azaphosphete [**3-4**]$^+$ *via* polarized intermolecular [2+2] cycloaddition, which was confirmed by multinuclear and 2D NMR spectroscopic techniques, as well as by HRMS. Heating is required for this reaction as the formation of [**3-2**$^{\mathbf{cyclo}}$]$^+$ by intramolecular cycloaddition is a competing reaction process. While [**3-2**$^{\mathbf{cyclo}}$]$^+$ can be observed *in situ*, it is eventually consumed at elevated temperatures, exclusively producing [**3-4**]$^+$. Compound [**3-4**]$^+$ shows a singlet at δ = -18.7 ppm in the phosphorus NMR spectrum which appears at a lower frequency than [**3-2**]$^+$ (δ = 43.9 ppm). The formation of [**3-4**]$^+$ is supported by $^{13}C\{^1H\}$ NMR experiments, revealing three diagnostic deshielded doublets, one centred at 187.9 ppm ($^2J_{CP}$ = 24 Hz) corresponding to the *sp* hybridized allene carbon, a second centred at 187.3 ppm ($^2J_{CP}$ = 25 Hz) attributed to the nitrogen-bound azaphosphete carbon atom, and a third at δ = 120.5 ppm ($^1J_{CP}$ = 70 Hz) which reflects the sp^2 carbon atom directly bound to phosphorus. The ^{1}H NMR signal of the acetonitrile derived methyl group in [**3-4**]$^+$ appears as a doublet at δ =1.35 ppm ($^4J_{HP}$ = 4 Hz) which collapses to a singlet upon ^{31}P decoupling.

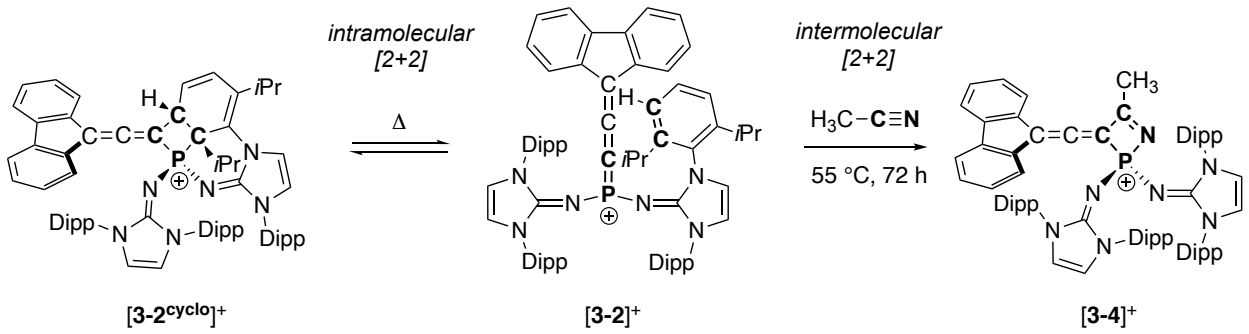

Scheme 3-20: Reversible intramolecular [2+2] cycloaddition of [**3-2**]$^+$, and intermolecular cycloaddition of [**3-2**]$^+$ with acetonitrile to give [**3-4**]$^+$.

The reaction of [**3-2**]$^+$ with acetonitrile stands in sharp contrast to the reactivity of most carbon-based cumulenes, which undergo [2+2] cycloadditions with electron-deficient substrates like tetrafluoroethylene (TFE), tetracyanoethylene (TCNE), bis(trifluoromethyl)acetylene, dimethyl acetylenedicarboxylate (DMAD) or C_{60}.[78,79,80,81] Compound [**3-2**]$^+$ can be viewed as a polarized ($P^{\delta+}$–$C^{\delta-}$) electron-deficient analog of a carbon cumulene, which is reflected in its facile reactivity

with an electron-rich substrate like a nitrile. Cation [**3-2**]$^+$ most resembles the reactivity of per halogenated cumulenes, like 1,1,4,4-tetrafluorobutatriene, which also reacts with π-electron rich unsaturated substrates. [82]

3.4 Conclusion and Outlook

Over a century since the synthesis of the first [3]cumulene by Brand,[83] and three decades after Bertrand's pioneering work on trigonal planar phosphorus cations,[84] here we demonstrate the preparation of a base-free allenylidene phosphonium cation [**3-2**]$^+$, the first main-group cumulene analog to feature a heavy element. Like other trigonal planar phosphorus cations, [**3-2**]$^+$ is a potent Lewis acid, evidenced experimentally by the preparation of a Lewis acid-base adduct with 4-dimethylaminopyridine, and fluoride ion affinity calculations. Solid-state structural data and quantum calculations indicate that [**3-2**]$^+$ features a conjugated P–C–C–C framework with a high degree of double-bond character for the terminal P–C1 and C2–C3 bonds, as well as the central C1–C2 bond. Remarkably [**3-2**]$^+$ undergoes an isomerization in solution to give [**3-2^{cyclo}**]$^+$, a rare example of a thermally reversible [2+2] cycloaddition between an unsaturated main-group motif and an inert arene. Additionally, [**3-2**]$^+$ can participate in a polarized intermolecular [2+2] cycloaddition as demonstrated by its reactivity with acetonitrile to yield [**3-4**]$^+$. Overall, this chapter illustrates the feasibility of replacing sp^2 carbon atoms with three-coordinate P(V) centers in π-conjugated molecules and serves to further strengthen the carbon-phosphorus diagonal relationship. While the structure and bonding analyses of [**3-2**]$^+$ provides comparisons to carbon [3]cumulenes and metal allenylidenes, the ability of [**3-2**]$^+$ to promote reversible bond activation supports the notion that unsaturated main group systems like trigonal planar phosphonium cations can facilitate reactivity patterns which are typically observed for transition metals complexes.

3.4.1 Heterocyclic Synthesis

While it was initially shown that [**3-2**]$^+$ can be used to prepare a four-membered heterocycle *via* [2+2] cycloaddition with acetonitrile, preliminary results indicate that [**3-2**]$^+$ is also a competent precursor towards the preparation of a six-membered ring system. We observed that in the presence of excess acetonitrile, with temperatures above 60 °C, a second equivalent of acetonitrile can be incorporated into [**3-4**]$^+$, yielding a new compound with a cationic PNNCCC ring [**3-5**]$^+$ (Scheme 3-21). Tentative assignment of this new species was provided by proton and heteronuclear NMR

spectroscopy, as well as by MS. Compound [**3-5**]$^+$ has a chemical shift of δ = -41.3 ppm in the ^{31}P NMR spectrum, which is shifted to lower frequency relative to [**3-4**]$^+$ (δ = -18.7 ppm). Conversion to [**3-5**]$^+$ from [**3-4**]$^+$ is sluggish, and heating beyond 75 ºC seemed to compromise selectivity. Interestingly, the transformation mimics work by Doxsee and co-workers, who demonstrated the sequential coupling of two nitriles to a titanium alkylidene surrogate, overall affecting the formation of a six-membered metallocycle (Scheme 3-21).[85] In their chemistry, the initial [2+2] cycloaddition occurs under relatively mild conditions, while the subsequent ring expansion reaction is more challenging. The formation of diazaphosphinine cation [**3-5**]$^+$ from [**3-4**]$^+$ has not been investigated computationally but is presumed to proceed by a hetero-Diels-Alder reaction similar to the ring expansion chemistry of oxophosphonium and thiophosphonium cations previously reported by Dielmann (Scheme 1-15). [86]

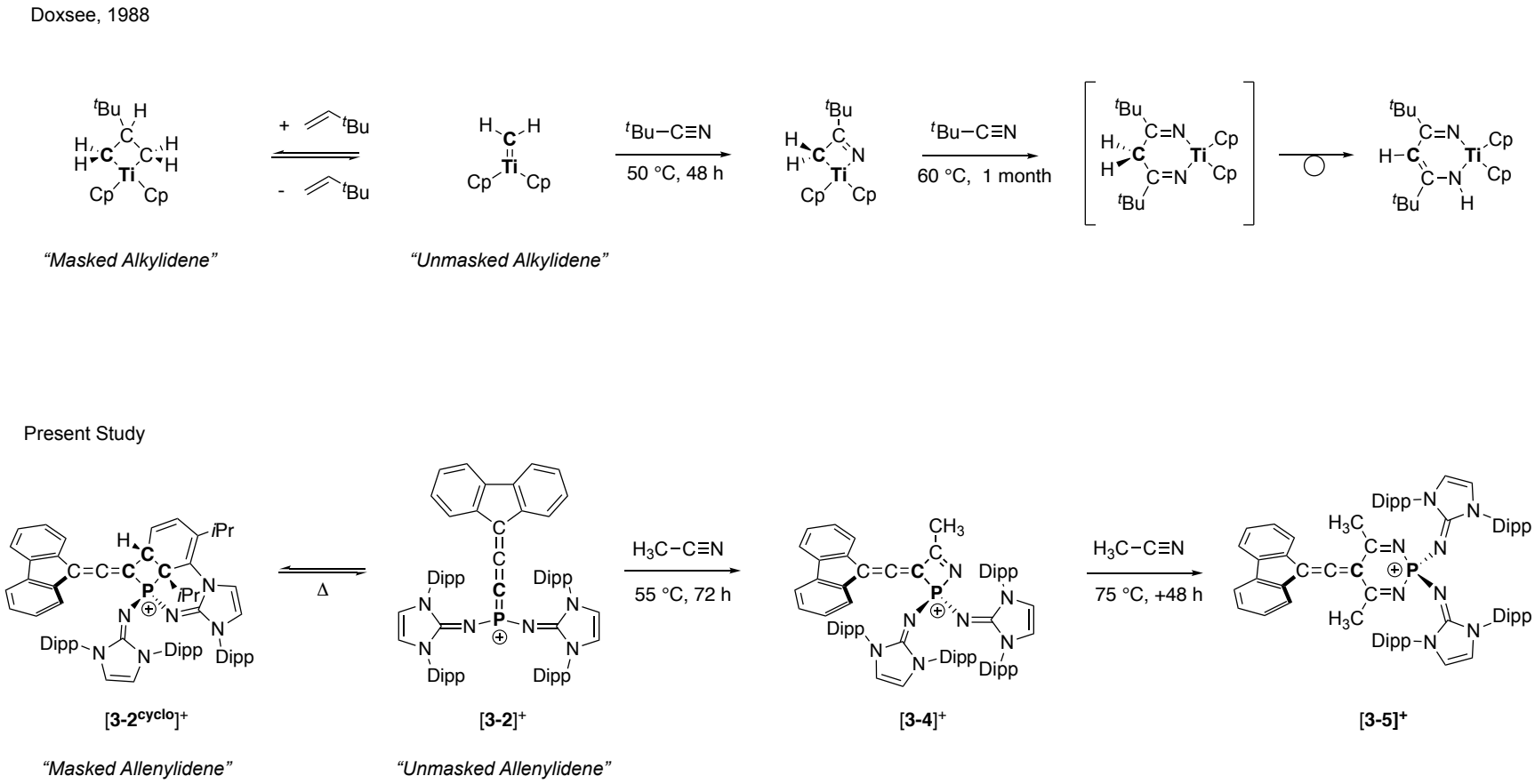

Scheme 3-20: Doxsee's nitrile addition to titanium alkylidene complex to initially give an azametallocyclobutene, followed by a subsequent ring expansion with a second nitrile (Cp = cyclopentadienyl). Reaction of allenylidene phosphonium with acetonitrile, and its subsequent expansion to the cationic diazaphosphinine [**3-5**]$^{+}$.

3.4.2 Derivatization

The feasibility of preparing an allenylidene phosphonium ion from the bis(imino)phosphine **3-1**^{b} remains an open question. Further investigation of this system would elucidate more precise electronic and steric requirements necessary for the isolation of such cationic species. Employing N-alkyl NHI substituents like NsI^{t}Bu in $[R_2P{=}C{=}C{=}CAr_2]^+$ cations is a promising prospect and provides several key benefits particularly for pursuing intermolecular reactions; a) this choice would prevent the intramolecular cycloaddition reaction that occurs with the phosphonium center when aryl-based NHI substituents are used (ex. [**3-2**]$^+$ →[**3-2**^{cyclo}]$^+$) b) the hypothetical cation [**3-2**^{b}]$^+$ would have a considerably less obstructive steric profile compared to [**3-2**]$^+$ rendering the P=C functional group more available for intermolecular cycloaddition reactions and c) the use of less electron-rich saturated NHI substituents would render [**3-2**^{b}]$^+$ a stronger Lewis acid and consequently would be more appropriate for polarized cycloadditions (Scheme 3-22). A current challenge when attempting to do cycloadditions with [**3-2**]$^+$ is that heating at relatively moderate temperatures is necessary to fully consume [**3-2**^{cyclo}]$^+$, which leads to very long reaction times. Unfortunately, it is not possible to obfuscate long reaction times by increasing reaction temperatures as doing so seems to result in decomposition of the anion $[B(OC_6F_5)_4]^-$.

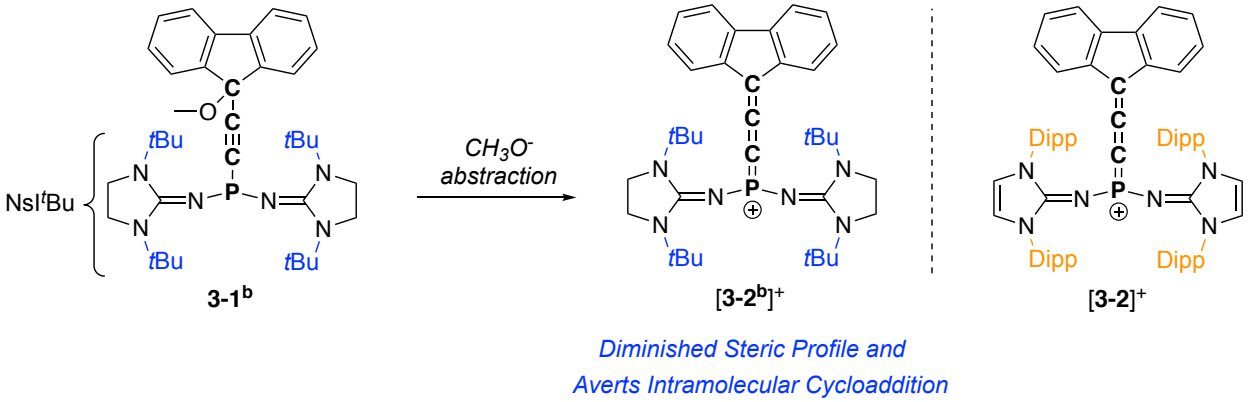

3-1^{b} **[3-2**^{b}**]**$^+$ **[3-2]**$^+$

Scheme 3-21: Our initially targeted allenylidene phosphonium cation [**3-2**^{b}]$^+$, which should be a superior candidate for pursuing cycloaddition chemistry.

Lastly, an initial screen of substrates including benzonitrile, benzaldehyde, CO_2, diphenylacetylene, and adamantyl azide was also performed in my studies and will be briefly summarized. The reaction of [**3-2**]$^+$ with benzonitrile appears to occur analogously to the reaction

of [**3-2**]$^+$ with MeCN, but requires higher temperatures and gives a less selective outcome. Reactions with diphenylacetylene and adamantyl azide resulted in no reaction even at high temperatures, presumably on account of the larger steric profile of the substrates. Reactions with terminal alkynes or less encumbered azides may be promising. Benzaldehyde, and CO_2 both gave instantaneous reactions but resulted in a mixture of species in ^{31}P NMR spectra, which could not be further deduced. A promising prospect would be to introduce ketones to [**3-2**]$^+$ in order to facilitate transfer of the cumulene unit C=C=CAr_2, although this can be done with synthetically more accessible phosphacumulene ylides like Ph_3P=C=C=CAr_2 **2-K** (highlighted previously in Scheme 2-9). [57]

3.5 Experimental

3.5.1 General Remarks

All manipulations were performed under an inert atmosphere of either dry argon (University of Innsbruck) or nitrogen (York University), employing standard Schlenk and glovebox techniques. Dry and oxygen-free solvents were utilized, which were obtained from a solvent purification system and then stored over molecular sieves. All glassware was oven-dried at 150 °C. ^{1}H, ^{11}B, ^{13}C, ^{19}F, and ^{31}P nuclear magnetic resonance (NMR) spectra were recorded on Bruker Neo 700 MHz, Bruker ARX 400 MHz, Bruker AVANCE (IV) Neo 400 MHz, Bruker ARX 300 MHz spectrometers, at either the NMR facilities at the University of Innsbruck or York University. Chemical shifts are given in parts per million (ppm) relative to $SiMe_4$ (^{1}H, ^{13}C), BF_3•Et_2O (^{11}B, ^{19}F), and 85% H_3PO_4 (^{31}P) and they were referenced to the residual solvent signals (CD_2Cl_2: ^{1}H δ_H =5.32, ^{13}C δ_C = 54.00; C_6D_6: ^{1}H d_H = 7.16, ^{13}C δ_C = 128.06; CD_3CN: δ_H =1.94, ^{13}C δ_C = 118.26; $CDCl_3$: δ_H =7.26, ^{13}C δ_C = 77.16;) or internally by the instrument after locking and shimming to the deuterated solvent (^{11}B, ^{19}F, ^{31}P). Coupling constants are reported in Hertz (Hz) and NMR multiplicities are abbreviated as follows: s = singlet, d = doublet, t = triplet, q = quartet, p = pentet, sext = sextet, sept = septet, m = multiplet, br = broad signal. Mass spectrometry was recorded using an Qexactive Orbitrap (Thermo Scientific) at the University of Innsbruck, or Mass spectrometry AIMS Mass Spectrometry Laboratory at the University of Toronto utilizing an AccuTOF 4G instrument. FT-IR absorption measurements were recorded with a Bruker Alpha FT-IR (Platinum ATR unit) spectrometer, within an argon atmosphere glovebox. UV-Vis absorption measurements were recorded with a Cary 5000 UV-Vis-NIR Spectrophotometer from Agilent Technologies. Recordings were obtained at 25 °C and taken with the instrument operating in dual beam mode and referenced to dichloromethane. All absorption experiments were conducted in quartz cuvettes (1 cm x 1 cm) equipped with a J-Young style Teflon tap. Cyclic voltammetry experiments were performed under an argon atmosphere using a Metrohm Autolab potentiostat. A three-electrode cell was utilized with a glassy carbon working electrode, platinum wire counter electrode, and a Ag/AgCl pseudo-reference electrode. Formal redox potentials were referenced to the Ag/AgCl redox couple. 0.1 M $^{n}Bu_4PF_6$ was used as the supporting electrolyte. 1,2-difluorobenzene was used as the solvent, and the scan rate was set to 100 mV/s. The voltammogram was recorded using the NOVA software package.

3.5.2 Reagents and Handling:

All compounds were purchased from commercial sources (Sigma Aldrich, Alfa Aesar, Tokyo Chemical Industry, Oakwood chemicals) and used as received, if not stated differently. $[(R^2)_2P]Cl$ (R^2 =1,3-bisdiisopropylphenylimidazolin-2-ylidenamino, NIDipp) [17] and $[(R^2)_2P]Cl$ (R^2 =1,3-ditertbutylimidazolidene-2-ylidenmino, NsI^{t}Bu) [31] and $B(OC_6F_5)_3$[32] were synthesized according to literature procedure.

Note 1: The synthesis of the phosphenium $[(NIDipp)_2P]Cl$ requires the silylated NHI (Me_3Si)-NIDipp. (Me_3Si)-NIDipp is typically prepared with azidotrimethylsilane (Me_3Si-N_3), which is extremely toxic, as well as an explosive hazard if stored incorrectly.

Note 2: The synthesis of the phosphenium $[(NsI^tBu)_2P]Cl$ requires the silylated NHI (Me_3Si)-NsI^{t}Bu. One of the steps to prepare (Me_3Si)-NsI^{t}Bu utilizes cyanogen bromide (BrCN). Contact with skin or inhalation of BrCN can be lethal, and it's highly recommended that if attempting to make (Me_3Si)-NsI^{t}Bu, it is done with an additional lab member who can help ensure the synthesis is executed safely.

3.5.3 Preparation of bis(imino)alkynylphosphine 3-1[a]

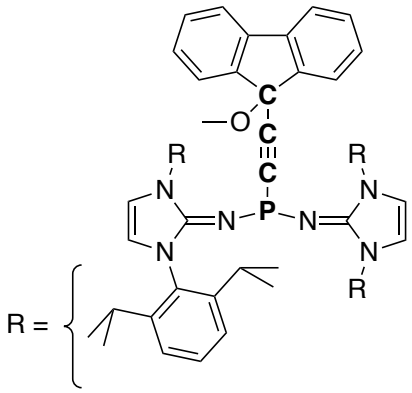

9-Ethynyl-9-methoxy-9H-fluorene **2-1^{Fl}** (50 mg, 0.23 mmol, 1.00 equiv) was dissolved in THF (~2 mL) and cooled to -78°C. n-BuLi (142 µL, 1.6 M in hexanes, 0.23 mmol, 1.00 equiv) was then added in a single portion. The reaction mixture was kept at -78°C and shaken periodically over the course of 30 minutes. The mixture was then added dropwise to a precooled (-78°C) solution of [(NIDipp)$_2$P][Cl] (198 mg, 0.23 mmol, 1.00 eq) in THF (~2 mL) and subsequently allowed to warm to room temperature to stir for 16 hours. All volatiles were removed *in vacuo*. The crude product was extracted with pentane (30 mL) and passed through a glass filter. The solvent was then removed in *in vacuo*, to provide the title compound as a yellow powder. Compound **3-1[a]** is soluble in THF, diethyl ether, benzene, and toluene, and sparingly soluble in *n*-pentane and *n*-hexane. It decomposes slowly in $CHCl_3$, CH_2Cl_2, and CH_3CN.

Yield: 140 mg (0.13 mmol, 58%).

^{1}H NMR (C_6D_6, 400 MHz, 298 K) δ (ppm) = 7.71 (d, $^3J_{HH}$ = 7.0 Hz, 2H, CH fluorenyl), 7.42 (d, d, $^3J_{HH}$ = 7.0 Hz, 2H, CH fluorenyl), 7.27 – 7.20 (m, 4H, CH fluorenyl), 7.19 (s, 2H, CH Dipp: *para*), 7.17 (s, 2H, CH Dipp: *para*), 7.14 – 7.09 (m, 4H, CH Dipp: *meta*), 6.94 – 6.89 (m, 4H, CH Dipp: *meta*), 5.79 (s, 4H, N-C<u>H</u>=C<u>H</u>-N), 3.20 (sept, $^3J_{HH}$ = 7.1 Hz, 4H, C<u>H</u>(CH$_3$)$_2$), 3.03-2.93 (m, 7H, C<u>H</u>(CH$_3$)$_2$ and C-OC<u>H</u>$_3$), 1.26 (d, $^3J_{HH}$ = 6.8 Hz, 12H, CH(C<u>H</u>$_3$)$_2$), 1.18 (d, $^3J_{HH}$ = 6.9 Hz, 12H, CH(C<u>H</u>$_3$)$_2$), 1.11 (d, $^3J_{HH}$ = 6.8 Hz, 12H, CH(C<u>H</u>$_3$)$_2$), 1.01 (d, $^3J_{HH}$ = 6.9 Hz, 12H, CH(C<u>H</u>$_3$)$_2$).

^{13}C{^{1}H} NMR (C_6D_6, 101 MHz, 298 K) δ (ppm) = 148.3 (C_q Dipp: *ortho*), 148.3 (C_q Dipp: *ortho*), 147.1 (C_q Dipp: *ortho*), 145.9 (C_q fluorenyl), 143.8 (d, $^2J_{CP}$ = 29.1 Hz, C_q N-C-N), 141.1 (C_q fluorenyl), 135.2 (C_q Dipp: *ipso*), 129.3 (CH fluorenyl), 128.9 (CH Dipp: *para*), 128 (overlapped with C_6D_6, CH fluorenyl), 126.9 (CH fluorenyl), 124.0 (CH Dipp: *meta*), 123.8 (CH Dipp: *meta*), 119.7 (CH fluorenyl), 115.1 (N-<u>C</u>H=<u>C</u>H-N), 94.9 (d , $^1J_{CP}$ = 65.4 Hz, P-<u>C</u>≡C-), 92 (d , $^2J_{CP}$ = 7.6 Hz, P-C≡<u>C</u>-), 81.2 (d, $^3J_{CP}$ = 2.4 Hz, <u>C</u>-OCH$_3$) 50.9 (C-O<u>C</u>H$_3$), 29.2 (<u>C</u>H(CH$_3$)$_2$), 28.9

(<u>C</u>H(CH$_3$)$_2$), 28.9 (<u>C</u>H(CH$_3$)$_2$), 24.9 (CH(<u>C</u>H$_3$)$_2$), 24.0 (CH(<u>C</u>H$_3$)$_2$), 23.9 (CH(<u>C</u>H$_3$)$_2$), 23.8 (CH(<u>C</u>H$_3$)$_2$), 23.8 (CH(<u>C</u>H$_3$)$_2$).

^{31}P NMR (C$_6$D$_6$, 162 MHz, 298 K) δ (ppm) = 51.9.

HR-ESI-MS: Calculated for [C$_{70}$H$_{84}$N$_6$OP]$^+$ ([3-1^a+H]$^+$) m/z = 1054.6444, found: m/z = 1055.6415.

3.5.4 Preparation of allenylidene phosphonium salt [3-2][B(OC$_6$F$_5$)$_4$]

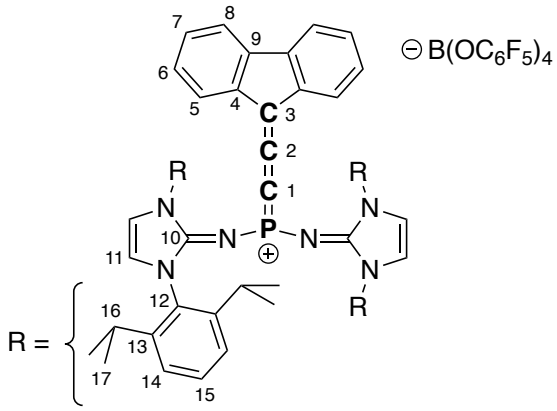

Phosphine **3-1^a** (40 mg, 0.038 mmol, 1.00 equiv) and B(OC$_6$F$_5$)$_3$ (30 mg, 0.054 mmol, 1.42 equiv) were each dissolved in *n*-pentane (5 mL). B(OC$_6$F$_5$)$_3$ solution was added dropwise to the solution of **3-1^a** at room temperature while vigorously stirring. The combined solution gradually became turbid with precipitation of a red solid. The reaction was allowed to stir for 30 minutes, and the red solid was left to settle to the bottom of the reaction container. The supernatant was decanted, and the solid residue was washed with pentane (3 x 10 mL) until the resulting supernatant appeared colorless. Afterwards, volatiles were removed *in vacuo*. The product was isolated as a red solid.

Yield: 47 mg (0.027 mmol, 71 %).

For NMR analysis, a solid sample of [3-2][B(OC$_6$F$_5$)$_4$] and CD$_2$Cl$_2$ were stored at -78 °C for several minutes before preparing the NMR sample. Once the solution was made, the NMR tube was stored in a dry ice/acetonitrile bath (-40 °C), until it was placed in the spectrometer, which was precooled to the listed acquisition temperatures. At approximately room temperature, [3-2]$^+$ begins to slowly convert to [3-2^{cyclo}]$^+$.

^{1}H NMR (CD$_2$Cl$_2$, 700 MHz, 258 K) δ (ppm) = 7.83 (d, $^3J_{HH}$ = 7.7 Hz, 2H, CH fluorenyl), 7.46 (t, $^3J_{HH}$ = 7.8 Hz, 4H, CH Dipp: *para*), 7.30 (t, $^3J_{HH}$ = 7.5 Hz, 2H, CH fluorenyl), 7.26 (t, $^3J_{HH}$ = 7.5

Hz, 2H, CH fluorenyl), 7.11 (d, $^{3}J_{HH}$ = 7.8 Hz, 8H, CH Dipp: *meta*), 7.08 (d, $^{3}J_{HH}$ = 7.7 Hz, 2H, CH fluorenyl), 7.02 (s, 4H, N-C<u>H</u>=C<u>H</u>-N), 2.41 (m, 8H, C<u>H</u>$(CH_3)_2$), 1.06 (d, $^{3}J_{HH}$ = 6.9, 24 H, CH(C<u>H</u>$_3)_2$), 0.81 (d, $^{3}J_{HH}$ = 6.9, 24 H, CH(C<u>H</u>$_3)_2$).

^{11}B NMR (CD_2Cl_2, 96 MHz, 253 K) δ (ppm) = 1.6.

^{13}C{^{1}H} NMR (CD_2Cl_2, 176 MHz, 258 K) δ (ppm) = 161.9 (d, $^{2}J_{CP}$ = 34 Hz, P=C=<u>C</u>=C), 145.6 (Dipp: *ortho*), 143.5 (d, $^{2}J_{CP}$ = 13 Hz, N-C-N), 142.1 (dm, $^{1}J_{CF}$ = 246 Hz, CF B$(OC_6F_5)_4$: *ortho*), 139.1 (d, $^{4}J_{CP}$ = 10 Hz, C_q fluorenyl), 137.7 (dm, $^{1}J_{CF}$ = 244 Hz, CF B$(OC_6F_5)_4$: *para*), 136.0 (d, $^{5}J_{CP}$ = 3 Hz, C_q fluorenyl), 134.9 (dm, $^{1}J_{CF}$ = 242 Hz, CF B$(OC_6F_5)_4$: *meta*), 133.0 (m, CF B$(OC_6F_5)_4$: *ipso*), 131.4 (Dipp: CH *para*), 129.0 (Dipp: *ipso*), 126.5 (CH fluorenyl), 126.3 (d, $^{6}J_{CP}$ = 3 Hz, CH fluorenyl), 124.9 (Dipp: CH *meta*), 121.7 (d, $^{5}J_{CP}$ = 4 Hz, CH fluorenyl), 120.8 (CH fluorenyl), 119.3 (N-CH=CH-N), 99.1 (d, $^{1}J_{PC}$ = 263 Hz, P=<u>C</u>=C=C), 94.6 (d, $^{3}J_{PC}$ = 31 Hz, P=C=C=<u>C</u>), 29.1 (<u>C</u>H$(CH_3)_2$), 25.2 (CH(<u>C</u>H$_3)_2$), 22.8 (CH(<u>C</u>H$_3)_2$).

^{19}F NMR (CD_2Cl_2, 282 MHz, 253 K) δ (ppm) = -156.9 (d, $^{3}J_{FF}$ = 20.4 Hz, 8F, CF B$(OC_6F_5)_4$: *ortho*), -167.9 (m, 8F, CF B$(OC_6F_5)_4$: *meta*), -171.2 (t, $^{3}J_{FF}$ = 20.4 Hz, 4F, CF B$(OC_6F_5)_4$: *para*).

^{31}P NMR (CD_2Cl_2, 121 MHz, 253 K) δ (ppm) = 42.9.

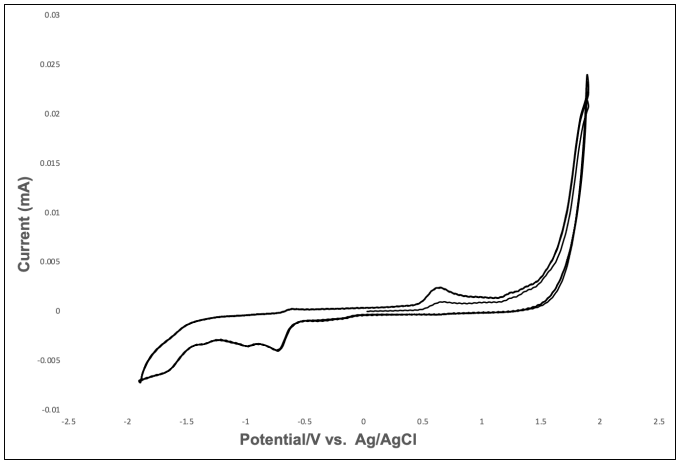

Figure 3-10: Cyclic voltammetry experiment of [**3-2**$^{+}$][B$(OC_6F_5)_4$] in 1,2-DFB (scan rate 100 mV/s, supporting electrolyte 0.1 M N^{n}Bu$_4$PF$_6$, potential versus Ag/AgCl, scanned from -1.9 V to 1.9 V (3 sweeps).

3.5.5 Preparation of [3-2•DMAP][B(OC$_6$F$_5$)$_4$]

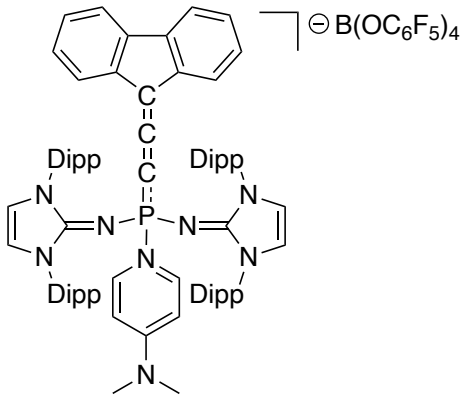

[**3-2**][B(OC$_6$F$_5$)$_4$] (50 mg, 0.028 mmol) was dissolved precooled (-40 °C) DCM (1 mL). A cooled (-40 °C) DCM solution of 4-dimethylaminopyridine (1.1 equiv, 3.8 mg, 0.031 mmol) was then added. The combination was stored overnight at -40 °C, then warmed to room temperature. Afterwards, all volatiles were removed *in vacuo*, and the resulting orange residue was washed with diethyl ether (3 x 1 ml), and benzene (3 x 1 ml). Removal of solvent afforded the title compound as a vibrant orange solid.

Yield: 33 mg (0.017 mmol, 62%).

^{1}H NMR (CD_2Cl_2, 400 MHz, 298 K) δ (ppm) = 7.97 (d, $^3J_{HH}$ = 7.7 Hz, 2H, CH fluorenyl), 7.75 (dd, $^3J_{HH}$ = 7.1. Hz, $^3J_{HP}$ = 8.2 Hz, 2H, DMAP *ortho*-H), 7.36 – 7.24 (m, 6H, CH Dipp; *para* and CH fluorenyl overlapped), 7.19 (t, $^3J_{HH}$ = 7.3 Hz, 2H, CH fluorenyl), 7.10 (dd, $^3J_{HH}$ = 7.8 Hz, 1.4 Hz, 4H, CH Dipp; *meta*), 7.06 (t, $^3J_{HH}$ = 7.3 Hz, 2H, CH fluorenyl), 6.97 (dd, $^3J_{HH}$ = 7.8 Hz, 1.4 Hz, 4H, CH Dipp; *meta*), 6.62 (s, 4H, N-C<u>H</u>=C<u>H</u>-N), 5.55 (d, $^3J_{HH}$ = 7.2 Hz, 2H, DMAP *m*-H), 3.03 (s, 6H, DMAP N(C<u>H</u>$_3$)$_2$), 2.92 (sept, $^3J_{HH}$ = 6.8 Hz, 4H, Dipp; C<u>H</u>(CH$_3$)$_2$), 2.52 (sept, $^3J_{HH}$ = 6.8 Hz, 4H, Dipp; C<u>H</u>(CH$_3$)$_2$), 1.10 (d, $^3J_{HH}$ = 6.8 Hz, 12H, Dipp; CH(C<u>H</u>$_3$)$_2$) 1.04 – 0.98 (m, 24H, Dipp; CH(C<u>H</u>$_3$)$_2$), 0.81 (d, $^3J_{HH}$ = 6.8 Hz, 12H, Dipp; CH(C<u>H</u>$_3$)$_2$).

^{13}C{^{1}H} NMR (CD_2Cl_2, 76 MHz, 298 K) δ (ppm) = 155.5 (DMAP *para*-C), 146.8, (Dipp: *ortho*) 146.3, (Dipp: *ortho*), 143.5 (d, $^2J_{CP}$ = 27.4 Hz, N-C-N), 144.4 (d, $^2J_{CP}$ = 43.5 Hz, P=C=<u>C</u>=C), 142.4 (quaternary carbon, fluorenyl), 142.38 (quaternary carbon, fluorenyl), 130.7 (quaternary carbon, fluorenyl), 138.64 ($^3J_{CP}$ = 6 Hz DMAP *meta*-C),138.64 ($^3J_{CP}$ = 6 Hz DMAP *ortho*-C), 132.4 (Dipp: *ipso*), 130.9 (Dipp; *para*), 125.4 (CH Dipp: *meta*), 125.1 (CH Dipp: *meta*), 124.3 (CH, fluorenyl), 120.1 (CH, fluorenyl), 119.6 (N-CH=CH-N), 119.3 (CH, fluorenyl), 118.7 (CH, fluorenyl), 106.8 ($^2J_{CP}$ = 5.3 Hz DMAP *ortho*-C), 106.8 ($^3J_{CP}$ = 5.3 Hz DMAP *meta*-C), 90.5 (d, $^1J_{CP}$ = 214.1 Hz, P=<u>C</u>=C=C), 75.8 (d, $^3J_{CP}$ = 11.6 Hz, P=C=C=<u>C</u>), 40.3 (DMAP; N(<u>C</u>H$_3$)$_2$), 29.4

(Dipp; $\underline{C}H(CH_3)_2$), 29.3 (Dipp; $\underline{C}H(CH_3)_2$), 25.4 (Dipp; $CH(\underline{C}H_3)_2$), 24.9 (Dipp; $CH(\underline{C}H_3)_2$), 23.4 (Dipp; $CH(\underline{C}H_3)_2$), 22.9 (Dipp; $CH(\underline{C}H_3)_2$).

Note: C-F carbons (*ortho/meta/para*) are too low in intensity, they can be observed in the baseline, but can't be definitively characterized. The data was acquired with 100,000 scans, and a concentrated sample.

^{11}B NMR (CD_2Cl_2, 96 MHz, 298 K) δ (ppm) = -1.2.

^{19}F NMR (CD_2Cl_2, 376 MHz, 298 K) δ (ppm) = -157.9 (d, $^3J_{FF}$ = 19 Hz, 8F, CF $B(OC_6F_5)_4$: *ortho*), -168.6 (t, $^3J_{FF}$ = 21 Hz, 8F, CF $B(OC_6F_5)_4$: *meta*), -172.6 (t, $^3J_{FF}$ = 22 Hz, 4F, CF $B(OC_6F_5)_4$: *para*).

^{31}P NMR (CD_2Cl_2, 162 MHz, 298 K) δ (ppm) = -30.4 (t, $^3J_{HP}$ = 8.2 Hz).

HR-ESI-MS: Calculated for $[C_{76}H_{90}N_8P]^+$ ([3-2•DMAP]$^+$) = 1145.7026 found: m/z = 1041.6256, Calculated for $[B(OC_6F_5)_4]^-$ = 742.9570, found: m/z = 742.9589.

The positive mass peak found corresponds to the calculated mass of $[3\text{-}2\bullet H_2O]^+$ = 1041.6288.

3.5.6 NMR Characterization of [3-2•H_2O][$B(OC_6F_5)_4$].

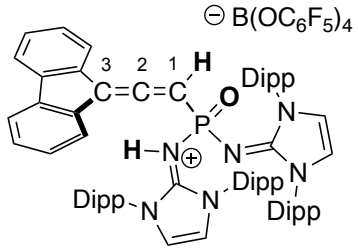

A single drop of water was added via syringe to a suspension of [**3-2**][$B(OC_6F_5)_4$] (~10 mg) in pentane which was stored under argon. The flask was shaken and periodically sonicated until the vibrant red color of [**3-2**]$^+$ completely subsided (took approximately 1 hour). Removal of the solvent and excess water afforded a beige powder which was directly dissolved in CD_2Cl_2 for NMR analysis.

^{1}H NMR (CD_2Cl_2, 400 MHz, 298 K) δ (ppm) = 7.79 (d, J_{HH} = 7.6, 2H, CH fluorenyl), 7.55 -7.45 (br, 4H, CH Dipp; *para*), 7.41 (t, J_{HH} = 7.6, 2H, CH fluorenyl), 7.28 (t, J_{HH} = 7.6, 2H, CH fluorenyl) 7.35 -7.15 (br, 8H, CH Dipp; *meta*), 7.10 (t, J_{HH} = 7.6, 2H, CH fluorenyl), 7.05-6.80 (br, 4H, N-C<u>H</u>=C<u>H</u>-N), 5.40 (broad s, 1H, allene CH), 2.65-2.35 (broad m, 8H, C<u>H</u>$(CH_3)_2$), 1.15-1.10 (broad doublet, 12H, CH(C<u>H</u>$_3)_2$), 1.05-0.90 (br, 24H, CH(C<u>H</u>$_3)_2$), 0.88-0.80 (broad doublet, 12H, CH(C<u>H</u>$_3)_2$).

Note: N-H proton is fluxional between the two exocyclic imine nitrogen atoms and cannot be detected at room temperature. At lower temperatures, the N-H proton appears as a broad singlet within the range 4.5-4.7 ppm. The fluctuation causes broadening of all the NHI related protons.

^{11}B NMR (CD_2Cl_2, 96 MHz, 296 K) δ (ppm) = 1.6.

^{13}C{^{1}H} NMR (CD_2Cl_2, 176 MHz, 298 K) δ (ppm) = 207.4 (s, P-HC=<u>C</u>=CR_2, position 2), 146.7 (C_q Dipp: *ortho*), 142.6 (dm, $^1J_{CF}$ = 245 Hz, CF $B(OC_6F_5)_4$: *ortho*), 139.0 (CH fluorenyl), 138.2 (dm, $^1J_{CF}$ = 246 Hz, CF $B(OC_6F_5)_4$: *para*), 136.9 (d, $^4J_{PC}$ = 7 Hz, CH fluorenyl),135.2 (dm, $^1J_{CF}$ = 241 Hz, CF $B(OC_6F_5)_4$: *meta*), 133.7 (m, CF $B(OC_6F_5)_4$: *ipso*), 129.1 (CH Dipp: *para*), 127.2, (CH fluorenyl), 126.0-124.5 (br, CH, Dipp; *meta*),123.8 (br, CH fluorenyl), 121.0, (CH fluorenyl), 107.7 (d, $^3J_{CP}$ = 16 Hz, position 3), 96.5 (d, $^1J_{CP}$ = 160 Hz, P-H<u>C</u>=C=CR_2, position 1), 29.5 (br, (<u>C</u>H$(CH_3)_2$), 25.3 (CH(<u>C</u>H$_3)_2$), 23.0 (br, CH(<u>C</u>H$_3)_2$)

Note: N-H proton fluctuation broadens the carbon resonances of the NHI substituents. The quaternary carbons including the Dipp *ipso* carbon, the central guanidine carbon ($N_2\underline{C}$=N) and the NHI backbone carbons (N-$\underline{C}$H=$\underline{C}$H-N) are too broad to be definitively assigned.

^{19}F NMR (CD_2Cl_2, 282 MHz, 296 K) δ (ppm) = -157.9 (d, $^3J_{FF}$ = 19.8 Hz, 8F, CF $B(OC_6F_5)_4$: *ortho*), -168.6 (m, 8F, CF $B(OC_6F_5)_4$: *meta*), -172.0 (m, 4F, CF $B(OC_6F_5)_4$: *para*).

^{31}P NMR (CD_2Cl_2, 121 MHz, 296 K) δ (ppm) = -15.3.

HR-ESI-MS: Calculated for $[C_{69}H_{82}N_6OP]^+$ ($[3\text{-}2{\bullet}H_2O]^+$) *m/z* = 1041.6286, found: *m/z* =1041.6288

3.5.7 Isomerization of [3-2][B(OC$_6$F$_5$)$_4$] to [3-2^{cyclo}][B(OC$_6$F$_5$)$_4$]

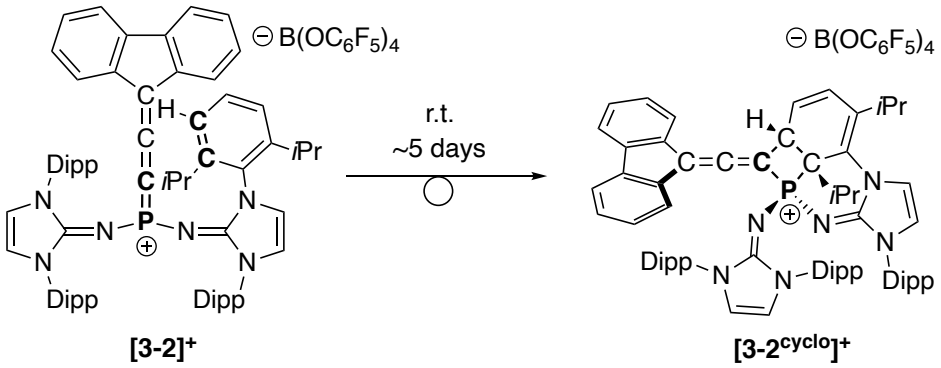

A solution of [**3-2**][$B(OC_6F_5)_4$] in dichloromethane was left to stand in the dark for 5 days. A color change of dark red to light red was noted. The product was obtained as a pale pink solid. The rearrangement/ isomerization reaction also occurs with the same selectively when polar halogenated solvents are used, including with trifluorotoluene, orthodifluorobenzene (1,2-DFB) and orthodichlorobenzene (1,2-DCB). Note: In THF, [**3-2**][$B(OC_6F_5)_4$] partially isomerizes to [**3-2^{cyclo}**][$B(OC_6F_5)_4$] but also decomposes to a new compound with a ^{31}P NMR resonance at 39.8 ppm which could not be identified. The decomposition in THF occurs in a ratio of roughly 2 to 1 (**[3-2^{cyclo}]$^+$** to unknown).

The characterized reaction was performed in CD_2Cl_2.

Note: partial assignment of the ^{13}C NMR was performed using 2D experiments.

^{1}H NMR (CD_2Cl_2, 400 MHz, 298 K) δ (ppm) = 7.80 (d, J_{HH} = 7.7, 1H, CH fluorenyl), 7.77 (d, J_{HH} = 7.7, 1H, CH fluorenyl), 7.47-7.36 (m, 2H CH fluorenyl, 1H CH Dipp: *para*), 7.32-7.22 (m, overlapped 2H CH fluorenyl, 2H CH Dipp; *para*, 2 CH Dipp; *meta*), 7.16-7.10 (m, overlapped 2H CH fluorenyl, 2H CH Dipp: *meta*), 7.01 (s, 2H, N-CH=CH-N, NIDipp), 6.90 – 6.97 (br, 2H, CH Dipp; *meta*), 6.72 (d, J_{HH} = 2.6, 1H, N-CH=CH-N, NIDipp dearomatized), 6.50 (d, J_{HH} = 2.6, 1H, N-CH=CH-N, NIDipp dearomatized), 6.05 (d, J_{HH} = 9.5 Hz, 1H, cyclohexadiene CH), 5.81 (dd, J_{HH} = 9.5 Hz, J_{HH} = 6.5 Hz, 1H, cyclohexadiene CH), 3.21 (sept, J_{HH} = 6.8 Hz, 1H, C<u>H</u>$(CH_3)_2$), 2.82 (dd, J_{HH} = 6.5 Hz, J_{PH} = 4.6 Hz, 1H, phosphacyclobutane C<u>H</u>), 2.80 – 2.71 (br, 1H, C<u>H</u>$(CH_3)_2$), 2.63 (sept, J_{HH} = 6.8 Hz, 2H, C<u>H</u>$(CH_3)_2$), 2.47-2.42 (overlapped septets, 2H, C<u>H</u>$(CH_3)_2$), 2.26 (sept, J_{HH} = 9.5 Hz, 1H, C<u>H</u>$(CH_3)_2$), 1.41 (m, 1H, phosphacyclobutane C-C<u>H</u>$(CH_3)_2$), 1.30-1.22 (m, 15H, CH(C<u>H</u>$_3)_2$), 1.12 (d, J = 6.6 Hz, 3H, CH(C<u>H</u>$_3)_2$), 1.07 (m, 6H, CH(C<u>H</u>$_3)_2$), 0.98 (d, J = 6.9 Hz, 3H, CH(C<u>H</u>$_3)_2$), 0.85-0.82 (m, 9H, CH(C<u>H</u>$_3)_2$), 0.75-0.70 (m, 6H, CH(C<u>H</u>$_3)_2$), 0.68 (d, J_{HH} = 6.9 Hz, 3H, CH(C<u>H</u>$_3)_2$), 0.61 (d, J_{HH} = 6.7 Hz, 3H, phosphacyclobutane C-CH(C<u>H</u>$_3)_2$).

^{11}B NMR (CD_2Cl_2, 96 MHz, 298 K) δ (ppm) = 1.2.

^{13}C{^{1}H} NMR (CD_2Cl_2, 101 MHz, 298 K) δ (ppm) = 194.2 (d, $^{2}J_{CP}$ = 10 Hz, allene C2), 152.7 (C_q C=N-P of NIDipp), 146.8, 146.8, 146.7, 146.3, 146.3, 146.1 and 146.0 (C_q aromatic), 142.7 (d, $^{2}J_{CP}$ = 7 Hz, C_q of cyclohexadiene), 142.1 (dm, $^{1}J_{CF}$ = 247 Hz, CF $B(OC_6F_5)_4$: *ortho*), 139.6 (d, J_{CP} = 2 Hz), 138.9 (d, 2 Hz), 137.7 (dm, $^{1}J_{CF}$ = 244 Hz, CF $B(OC_6F_5)_4$: *para*), 137.6 (d, J_{CP} = 8 Hz,) 137.6 (d, J_{CP} = 8 Hz),134.9 (dm, $^{1}J_{CF}$ = 242 Hz, CF $B(OC_6F_5)_4$: *meta*), 133.3 (m, $B(OC_6F_5)_4$: *ipso*), 131.7, 131.5, 130.6 and 130.5 (CH aromatic), 129.6 (d, J_{CP} = 2 Hz), 129.5 (d, J_{CP} = 2 Hz), 127.9, 127.7 (d, J_{CP} = 2 Hz), 127.3 (d, J_{CP} = 2 Hz), 125.2, 125.0 (d, J_{CP} = 4 Hz, cyclohexadiene CH), 124.7, 124.6, 124.4, 123.9, 123.6 (d, J_{CP} = 2 Hz), 122.5 (d, J_{CP} = 2 Hz), 122.2 (d, J_{CP} = 11 Hz), 121.3, 121.1, 119.4 (N-<u>C</u>H=<u>C</u>H-N, NIDipp), 116.9 (N-<u>C</u>H=<u>C</u>H-N, NIDipp dearomatized), 113.9 ($^{4}J_{CP}$ = 2 Hz, N-<u>C</u>H=<u>C</u>H-N, NIDipp dearomatized), 110.5 (d, $^{1}J_{CP}$ = 60 Hz, allene C1), 52.5 (overlapped with CD_2Cl_2, phosphacyclobutane P-<u>C</u>-CH$(CH_3)_2$), 47.3 ($^{2}J_{CP}$ = 5 Hz, phosphacyclobutane <u>C</u>H), 34.9 (d, $^{2}J_{CP}$ = 4 Hz, phosphacyclobutane P-C-<u>C</u>H$(CH_3)_2$), 29.7 (<u>C</u>H$(CH_3)_2$), 29.3 (<u>C</u>H$(CH_3)_2$), 29.2 (<u>C</u>H$(CH_3)_2$), 28.9 (<u>C</u>H$(CH_3)_2$), 28.2 (<u>C</u>H$(CH_3)_2$), 26.1 (CH(<u>C</u>H$_3)_2$), 25.6 (CH(<u>C</u>H$_3)_2$), 25.4 (CH(<u>C</u>H$_3)_2$), 24.5 (CH(<u>C</u>H$_3)_2$), 23.4 (CH(<u>C</u>H$_3)_2$), 23.3 (CH(<u>C</u>H$_3)_2$), 23.2 (CH(<u>C</u>H$_3)_2$), 23.1 (CH(<u>C</u>H$_3)_2$), 22.9 (CH(<u>C</u>H$_3)_2$), 22.1 (CH(<u>C</u>H$_3)_2$), 21.3

(CH(CH$_3$)$_2$), 20.2, ($^3J_{CP}$ = 3 Hz, P-C-CH(CH$_3$)$_2$), 19.8 (CH(CH$_3$)$_2$), 19.8 (CH(CH$_3$)$_2$), 17.7 (d, $^3J_{CP}$ = 13 Hz, P-C-CH(CH$_3$)$_2$).

^{19}F NMR (CD_2Cl_2, 376 MHz, 298 K) δ (ppm) = -157.9 (d, $^3J_{FF}$ = 19.6 Hz, 8F, CF B(OC_6F_5)$_4$: *ortho*), -168.6 (t, $^3J_{FF}$ = 20.8 Hz, 8F, CF B(OC_6F_5)$_4$: *meta*), -172.1 (t, $^3J_{FF}$ = 22.3 Hz, 4F, CF B(OC_6F_5)$_4$: *para*).

^{31}P NMR (CD_2Cl_2, 121 MHz, 298 K) δ (ppm) = 16.3.

HR-ESI-MS: Calculated for [$C_{69}H_{80}N_6P$]$^+$ ([3-2^{cyclo}]$^+$) = 1023.6182, found: m/z =1023.6154, Calculated for [B(OC_6F_5)$_4$]$^-$ = 742.9570, found: m/z = 742.9585.

3.5.8 Cycloreversion of [3-2^{cyclo}]$^+$; Trapping reaction with DMAP

To a J-Young NMR tube containing a solution of [**3-2^{cyclo}**][B(OC_6F_5)$_4$] (10 mg, 0.0057 mmol) in 1,2-DFB, 10 equivalents of DMAP (6.9 mg 0.057 mmol) were added. The reaction was monitored by heteronuclear NMR spectroscopy, beginning with a heating period of 40 °C, then increasing the temperature in 10-degree increments. Complete cycloreversion occurs at ~60 °C over a total time period of approximately 16 hours. Once conversion was complete, the NMR sample was reduced to a solid residue and directly reconstituted in deuterated acetonitrile.

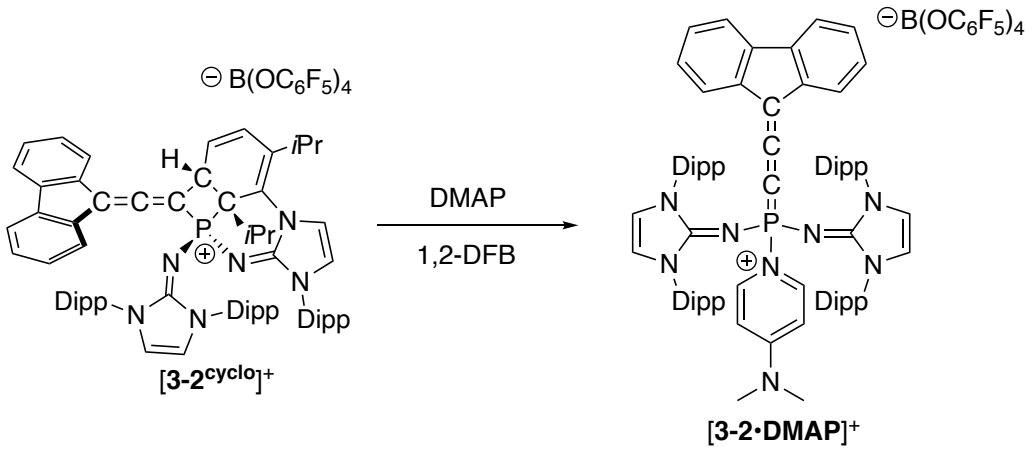

[**3-2^{cyclo}**]$^+$ [**3-2·DMAP**]$^+$

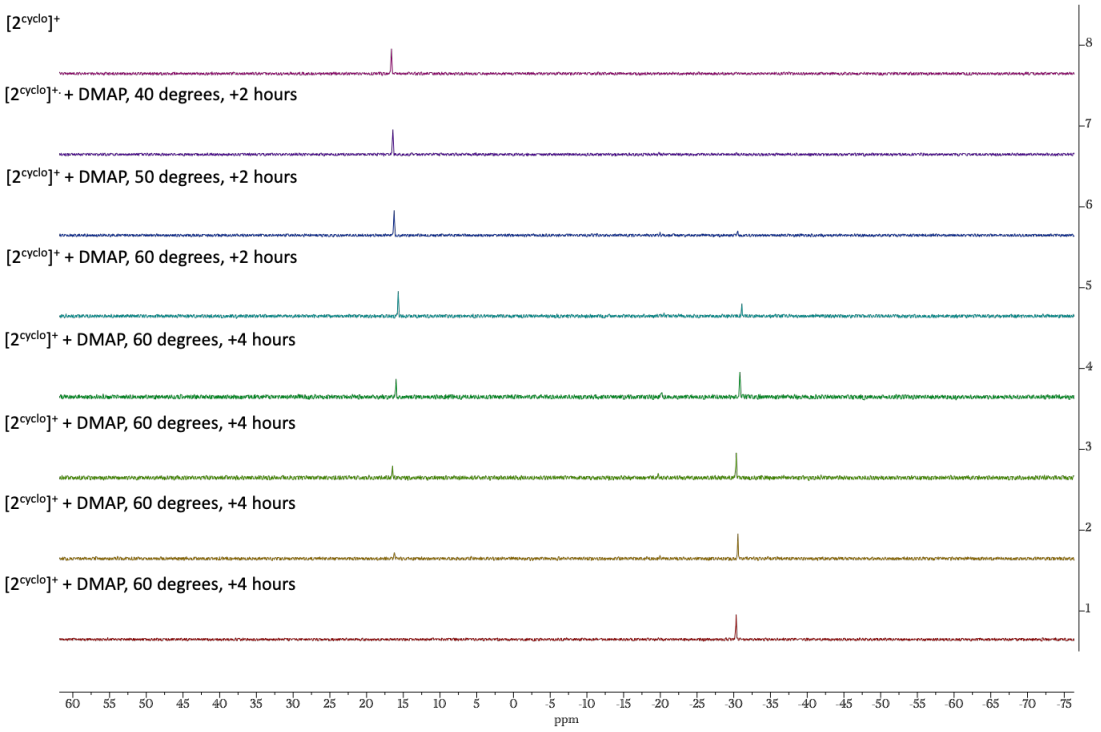

Figure 3-11: Stacked $^{31}P\{^{1}H\}$ NMR spectra monitoring the conversion of [**3-2^{cyclo}**][$B(OC_6F_5)_4$] to [**3-2•DMAP**][$B(OC_6F_5)_4$] in 1,2-DFB.

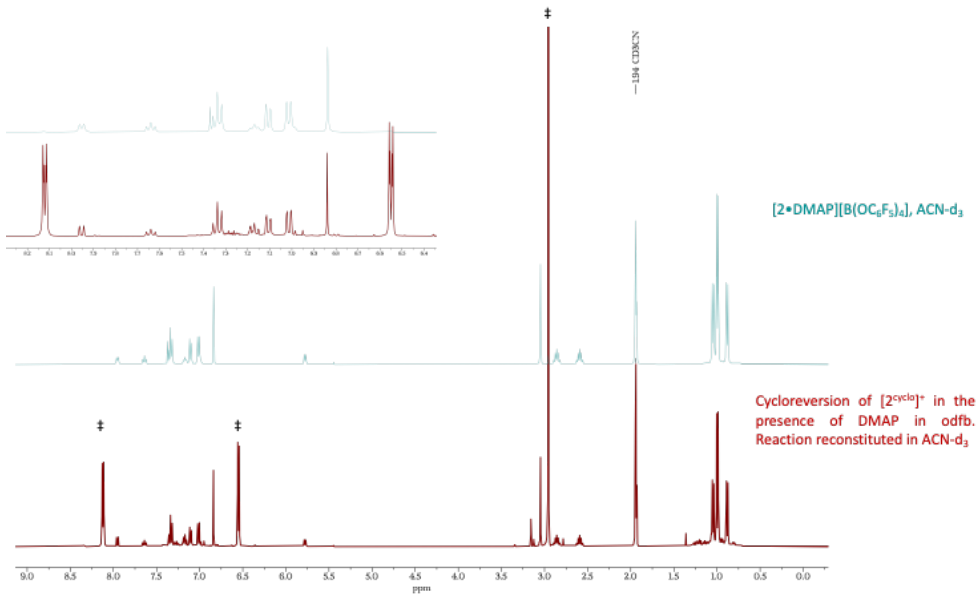

Figure 3-12: Stacked ^{1}H NMR spectra, the top trace corresponds to an isolated sample of [**3-2^{cyclo}**][$B(OC_6F_5)_4$] in ACN-d_3, the bottom trace corresponds to experiment 1.3. Following the reaction of [**3-2^{cyclo}**][$B(OC_6F_5)_4$] with DMAP, 1,2-DFB was removed under reduced pressure and

the residue was directly dissolved in acetonitrile-d_3. The ‡'s reflects the ^{1}H NMR resonances of excess DMAP.

3.5.9 Preparation of [3-4][B(OC$_6$F$_5$)$_4$].

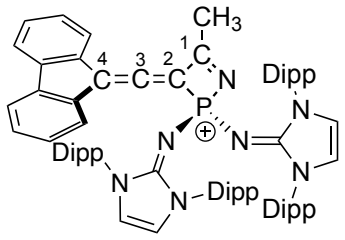

[**3-2**][B(OC$_6$F$_5$)$_4$] (25 mg, .142 mmol, 1.00 equiv) was dissolved in pre-cooled DCM (-40°C), and an excess of acetonitrile (75 uL, 1.4 mmol, 100 equiv) was added. The reaction was allowed to heat to 55°C for 72 hours. Once cooled, the solvent was evaporated in vacuo and the residue was washed with pentane (3 x 2 mL). The title compound was isolated as a light orange powder.

Yield: 25 mg (0.142 mmol, quantitative).

^{1}H NMR ($CDCl_3$, 700 MHz, 298 K) δ (ppm) = 7.75 (d, $^3J_{HH}$ = 7.8 Hz, 2H, CH fluorenyl), 7.43 (t, $^3J_{HH}$ = 7.8 Hz, 2H, CH fluorenyl), 7.39 (t, $^3J_{HH}$ = 7.8 Hz, 4H, CH Dipp; *para*), 7.24 (t, $^3J_{HH}$ = 7.5 Hz, 2H, CH fluorenyl), 7.16 (d, $^3J_{HH}$ = 7.9 Hz, 2H, CH fluorenyl), 7.14 (d, $^3J_{HH}$ = 7.8 Hz, 4H, CH Dipp; *meta*), 7.07 (d, $^3J_{HH}$ = 7.8 Hz, 4H, CH Dipp; *meta*), 6.63 (s, 4H, N-C<u>H</u>=C<u>H</u>=N), 2.62 (sept, $^3J_{HH}$ = 6.9 Hz, 4H, C<u>H</u>(CH$_3$)$_2$), 2.51 (sept, $^3J_{HH}$ = 6.8 Hz, 4H, C<u>H</u>(CH$_3$)$_2$), 1.35, (d, $^4J_{HP}$ = 4.1 Hz, 3H, P-N=C(C<u>H</u>$_3$)), 1.16 (d, $^3J_{HH}$ = 6.8 Hz, 12H, CH(C<u>H</u>$_3$)$_2$), 1.02 (d, $^3J_{HH}$ = 6.8 Hz, 12H, CH(C<u>H</u>$_3$)$_2$), 0.87 (d, $^3J_{HH}$ = 6.9 Hz, 12H, CH(C<u>H</u>$_3$)$_2$), 0.76 (d, $^3J_{HH}$ = 6.8 Hz, 12H, CH(C<u>H</u>$_3$)$_2$).

^{11}B NMR ($CDCl_3$, 128 MHz, 297 K) δ (ppm) = 1.2

^{13}C{^{1}H} NMR ($CDCl_3$, 101 MHz, 298 K) δ (ppm) = 187.9 (d, $^2J_{CP}$ = 24 Hz, P-C=<u>C</u>=CR$_2$, position 3), 187.3 (d, $^2J_{CP}$ = 25 Hz, P-N=<u>C</u>(CH$_3$), position 1), 145.9, (C$_q$ Dipp: *ortho*), 145.4 (C$_q$ Dipp: *ortho*), 143.0 (d, $^2J_{CP}$ = 24 Hz, N-C-N), 142.3 (dm, $^1J_{CF}$ = 238 Hz, CF B(OC$_6$F$_5$)$_4$: *ortho*), 139.6 (C$_q$ fluorenyl), 137.8 (dm, $^1J_{CF}$ = 245 Hz, CF B(OC$_6$F$_5$)$_4$: *para*), 136.1 (J_{CP} = 10 Hz, C$_q$ fluorenyl), 135.0 (dm, $^1J_{CF}$ = 243 Hz, CF B(OC$_6$F$_5$)$_4$: *meta*), 133.5 (m, B(OC$_6$F$_5$)$_4$: *ipso*), 131.6 (Dipp: *ipso*) 130.7 (CH Dipp: *para*),130.0 (CH fluorenyl), 127.0 (CH fluorenyl), 125.0 and 124.9 (CH Dipp; *meta*), 123.7 (CH fluorenyl), 121.2 (CH fluorenyl), 120.5 (d, $^1J_{CP}$ = 70 Hz, P-<u>C</u>=C=CR$_2$, position 2), 118.5 (N-<u>C</u>H=<u>C</u>H=N), 110.1 (d, $^3J_{CP}$ = 20 Hz, P-C=C=<u>C</u>R$_2$, position 4) 29.0 (<u>C</u>H(CH$_3$)$_2$),

29.0(<u>C</u>H(CH$_3$)$_2$), 25.1 (CH(<u>C</u>H$_3$)$_2$), 24.6 (CH(<u>C</u>H$_3$)$_2$), 23.9 (CH(<u>C</u>H$_3$)$_2$), 22.5 (CH(<u>C</u>H$_3$)$_2$), 21.1 (d, $^3J_{CP}$ = 42 Hz, P-N=C(<u>C</u>H$_3$).

^{19}F NMR ($CDCl_3$, 282 MHz, 298 K) δ (ppm) = -157.1 (d, $^3J_{FF}$ = 19.8 Hz, 8F, CF B(OC_6F_5)$_4$: *ortho*), -163.4 - -169.8 (m, 8F, CF B(OC_6F_5)$_4$: *meta*), -171.6 (t, , $^3J_{FF}$ = 22.4 Hz, 4F, CF B(OC_6F_5)$_4$: *para*).

^{31}P NMR ($CDCl_3$, 101 MHz, 298 K) δ (ppm) = -18.7

HR-ESI-MS: Calculated for $[C_{71}H_{83}N_7P]^+$ ([**3**]$^+$) *m/z* = 1064.6442, found: *m/z* =1064.6452.

3.5.10 Stability of [3-2^{cyclo}][B(OC_6F_5)$_4$] to ambient atmosphere

A J-Young NMR tube containing a solution of [**3-2^{cyclo}**][B(OC_6F_5)$_4$] in CD_2Cl_2 was opened to ambient atmosphere, and its decomposition monitored over 16 hours. The ^{1}H and ^{31}P NMR suggest minimal/ no decomposition of the phosphorus cation, while the ^{19}F NMR spectrum indicates a decomposition pathway for the borate anion.

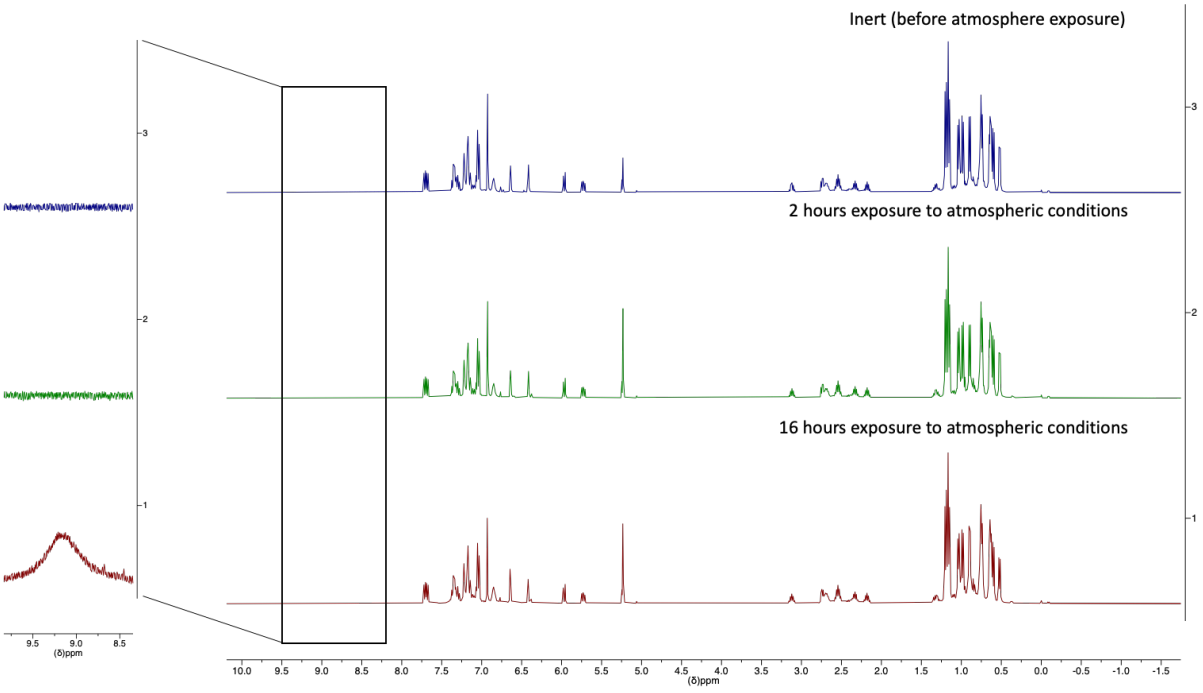

Figure 3-13: ^{1}H NMR spectra of a solution state sample of [**3-2^{cyclo}**][B(OC_6F_5)$_4$] in CD_2Cl_2 before and after exposure to air for up to 16 hours.

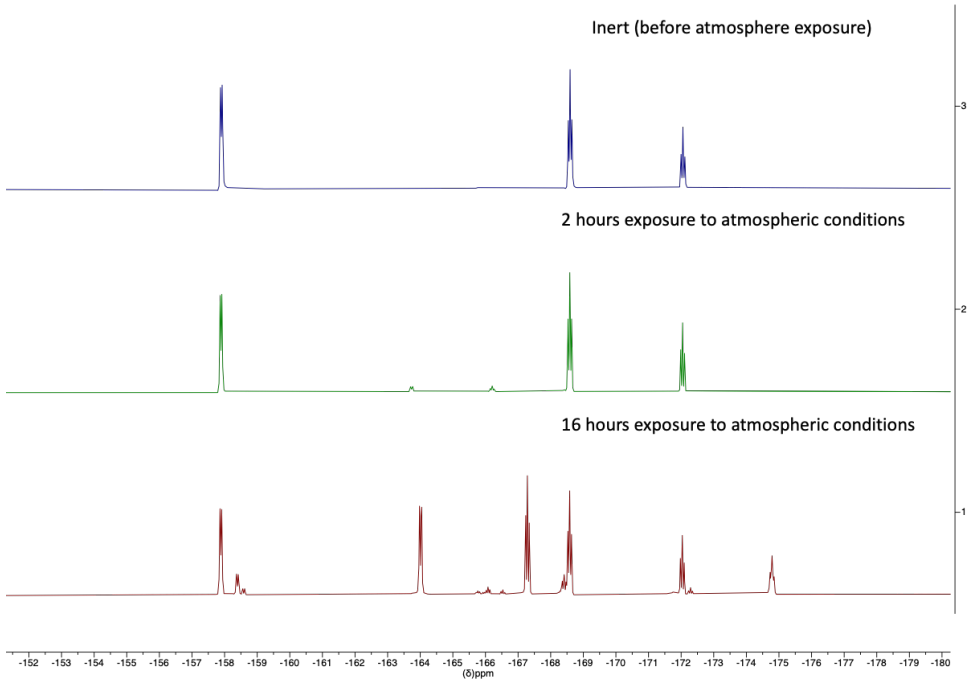

Figure 3-14: $^{19}F\{^{1}H\}$ NMR spectra of a solution state sample of [**3-2^{cyclo}**][$B(OC_6F_5)_4$] in CD_2Cl_2 before and after exposure to air for up to 16 hours.

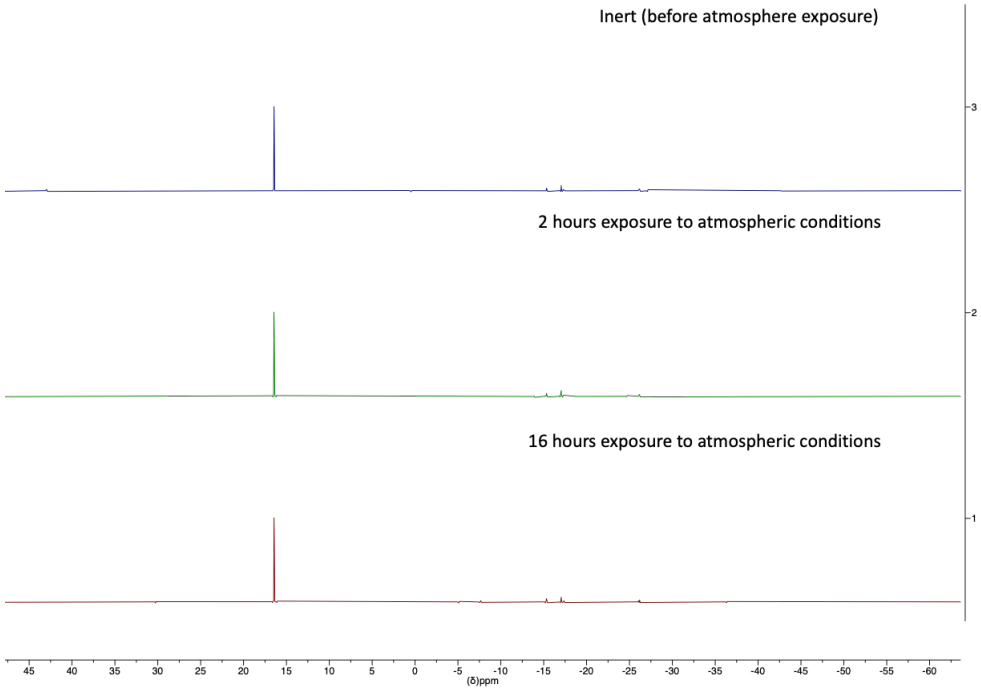

Figure 3-15: $^{31}P\{^{1}H\}$ NMR spectra of a solution state sample of [**3-2^{cyclo}**][$B(OC_6F_5)_4$] in CD_2Cl_2 before and after exposure to air for up to 16 hours.

3.5.11 Attempted Determination of Gutmann Beckett Acceptor number for [3-2]$^+$

A cooled (-40 °C) CD_2Cl_2 solution of [**3-2**]$^+$ (0.019 mmol) was combined with a cooled (-40 °C) CD_2Cl_2 solution of excess Et_3PO (2 equiv) and then allowed to gradually warm to room temperature. The solutions were precooled to minimize [**3-2**]$^+$ to [**3-2**^{cyclo}]$^+$ conversion. The mixture was prepared in a J-Young tube and monitored by NMR approximately two hours after combining.

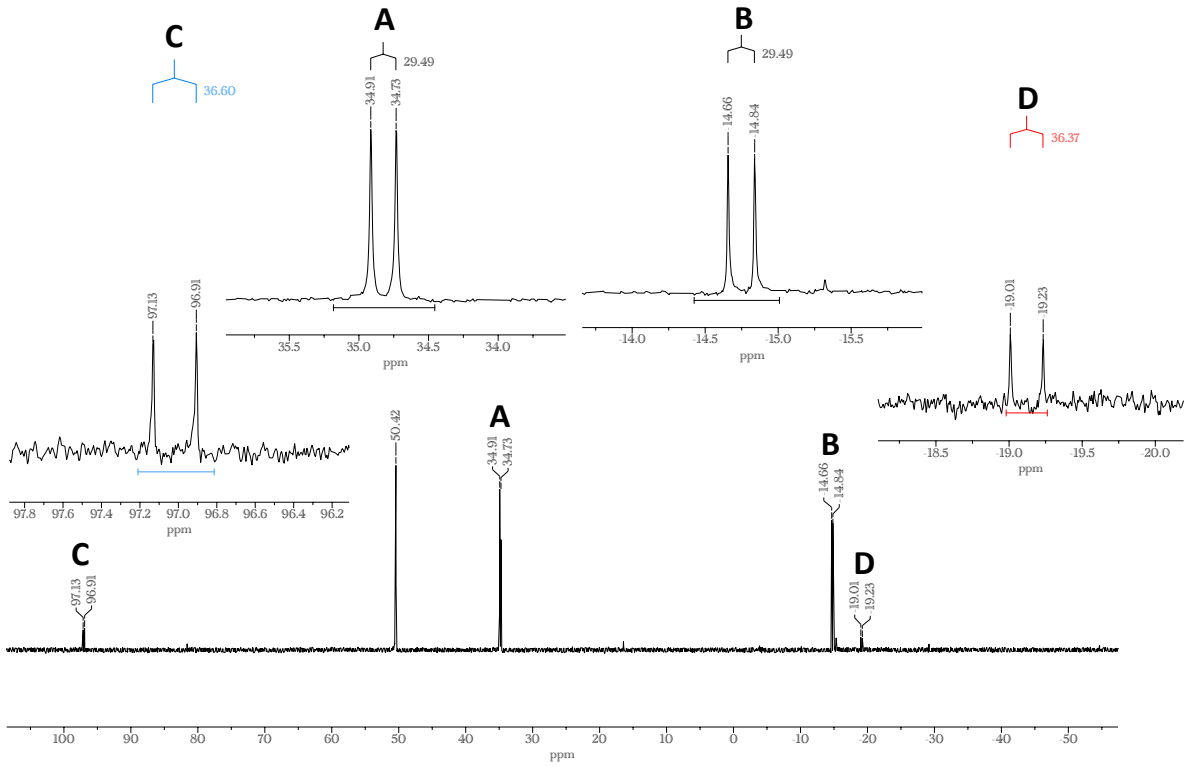

Figure 3-16: $^{31}P\{^1H\}$ NMR spectrum following the addition of Et_3PO to [**3-2**][$B(OC_6F_5)_4$] in CD_2Cl_2.

The reaction gives rise primarily to a set of doublet resonances (δ (ppm) = +34.8 **A** and δ = –14.6 **B**) in the $^{31}P\{^1H\}$ NMR spectrum which exhibit a J_{PP} coupling constant of 29 Hz, corresponding to the proposed cation [**3-3**]$^+$. Excess Et_3PO can also be seen in the reaction mixture (50.4 ppm). We speculated that an additional minor set of doublets (denoted **C** and **D**) could be the intact Et3PO:⟶ [**3-2**]$^+$ adduct. However this would attribute an AN of 124 to [**3-2**]$^+$, exceeding the Lewis acidity of Dielmann's phosphorandylium dications $[R_3P]^{2+}$ (AN = 117), [7] and Stephan's organofluophosphonium cation (AN = 111), [53] which is possible but unsupported by computational evaluation.

3.5.12 Double Nitrile Addition to Allenylidene Phosphonium [3-2]$^+$ to give [3-5]$^+$.

[**3-2**][$B(OC_6F_5)_4$] (25 mg, 0.142 mmol, 1.00 equiv) was dissolved in pre-cooled DCM (-40°C), and an excess of acetonitrile (75 uL, 1.4 mmol, 100 equiv) was added. The reaction was allowed initially heated to 50°C, then eventually brought up to a final temperature 70°C. Conversion was monitored over several days (Figure 3-18). Alternatively, the reaction mixture can immediately be brought to 75°C, and is complete after 4 days. The product was then dried in vacuum, washed with hexanes, dried again, and subsequently taken up in NMR solvent for analysis.

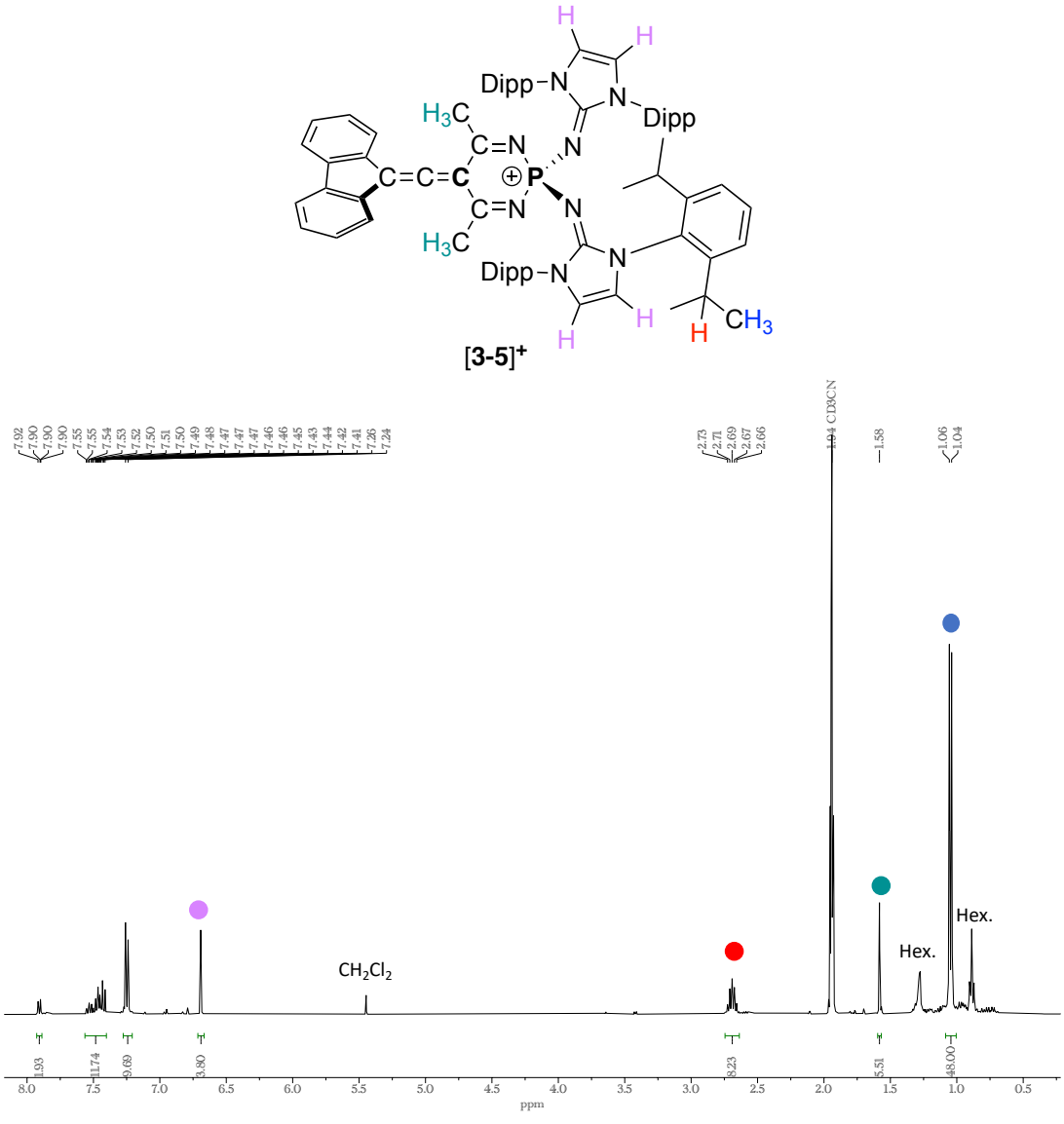

Figure 3-17: ^{1}H NMR spectrum of **[3-5]**$^+$in CD_3CN.

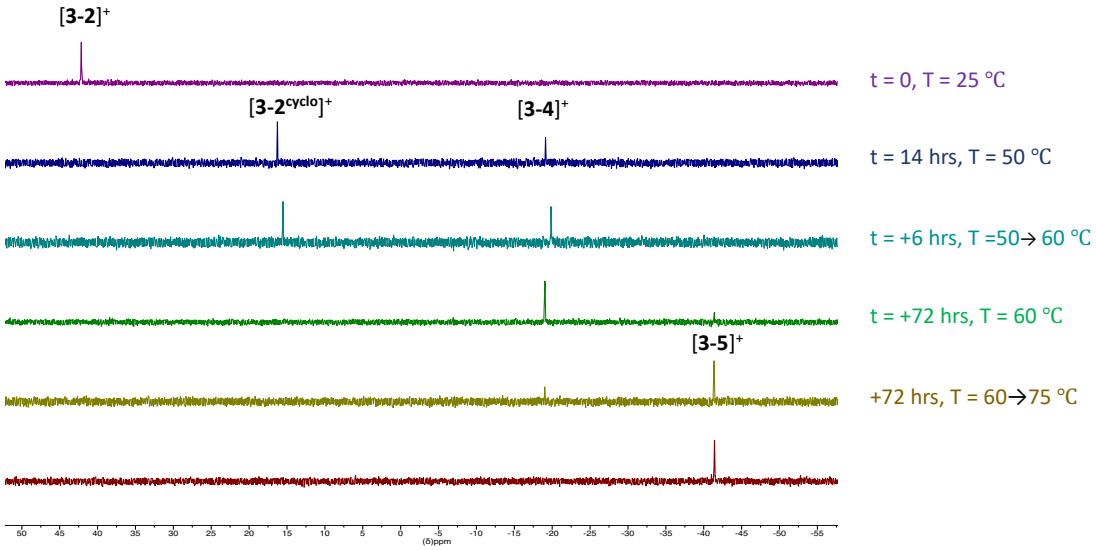

Figure 3-18: Stacked $^{31}P\{^{1}H\}$ NMR spectra (121 MHz) monitoring the conversion of [**3-2**]$^{+}$ to [**3-5**]$^{+}$.

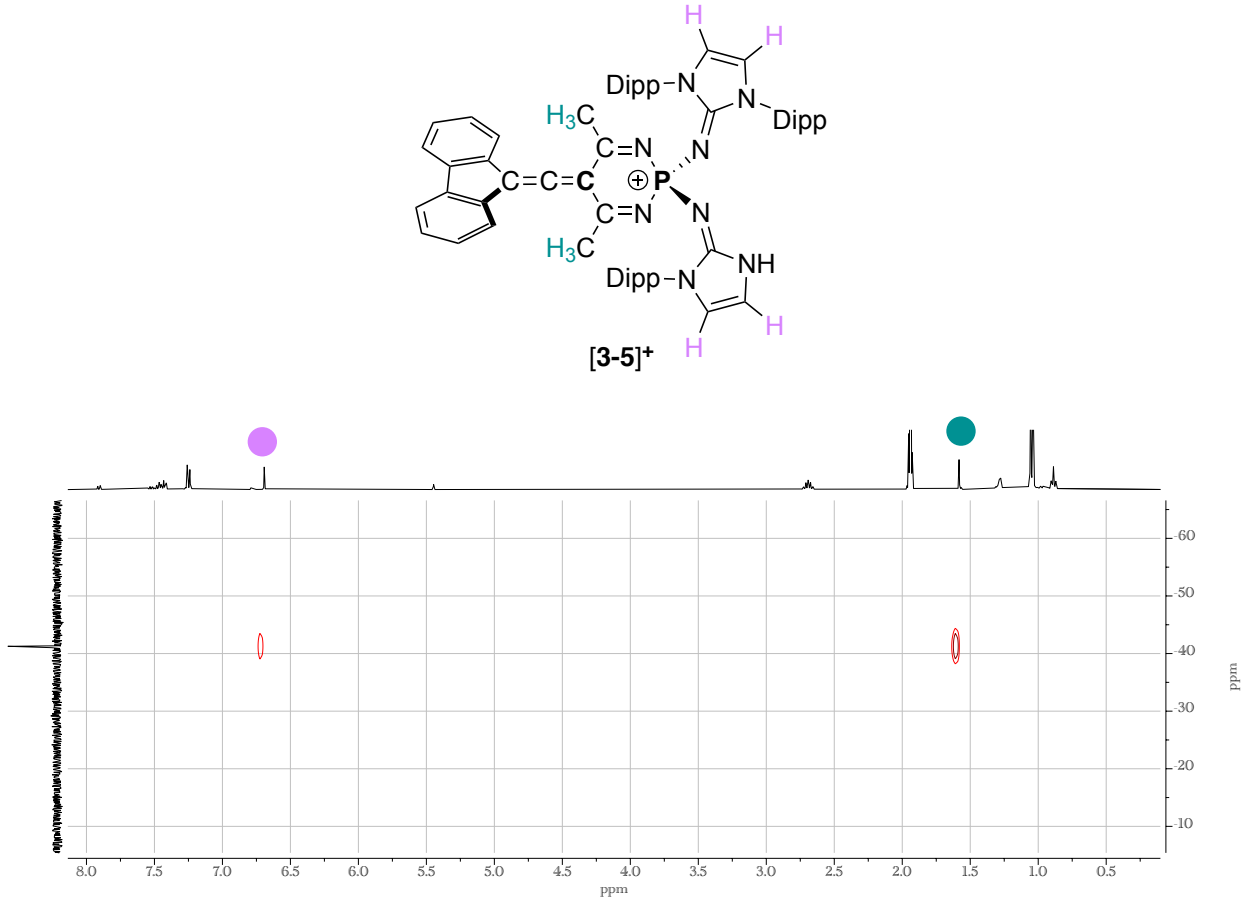

Figure 3-19: $^{1}H/^{31}P$ NMR HMBC spectrum of a crude sample of [**3-5**]$^{+}$ CD_3CN.

ESI-MS of Crude Mixture: Calculated for $[C_{76}H_{90}N_8P]^+$ ([**3-5**]$^+$) = 1105.67 found: m/z = 1105.67

3.5.13 SCXRD Analyses

Single-crystal X-ray diffraction data were collected on a Bruker APEX-II CCD detector or with a Bruker D8 QUEST PHOTON III C14, both using Mo-Kα radiation sources (l = 0.71073 Å). Crystals were selected under oil, mounted on either glass fibre or nylon loops and then immediately placed in a cold stream of N_2 on a diffractometer. The APEX2[S1] and APEX4[S2] software was used to operate the diffractometers. The data was integrated with SAINT15[S3] and corrected for absorption effects based on Gaussian numerical integration and scaled with SADABS.[S4] Using Olex2,[S5] the structures were solved with the Superflip[S6] Olex2.solve [S7], ShelXS [S8], ShelXD [S8] or ShelXT[S9] using charge flipping, direct, or dual methods. The refinement was done with ShelXL[S8] using Least Squares minimization or Olex2.refine[S7] using Gauss-Newton minimization.

Crystallographic data has been deposited with the Cambridge Crystallographic Data Centre as supplementary publication no. CCDC-2371603 (**3-1^a**), CCDC-2371604 (**[3-2][B(OC$_6$F$_5$)$_4$]**), CCDC-2371602 **[3-2^{cyclo}][B(OC$_6$F$_5$)$_4$]**, CCDC-2371601 **[3-2•DMAP][B(OC$_6$F$_5$)$_4$]**. These data can be obtained free of charge via www.ccdc.cam.uk/data_request/cif (or from the CCDC, 12 Union Road, Cambridge CB2 1EZ, UK; fax: (+44) 1223-336-033; or deposit@ccdc.cam.ac.uk). Phosphine (**3-1^b**) has not been deposited.

Phosphine **3-1^a**: Yellow single crystals were obtained by storing a concentrated *n*-hexane solution at -40 °C. Compound **3-1^a** crystallizes in the $P2_1/c$ space group and contains four molecule per unit cell. The assymetric unit contains one molecule of **3-1^a**.

Phosphine **3-1^b**: Colorless single crystals were obtained by storing a concentrated crude reaction mixture in pentane at -40 °C.

[3-2][B(OC$_6$F$_5$)$_4$]: Red single crystals were obtained from a mixed CH_2Cl_2/ pentane solution which was stored at -40 °C. **[3-2][B(OC$_6$F$_5$)$_4$]** crystalizes in the orthorhombic Pccn space group and contains one molecule per unit cell.

[3-2•DMAP][B(OC$_6$F$_5$)$_4$]: Orange single crystals were obtained by slow evaporation of a concentrated ether solution. **[3-2•DMAP][B(OC$_6$F$_5$)$_4$]** crystalizes in the P2$_1$/c space group and contains one molecule of **[3-2•DMAP][B(OC$_6$F$_5$)$_4$]** and one molecule of diethyl ether per unit cell.

[3-2^{cyclo}][B(OC$_6$F$_5$)$_4$]: Colorless single crystals were obtained by slow evaporation of a concentrated CH_2Cl_2. Compound **[3-2^{cyclo}][B(OC$_6$F$_5$)$_4$]** crystalizes in the P2$_1$/c space group and contains one molecule per unit cell.

[3-2•H$_2$O][B(OC$_6$F$_5$)$_4$]: Yellow single crystals were obtained by exposing **[3-2][B(OC$_6$F$_5$)$_4$]** to ambient atmosphere while suspended in paratone oil. The data is of very poor quality but the reflection files are available upon request

Table 3-1: Crystal structure refinement data **3-1**[a], **3-1**[b], and [**3-2**][$B(OC_6F_5)_4$].

Compound	**3-1**[a]	**3-1**[b]	**[3-2][B(OC$_6$F$_5$)$_4$]**
CCDC	2371603	*Not deposited*	2371604
Emp. formula	$C_{70}H_{83}N_6OP$	$C_{39}H_{56}N_6OP$	$C_{108}H_{116}BF_{20}N_6O_4P$
Formula weight	1055.39	655.86	1983.84
Temperature/K	173.00K	173.00K	173.00K
Crystal system	Monoclinic	Monoclinic	Orthorhombic
Space group	$P2_1/c$	$P2_1/c$	*P*ccn
a/Å	23.702(3)	10.7038(6)	25.7844(10)
b/Å	12.4334(14)	19.7416(9)	31.3106(13)
c/Å	21.898(2)	19.7288(11)	24.0922(10)
α/°	90	90	90
β/°	108.088(3)	96.428(2)	90
γ/°	90	90	90
Volume/Å^3	6134.3(12)	3723.0(4)	19450.2(14)
Z	4	4	8
r_{calc}g/cm^3	1.143	1.170	1.355
μ/mm^{-1}	0.092	0.112	0.124
F(000)	2272	1420.0	8304.0
Crystal size/mm^3	0.18 × 0.13 × 0.015	0.1 x 0.05 x 0.05	0.015 × 0.01 × 0.005
Radiation	MoK_a (l = 0.71073)	MoK_a (l = 0.71073)	MoK_a (l = 0.71073)
2Θ range for data collection/°	1.977 to 25.117	4.148 to 55.088	3.38 to 52.744
Index ranges	-28 ≤ h ≤ 28, -14 ≤ k ≤ 14, -26 ≤ l ≤ 25	-13≤ h ≤ 13, -23 ≤ k ≤ 23, -25 ≤ l ≤ 25	-32 ≤ h ≤ 32, -39 ≤ k ≤ 39, 30 ≤ l ≤ 27
Reflections col.	102976	71656	254219
Independent ref.	10673 [R_{int} = 0.1083, R_{int} = 0.0744]	8563 [R_{int} = 0.0913, R_{int} = 0.0497]	19878 [R_{int} = 0.1000, R_{sigma} = 0.0452]
D/R/P	10673/0/721	8563/57/574	19878/0/1142
Goodness-of-fit on F^2	1.016	1.023	1.138
Final R indexes [I>2s (I)]	R_1 = 0.0597, wR_2 = 0.1493	R_1 = 0.0717, wR_2 = 0.1728	R_1 = 0.0956, wR_2 = 0.1972
Final R indexes [all data]	R_1 = 0.1086, wR_2 = 0.1804	R_1 = 0.1212, wR_2 = 0.2075	R_1 = 0.1180, wR_2 = 0.2083
Largest diff. peak/hole/ eÅ^{-3}	0.35/-0.30	1.22/0-71	0.41/-0.51

Table 3-2: Crystal structure refinement data [**3-2^{cyclo}**][$B(OC_6F_5)_4$] and [**3-2•DMAP**][$B(OC_6F_5)_4$].

Compound	**[3-2^{cyclo}][$B(OC_6F_5)_4$]**:	**[3-2•DMAP][$B(OC_6F_5)_4$]**
CCDC	2371602	2371601
Emp. formula	$C_{93}H_{80}BF_{20}N_6O_4P$	$C_{100}H_{90}BF_{20}N_8O_4P$ x $2C_4H_{10}O$
Formula weight	1767.71	2037.81
Temperature/K	173.00K	173.00K
Crystal system	Monoclinic	Triclinic
Space group	$P2_1/c$	P-1 (no. 2)
a/Å	14.4058(6)	14.223(3)
b/Å	22.2218(11)	17.793(4)
c/Å	26.6962	20.317(4)
α/°	90	85.519 (5)
β/°	101.691(2)	76.625 (4)
γ/°	90	87.233 (5)
Volume/Å^3	8368.8(7)	4984.5 (18)
Z	4	2
r_{calc}g/cm^3	1.403	1.358
μ/mm^{-1}	0.134	0.125
F(000)	3648	2124
Crystal size/mm^3	0.186 × 0.088 × 0.045	0.14 × 0.09 × 0.06
Radiation	MoK_a (l = 0.71073)	MoK_a (l = 0.71073)
2Θ range for data collection/°	3.614 to 50.866	2.246 to 25.110
Index ranges	-17 ≤ h ≤ 17, -26 ≤ k ≤ 26, -32 ≤ l ≤ 32	-16 ≤ h ≤ 16, -21 ≤ k ≤ 21, -24 ≤ l ≤ 24
Reflections col.	145065	121104
Independent ref.	15419 [R_{int} = 0.0983, R_{sigma} = 0.0518]	17684 [R_{int} = 0.0714, R_{sigma} = 0.0517]
D/R/P	15419/0/1153	17684/0/1272
Goodness-of-fit on F^2	1.008	1.032
Final R indexes [I>2s (I)]	R_1 = 0.0488, wR_2 = 0.1131	R_1 = 0.0580, wR_2 = 0.1573
Final R indexes [all data]	R_1 = 0.0869, wR_2 = 0.1350	R_1 = 0.0977, wR_2 = 0.1835
Largest diff. peak/hole/ eÅ^{-3}	0.28/-0.30	0.373/-0.457

3.5.12 Computational Details:

All Density Functional Theory (DFT) calculations have been performed using the Gaussian 16 program package.[S10] All geometry optimizations were performed at B3LYP [S11] level of theory using Grimme's D3 dispersion model with Becke-Johnson Damping (D3-BJ) [S12] using def2-TZVP [S13] basis sets employing a universal solvation model based on density (SMD) for dichloromethane.[S14] Frequency calculations confirmed with no imaginary frequencies confirmed the attainment of the stationary points on the potential energy surface (PES). UV-vis absorption spectrum was simulated at B3LYP/6-311+G(d) using SMD for CH_2Cl_2. Transition state geometry produced a single imaginary frequency confirming a first-order saddle point on the PES. The Cartesian coordinates and energies of all optimized molecules are provided in a supplementary *.xyz file. The % s/p-character of the phosphorus atom and cumulenic carbon atoms of [**3-2**]$^+$ were calculated by the natural bond orbital analyses using NBO 3.1 module as implemented in the Gaussian 16 programs in B3LYP/Lanl2dz method.[S15] The Hirshfeld charges and the Mayer bond orders of [**3-2**]$^+$ were calculated using Multiwfn 3.7 software package.[S16] Molecular orbitals and the electrostatic potential map were visualized using GaussView 6 program. The fluoride ion affinity (FIA) of [**3-2**]$^+$ was calculated in the gas phase and in dichloromethane. For the latter the SMD (dichloromethane) solvent correction was applied. The FIAs were calculated according to the reported procedure by Christe [S17] anchored to COF_2.

3.6 References

1. T. Ochiai, D. Franz, S. Inoue, *Chem. Soc. Rev.* **2016**, *45*, 6327–6344.
2. M. D. Roy, E. Rivard, *Acc. Chem. Res.* **2017**, *50*, 2017–2025.
3. Y. K. Loh, L. Ying, M. Ángeles Fuentes, D. C. H. Do, S. Aldridge, *Angew. Chem. Int. Ed.* **2019**, *58*, 4847–4851.
4. M. Peters, A. Doddi, T. Bannenberg, M. Freytag, P.G. Jones, M. Tamm, *Inorg. Chem.* **2017**, *56*, 10785–10793.
5. A. Doddi, D. Bockfeld, T. Bannenberg, M. Tamm, *Chem. Eur. J.* **2020**, *26*, 14878–14887.
6. M. E. Doleschal, A. Espinosa Ferao, A. Kostenko, F. J. Kiefer, S. Inoue, *Angew. Chem. Int. Ed.* **2025**, *64, e202422186.*
7. P. Mehlmann, T. Witteler, L. F. B. Wilm, F. Dielmann, F. *Nat. Chem.* **2019**, *11*, 1139–1143.
8. L. F. B. Wilm, T. Eder, C. Mück-Lichtenfeld, P. Mehlmann, M. Wünsche, F. Buß, Dielmann, *Green Chem.* **2019**, *21*, 640–648.
9. M. Zhong, M. Yuan, *RSC Adv*. **2025**, *15*, 15052–15085.
10. N. Kuhn, R. Fawzi, M. Stiemann, J. Wiethoff, *Chem. Ber.* **1996**, *129*, 479–482.
11. P. Mehlmann, C. Mück-Lichtenfeld, T. T. Y. Tan, F. Dielmann, *Chem. Eur. J.* **2017**, *23*, 5929–5933.
12. O. Back, B. Donnadieu, M. von Hopffgarten, S. Klein, R. Tonner, G. Frenking, G. Bertrand, *Chem. Sci.* **2011**, *2*, 858–861.
13. F. Dielmann, O. Back, M. Henry-Ellinger, P. Jerabek, G. Frenking, G. Bertrand, *Science* **2012**, *337*, 1526–1528.
14. F. Dielmann, C. E. Moore, A. L. Rheingold, G. Bertrand, *J. Am. Chem. Soc.* **2013**, *135*, 14071–14703.
15. M. A. Wünsche, T. Witteler, F. Dielmann, *Angew. Chem. Int. Ed.* **2018**, *57*, 7234–7239.
16. P. Löwe, T. Witteler, F. Dielmann, *Chem. Comm.* **2021**, *57*, 5043–5046.

17. P. Löwe, M. A. Wünsche, F. R. S. Purtscher, J. Gamper, T. S. Hofer, L. F. B. Wilm, M. B. Röthel, F. Dielmann, *Chem. Sci.* **2023**, *14*, 7928–7935.
18. M. A. Wünsche, dissertation, Westfälische Wilhelms-Universität Münster, **2018**.
19. P. Löwe, dissertation, Westfälische Wilhelms-Universität Münster, **2022**.
20. D. Sarkar, P. Vasko, L. Ying, J. J. C. Struijs, L. P. Griffin, S. Aldridge, *Angew. Chem. Int. Ed.* **2025**, *64*, e202502326.
21. D. Sarkar, P. Vasko, A. F. Roper, A. E. Crumpton, M. D. Roy, L. P. Griffin, C. Bogle, S. Aldridge, *J. Am. Chem. Soc.* **2024**, *146*, 11792–11800.
22. J. T. Boronski, A. E. Crumpton, A. F. Roper, S. Aldridge, *Nat. Chem.* **2024**, *16*, 1295–1300.
23. D. Sarkar, P. Vasko, T. Gluharev, L. P. Griffin, C. Bogle, J. J. C. Struijs, J. Tang, A. F. Roper, A. E. Crumpton, S. Aldridge, *Angew. Chem. Int. Ed.* **2024**, *63*, e202407427.
24. M. Balmer, Y. J. Franzke, F. Weigend, C. von Hänisch, *Chem. Eur. J.* **2020**, *26*, 192–197.
25. M. Doleschal, A. Kostenko, J. Y. Liu, S. Inoue, *Nat. Chem.* **2024**, *16*, 2009–2016.
26. V. Nesterov, R. Baierl, F. Hanusch, A. E. Ferao, S. Inoue, *J. Am. Chem. Soc.* **2019**, *141*, 14576–14580.
27. T. F. Leung, D. Jiang, M-C. Wu, D. Xiao, W-M. Ching, G. P. A. Yap, T. Yang, L. Zhao, T-G. Ong, G. Frenking, *Nat. Chem.* **2021**, *13*, 89–93.
28. L. C. Torres, R. Dobrovetsky, C. B. Caputo, *Chem. Comm.* **2021**, *57*, 8272–8275.
29. L. C. Torres, A. Brar, J. LeBlanc, C B. Ameyaw, C. B. Caputo, *Z. Anorg. Allg. Chem.* **2023**, *649*, e202200383.
30. O. Ekkert, G. Kehr, R. Fröhlich, G. Erker, *Chem. Commun*. **2011**, *47*, 10482–10484.
31. M. D. Böhme, T. Eder, M. B. Röthel, P. D. Dutschke, L. F. B. Wilm, E. Hahn, F. Dielmann, *Angew. Chem. Int. Ed.* **2022**, *61*, e202202190.
32. D. Naumann, H. Butler, R. Gnann, *Z. Anorg. Allg. Chem.* **1992**, *618*, 74–76.
33. A. D. Hendsbee, N. A. Giffin, Y. Zhang, C.C. Pye, J. D. Masuda, *Angew. Chem. Int. Ed.*

2012, *51*, 10836–10840.

34. R. Heyes, J. C. Lockhart, *J. Chem. Soc. A*. **1968**, 326–328.

35. H. C. Brown, S. K. Gupta, *J. Am. Chem. Soc*. **1970**, *93*, 6983–6984.

36. D. J. Pasto, V. Balasubramaniyan, P. W. Wojtkowski, *Inorg. Chem*. 1969, *8*, 594–598.

37. Y. Hasegawa, G. Kehr, S. Ehrlich, S. Grimme, C. G. Daniliuc, G. Erker, *Chem. Sci*. **2014**, *5*, 797–803.

38. F. Lavigne, E. Maerten, G. Alcaraz, N. Saffon-Merceron, C. Acosta-Silva, V. Branchadell, A. Baceiredo, *J. Am. Chem. Soc.* **2010**, *132*, 8864–8865.

39. U. Heim, H. Pritzkow, H. Schönberg, H. Grützmacher, *J. Chem. Soc. Chem. Commun.* **1993**, 673–674.

40. J. A. Januszewski, R. R. Tykwinksi, *Chem. Soc. Rev*. **2014**, *43*, 3184–3203.

41. D. Wendinger, R. R. Tykwinksi, *Acc. Chem. Res*. **2017**, *50*, 1468−1479.

42. E. Weber, W. Seichter, R-J. Wang, T. C. W. Mak, *Bull. Chem. Soc. Jpn.* **1991**, *64*, 659−667.

43. M. Franz, J. A. Januszewski, D. Wendinger, C. Neiss, L. D. Movsisyan, F. Hampel, H. L. Anderson, A. Görling, R. R. Tykwinski, *Angew. Chem. Int. Ed.* **2015**, *54*, 6645–6649.

44. Y. Li, K. C. Mondal, P. P. Samuel, H. Zhu, C. M. Orben, S. Panneerselvam, B. Dittrich, B. Schwederski, W. Kaim, T. Mondal, D. Koley, H. W. Roesky, *Angew. Chem. Int. Ed.* **2014**, *53*, 4168–4172.

45. L. Jin, M. Melaimi, L. L. Liu, G. Bertrand, *Org. Chem. Front.* **2014**, *1*, 351–354.

46. A. D. Becke, *J. Chem. Phys.* **1993**, *98*,1372–1377.

47. F. Weigend, R. Ahlrichs, *Phys. Chem. Chem. Phys*. **2005**, *7*, 3297–3305.

48. S. Grimme, S. Ehrlich, L. Goerigk, *J. Comput. Chem.* **2011**, *32*,1456–1465.

49. N. E. Kolobova, L. L. Ivanov, O. S. Zhvanko, O. M. Khitrova, A. S. Batsanov, Y. T. Struchkov, *J. Organomet. Chem.* **1984**, *262*, 39−47.

50. M. I. Bruce, *Chem. Rev*. **1991**, *91*, 197−257.

51. O. Ordoñez, X. Yu, M. A. Schuerlein, G. Wu, J. Autschbach, T. W. Hayton, *J. Am. Chem. Soc.* **2024**, *146*, 28306−28319.

52. K. O. Christe, D. A. Dixon, D. McLemore, W. W. Wilson, J. A. Sheehy, J. A. Boatz, *J. Fluor. Chem.* **2000**, *101*, 151–153.

53. C. B. Caputo, L. J. Hounjet, R. Dobrovetsky, D. W. Stephan, *Science*. **2013**, *341*, 1374–1377.

54. D. Roth, J. Stirn, D. W. Stephan, L. Greb, *J. Am. Chem. Soc.* **2021**, *143*, 15845–15851.

55. U. Mayer, V. Gutmann, W. Gerger, *Monatsh. Chem.* **1975***, 106*, 1235–1257.

56. M. A. Beckett, D. S. Brassington, S. J. Coles, M. B. Hursthouse, *Inorg. Chem. Commun.* **2000**, *3*, 530–533.

57. H. J. Bestmann, *Angew. Chem. Int. Ed*. *Engl*. **1977**, *16*, 349–364.

58. R. Wei, X-F. Wang, D. A. Ruiz, L. L. Liu, *Angew. Chem. Int. Ed*. **2023**, *62*, e202219211.

59. A. Brar, D. K, Unruh, A. J. Aquino, C. Krempner, *Chem. Comm.* **2019**, *55*, 3513–3516.

60. H. Burzlaff, R. Hagg, E. Wilhelm, H. J. Bestmann, *Chem. Ber.* **1985**, *118*, 1720–1723.

61. U. Heim, H. Pritzkow, U. Fleischer, H. Grützmacher, *Angew. Chem. Int. Ed*. **1993**, *32*, 1359–1361.

62. E. Buchner, T. Curtius, *Ber. Dtsch. Chem. Ges.* **1885**, *18*, 2377–2379. b) E. Buchner, T. Curtius, *Ber. Dtsch. Chem. Ges.* **1885**, *18*, 2371–2377.

63. T. Ye and M. A. McKervey, *Chem. Rev.* **1994**, *94*, 1091–1160.

64. Y. Chen, P. Su, D. Wang, Z. Ke, G. Tan, *Nat. Commun.* **2024**, *15*, 4579.

65. L. L. Liu, J. Zhou, R. Andrews, D. W. Stephan, *J. Am. Chem. Soc.* **2018**, *140*, 7466–7470.

66. L. L. Liu, J. Zhou, L.L. Cao, R. Andrews, R. L. Falconer, C. A. Russell, D. W. Stephan, *J. Am. Chem. Soc.* **2018**, *140*, 147–150.

67. M. Kira, S. Ishida, T. Iwamoto, C. Kabuto, *J. Am. Chem. Soc.* **2002**, *124*, 3830–3831.

68. T. Kosai, S. Ishida, T. Iwamoto, *Angew. Chem. Int. Ed.* **2016**, *55*, 15554–15558.

69. T. Kosai, S. Ishida, T. Iwamoto, *Chem. Commun.* **2015**, *51*, 10707–10709.

70. H. Suzuki, N. Tokitoh, R. Okazaki, *J. Am. Chem. Soc.* **1994**, *116*, 11572–11573.

71. D. Wendel, A. Porzelt, F. A. D. Herz, D. Sarkar, C. Jandl, S. Inoue, B. Rieger, *J. Am. Chem. Soc.* **2017**, *139*, 8134–8137.

72. C. Xu, Z. Ye, L. Xiang, S. Yang, Q. Peng, X. Leng, Y. Chen, *Angew. Chem. Int. Ed.* **2021**, *60*, 3189–3195.

73. H. Zhu, A. Kostenko, D. Franz, F. Hanusch, S. Inoue. *J. Am. Chem. Soc.* **2023**, *145*, 1011–1021.

74. X. Zhang, L. L. Liu, *Angew. Chem. Int. Ed.* **2022**, *134*, e202116658.

75. L. L. Liu, J. Zhou, L.L. Cao, Y. Kim, D. W. Stephan, *J. Am. Chem. Soc*. **2019**, *141*, 8083–8087.

76. D. Raiser, C. P. Sindlinger, H. Schubert, L. Wesemann, *Angew. Chem. Int. Ed.* **2020**, *59*, 3151–3155.

77. Y. K. Loh, M. Melaimi, D. Munz, G. Bertrand, *J. Am. Chem. Soc.* **2023**, *145*, 2064–2069.

78. H. D. Hartzler, *J. Am. Chem. Soc.* **1966**, *88*, 3155–3156.

79. H. D. Hartzler, *J. Am. Chem. Soc.* **1971**, *93*, 4527–4531.

80. B. Bildstein, M. Schweiger, H. Angleitner, H. Kopacha, K. Wurst, K. H. Ongania, M. Fontani, P. Zanello, *Organometallics.* **1999**, *18*, 4286–4295.

81. J. A. Januszewski, F. Hampel, C. Neiss, A. Görling, R. R. Tykwinksi, *Angew. Chem. Int. Ed. Engl.* **2014**, *53*, 3743–3747.

82. C. Ehm, D. Lentz, *Chem. Commun.* **2010**, *46*, 2399–2401.

83. K. Brand, *Ber. Dtsch. Chem. Ges. B*. **1921**, *54*, 1987–2006.

84. A. Igau, A. Baceiredo, H. Grützmacher, H. Pritzkow, G. Bertrand, *J. Am. Chem. Soc.* **1989**, *111*, 6853–6854.

85. J. B. Farahi, K. M. Doxsee, *J. Am. Chem. Soc.* **1988**, *110*, 7240–7242.

86. P. Löwe, M. Feldt, M. A. Wünsche, L. F. B. Wilm, F. Dielmann, *J. Am. Chem. Soc.* **2020**, *142*, 9818–9826.

3.6.2 Crystallographic and Computational References

S1. APEX2 Version 2.1 – 0; Bruker AXS Inc. Madison, **2004**.

S2. APEX4; Bruker AXS Inc. Madison, **2021**.

S3. SAINT version 7.46a, Bruker AXS Inc. Madison **2004**.

S4. G. Sheldrick GM SADABS. University of Göttingen, Göttingen **1996**.

S5. O. V. Dolomanov, L. J. Bourhis, R. J. Gildea, J. A. K. Howard and H. Puschmann, *J. Appl. Crystallogr.* **2009**, *42*, 339–341.

S6. a) L. Palatinus, G. Chapuis, *J. Appl. Cryst.* **2007**, 40, 786-790; b) L. Palatinus, A. van der Lee, *J. Appl. Cryst.* **2008**, 41, 975-984; c) L. Palatinus, S. J. Prathapa, S. van Smaalen, *J. Appl. Cryst.* **2012**, *45*, 575-580.

S7. L. J. Bourhis; O. V. Dolomanov; R. J. Gildea; J. A. K. Howard; H. Puschmann, *Acta crystallogr. A*. **2015**, *71*, 59–75.

S8. G. M. Sheldrick, *Acta crystallogr. A*. **2008**, *64*, 112–122.

S9. G. M. Sheldrick, *Acta crystallogr. A*. **2015**, *71*, 3–8.

S10. Gaussian 16, Revision C.01, M. J. Frisch, G. W. Trucks, H. B. Schlegel, G. E. Scuseria, M. A. Robb, J. R. Cheeseman, G. Scalmani, V. Barone, G. A. Petersson, H. Nakatsuji, X. Li, M. Caricato, A. V. Marenich, J. Bloino, B. G. Janesko, R. Gomperts, B. Mennucci, H. P. Hratchian, J. V. Ortiz, A. F. Izmaylov, J. L. Sonnenberg, D. Williams-Young, F. Ding, F. Lipparini, F. Egidi, J. Goings, B. Peng, A. Petrone, T. Henderson, D. Ranasinghe, V. G. Zakrzewski, J. Gao, N. Rega, G. Zheng, W. Liang, M. Hada, M. Ehara, K. Toyota, R. Fukuda, J. Hasegawa, M. Ishida, T. Nakajima, Y. Honda, O. Kitao, H. Nakai, T. Vreven, K. Throssell, J. A. Montgomery, Jr., J. E. Peralta, F. Ogliaro, M. J. Bearpark, J. J. Heyd, E. N. Brothers, K. N. Kudin, V. N. Staroverov, T. A. Keith, R. Kobayashi, J. Normand, K.

Raghavachari, A. P. Rendell, J. C. Burant, S. S. Iyengar, J. Tomasi, M. Cossi, J. M. Millam, M. Klene, C. Adamo, R. Cammi, J. W. Ochterski, R. L. Martin, K. Morokuma, O. Farkas, J. B. Foresman, and D. J. Fox, Gaussian, Inc., Wallingford CT, **2016**.

S11. A. D. Becke, *J. Chem. Phys*, **1993**, *98*, 5648–5652; b) C. Lee, W. Yang, R. G. Parr, *Phys. Rev. B.* **1998**, *37*, 785–789; c) S. H. Vosko, L. Wilk, M. Nusair, *Can. J. Phys*. **1980**, *58*, 1200-1211; d) P. J. Stephens, F. J. Devlin, C. F. Chabalowski, M. J. Frisch, *J. Phys. Chem*. **1994**, *98*, 11623–11627.

S12. a) L. Goerigk, S. Grimme, *J. Chem. Theory Comput.* **2011**, *7*, 291–309; b) L. Goerigk, A. Hansen, C. Bauer, S. Ehrlich, A. Najibi, S. Grimme, *Phys. Chem. Chem. Phys.* **2017**, *19*, 32184–32215; c) B. G. Johnson, M. J. Frisch, *J. Chem. Phys.* **1994**, *100*, 7429–7442.

S13. F. Weigend, R. Ahlrichs, *Phys. Chem. Chem. Phys.* **2005**, *7*, 3297–3305; b) F. Weigend, *Phys. Chem. Chem. Phys.* **2006**, *8*, 1057–1065.

S14. A. V. Marenich, C. J. Cramer, D. G. Truhlar, *Phys. Chem. B*. **2009**, *113*, 6378–6396.

S15. a) F. Weinhold, C. R. Landis (Eds.) Discovering Chemistry with Natural Bond Orbitals, John Wiley & Sons, Inc, Hoboken, NJ, USA, **2012**; b) J. P. Foster, F. Weinhold, *J. Am. Chem. Soc.* **1980**, 102, 7211–7218; c) A. E. Reed, R. B. Weinstock, F. Weinhold, *J. Chem. Phys.* **1985**, 83, 735–746; d) J. E. Carpenter, F. Weinhold, *J. Mol. Struct.: THEOCHEM*. **1988**, 169, 41–62; e) F. Weinhold, J. E. Carpenter, *The Structure of Small Molecules and Ions*, R. Naaman and Z. Vager, Springer US, Boston, MA, **1988**, 227–236.

S16. T. Lu, F. Chen, *J. Comput. Chem.* **2012**, *33*, 580–592.

S17. K. O. Christe, D. A. Dixon, D. McLemore, W. W. Wilson, J. A. Sheehy, J. A. Boatz, *J. Fluorine Chem*. **2000**, *101*, 151–153.

Chapter Four: Synthesis, Characterization and Reactivity of Alkyl-Imino-Phosphenium Cations.

The synthesis of all new compounds in this chapter was performed by the primary author. Computations were performed by Avik Bhattacharjee (FMOs, Mayer Bond Order Calculations, NBO analysis, Hirshfeld Charge analysis and TD-DFT) and Pawel Löwe (FMO and FIA calculations). SCXRD data collection and solving was performed by Casey Lenart, Michael Seidl and Klaus Wurst.

This thesis will contain 4 derivatives of phosphenium cations derived from different N-heterocyclic imines. The purpose of synthesizing these derivatives was to delineate how differences in the steric and electronic properties of the NHI component would modulate the subsequent reactivity of this family of phosphenium cations. The synthesis of these phosphenium cations and their phosphine precursors was initially performed at the University of Innsbruck, with the intention being to study their reactivity at York University. Unfortunately, a package containing the precursors for 3 out of 4 of these derivatives was lost by the shipping courier (UPS) during their transport back to Toronto, and it was ultimately decided due to time constraints not to pursue their re-synthesis, however their preparation will still be outlined, and some computational insight for the compounds will be provided.

4.1 Introduction

4.1.1 Ambiphilic Main Group Carbenoids

The orthogonal arrangement of occupied and unoccupied orbitals at dicoordinate carbenoid centers $(R_2E:)^n$ (n = charge) (E = Group 13-15 elements) enables their reactivity towards the cleavage of high energy bonds. As a collective, $R_2E:^n$ species have demonstrated insertion into a range of bonds, including those commonly found in organic compounds like N–H, O–H, C–X (F, Cl, Br, I), homoatomic bonds like H–H, P–P, as well as inorganic heteroatomic bonds like B–H, Si–H, P–H. [1,2] Although considerably less common, subsequent reductive eliminations have also been shown to occur from activated carbenoid centers, seeding the question as to whether there is a future where main-group elements replace organometallic complexes.[1,3] Generally, closer convergence of the HOMO and LUMO energies of $R_2E:^n$ compounds crudely correlates with more pronounced reactivity.[1,2] As discussed in the introduction (Section 1.1.4) and illustrated by comparison of the electronic properties of NHCs and CAACs, the most well-studied approach to modifying the FMO energies of $R_2E:^n$ species occurs by changing the electronic nature of the substituents (R).[4] The bond angle of the substituents about the E center (∠R–E–R) is also influential. As $R_2E:^n$ systems approach linearity, the HOMO and LUMO at E adopt more *p* character and become degenerate. Consequently, cyclic carbenoids of larger ring size or acyclic variants which allow for very obtuse ∠R–E–R angles, are more ambiphilic.[5]

4.1.2 Reactivity of Phosphenium Cations

Alluded to in Chapter 1, phosphenium cations $[R_2P:]^+$ predate most other dicoordinate carbenoid species, and their potential to perform oxidative addition type transformations on account of their ambiphilic character was recognized as early as 1982 through various [n+1] cycloaddition reactions and by intramolecular C–H activation (Scheme 1-7).[6] Analogous cheletropic cycloaddition chemistry has also been observed between the cyclic phosphenium [**4-A**]$^+$ and diazabutadienes, and is even reversible with extreme steric pressure (Scheme 4-1).[7] Additionally, surrogate sources of $[R_2P:]^+$ like $[Ph_2ClP:\rightarrow GaCl_3]$ **4-B** have been shown to oxidatively insert into P_4.[8] In 2013, Vidović and co-workers reported a dicationic phosphenium cation [**4-C**]$^{2+}$ stabilized by a π-electron rich carbodiphosphorane $(-C(PPh_3)_2)$.[9] The compound can be viewed as analogous to a monocationic phosphenium $[R_2P:]^+$, albeit with a secondary positive charge mostly

localized on the adjacent -C(PPh_3)$_2$ substituent. The group would show in a subsequent study the following year that [**4-C**]$^{2+}$ reacts with a stoichiometric amount of water or methanol to afford the corresponding hydrido-hydroxyphosphonium dication by formal oxidative addition.[10] In 2021, Olaru, Mebs, and Beckmann would prepare diaryl phosphenium cations [**4-D**]$^+$ (Ar = Ph) and [**4-D**]$^+$ (Ar = Mes) with a very encumbered dispiro[fluorene-9,3'-(1',1',7',7'-tetr-4'-yl)-5',9''-fluorene] (Fluid) substituent, which combines with atmospheric water to afford the analogous O–H insertion product.[11]

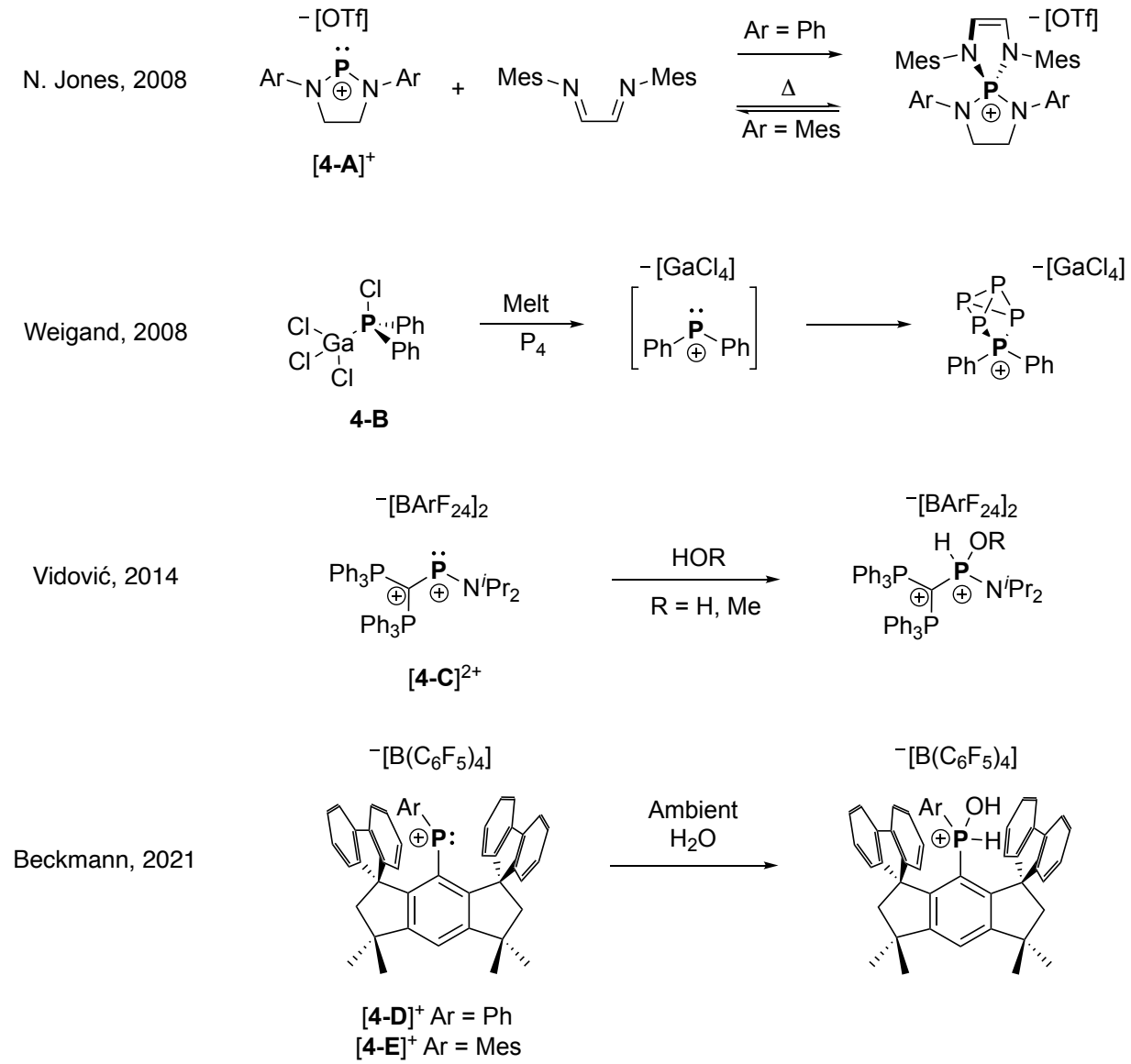

Scheme 4-1: Select examples of oxidative additions across phosphenium cations.

In a later study, Vidović's group would prepare two more phosphenium dications $[R_2P:]^{2+}$ [**4-F**]$^{2+}$ (R = Ph) and [**4-G**]$^{2+}$ (R = N^{i}Pr$_2$) based on an electronically similar carbodicarbene substituent (–C(NHC)$_2$).[12] The team posited that the high electrophilicity of the dications would allow for the activation of hydridic Si–H and B–H bonds, and to a lesser extent hydridic C–H substrates (Scheme 4-2). [**4-F**]$^{2+}$ and [**4-G**]$^{2+}$ were found to activate silanes by H$^-$ abstraction, resulting in the formation of cationic hydrido phosphines and free silylium cations. By comparison, [**4-F**]$^{2+}$ and [**4-G**]$^{2+}$ were found to activate B–H bonds, affording mostly H–P–B oxidative addition products with trace amounts of hydrido phosphines. Moreover, [**4-G**]$^+$ was observed to undergo oxidative addition with C*sp*^{3}–H when provided a stoichiometric amount of either 1,3,5-cyclohexatriene or xanthene. With 1,3,5-cycloheptatriene, a product directly arising from H$^-$ abstraction and a [4+1] cycloadduct were also observed.

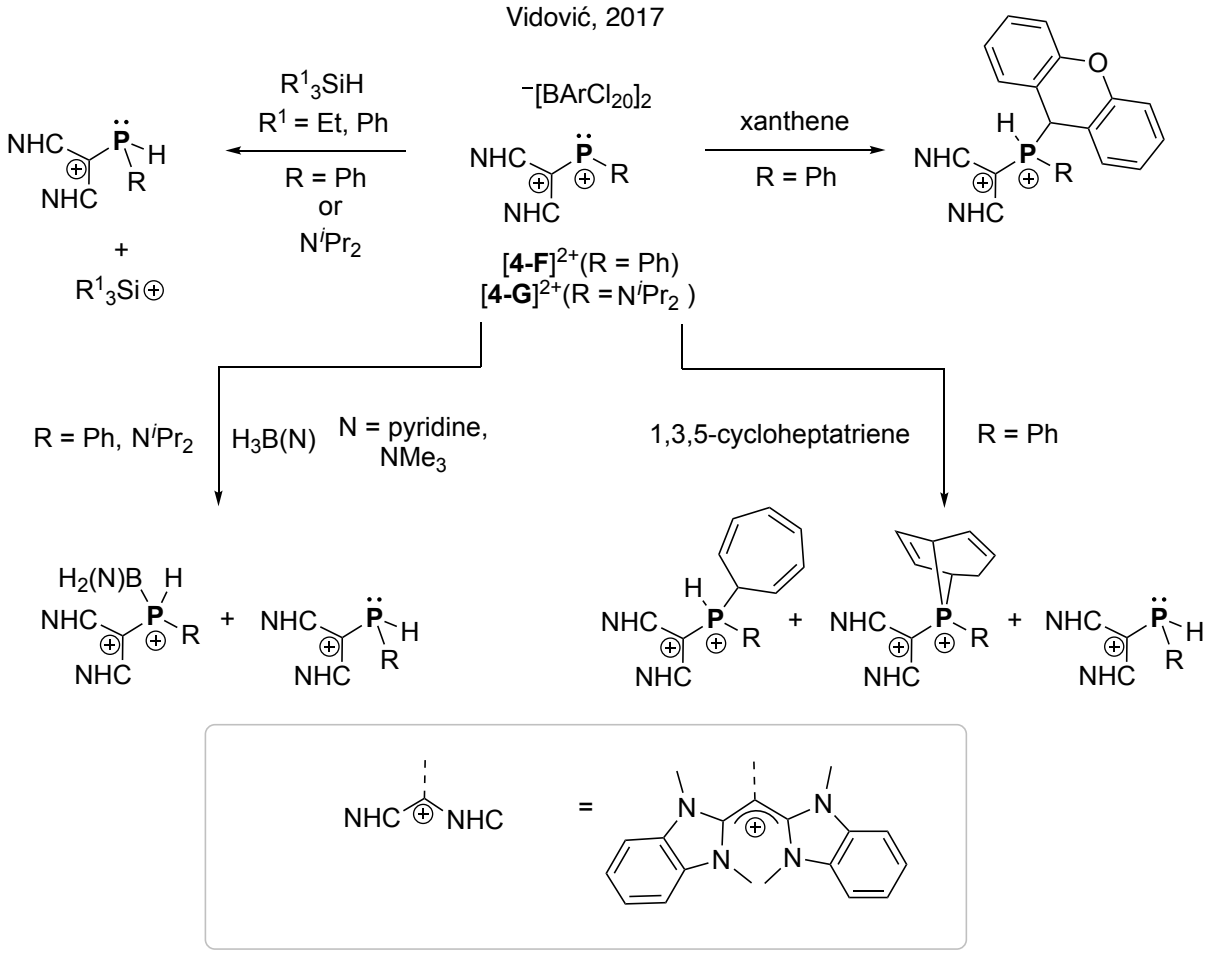

Scheme 4-2: Oxidative additions with phosphenium dications. Anions excluded from the products for clarity.

Beyond the aforementioned reports, investigations of discrete $[R_2P:]^+$ species towards bond activation are becoming increasingly scarce. This may be attributed to burgeoning interest in geometrically constrained main group systems.[13,14,15] Positioning main-group elements within restrictive substituents is known to cause orbital rehybridization on account of preventing the element from adopting typical VSEPR geometries. In molecular phosphorus chemistry, this concept is most frequently applied to tricoordinate phosphines, where pincer ligands are used to enforce strongly distorted trigonal pyramidal or T-shaped geometries. These perturbed geometries afford phosphines with ambiphilic character, which are capable of oxidatively adding various substrates to form P(V) phosphoranes. An illustrative example of this is shown with a NNN pincer supported phosphine **4-H** studied by Radosevich and coworkers in 2014, which can activate N–H and O–H bonds (Scheme 4-3).[16] Remarkably, substrate additions are entirely reversible which would be an early indication of the potential application of these types of systems in catalysis. Constraining substituent manifolds have also been applied more recently to phosphenium cations, which when compared to constrained phosphines, are more electrophilic due to being positively charged.[17,18,19,20] The phosphenium cations in these systems are tri-coordinate and usually described with a bonding representation $[LB:\rightarrow PR_2]^+$ where LB is a donor group within the pincer substituent. A depictive example of this is a recently reported CNC pyridine bis-carborane pincer phosphenium cation [**4-I**]$^+$ by the Dobrovetsky group.[21] As the chemistry of constrained phosphines and phosphenium cations in bond activation and catalysis has been the subject of reviews,[13,15] and the chemistry of this Chapter concerns the reactivity of dicoordinate phosphenium cations $[R_2P:]^+$, geometrically constrained P compounds are not extensively covered. Rather, comparisons to such systems will be made throughout the discussion when relevant.

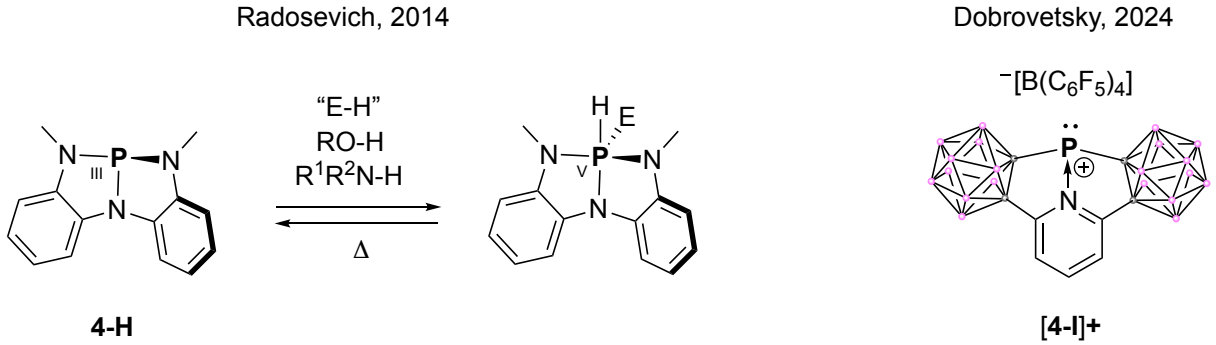

Scheme 4-3: Selected examples of bond activation by geometrically constrained phosphorus compounds.

4.2. Chapter Objectives: N-Heterocyclic Imine Substituted Phosphenium Cations

Emphasized previously in this thesis, NHIs are a privileged substituent platform for enabling the isolation of many reactive phosphorus compounds, including several TPPCs like the allenylidene phosphonium cation [**3-2**]$^+$ (other examples featured in Schemes 3-3, 3-4, 3-7). Taking a retrosynthetic stance, in many instances the imine groups are introduced simultaneously into these structures along with the phosphorus atom *via* cationic bis(imino)-phosphenium precursors like $[(NIDipp)_2P]^+$[22] and $[(NsI^tBu)_2P]^+$.[23] Two π-donating imine substituents make bis(imino)phosphenium cations highly stabilized and weakly electrophilic. For instance, both cations are inert or show no discernable interactions with donating solvents like acetonitrile and are charge separated from anions that are typically coordinating like Cl^-. Almost without exception in literature, bis(imino)phosphenium cations are functionalized by salt metathesis reactions with anionic nucleophiles. As carbenoid analogs, it is conceivable that these salts exhibit some degree of nucleophilic character, although direct functionalization of the P lone pair of bis(imino)-phosphenium cations has not yet been reported. In this Chapter, we envisioned the preparation of more electrophilic phosphenium cations based on NHIs which could be subsequently deployed in two contexts. The first intended application of these compounds was to investigate their reactivity towards small molecules. The NHI motif has long standing use in the preparation of ambiphilic tetralenes R_2E: (E = group 14 element). In particular, we were inspired by recent developments delineated by the Inoue group,[24] who have shown that the NHI substituent affords silylenes capable of a range of transformations, including the remarkable intermolecular dearomatization of arenes (Scheme 4-4).

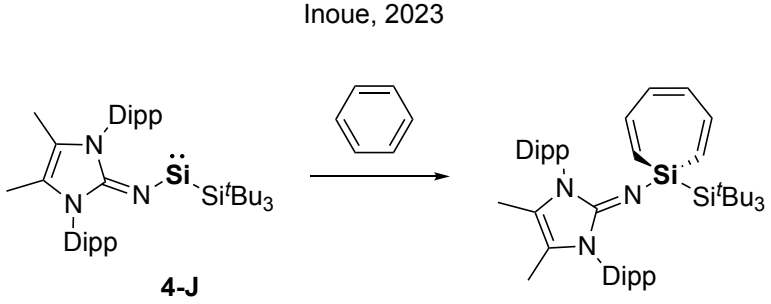

Scheme 4-4: Intermolecular dearomatization of benzene by an NHI substituted acyclic silylene.

The second intended application was inspired by the ketenation of electrophilic carbenes like CAACs (Scheme 1-3).[25] We anticipated that a bulky electrophilic phosphenium cation might be used to approach the synthesis of new allene-type TPPCs, namely ketenyl phosphonium $[R_2P{=}C{=}O]^+$ and keteniminyl phosphonium $[R_2P{=}C{=}N{-}R]^+$ cations by direct homologation of $[R_2P{:}]^+$ with carbon monoxide or an isocyanide, respectively. The latter cation, $[R_2P{=}C{=}N{-}R]^+$ had previously been sought after by Sanchez, Majoral, and co-workers in 1989, who proposed its intermediacy (Scheme 4-5).[26] The author's noted that there is ambiguity between whether the keteniminyl phosphonium cation is represented by an allene bonding description $[R_2P{=}C{=}N{-}R]^+$ which features a planarized phosphorus center, or as a Lewis base adduct $[R_2P{\leftarrow}{:}C{\equiv}N{-}R]^+$ where phosphorus is pyramidal. To date, isoelectronic main group ketenes $(R_2E{=}C{=}Y)^n$ (Y = O, NR) are rare. Aside from the ketenation of carbenes, base-stabilized borylenes,[27] as well as silylenes,[28 29] can also form stable adducts with CO. Importantly, the latter compounds featuring silicon are most appropriately described as donor-acceptor complexes $[R_2Si{\leftarrow}{:}C{\equiv}O]^+$ rather than ketenes, emphasizing a lack of multiple bond character between Si and C. This Lewis structure depiction is made on the basis that displacement of CO occurs upon addition of stronger donors, and crystallographic data which shows pyramidalized Si centers. We reasoned that reaction of CO or isocyanide with a phosphenium cation may be more promising for forming a heavier main group ketene, with phosphorus generally showing a higher tendency to form multiple bonds with carbon.

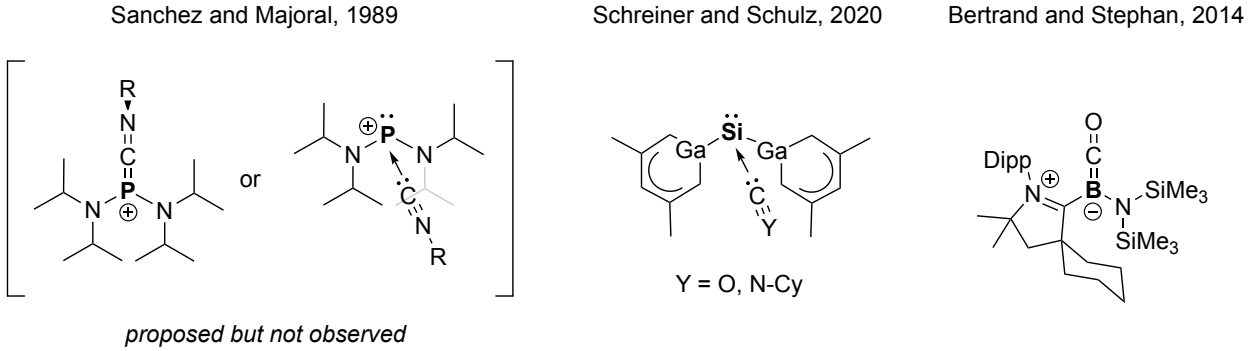

Scheme 4-5: Proposed keteniminyl phosphonium cation by Sanchez and Majoral. Other main-group carbenoid homologations with either carbon monoxide or isocyanides.

Herein, the electrophilic properties of NHI substituted phosphenium cations are modulated using substituent effects. From bis(imino)-phosphenium cations, one strong π-donating imine substituent is forgone in favor an alkyl-based substituent, lessening the degree of mesomeric stabilization at the cationic P center. To retain similar steric properties and to ensure a wide R–P–R bond angle, the alkyl substituent was chosen to be a ^{t}Bu group, which can be introduced readily by commercial reagents.

4.3 Results and Discussion

4.3.1 Synthesis of Electrophilic NHI-substituted Phosphenium Cations

Alkyl-imino-chlorophosphines **4-1**$^{(a-d)}$ were first prepared in a reaction with one equivalent of the silyl-imines and ^{t}BuPCl$_2$ *via* elimination of Me$_3$SiCl, following Kuhn's original NHI-phosphine synthesis route (Scheme 4-6).[30] All phosphines were isolated in moderate-good yield following the removal of residual ^{t}BuPCl$_2$ by sublimation. Phosphines **4-1**^{a} and **4-1**^{b} are slightly beige powders while **4-1**^{c} and **4-1**^{d} are white powders. The ^{31}P NMR resonances of **4-1**^{a} to **4-1**^{d} appear with decet coupling patterns due to the appended ^{t}Bu substituent and are all centered within the range of δ = 150 - 190 ppm. SCXRD studies of **4-1**^{a}, **4-1**^{c}, and **4-1**^{d}, confirmed their connectivity. The solid-state structures are highly disordered as the phosphines are racemic, co-crystallizing as enantiomers and featuring long P–Cl bonds (**4-1**^{a}; avg 2.25 Å, **4-1**^{c}; avg 2.25 Å, **4-1**^{d}; 2.213(15) Å), likely an artifact of π-donation from the NHI substituent into the P–Cl σ* orbital (Figure 4-1).[31] From chlorophosphines **4-1**$^{(a-d)}$, acyclic alkyl-imino-phosphenium cations [**4-2**$^{(a-d)}$]$^{+}$ are affected by chloride abstraction with an alkali salt, sodium or potassium tetrakis(pentafluorophenyl)borate ([B(C$_6$F$_5$)$_4$]).

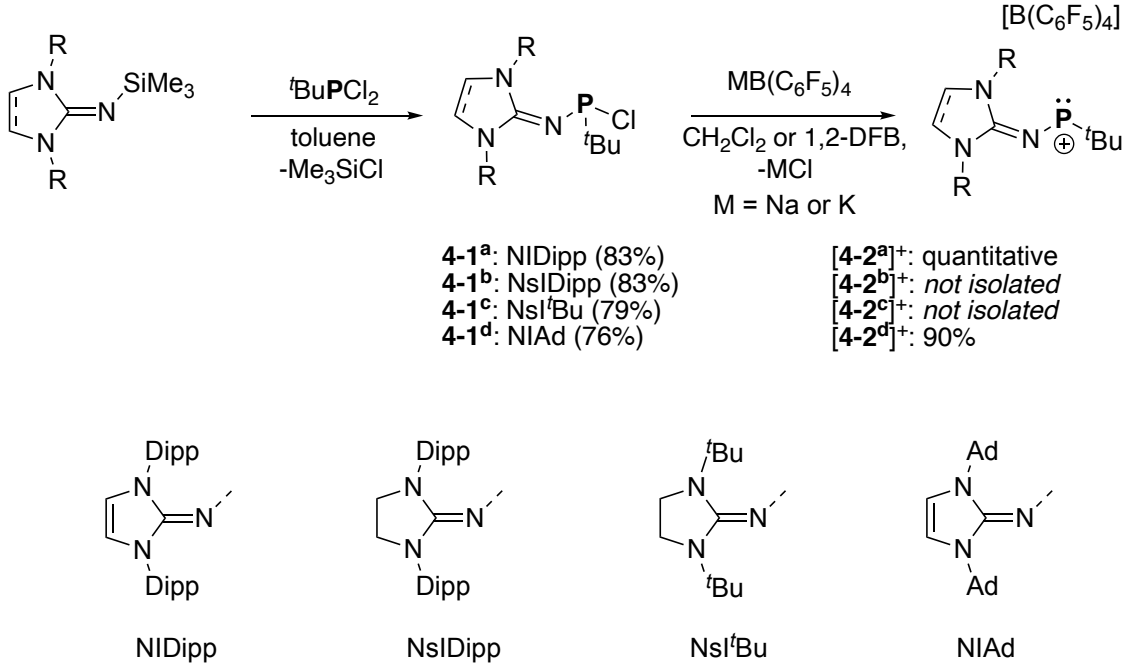

Scheme 4-6: Synthesis of alkyl-imino chlorophosphines **4-1**^{a} to **4-1**^{d}, and their phosphenium [B(C$_6$F$_5$)$_4$] salts [**4-2**^{a}]$^{+}$ to [**4-2**^{d}]$^{+}$.

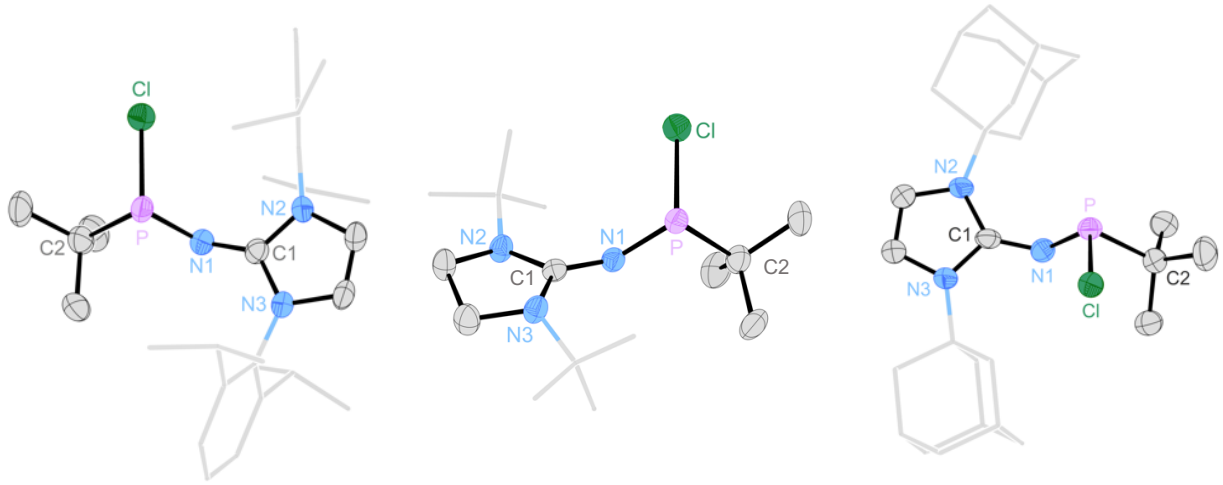

Figure 4-1: Solid-state structures of **4-1**[a] (left) **4-1**[c] (middle), and **4-1**[d] (right). Hydrogen atoms are omitted for clarity. Ellipsoids are drawn at 50% probability. NHI bound Dipp, *tert*-butyl, and adamantyl groups are shown in wireframe. For each phosphine, one enantiomer is shown.

Along this thought **4-1**[a] was added to a stirring suspension of $NaB(C_6F_5)_4$ or $KB(C_6F_5)_4$ in either CH_2Cl_2 or 1,2-DFB, resulting in a highly evident color change and the precipitation of NaCl or KCl. Phosphine **4-1**[a] appears slightly yellow in solution, but following chloride abstraction, the reaction mixture appears red. After workup, [**4-2**[a]][$B(C_6F_5)_4$] was isolated as a bright red-pink solid. ^{31}P NMR analysis of [**4-2**[a]][$B(C_6F_5)_4$] in CD_2Cl_2 revealed an extremely downfield chemical shift at $\delta = 596$ ppm, over 400 ppm units apart from the starting material. ^{11}B and ^{19}F NMR spectra showed signals consistent with $[B(C_6F_5)_4]^-$ anion. Comparable acyclic phosphenium cations exhibit similarly downfield phosphorus NMR shifts. This includes a structurally related amino-alkyl phosphenium $[t\text{BuPNMe}_2]^+$ (513.2 ppm) prepared by Cowley,[32] and the diaryl phosphenium cations [**4-D**]$^+$ and [**4-E**]$^+$ (542.0 ppm and 573.1 ppm) reported recently by Beckmann, the latter being the phosphenium cation with the most downfield chemical shift.[11] Thus [**4-2**[a]]$^+$ is to the best of our knowledge, the new record holder for this moniker. Unfortunately, all attempts to confirm the solid-state structure of [**4-2**[a]][$B(C_6F_5)_4$] failed owing to the tendency for $[B(C_6F_5)_4]^-$ salts to form oils. Colorless single crystals were extracted from a red oil following a crystallization attempt from a concentrated chlorobenzene-CH_2Cl_2 mixture, corresponding to the molecular structure of [**4-3**][$B(C_6F_5)_4$], a phosphino-phosphenium salt (Figure 4-2).

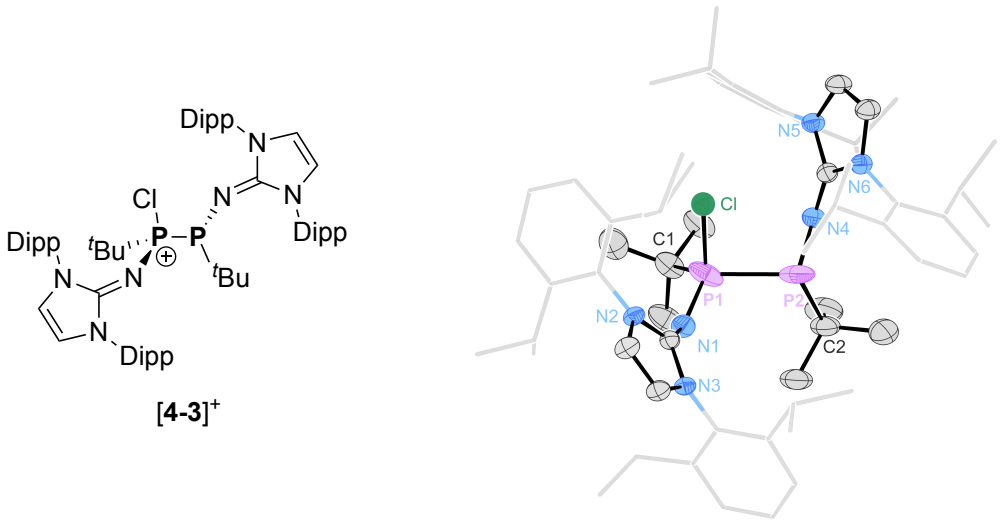

Figure 4-2: Solid-state structure of phosphino-phosphenium salt [**4-3**][$B(C_6F_5)_4$]. Hydrogen atoms and the [$B(C_6F_5)_4$] anion are omitted for clarity. Ellipsoids are drawn at 50% probability. NHI bound Dipp groups are shown in wireframe. Selected bond length [Å] [**4-3**]$^+$; P1–P2 2.288(1).

Spectroscopic evidence of [**4-3**]$^+$ has never been observed in solution state NMR experiments, suggesting that [**4-3**]$^+$ may be a decomposition product of [**4-2^a**]$^+$ that occurs slowly while concentrating in the chlorobenzene-CH_2Cl_2 mixture. Analogous chloride abstractions with salts of weakly coordinating anions were attempted on **4-1^a** to alter the solubility and to encourage the crystallization of [**4-2^a**]$^+$. In this effort, abstraction with silver trifluoromethanesulfonate (AgOTf), silver bis(trifluoromethane)sulfonimide ($AgNTf_2$) and silver hexafluorophosphate ($AgPF_6$) were all attempted but led to intractable reaction mixtures. Gratifyingly, chloride abstraction with $AlCl_3$ affected the formation of [**4-2^a**][$AlCl_4$]. The [$AlCl_4$]$^-$ counterion does not influence the ^{31}P NMR resonance of [**4-2^a**]$^+$ to a significant degree (δ = 594.4 ppm) which indicates its ionic behavior in the solution state. [**4-2^a**][$AlCl_4$] exhibited little signs of decomposition in CD_2Cl_2 at room temperature after 1 week although gently heating solutions (~60 °C) [**4-2^a**][$AlCl_4$] leads to unselective complex decomposition mixtures. Red block single crystals suitable for an SCXRD study were obtained by layering a CH_2Cl_2 solution with hexane (1:2) and storing it at room temperature for a few days (Figure 4-3). The P–N1 bond length of [**4-2^a**]$^+$ is shorter (1.578(8) Å) relative to the phosphine precursor **4-1^a** (1.614(9) Å) which indicates some multiple bond character for [**4-2^a**]$^+$ arising from π-donation from the exocyclic imine nitrogen atom to phosphorus. The P–C2 bond length of [**4-2^a**]$^+$ is 1.827(9) Å and is consistent with a P–C single bond. The cationic and anionic components are well separated, with no obvious Al–Cl···P interion contacts.

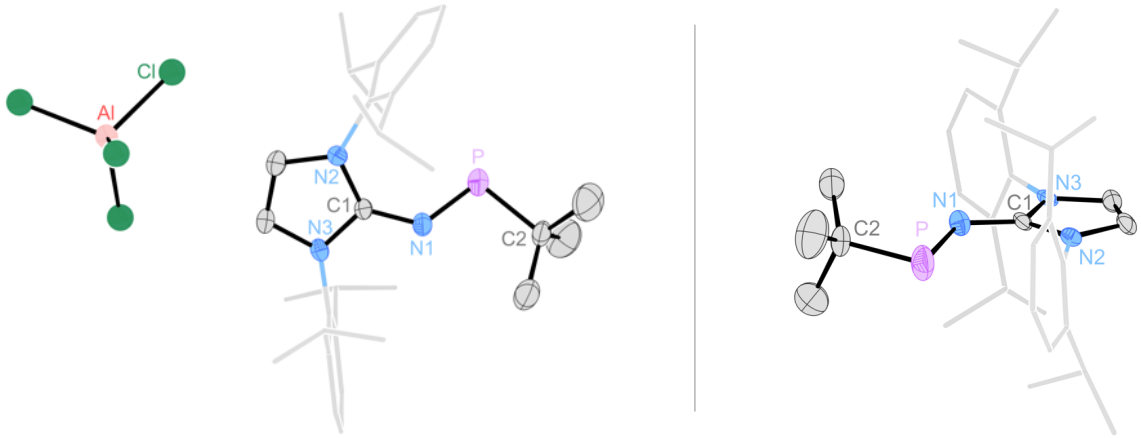

Figure 4-3: Solid-state structure of [**4-2**^{a}][$AlCl_4$] from different perspectives. The depiction on the right excludes the anion for clarity. Additionally, hydrogen atoms are omitted and the Dipp substituents are shown in wireframe for clarity. Ellipsoids are drawn at 50% probability. Selected bond lengths [Å] and angles [°]: [**4-2**^{a}]: P–N1 1.575(8), N1–C1 1.359(1), P–C2 1.827(9), C2–P–N1 103.5(4), P–N1–C1 128.1(6).

[**4-2**^{a}]$^{+}$ features a N1–P–C2 angle of 103.5(4)°, which is similar to the N–Si–Si bond angle (106.2(9)°) of the isoelectronically analogous silylene **4-J** [24] prepared by Inoue and the N–P–N bond angle (105.5(3)°) of [$(NIDipp)_2P$]$^{+}$.[33] The acyclic dicationic phosphenium [**4-C**]$^{2+}$ that has been shown to facilitate O–H bond cleavage, features a central atom bond angle of 117.7(3) °. [9] Phosphines **4-1**$^{b-d}$ could be used to generate their corresponding [$B(C_6F_5)_4$]$^{-}$ phosphenium salts. The formation of [**4-2**^{b}]$^{+}$ and [**4-2**^{c}]$^{+}$ is suggested by *in-situ* ^{31}P NMR spectroscopic experiments which indicated similar downfield chemical shifts of the ^{31} P NMR resonances upon chloride abstraction ([**4-2**^{b}]$^{+}$ δ = 556 ppm; [**4-2**^{c}]$^{+}$ δ = 544 ppm). Cl^{-} abstraction of **4-1**^{d} with Na[$B(C_6F_5)_4$] afforded salt [**4-2**^{d}][$B(C_6F_5)_4$] as a purple compound which was characterized by proton and heteronuclear NMR spectroscopy. Similar to [**4-2**^{a}][$B(C_6F_5)_4$], the [$B(C_6F_5)_4$]$^{-}$ salt of [**4-2**^{d}]$^{+}$ had a tendency to oil out of solution during crystallization attempts. The reluctance of the [**4-2**^{a}][$B(C_6F_5)_4$] system to crystalize was also a challenge with its subsequent reaction products (*vide infr*a).

4.3.2 Electronic Structure of Acyclic Alkyl-Imino Phosphenium Cations

The electronic structures of [**4-2**^{a}]$^{+}$ and its analog were investigated with DFT at B3LYP-D3BJ/def2-TZVP level of theory [34,35,36] As [**4-2**^{a}]$^{+}$ was used in subsequent reactivity studies, it

will be the primary point of discussion. The HOMO of [**4-2**^{a}]$^{+}$ has contributions from the π-system of the imidazole ring, as well as a lone pair on both the exocyclic nitrogen atom and the phosphorus atom. The depiction of the LUMO shows that [**4-2**^{a}]$^{+}$ is predominantly comprised of large diffuse lobe of *p* character on phosphorus, as well as an antibonding combination along the C–N. The HOMO-LUMO gap of [**4-2**^{a}]$^{+}$ is 3.31 eV (319 kJ mol^{-1}), which is marginally higher than Inoue's silylene **4-J** (3.22 eV).[24]

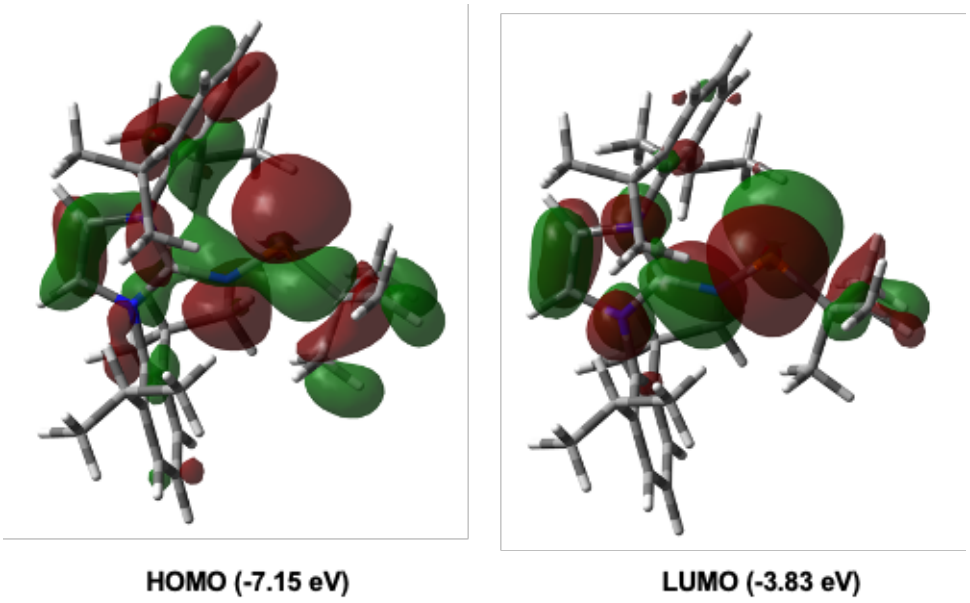

Figure 4-4: Selected molecular orbitals of [**4-2**^{a}]$^{+}$ (HOMO and LUMO) at the B3LYP-D3BJ/def2-TZVP level of theory (top), isovalue = 0.02.

For [**4-2**^{a}]$^{+}$, Mayer bond orders P–N1 (1.6) and C1–N1 (1.4) indicate significant π-bonding character within the C=N–P fragment. Charges obtained by Natural Bond Orbital (NBO) analysis confirm phosphorus as the most electrophilic site of [**4-2**^{a}]$^{+}$ and that the compound features a polarized P$^{\delta+}$–N$^{\delta-}$ bond (P: +1.13 a.u. and N: -0.91 a.u). Hirshfeld charge analysis tells a similar story, showing a positively charged P atom (+0.45 a.u.) and negatively charged (-0.35 a.u.) exocyclic nitrogen atom.

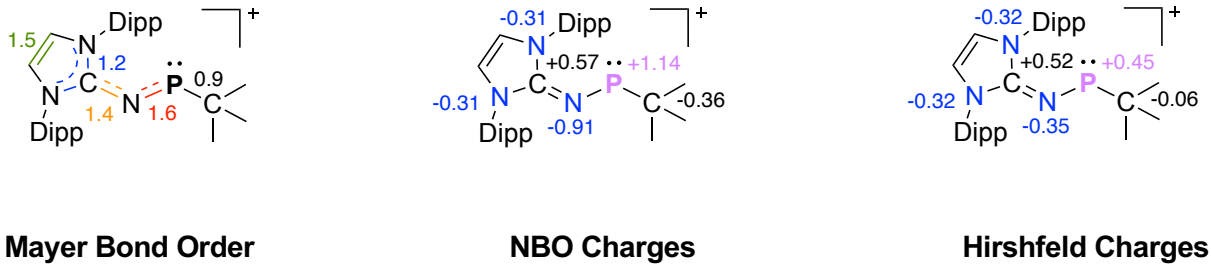

Figure 4-5: Calculated Mayer bond order analysis, as well as NBO and Hirshfeld Charges of [**4-2^{a}**]$^{+}$.

4.3.3 Electrophilicity of Acyclic Alkyl-Imino Phosphenium Cations

For reactivity studies, [**4-2^{a}**]$^{+}$ was always generated *in situ* from phosphine **4-1^{a}** and K[B(C_6F_5)$_4$]. To qualitatively evaluate the Lewis acidity of the titular compound [**4-2^{a}**]$^{+}$, addition of the Lewis base DMAP to [**4-2^{a}**][B(C_6F_5)$_4$] led to an immediate dissipation of the cation's characteristic red color (Scheme 4-7). Multinuclear NMR analysis confirmed the formation of a new product, which formed quantitatively and was determined to be the acid-base adduct [**4-2^{a}**•DMAP][B(C_6F_5)$_4$]. Phosphenium [**4-2^{a}**][B(C_6F_5)$_4$] was then combined with Et_3PO for an effective Lewis acidity measure by the Gutmann Beckett method.[37,38] The ^{31}P NMR spectroscopy resonance that corresponds to the Et_3PO moiety of adduct [**4-2^{a}**•Et_3PO][B(C_6F_5)$_4$] has a chemical shift of δ = 85.3 ppm (CD_2Cl_2), which was used to determine an acceptor number (AN) of 98.

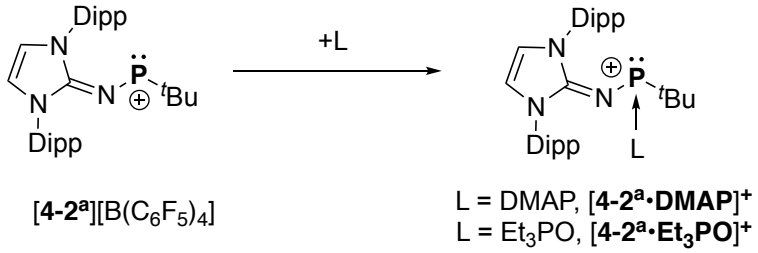

Scheme 4-7: Reaction of [**4-2^{a}**][B(C_6F_5)$_4$] with DMAP and Et_3PO.

The effective Lewis acidity of [**4-2^{a}**][B(C_6F_5)$_4$] determined by the Gutmann-Beckett method exceeds the ubiquitous borane Lewis acid B(C_6F_5)$_3$ (AN 82).[39] Compared to other acyclic P(III) cations, [**4-2a**][B(C_6F_5)$_4$] is an inferior Lewis acid to Beckmann's diaryl phosphenium salts [**4-E**]$^{+}$ (AN 132) and [**4-D**]$^{+}$ (AN 137),[11] as well as the bis(ferrocenyl)phosphenium ion [**1-J**]$^{+}$ (AN 117)

(Scheme 4-8).[40] This observation can be rationalized on the basis that [**4-D**]$^+$, [**4-E**]$^+$, and [**1-J**]$^+$ lack any stabilizing π-donor substituents. With respect to other phosphorus cations that implement NHI substitution, the P(V) phosphorandylium species [**3-L$^{NI(Benz)iPr)}$**]$^{2+}$ (AN 129) and [**3-L$^{NI(Me)iPr)}$**]$^{2+}$ (AN 117)[41] are unsurprisingly more electrophilic on account of being doubly charged (Scheme 4-8). Lastly the P(V) oxophosphonium [**3-I**]$^+$ (AN 102) owes its Lewis acidity to a highly electron withdrawing O atom, and just slightly exceeds the Lewis acidity of [**4-2^a**][$B(C_6F_5)_4$].[31] As a control, the bis(imino)phosphenium chloride [$(NIDipp)_2P$][Cl] showed no interaction with Et_3PO in our testing.

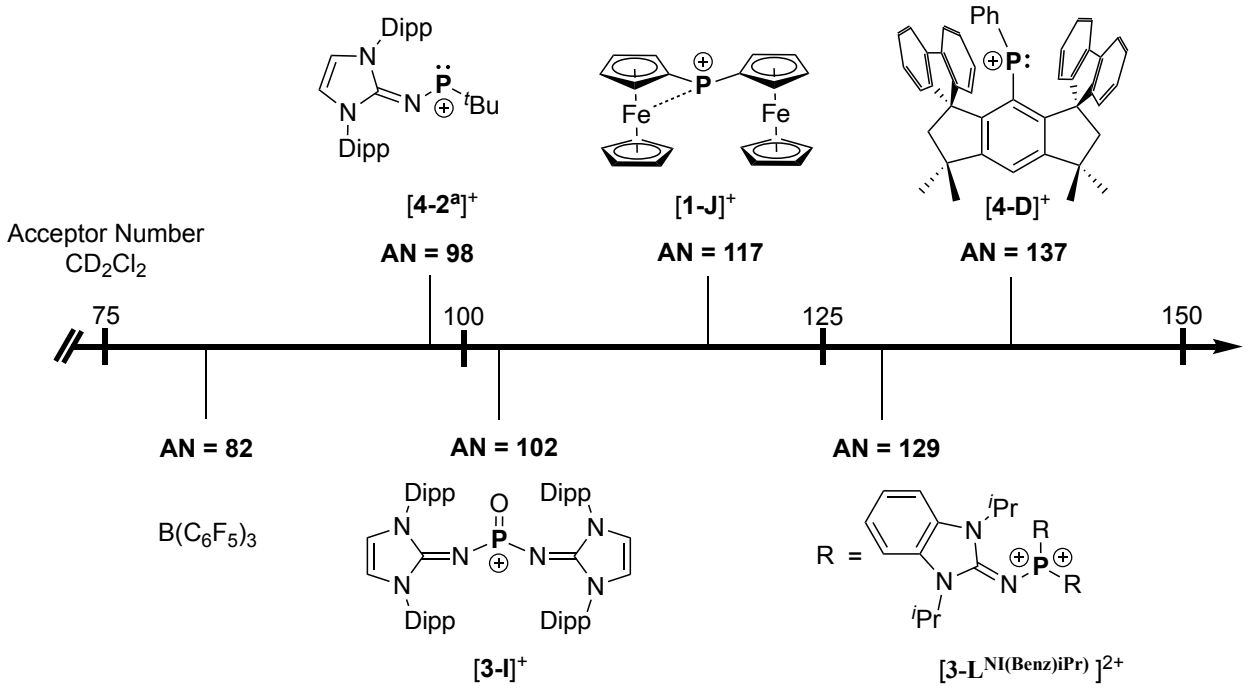

Scheme 4-8: Gutmann-Beckett acceptor numbers of selected phosphenium cations, and other NHI substituted phosphorus (di)cations.

4.3.4 Probing the Ambiphilic Character of Acyclic Alkyl-Imino Phosphenium Cations

We next pursued cheletropic cycloaddition reactions with unsaturated hydrocarbons to crudely probe the ambiphilic character of [**4-2^a**]$^+$. The reaction with of diphenylacetylene with [**4-2^a**]$^+$ afforded the P(V) phosphirenium salt [**4-4**][$B(C_6F_5)_4$] by a [2+1] cycloaddition (Scheme 4-9).[6] Similarly, combining 2,3-dimethyl-1,3-butadiene with [**4-2^a**][$B(C_6F_5)_4$] cleanly afforded the cyclic P(V) phospholenium [**4-5**][$B(C_6F_5)_4$] *via* [4+1] cycloaddition. Employing 1,1-diphenylethylene

afforded [**4-6**][B(C_6F_5)$_4$], which was supported using 2D NMR spectroscopic methods. Notably, ^{1}H NMR analysis shows environments indicative of a cyclohexabutadiene fragment, resulting from arene dearomatization. The ^{31}P NMR resonance of [**4-6**][B(C_6F_5)$_4$] is shifted to low field frequency (δ = 63.4 ppm) relative to phosphenium [**4-2^a**]$^+$, as is the case with the tetracoordinate phospholenium salt [**4-5**][B(C_6F_5)$_4$] (δ = 43.9 ppm). Phosphirenium salt [**4-4**][B(C_6F_5)$_4$] appeared at even lower frequency in the ^{31}P spectrum (δ = -82.5 ppm). [**4-4**]$^+$ and [**4-5**]$^+$ closely agree with reported literature compounds.[42,43]

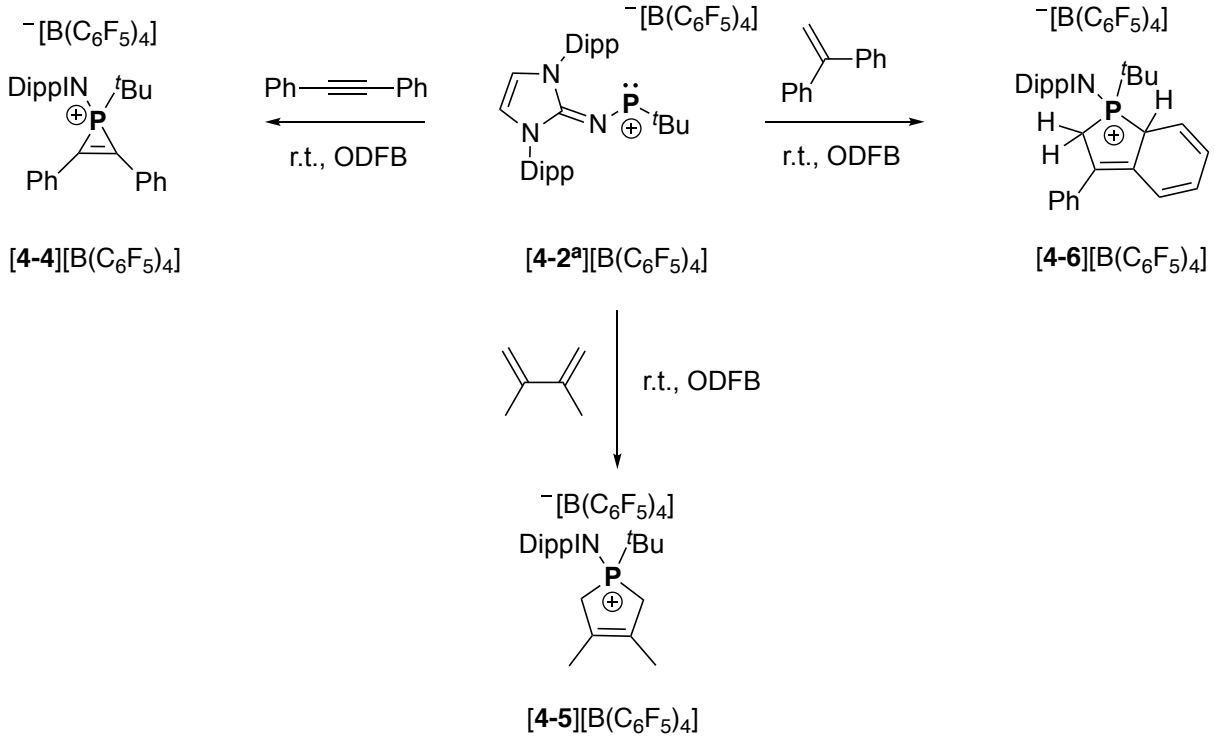

Scheme 4-9: Cycloadditions with phosphenium salt [**4-2^a**][B(C_6F_5)$_4$] and unsaturated substrates.

4.3.5 Oxidative Addition of O–H and N–H compounds

In light of the increased prominence of geometrically constrained P systems capable of E–H bond activation (E = O and N), we wanted to explore the reactivity of [**4-2^a**][B(C_6F_5)$_4$] towards alcohols and amines. First, [**4-2^a**][B(C_6F_5)$_4$] was reacted independently with stoichiometric amounts methanol (MeOH) at room temperature, resulting in the formation of a single new product. Multinuclear NMR experiments revealed that the new compound was the result of O–H bond activation at phosphorus, evident by J_{HP} splitting (514 Hz) in the ^{1}H and ^{31}P NMR spectra (Scheme

4-10). The large J_{HP} coupling constant is consistent with the formation of a P–H bond. The ^{31}P NMR chemical shift (δ = 35.2 ppm) suggests a tetrahedral environment for phosphorus. Additionally, proton-phosphorus coupling can be observed for the –OCH_3 moiety ($^3J_{HP}$ = 13 Hz). Taken together, the data suggests that both P–H and P–O bond formation events occur, with a change in oxidation state from P(III) to P(V) (Scheme 4-10), giving phosphonium cation [**4-7**]$^+$. The analogous P(V) oxidative addition product, [**4-2^a•H$_2$O**]$^+$, is speculated to form by addition of degassed water (^{31}P NMR δ = 30.4 ppm, $^1J_{HP}$ = 557 Hz), but appeared as the major component of a rather complex reaction mixture. Similarly, phenol (PhOH) gave spectroscopic features consistent with oxidative addition across the O–H bond (^{31}P NMR δ = 27.5 ppm, $^1J_{HP}$ = 522 Hz) when monitored *in-situ,* but upon workup was isolated along with an unidentified minor impurity. Surprisingly, when [**4-2a**][$B(C_6F_5)_4$] was reacted with *tert*-butanol (^{t}BuOH), it was immediately apparent that P–H bond formation had not occurred given the absence of $^1J_{HP}$ coupling features in either the ^{1}H and ^{31}P NMR spectra. Curiously, the ^{31}P NMR spectrum showed one new feature at δ = 125.5 ppm, which is shifted slightly downfield of phosphine **4-1^a** (δ = 157.6 ppm), indicating that ^{t}BuOH activation likely leads to a compound with a tricoordinate P(III) centre. Correlations in the ^{1}H/^{13}C HMBC spectrum were used to identify this species as a cationic phosphonamidite [**4-9**]$^+$, where both P–O bond and N–H bond formation occur. The addition of ^{t}BuOH across the P–N bond of [**4-2^a**][$B(C_6F_5)_4$] is reminiscent of alcohol additions to Dielmann's oxophosphonium [**3-I**]$^+$,[31] and Markovski's oxo(imino)phosphorane R-P(=O)(=N^{t}Bu) (R = 2,4,6-^{t}Bu$_3$C$_6$H$_2$).[44]

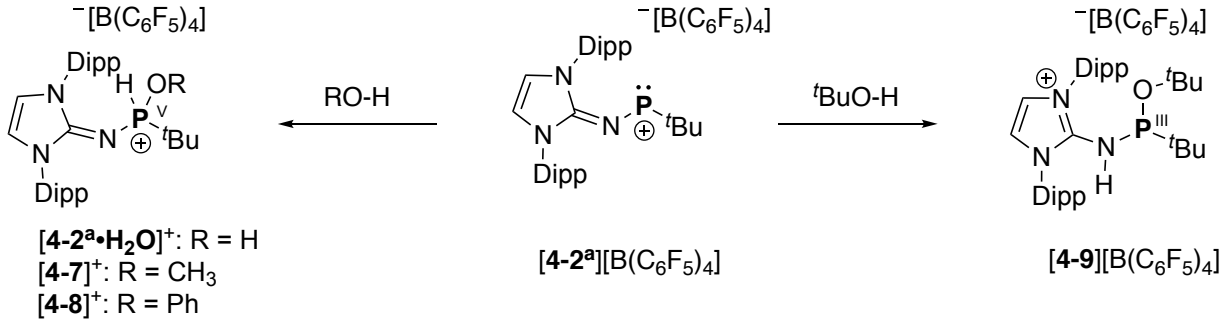

Scheme 4-10: Divergent reaction pathways for the activation of O-H compounds by [**4-2^a**]$^+$.

Both involve new P–O and N–H bonds being formed, but are additions to planar P(V) centers. Additionally, 1,2-addition products have been observed to occur with NHI-substituted phosphorandylium dications (Scheme 1-17).[41]

The P(V) oxidative addition product with ^{t}BuOH could be precluded due to steric crowding. Phosphonamidite [**4-9**]$^+$ may better accommodate its –NIDipp, –^{t}Bu and –O^{t}Bu substituents when the phosphorus center is trigonal pyramidal rather than tetrahedral. Substrate selective outcomes resulting from alcohol activation with P(III) compounds has been shown previously, specifically with the aforementioned NNN pincer phosphine **4-H** studied by Radosevich.[16] Their group found that with most alcohols **4-H** is quickly converted to the corresponding phosphorane (Scheme 4-11). However, with ^{t}BuOH, ^{31}P NMR experiments initially identified a mixture of two species, the expected phosphorane and a P(III) phosphordiamidite.

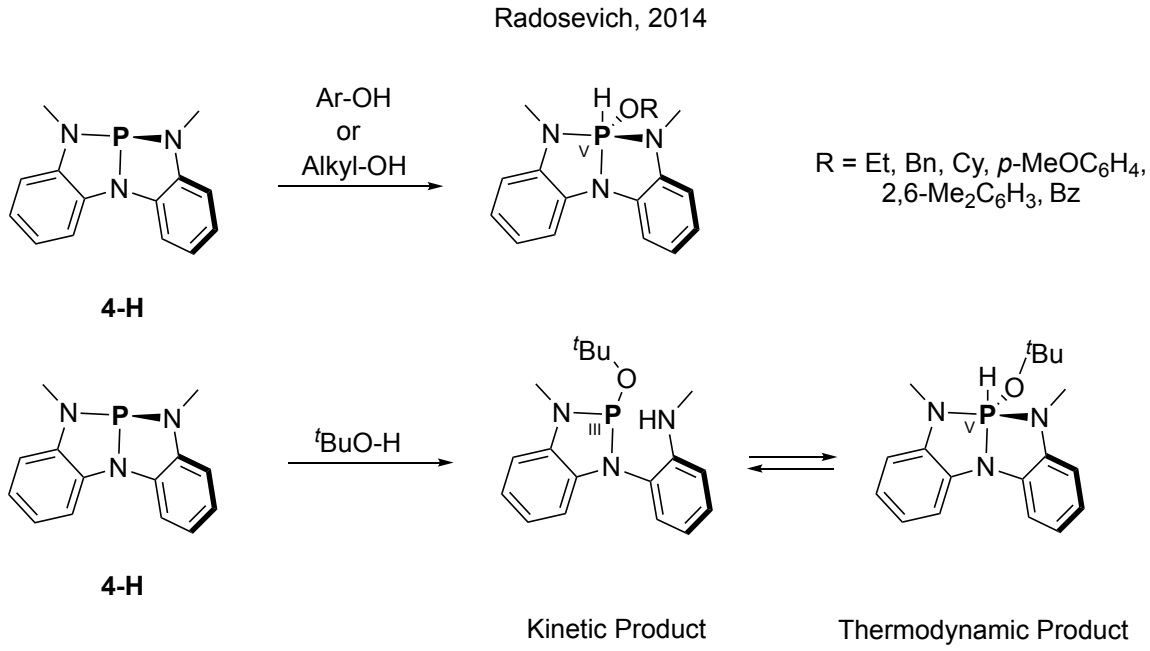

Scheme 4-11: Activation of alcohols by a C_s symmetric phosphorous triamide **4-H.**

At room temperature, the products eventually converge to the exclusive formation of the phosphorane, suggesting it to be a thermodynamic product while the phosphordiamidite is a kinetic product. The observation led the authors to the conclusion that O–H activation by **4-H** is likely a result of cooperativity between the electrophilic phosphorus center and one of its basic pendent

nitrogen substituents to give phosphordiamidites, which would eventually tautomerize into phosphoranes.

In our case, the isolation of both phosphonium cations like [**4-7**]$^+$ and [**4-8**]$^+$, and a cationic phosphonamidite [**4-9**]$^+$ implicates atleast two possible mechanisms for alcohol activation by [**4-2^a**]$^+$. The first possibility involves a reaction pathway which proceeds *via* direct P–O and P–H bond formation at the P(III) center to give P(V) products, and the formation of P(III) phosphonamidites arises from a subsequent proton migration from the phosphorus atom to the guanidine unit (Scheme 4-12a). Alternatively, a second pathway could be considered, which sees the initial P–O and N–H bond formation occur across the N–P fragment giving phosphonamidites (Scheme 4-12b). This pathway would suggest cooperativity of the imine substituent. Formal oxidative addition products would form by subsequent proton migration to the phosphorus center from the exocyclic NHI nitrogen atom, if not impeded by sterics.

a)

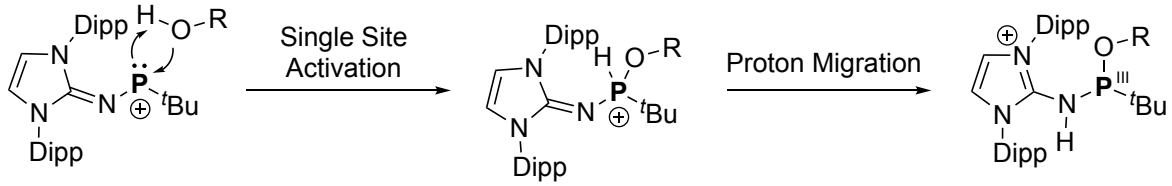

b)

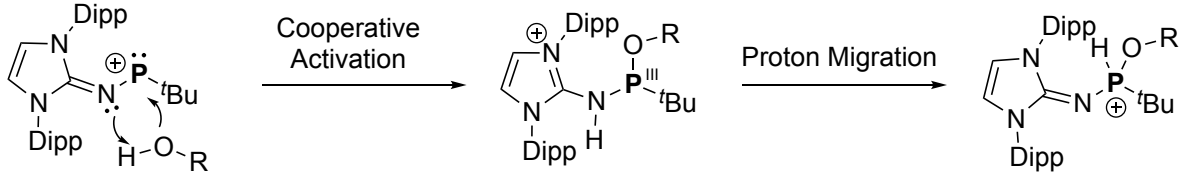

Scheme 4-12: Simplified reaction pathways for alcohol activation by phosphenium [**4-2^a**]$^+$. A) Single site activation of alcohols by [**4-2^a**]$^+$. B) Substituent assisted O-H activation by [**4-2^a**]$^+$.

Currently, we have not observed isomerization of phosphonamidite product [**4-9**]$^+$ to a formal oxidative addition product by either allowing it to stand in solution for long periods of time or by

refluxing it in the NMR solvent ($CDCl_3$) for several hours. Investigation of O–H activation by [**4-2^a**]$^+$ by quantum chemical calculations will be pursued in due course. In an attempt to demonstrate reductive elimination of O–H bonds, [**4-7**]$^+$ was heated under reduced pressure (10^{-3} mbar) up to 150 °C, which showed no signs of decomposition, reformation of [**4-2^a**]$^+$, or loss of methanol. Moreover, a $CDCl_3$ solution of [**4-7**]$^+$ was refluxed (90 °C) with added CD_3OD (methanol-d_4), which showed no evidence for the incorporation of –OCD_3, further suggesting the O–H activation of methanol by [**4-2^a**]$^+$ is irreversible.

[**4-2^a**][$B(C_6F_5)_4$] was also found to react with primary or secondary aryl amines to give P(V) oxidative addition through N–H bond activation (Scheme 4-13). Equimolar amounts of aniline and [**4-2^a**][$B(C_6F_5)_4$] cleanly afforded [**4-10**][$B(C_6F_5)_4$], evidenced by the appearance of a doublet of doublet of decets centred at δ = 13.7 ppm ($^1J_{PH}$ = 490 Hz, $^2J_{PH}$ = 5.9 Hz) in the ^{31}P NMR spectrum. Qualitatively, the reaction occurs within moments of mixing, suggested by rapid dissipation of the red color of cation [**4-2^a**]$^+$. The corresponding ^{1}H NMR spectrum shows features at δ = 6.47 ppm ($^1J_{PH}$ = 490 Hz, $^2J_{PH}$ = 5.9 Hz) and 4.47 ppm, attributed to the P–H and P–N(H)–Ph environments, respectively. ^{1}H/ ^{13}C HMBC experiments confirm the location of the proton as amine bound and not bound to the exocyclic nitrogen atom of the NIDipp substituent. Likewise [**4-2^a**][$B(C_6F_5)_4$] appears to react with secondary aryl amines. The addition of *N,N*-diphenylamine to [**4-2^a**][$B(C_6F_5)_4$] also furnished the corresponding phosphonium cation [**4-11**]$^+$ with a ^{31}P NMR chemical shift of 21.4 ppm ($^1J_{HP}$ = 504), but only after heating between 60-70 °C for several weeks (~20 days). A qualitative assessment of the mixture suggested that the reaction occurs very slowly, with dissipation of the red color of [**4-2^a**]$^+$ gradually occurring over several hours. *In situ* analysis by ^{31}P NMR spectroscopy suggests that [**4-2^a**]$^+$converts to [**4-11**]$^+$ *via* an intermediate that has a characteristic chemical shift at δ = 72.7 ppm, notably lacking any obvious multiplicity features that would indicate a P–H bond. We speculate this intermediate could be a Lewis adduct of *N,N*-diphenylamine and phosphenium cation [**4-2^a**]$^+$. In-depth NMR characterization of this intermediate may provide mechanistic insight for the activation of amines by [**4-2^a**]$^+$ and will be delineated in due course. By contrast, a preliminary reaction of [**4-2^a**]$^+$ and *N,N*-methyl-phenyl amine occurred rapidly, providing a phosphonium salt by insertion into the N–H bond, which suggests that weakly basic or sterically encumbered amines like *N,N*-diphenylamine are perhaps more challenging substrates. To the best of our knowledge, this would be the first example of N–H

oxidative addition at an acyclic phosphenium cation, although strictly alkyl amines and ammonia have not been attempted.

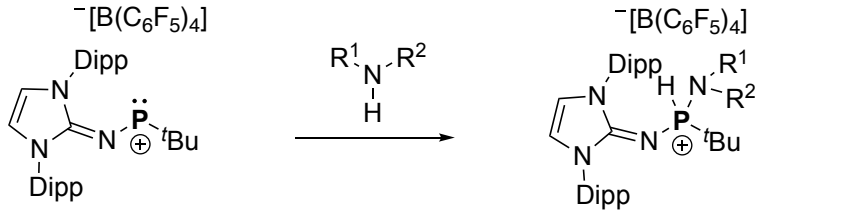

[**4-2**$^{\mathbf{a}}$]$^+$

[**4-10**]$^+$: R^1 = H, R^2 = Ph
[**4-11**]$^+$: R^1 = R^2 = Ph
[**4-12**]$^+$: R^1 = CH_3, R^2 = Ph

Scheme 4-13: Reactions of [**4-2**$^{\mathbf{a}}$]$^+$ with aromatic amines.

4.3.6 Attempted Carbenoid Homologation Reaction

In our pursuit of a ketenyl phosphonium $[R_2P{=}C{=}O]^+$ cation, a 1,2-DFB solution of [**4-2**$^{\mathbf{a}}$][$B(C_6F_5)_4$] was frozen in liquid nitrogen in a J-Young style NMR tube, and the headspace was evacuated and subsequently pressurized to 1 atmosphere of CO. Warming led to a gradual discoloration of the solution. Unfortunately, the reaction failed to produce any evidence for a $[R_2P{=}C{=}O]^+$ species, with ^{31}P NMR analysis showing atleast seven unique NMR resonances. In contrast, addition of cyclohexyl isocyanide (:C≡N–Cy) led to the selective formation of one phosphorus-containing product (Scheme 4-14). The new compound is a colorless substance, which is insoluble in hydrocarbon solvents like pentane, and has a characteristic ^{31}P NMR chemical shift at δ = 140.6 ppm, approximately 15 ppm units upfield of the respective chlorophosphine **4-1**$^{\mathbf{a}}$. ^{1}H NMR analysis suggest that both the ^{t}Bu and NIDipp substituents at phosphorus are intact. At the present moment, NMR analysis alone is insufficient to deduce a structure for the product, given the complexity of the upfield regions of the ^{1}H NMR resulting from aliphatic isopropyl groups of the NIDipp substituent, the ^{t}Bu substituent, and the Cy ring. Attempts to identify this compound *via* an SCXRD study have yet to be successful. We speculate that the identity of this compound could be an adduct $[R_2P{\leftarrow}{:}C{\equiv}N{-}Cy]^+$ or a cyano phosphine $R_2P{-}C{\equiv}N$, both of which would feature tricoordinate pyramidalized phosphorus centers, and would be consistent with the ^{31}P NMR chemical shift being in a similar range to pyramidalized chlorophosphine **4-1**$^{\mathbf{a}}$ (Scheme 4-14). The formation of a cyano phosphine $R_2P{-}C{\equiv}N$ directly from a phosphenium cation and an isocyanide

would not be unprecedented. When studying the reactivity of a diaminophosphenium triflate salt [(^{i}Pr$_2$N)$_2$P][OTf] with ^{t}Bu isocyanide (:C≡N–^{t}Bu), Sanchez and Majoral noted the formation of (^{i}Pr$_2$N)$_2$P–C≡N, although this occurred with concomitant production of isobutene and [^{i}Pr$_2$NH$_2$][OTf].[26] Moreover, highly Lewis acidic main-group species have been shown to abstract [C≡N]$^-$ from isocyanides.[45] In our specific case, we do not observe the formation of any reaction by-products that would directly imply that [C≡N]$^-$ abstraction had occurred. For further studies, it is recommended that bulky aromatic isocyanides that have easily distinguishable ^{1}H NMR handles are employed, like *m*-xylyl isocyanide for example.

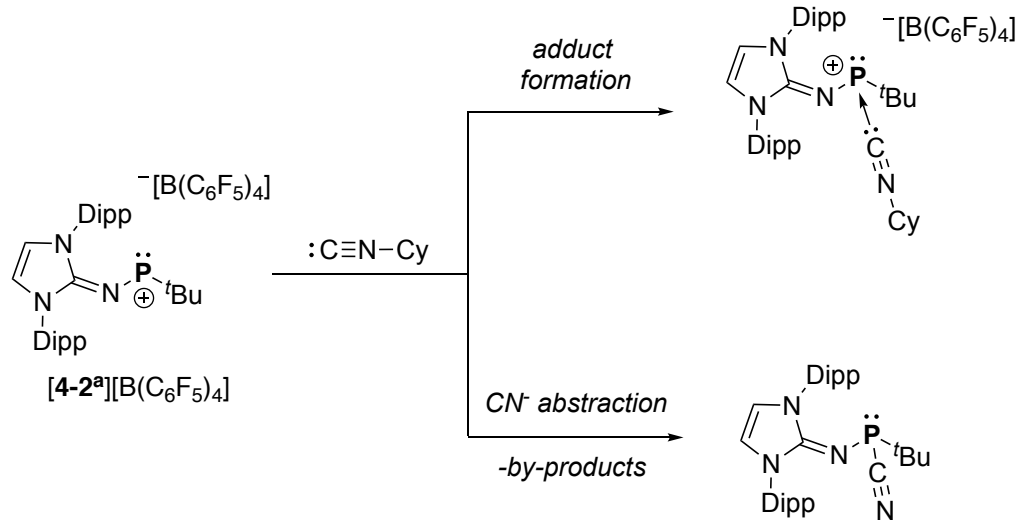

Scheme 4-14: Speculative products resulting from the reaction of phosphenium cation [**4-2^a**][B(C$_6$F$_5$)$_4$] and cyclohexyl isocyanide.

4.4 Conclusions and Outlook

In conclusion, the synthesis of acyclic alkyl (^{t}Bu) and imino (N-heterocyclic imine) substituted phosphenium cations has been delineated. Assessment of the electrophilic character of phosphenium cation [**4-2^a**]$^+$ was experimentally shown by the formation of a base adducts with DMAP, and with Et$_3$PO, the latter providing a quantitative measure of Lewis acidity *via* the Gutmann-Beckett method. [**4-2^a**]$^+$ was also found to react as an ambiphile, combining with various unsaturated hydrocarbon substrates in cheletropic cycloaddition reactions. Oxidative addition reactions extend to the cleavage of E–H bonds. O–H activation by [**4-2^a**]$^+$ was proposed to occur with two reaction outcomes, either an oxidative addition product which is a P(V) phosphonium cation, or the formation of a cationic P(III) phosphonamidite. The currently explored substrate

scope is limited, although it appears that the reaction outcome may be biased by the steric demand of the alcohol. As a first for non-geometrically constrained molecular phosphorus species, [**4-2^{a}**]$^{+}$ was shown to insert into N–H bonds, demonstrated with various aromatic amines. Unfortunately, one of our initial ambitions for preparing these phosphenium cations, which was to exploit them towards the synthesis of two new TPPCs, the ketenyl phosphonium [$R_2P{=}C{=}O$]$^{+}$ and keteniminyl phosphonium [$R_2P{=}C{=}N{-}R$]$^{+}$ cation, has not yet been realized. The latter compound, [$R_2P{=}C{=}N{-}R$]$^{+}$, warrants revisiting, by exploring reactions of [**4-2^{a}**]$^{+}$ with different isocyanides. Yet to be explored is the reactivity of [**4-2^{a}**]$^{+}$ towards B–H and Si–H bonds, as well as with small molecules like P_4, and NH_3.

4.4.1 Attempted H_2 Activation

In the last several decades, numerous dicoordinate carbenoid species have shown to be capable of H_2 activation by oxidative addition, almost all of them featuring group 13 or 14 elements (Scheme 4-15).[1,46,47,48,49,50] In most cases, the addition of H_2 addition across a $R_2E{:}^{n}$ species is considerably exergonic process, and thus the resulting dihydrogen compounds are formed irreversibly, deterring the subsequent transfer of "H_2" to a substrate. Very recently, Dobrovetsky and co-workers showed that the geometrically constrained phosphenium [**4-I**]$^{+}$ can split H_2 and subsequently transfer it to an unsaturated C–C bond. [21] While H_2 activation by [**4-I**]$^{+}$ is irreversible, H_2 transfer to unsaturated substrates by dihydrophosphonium [**4-I•H$_2$**]$^{+}$ is still achievable. This is possible because the dihydrophosphonium cation [**4-I•H$_2$**]$^{+}$ possesses a high Brønsted acidity, which initiates hydrogenation *via* the protonation of C=C functional groups. The secondary phosphine **4-I•H** that results from the protonation step functions as a hydride donor to the intermediate carbocation, completing one hydrogenation cycle and regenerating phosphenium cation [**4-I**]$^{+}$.

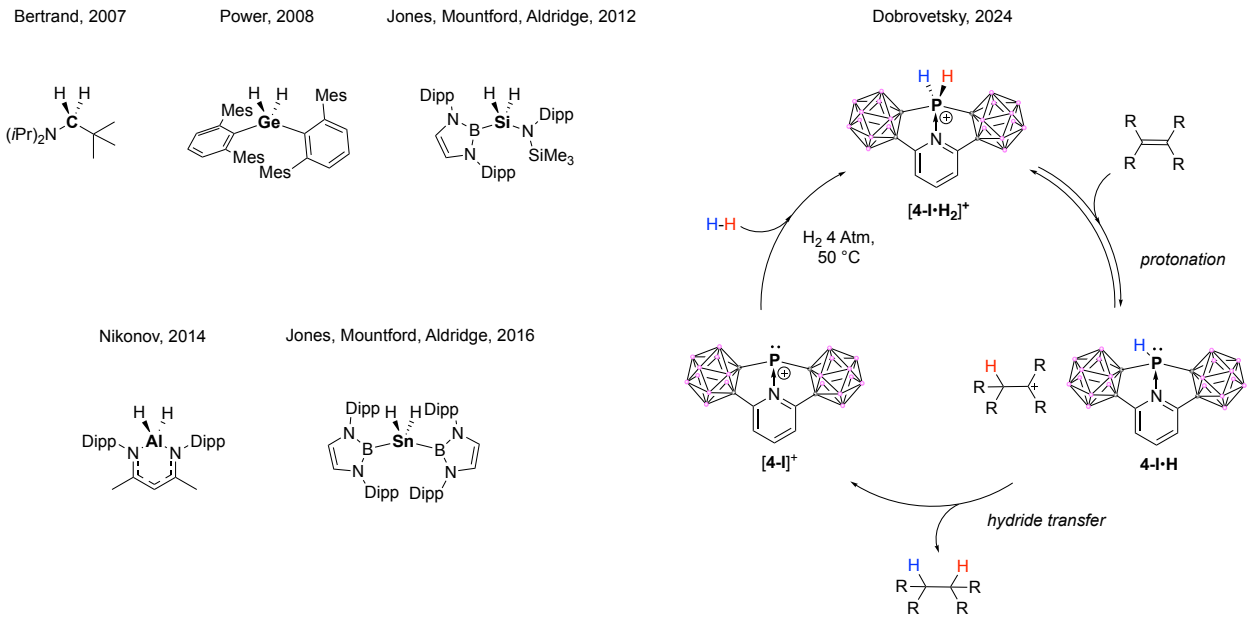

Scheme 4-15: Selected examples of H_2 activated main group centers. Alkene hydrogenation directly from dihydrogen using a geometrically constrained phosphenium cation.

Designing phosphenium systems to facilitate hydrogenation catalysis appears to have several inherent advantages. Foremost, phosphorus can cycle between two relatively stable redox states, in this case as phosphenium P(III) and dihydrophosphonium P(V) cations. When we initially targeted the acyclic-alkyl-imino-phosphenium cations delineated in this Chapter, we wanted to investigate whether they could facilitate H_2 activation, as at the time, H_2 activation by [**4-I**]$^+$ was unreported. Nonetheless, there remains no published examples of acyclic phosphenium cations activating H_2. Unfortunately, no evidence of a reaction between [**4-2^a**][$B(C_6F_5)_4$] and H_2 could be observed (1 atm and at room temperature). Applying more forcing conditions (refluxing in CH_2Cl_2 at 100 °C in a pressure vessel) only led to highly unselective outcomes with no indication of any P–H bond formation. One rationale for the inertness of [**4-2^a**]$^+$ towards H_2 could be that [**4-2^a**]$^+$ has a larger HOMO-LUMO gap (3.3 eV) compared to [**4-I**]$^+$ (3.0 eV).

As an alternative, ammonia-borane (H_3NBH_3)**,** a chemical H_2 surrogate which has been shown to furnish dihydrophosphoranes from phosphines,[51] was employed towards cation [**4-2^a**]$^+$. The reaction between [**4-2^a**]$^+$ and a large excess (20-fold) of H_3NBH_3 furnished a mixture of two phosphorus-containing compounds, one which appears as a doublet of decets ($^1J_{PH}$ = 208 Hz)

centered at δ = 37.1 ppm in ^{31}P NMR spectrum, and a second appearing as a triplet of decets ($^{1}J_{PH}$ = 460 Hz) centered at δ = -4.4 ppm (Scheme 4-16). The doublet resonance was proposed to be the secondary phosphine **4-13**, which was confirmed by its independent synthesis from chlorophosphine **4-1^{a}** and sodium tri-*sec*-butylborohydride (*N*-Selectride®). For the latter ^{31}P NMR feature, its low frequency chemical shift (δ = -4.4 ppm) suggests a tetracoordinate phosphorus environment, while its large triplet splitting pattern indicates ^{31}P coupling to two equivalent hydrogen nuclei. Taken together, we assigned this feature to be the dihydrophosphonium salt [**4-14**]$^{+}$. *In situ* analysis by ^{31} P NMR spectroscopy of the crude reaction mixture indicates that the two compounds initially form in a ratio of 7:3 (phosphine to phosphonium), which slowly evolved to a ratio of 6:4 after 72 hours. While complete conversion to [**4-14**]$^{+}$ could not be observed, the reaction with H_3NBH_3 suggests that the intermediates that would be conceivably necessary for alkene hydrogenation are synthetically viable from [**4-2^{a}**]$^{+}$. A potential next step would be to screen mixtures of [**4-2^{a}**]$^{+}$, H_3NBH_3, and various olefin substrates.

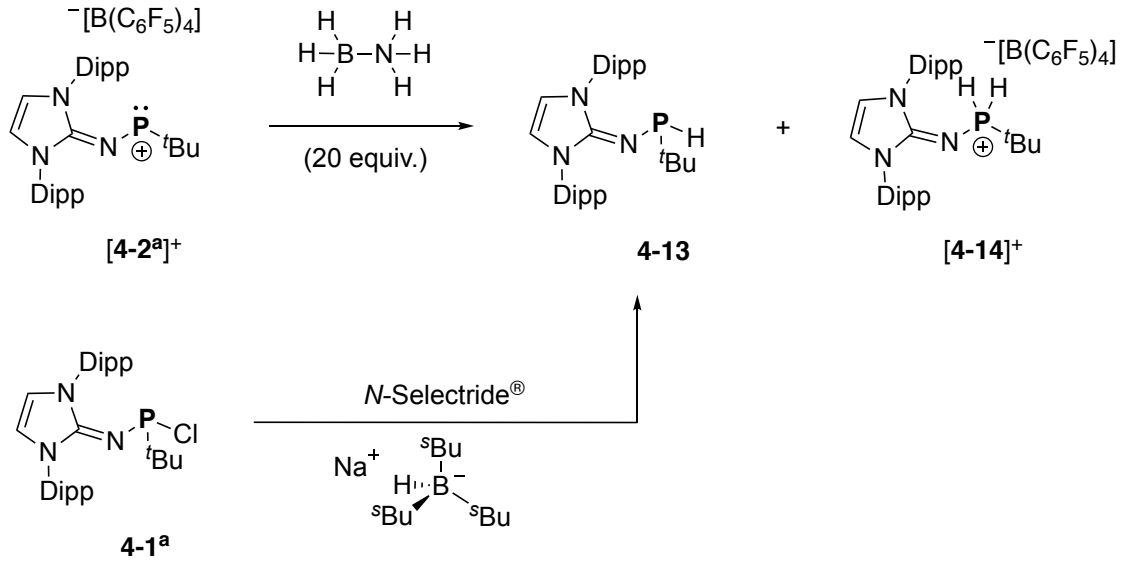

Scheme 4- 16: Reaction of phosphenium cation [**4-2^{a}**]$^{+}$ with ammonia borane, generating a mixture of secondary phosphine **4-13** and dihydrophosphonium cation [**4-14**]$^{+}$. Independent synthesis of **4-13** from N-Selectride® and chlorophosphine **4-1^{a}**.

4.4.2 Electronics of Phosphenium Cation Analogs

While the reactivity of the structural analogs of [**4-2**$^{\mathbf{a}}$]$^+$ was not performed, computations might provide some insight as to how they may differ. All alkyl-iminophosphenium cations have more accessible LUMOs than [NIDipp$_2$P]$^+$ (-2.72 eV) for reference. Most notably, of all the derivatives, cation [**4-2**$^{\mathbf{d}}$]$^+$ exhibits the narrowest HOMO-LUMO gap at (3.13 eV), and thus may be the most worthwhile to explore in oxidative addition type reactions (Figure 4-6). We can speculate as to why this might be, and the leading theory is that steric repulsion of the NIAd substituent and ^{t}Bu may force [**4-2**$^{\mathbf{d}}$]$^+$ to adopt a wider geometry, bringing closer convergence of the FMOs. In support of this thought, structural optimization of [**4-2**$^{\mathbf{d}}$]$^+$ in CH_2Cl_2 (cPCM solvation) predicts a N–P–C bond angle of 103.98°, compared to the solvated structure for [**4-2**$^{\mathbf{a}}$]$^+$ which has a narrower N–P–C bond angle of 102.14°. Alternatively, with respect to tuning the electronics of these NHI substituted phosphenium cations NHI-P-(^{t}Bu), one can entertain replacing the –^{t}Bu, for instance with a bulkier carbon-based substituent like a Mes or Dipp.

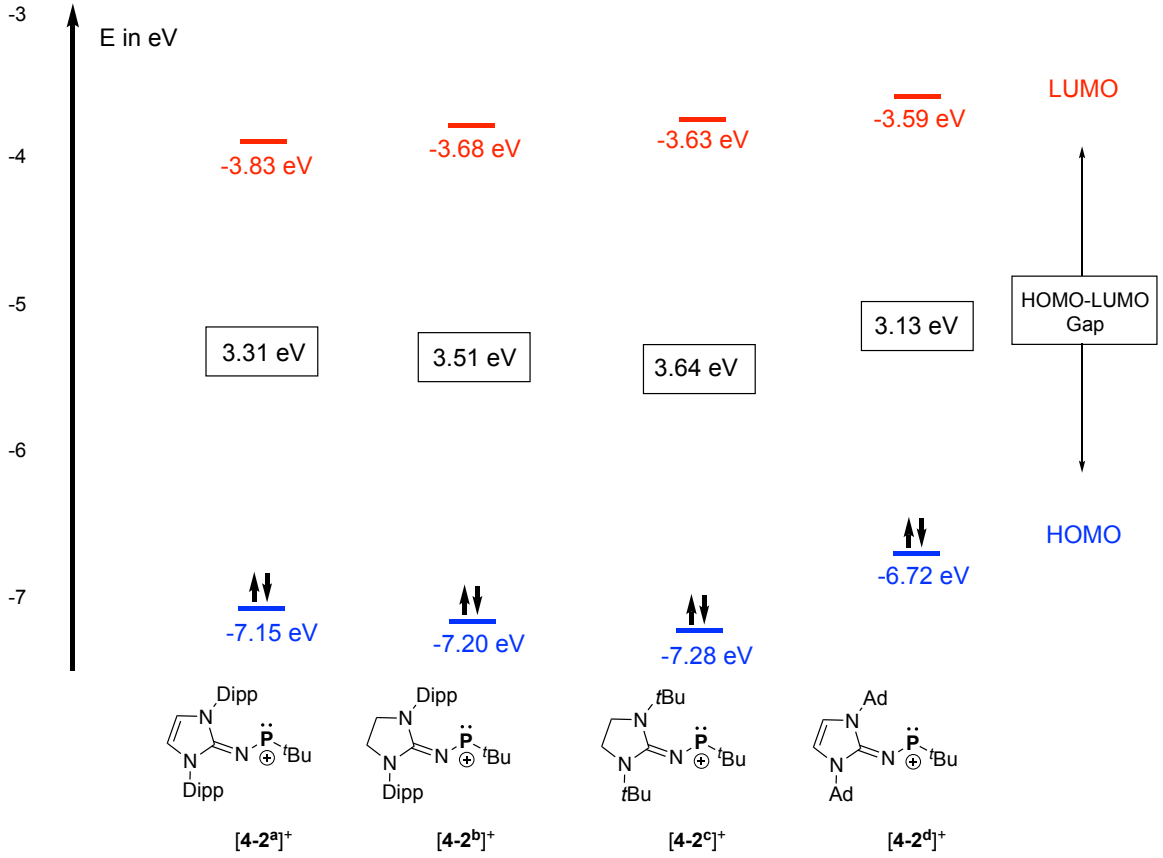

Figure 4-6: Comparison of FMO energies calculated at the B3LYP-D3BJ/def2-TZVP level of theory between alkyl-iminophosphenium cations [**4-2**$^{\mathbf{a}}$]$^+$, [**4-2**$^{\mathbf{b}}$]$^+$, [**4-2**$^{\mathbf{c}}$]$^+$ and [**4-2**$^{\mathbf{d}}$]$^+$.

Discussed previously in this thesis (Section 3.1.2), phosphorus cations based on NHIs can be made more Lewis acidic by modifying the heterocyclic backbone of the substituent. This was our initial reason for preparing alkyl-imino-phosphenium cations based on both unsaturated (more electron rich) and saturated (less electron rich) imines. To crudely probe the effect of this modification computationally, gas phase FIA calculations were performed on two truncated structures.[52] [^{unsat}NHI-P(^{t}Bu)]$^+$ and [^{sat}NHI-P(^{t}Bu)]$^+$, where both models have methyl groups at the endocyclic nitrogen atoms of the NHIs. Within the context of FIAs, [^{sat}NHI-P(^{t}Bu)]$^+$ (700/kJ mol^{-1}) is predicted to be only slightly more electrophilic than [^{unsat}NHI-P(^{t}Bu)]$^+$ (691/kJ mol^{-1}).

4.4.3 Future Directions

A new paradigm was set in 2021 with Beckmann's diaryl phosphenium cation [**4-D**]$^+$, which disintegrated the notion that at least one mesmerically stabilizing π-donor substituent was mandatory to prepare phosphenium cations.[11] From the perspective of isolation, one of the last uncharted frontiers still remaining in phosphenium chemistry are "monosubstituted" species [RHP:]$^+$. The parent phosphenium cation [H_2P:]$^+$ has been calculated to have a singlet ground state but is far too reactive to be isolated.[53] Theoretically, [H_2P:]$^+$ has been determined to be the most electrophilic [R_2P:]$^+$ species, with a gas phase FIA of 1100 kJ mol^{-1}.[54] In the absence of their isolation, both [H_2P:]$^+$ and [RHP:]$^+$ species have been investigated as Lewis base adducts of carbenes [NHC:→PR_2]$^+$.[55] With respect to dicoordinate carbenoids R_2E:^{n}, the only hydrogen substituted species R(H)E:^{n} was reported by Bertrand's group, who prepared a R(H)C: carbene based on an extremely bulky amino substituent.[56] This was experimentally determined to be the most electrophilic carbene ever isolated, underscoring the electronic influence of an H substituent in these systems. Approaching a [RHP:]$^+$ species presents a unique challenge for two reasons. 1) phosphenium cations are usually prepared by halide abstraction (X^-), most commonly a chloride, from a halophosphine R_2PX precursor. Compounds with P–H and P–Cl bonds are generally incompatible, where concomitant loss of HCl drives the formation of P–P bonds,[57] thus a [RHP:]$^+$ compound would likely not be attainable *via* a RHPCl precursor. 2) [RHP:]$^+$ would be considerably electrophilic which may be tackled with the electronic properties of the NHI substituent platform. Finding the correct steric environment for [RHP:]$^+$ is the biggest obstacle, which would first require an innovation in the steric properties of NHIs, as N-Dipp and N-Ad substituted systems are likely too small to support a phosphenium cation where the phosphorus center can only be

encumbered on one end. Nonetheless, this is one potential avenue for future work concerning the intersection of NHI and phosphenium chemistry (Scheme 4-17).

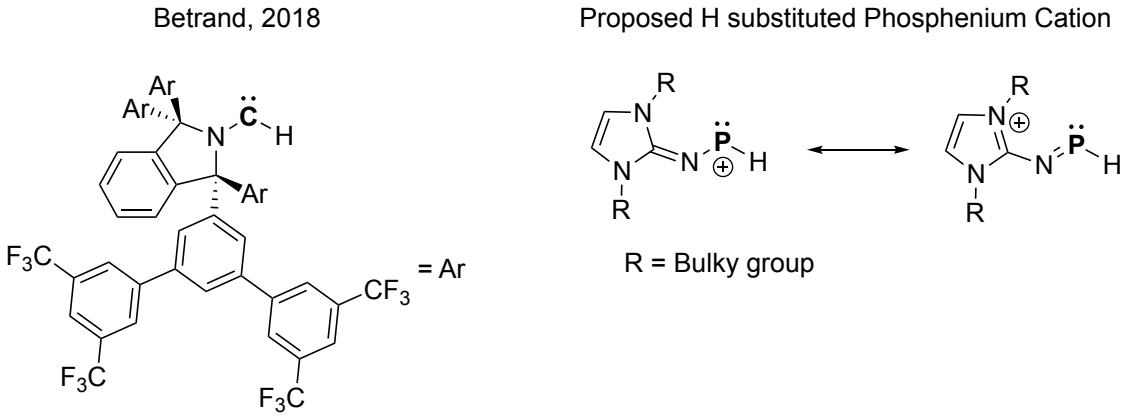

Scheme 4-17: The only H atom substituted dicoordinate carbenoid, a monosubstituted carbene stabilized by extreme steric bulk. Proposed H-substituted phosphenium cation based on an NHI.

4.5 Experimental Procedures

4.5.1 General Remarks: All manipulations were performed under an inert atmosphere of either dry argon (University of Innsbruck) or nitrogen (York University), employing standard Schlenk and glovebox techniques. Dry and oxygen-free solvents were utilized, which were obtained from a solvent purification system and then stored over molecular sieves. All glassware was oven-dried at 150 °C. ^{1}H, ^{11}B, ^{13}C, ^{19}F, and ^{31}P nuclear magnetic resonance (NMR) spectra were recorded on Bruker Neo 700 MHz, Bruker ARX 400 MHz, Bruker AVANCE (IV) Neo 400 MHz, Bruker ARX 300 MHz spectrometers, at either the NMR facilities at the University of Innsbruck or York University. Chemical shifts are given in parts per million (ppm) relative to $SiMe_4$ (^{1}H, ^{13}C), BF_3•Et_2O (^{11}B, ^{19}F), and 85% H_3PO_4 (^{31}P) and they were referenced to the residual solvent signals (CD_2Cl_2: ^{1}H δ_H =5.32, ^{13}C δ_C = 54.00; C_6D_6: ^{1}H δ_H = 7.16, ^{13}C δ_C = 128.06; CD_3CN: δ_H =1.94, ^{13}C δ_C = 118.26; $CDCl_3$: δ_H =7.26, ^{13}C δ_C = 77.16;) or internally by the instrument after locking and shimming to the deuterated solvent (^{11}B, ^{19}F, ^{31}P). Coupling constants are reported in Hertz (Hz) and NMR multiplicities are abbreviated as follows: s = singlet, d = doublet, t = triplet, q = quartet, p = pentet, sext = sextet, sept = septet, m = multiplet, br = broad signal. Mass spectrometry was recorded using an Qexactive Orbitrap (Thermo Scientific) at the University of Innsbruck, or Mass spectrometry AIMS Mass Spectrometry Laboratory at the University of Toronto utilizing an AccuTOF 4G instrument.

4.5.2 Reagents and Handling: All compounds were purchased from commercial sources (Sigma Aldrich, Alfa Aesar, Tokyo Chemical Industry, Oakwood chemicals, Ambeed) and used as received, if not stated differently. Me_3Si-NIDipp [58] and Me_3Si-NsI^{t}Bu [23], and $NaB(C_6F_5)_4$[17] were synthesized according to literature procedure. $NaB(C_6F_5)_4$ and $KB(C_6F_5)_4$ were dried at 140+ °C under dynamic vacuum for several days prior to use.

Note 1: The synthesis of the phosphenium cations in this Chapter requires silylated NHIs (Me_3Si-NIDipp, Me_3Si-NsI^{t}Bu, Me_3Si-NIAd, and Me_3Si-NsIDipp). These are prepared by one of two cited methods. [23,58] One route uses azidotrimethylsilane (Me_3Si-N_3), which is extremely toxic, as well as an explosive hazard if stored incorrectly. It should be stored under argon with ground glass contacts, at low temperature. The second route utilizes cyanogen bromide (BrCN). Contact with

skin or inhalation of BrCN can be lethal. If attempting to make any of these compounds, please consult with your supervisor and lab members prior to doing so.

Note 2: $NaB(C_6F_5)_4$ was prepared *via* a route that involves lithium halogen exchange of bromopentafluorobenzene (BrC_6F_5). It is very important that when lithiating bromopentafluorobenzene (BrC_6F_5), cryogenic temperatures are judiciously kept. Not doing so is very risky and can cause a detonation on account of LiF elimination and the formation of benzyne. Please be careful.

4.5.3 Synthetic Procedure

Protocol 1: Procedure for alkyl-imino-chlorophosphines **P(NHI)^{t}BuCl:** The respective silylated imine precursor, Me_3Si-(NHI) (1 eq) was dissolved in toluene and then added slowly *via* cannula transfer to a stirring toluene solution of ^{t}BuPCl$_2$ (1.05 eq) which had been cooled to -78 °C with a dry ice/acetone cooling bath. The reaction mixture was stirred for 30 minutes while keeping it at -78 °C, then allowed warm up to room temperature and stirred for an additional 16 h. All volatiles were then removed *in vacuo.* Excess ^{t}BuPCl$_2$ in the reaction mixture was removed by sublimation (60 °C at 10^{-3} mbar) affording the appropriate phosphines precursors.

Protocol 2: Protocol for reactivity investigations with **[4-2^a][B(C$_6$F$_5$)$_4$]:** Phosphine **4-1^a** (13.1 mg, 0.025 mmol) was dissolved in 1,2-DFB (1 ml) then added to a suspension of KB(C$_6$F$_5$)$_4$ (17.9 mg, 0.025 mmol) at room temperature. The reaction was allowed to stir for 1 hour, followed by addition of the substrate, which was always added in a very slight excess (0.026 mmol). For liquid reagents, Eppendorf style pipettes were used to measure volumes. Usually, an aliquot of the reaction mixture was analyzed by ^{31}P NMR spectroscopy to monitor reaction progress. Once reactions were complete, the solvent was removed *in vacuo*. The residue was taken up in CH_2Cl_2, filtered to remove KCl, concentrated and dried to a solid. Subsequently the solid residue was washed with pentane (3 x 2 ml) and then re-dried under high vacuum prior to analysis by NMR spectroscopy.

4.5.4 Preparation of P(NIDipp)^{t}BuCl (4-1^a)

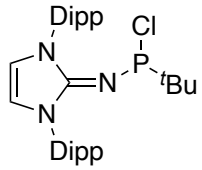

Following protocol **1** (NIDipp)SiMe$_3$ (1.00 g, 2.10 mmol, 1 eq) and ^{t}BuPCl$_2$ were combined (350 mg, 2.20 mmol, 1.05 eq). The title compound was isolated as a beige/ white powder.

Yield: 913 mg (1.74 mmol, 83%).

^{1}H NMR (400 MHz, C_6D_6, T= 298 K): δ (ppm) = 7.24 (t, $^3J_{HH}$= 7.7 Hz, 2H, Dipp; *para*), 7.13 (m, 4H, Dipp; *meta*), 5.98 (s, 2H, N-C<u>H</u>=C<u>H</u>-N), 3.16 (sept, $^3J_{HH}$ = 6.9 Hz, 2H, C<u>H</u>(CH$_3$)$_2$), 2.98 (sept, $^3J_{HH}$ = 6.9 Hz, 2H , C<u>H</u>(CH$_3$)$_2$), 1.48 (d, $^3J_{HH}$ = 6.9 Hz, 6H, CH(C<u>H</u>$_3$)$_2$), 1.42 (d, $^3J_{HH}$ = 6.9 Hz, 6H, CH(C<u>H</u>$_3$)$_2$), 1.15 (d, $^3J_{HH}$ = 2.3 Hz, 6H, CH(C<u>H</u>$_3$)$_2$), 1.13 (d, $^3J_{HH}$ = 2.4 Hz, 6H, CH(C<u>H</u>$_3$)$_2$), 0.96 (d, $^3J_{HP}$ = 13 Hz, 9H, P-C(C<u>H</u>$_3$)$_3$).

^{13}C{^{1}H} NMR (C_6D_6, 101 MHz, 298 K) δ (ppm) = 150.4 (d, $^2J_{CP}$ = 14 Hz, N$_2$<u>C</u>=N-P), 147.6 (Dipp: *ortho*), 147.6 (Dipp: *ortho*), 147.1, (Dipp: *ortho*), 133.6, (Dipp: *ipso*), 130.3 (CH Dipp: *para*), 124.3 (CH Dipp: *meta*), 124.0 (CH Dipp: *meta*), 116.3 (N-<u>C</u>H=<u>C</u>H-N), 36.7 (d, $^1J_{CP}$ = 24 Hz, 29.3 (Ph-<u>C</u>H(CH$_3$)$_2$), 29.3 (Ph-<u>C</u>H(CH$_3$)$_2$), 29.2 (Ph-<u>C</u>H(CH$_3$)$_2$), 25.0 (Ph-CH(<u>C</u>H$_3$)$_2$), 24.9 (Ph-CH(<u>C</u>H$_3$)$_2$), 24.8 (d, $^2J_{CP}$ = 18 Hz, P-C(<u>C</u>H$_3$)$_3$, 23.3 (Ph-CH(<u>C</u>H$_3$)$_2$), 22.9 (Ph-CH(<u>C</u>H$_3$)$_2$), 22.8 (Ph-CH(<u>C</u>H$_3$)$_2$).

^{31}P NMR (C_6D_6, 162 MHz, 298 K) δ (ppm) = 157.6 (decet, $^3J_{PH}$ = 13 Hz).

DART-HRMS: Calculated for $[C_{31}H_{46}ClN_3P]^+$ ([**4-1^a**+H])$^+$: *m/z* = 526.3112, found: *m/z* =526.3123

4.5.5 Preparation of P(NsIDipp)^{t}BuCl (4-1^b)

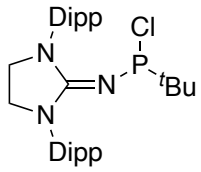

Following protocol **1** (sIDippN)SiMe$_3$ (1.03 g, 2.15 mmol, 1 eq) and ^{t}BuPCl$_2$ were combined (360 mg, 2.26 mmol, 1.05 eq). The title compound was isolated as a beige/ white powder.

Yield: 939 mg (1.78 mmol, 83%).

^{1}H NMR (C_6D_6, 400 MHz, T = 298 K): δ (ppm) = 7.22 (d, $^3J_{HH}$ = 7.7 Hz, 2 H, Dipp; *para*), 7.14-7.10 (m, 4 H, Dipp; *meta*), 3.44 (m, 4 H, N-C$\underline{H}_2$- C$\underline{H}_2$-N), 3.36 (m, 2 H, C$\underline{H}$Me$_2$), 3.29 (m, 2 H, C$\underline{H}$Me$_2$), 1.54 (d, $^3J_{HH}$ = 6.8 Hz, 6H, CH(C$\underline{H}_3$)$_2$), 1.49 (d, $^3J_{HH}$ = 6.8 Hz, 6H, CH(C$\underline{H}_3$)$_2$), 1.22 (d, $^3J_{HH}$ = 6.9 Hz, 12H, CH(C$\underline{H}_3$)$_2$), 0.90 (d, $^3J_{HP}$ = 13 Hz, 9H, P-C(C$\underline{H}_3$)$_3$).

^{13}C{^{1}H} NMR (C_6D_6, 101 MHz, T = 298 K): δ (ppm) = 158.0 (d, $^2J_{CP}$ = 10 Hz, N$_2$C=N), 148.6 (Dipp, *ortho*), 148.0 (Dipp, *ortho*), 135.1 (Dipp; *ipso*), 129.5 (Dipp; *ipso*), 124.5 (Dipp; *para*), 124.4 (Dipp; *meta*), 49.0 (N-$\underline{C}$H$_2$-$\underline{C}$H$_2$-N), 36.8 (d, $^1J_{CP}$ = 24.4 Hz, P-$\underline{C}$(CH$_3$)$_3$, 29.12 (Ph-$\underline{C}$H(CH$_3$)$_2$), 29.11 (Ph-$\underline{C}$H(CH$_3$)$_2$), 25.7 (Ph-CH(C$\underline{H}_3$)$_2$), 25.6 (Ph-CH(C$\underline{H}_3$)$_2$), 24.8 (d, $^2J_{CP}$ = 18.2 Hz, P-C(C$\underline{H}_3$)$_3$, 23.67 (Ph-CH(C$\underline{H}_3$)$_2$), 23.62 (Ph-CH(C$\underline{H}_3$)$_2$).

^{31}P NMR (162 MHz, C_6D_6, T = 298 K): δ (ppm) = 148.2 (decet, $^3J_{HP}$ = 13 Hz).

4.5.5 Preparation of P(NsI^{t}Bu)^{t}BuCl (4-1^c)

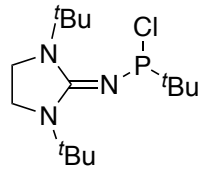

Following protocol **1**, (NsI^{t}Bu)SiMe$_3$ (1.62 g, 6.03 mmol, 1 eq) and ^{t}BuPCl$_2$ were combined (1.01 g, 6.33 mmol, 1.05 eq). The title compound was isolated as a white powder.

Yield: 1.60 g (5.01 mmol, 79 %).

^{1}H NMR (400 MHz, C_6D_6, T= 298K): δ (ppm) 2.62 (m, 4H, N-C$\underline{H}_2$-C$\underline{H}_2$-N), 1.47 (d, $^3J_{HP}$ = 11.9 Hz, 9H, P-C(C$\underline{H}_3$)$_3$), 1.34 (s, 18H, N-C(C$\underline{H}_3$)$_3$).

^{13}C{^{1}H} NMR (101 MHz, C_6D_6, T = 300 K): δ (ppm) 160.2 (d $^2J_{cp}$ = 15.8 Hz, N$_2\underline{C}$=N), 54.6 (N-$\underline{C}$(CH$_3$)$_3$), 42.4 (N-$\underline{C}$H$_2$-$\underline{C}$H$_2$-N), 38.2 (d, $^1J_{cp}$ = 30.4 Hz, P-$\underline{C}$(CH$_3$)$_3$), 29.1 (N-C($\underline{C}$H$_3$)$_3$), 29.0 (N-C($\underline{C}$H$_3$)$_3$), 26.2 ($^2J_{cp}$ = 18.1 Hz, P-C($\underline{C}$H$_3$)$_3$).

^{31}P NMR (162 MHz, C_6D_6, T = 298 K): δ (ppm) = 174.43 (decet, $^3J_{HP}$ = 11.7 Hz).

4.5.6 Preparation of P(NIAd)^{t}BuCl (4-1^d)

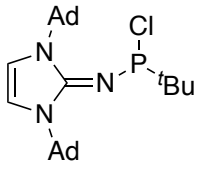

Following protocol **1** (NIAd)SiMe$_3$ (999 mg, 2.35 mmol, 1 eq) and ^{t}BuPCl$_2$ were combined (395 mg, 2.48 mmol, 1.05 eq). The title compound was isolated as a white powder.

Yield: 851 mg (1.80 mmol, 76 %).

^{1}H NMR (400 MHz, C_6D_6, T= 298K): δ (ppm) 6.24 (s, 2H, N-C<u>H</u>=C<u>H</u>-N), 2.63 – 2.19 (m, 12H, adamantyl-CH_2), 1.99 (s, 6H, adamantyl-CH), 1.68 – 1.61 (m, 6H, adamantyl-CH_2), 1.57 (d, $^3J_{HP}$ = 12.1 Hz, 9H, P-C(C<u>H</u>$_3$)$_3$), 1.51 – 1.44 (m, 6H, adamantyl-CH_2).

^{13}C{^{1}H} NMR (101 MHz, C_6D_6, T = 300 K): δ (ppm) 149.9 (N_2<u>C</u>=N), 110.1 (N-<u>C</u>H=<u>C</u>H-N), 58.0 (N-Ad quaternary C), 41.0 (Adamantyl-<u>C</u>H_2), 41.0 (Adamantyl-<u>C</u>H_2), 38.3 (d, $^1J_{CP}$ = 29.8 Hz, P-<u>C</u>(CH$_3$)$_3$), 30.3 (Adamantyl-<u>C</u>H), 26.3 (d, $^2J_{CP}$ = 17.9 Hz, P-C(<u>C</u>H$_3$)$_3$).

^{31}P NMR (162 MHz, C_6D_6, T = 298 K): δ (ppm) = 189.4 (decet, $^3J_{HP}$ = 11.6 Hz)

4.5.7 Preparation of Phosphenium Salt [4-2^{a}][AlCl$_4$]

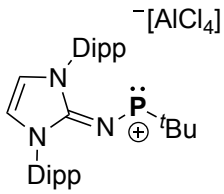

A dichloromethane solution (2 mL) of alkyl-imido-chlorophosphine **4-1^{a}** (39.5 mg, 0.075 mmol, 1 eq) was added directly to solid $AlCl_3$ (10 mg, 0.075 mmol, 1 eq) resulting in an instantaneous color change to bright red. The solution was allowed to stir for 30 minutes then all volatiles were removed *in vacuo* and the resulting red residue was washed with pentane. Once dried under reduced pressure the title compound was isolated as a pink-red solid.

Yield: Quantitative.

^{1}H NMR (700 MHz, CD_2Cl_2, T= 298K): δ (ppm) 7.62 (t, $^{3}J_{HH}$ = 7.8 Hz, 2H, Dipp; *para*), 7.60 (s, 2H, N-C<u>H</u>=C<u>H</u>-N), 7.40 (d, 4H, Dipp; *meta*), 2.50 (sept, $^{3}J_{HH}$ = 6.9 Hz, 2H , C<u>H</u>$(CH_3)_2$), 1.29 (d, $^{3}J_{HH}$ = 6.9 Hz, 6H, CH(C<u>H</u>$_3)_2$), 1.15 (d, $^{3}J_{HH}$ = 6.9 Hz, 6H, CH(C<u>H</u>$_3)_2$), 0.88 (d, $^{3}J_{HP}$ = 10.1 Hz, 9H, P-C(C<u>H</u>$_3)_3$).

^{13}C{^{1}H} NMR (176 MHz, CD_2Cl_2, T = 298 K): δ (ppm) 147.7 (s, N_2<u>C</u>=N-P), 145.8 (Dipp: *ortho*), 133.0 (CH Dipp: *para*), 129.2 (Dipp: *ipso*), 125.6 (CH Dipp: *meta*), 123.5 (N-<u>C</u>H=<u>C</u>H-N), 50.3 (d, $^{1}J_{CP}$ = 46.6 Hz, P-<u>C</u>$(CH_3)_3$), 29.8 (Ph-<u>C</u>H$(CH_3)_2$), 24.7 (Ph-CH(<u>C</u>H$_3)_2$), 23.5 (d, $^{2}J_{CP}$ = 46.6 Hz, P-C(<u>C</u>H$_3)_3$), 23.2 (Ph-CH(<u>C</u>H$_3)_2$).

^{27}Al NMR δ (78 MHz, CD_2Cl_2, T = 296 K): δ (ppm) 104.4

^{31}P NMR (121 MHz, CD_2Cl_2, T = 296 K): δ (ppm) = 594.4 (broad multiplet).

DART-HRMS: Calculated for $[C_{31}H_{45}N_3P]^+$ ([**4-2^{a}**])$^+$: *m/z* = 490.3351, not found. Highest intensity *m/z* corresponds to the oxidative addition of [**4-2^{a}**]$^+$ with water $[C_{31}H_{45}N_3P{\bullet}H_2O]^+$ *m/z* = 508.35

Alternatively, a CH_2Cl_2 solution of **4-1^{a}** can be added to an equimolar suspension of Na[B$(C_6F_5)_4$] or K[B$(C_6F_5)_4$]. After atleast 30 minutes, the solution is passed through glass, dried, washed with either hexane or pentane, dried again and collected as a red/pink solid.

Note: for the $[B(C_6F_5)_4]^-$ derivative of $[\mathbf{4\text{-}2^a}]^+$ the ^1H and ^{13}C resonances corresponding to the cation are very similar but broadened, presumably due to worse solubility. The multinuclear NMR data for this compound is listed as follows.

^{11}B NMR (101 MHz, CD_2Cl_2, T = 298 K): δ (ppm) = -16.7 ppm.

^{19}F NMR (282 MHz, CD_2Cl_2, T = 295 K): δ (ppm) = -133.1 (m, 8F), -163.7 (t, $^3J_{FF}$ = 20.4 Hz), -167.6 (t, $^3J_{FF}$ = 19.8 Hz).

4.5.8 Confirmation of Phosphenium cations $[\mathbf{4\text{-}2^b}]^+$ and $[\mathbf{4\text{-}2^c}]^+$

Following the reaction of either phosphine **4-1b** and **4-1c** with $Na[B(C_6F_5)_4]$ (1.05 equiv.), the reaction mixtures were filtered through glass to remove NaCl, and dried to a residue. After washing with hexanes the remaining solids were taken up in CD_2Cl_2. The large downfield resonances ($[\mathbf{4\text{-}2^b}]^+$: 555.6 ppm, $[\mathbf{4\text{-}2^c}]^+$: 543.9 ppm) confirms the formation of phosphenium cations.

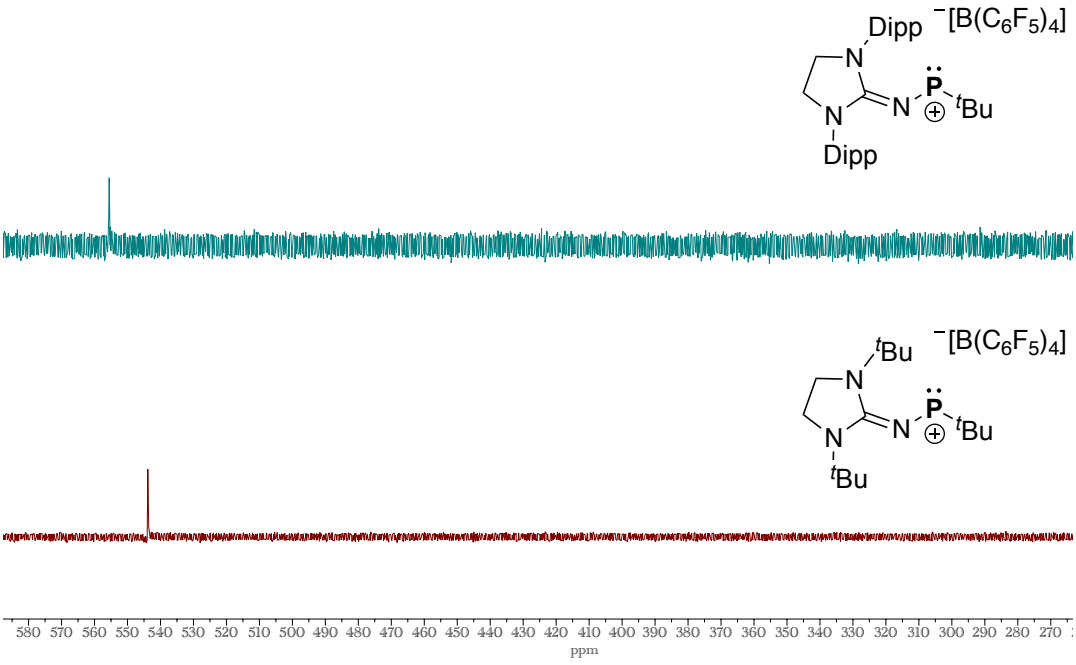

Figure 4-7: Stacked $^{31}P\{^1H\}$ NMR spectra of phosphenium cations $[\mathbf{4\text{-}2^b}]^+$ and $[\mathbf{4\text{-}2^c}]^+$.

4.5.9 Preparation of Phosphenium Salt [4-2^{d}][$B(C_6F_5)_4$]

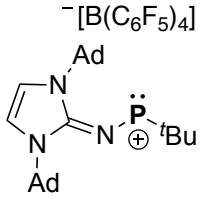

4-1^{d} (20 mg, 0.042 mmol, 1 eq) was dissolved in dichloromethane (1 ml) and then added dropwise to a stirring suspension of $NaBArF_{20}$ (31.1 mg, 0.044 mmol) in dichloromethane (1 ml). The solution immediately changes from colorless to bright purple. The solution was allowed to stir for 1 hour, then filtered through glass. Solvent was removed *in vacuo*, and the residue was washed with hexanes (1 x 3 ml). Drying *in vacuo* gave the title phosphenium salt as a lavender colored powdery solid.

Yield: 42.6 mg (0.038 mmol, 90 %).

^{1}H NMR (400 MHz, CD_2Cl_2, T= 298 K): δ (ppm) 7.25 (s, 2H, N-C<u>H</u>=C<u>H</u>-N), 2.29 (s, 6H, adamantyl-CH), 2.20 (m, 12H, adamantyl-CH_2), 1.91 – 1.74 (m, 6H, adamantyl-CH_2), 1.70 – 1.64 (m, 6H, adamantyl-CH_2). 1.53 (d, $^{3}J_{HP}$ = 11.8 Hz, 9H, P-C(C<u>H</u>$_3$)$_3$),

^{11}B NMR (101 MHz, CD_2Cl_2, T = 298 K): δ (ppm) = -16.6 (s)

^{13}C{^{1}H} NMR (101 MHz, CD_2Cl_2, (T= 298 K): δ (ppm) 148.6 (dm, $^{1}J_{CF}$ = 242 Hz, CF $B(C_6F_5)_4$: *ortho*), 147.9 (d, $^{2}J_{CP}$ = 10 Hz, N_2<u>C</u>=N-P), 138.7 (dm, $^{1}J_{CF}$ = 245 Hz, CF $B(C_6F_5)_4$: *ortho*), 136.7 (dm, $^{1}J_{CF}$ = 247 Hz, CF $B(C_6F_5)_4$: *ortho*), 123.9 (br, $B(C_6F_5)_4$: *ipso*), 115.8 (N-<u>C</u>H=<u>C</u>H-N), 63.1 (N-Ad quaternary C), 50.3 ($^{1}J_{CP}$ = 48 Hz, P-<u>C</u>(CH_3)$_3$), 42.7 (adamantyl-<u>C</u>H_2), 35.7 (adamantyl-<u>C</u>H_2), 30.26 (adamantyl-<u>C</u>H_2), 24.0 ($^{2}J_{CP}$ = 12 Hz, P-C(<u>C</u>H_3)$_3$). * $B(C_6F_5)_4$ *Ipso* not observed.

^{19}F NMR (101 MHz, CD_2Cl_2, T = 298 K): δ (ppm) = -128 – -135 (m, 8F, ortho-F), -163.65 (t, $^{1}J_{FF}$ = 20 Hz, 4F, para-F), 167.53 (t, $^{1}J_{FF}$ = 19 Hz, 8F, meta-F)

^{31}P NMR (162 MHz, CD_2Cl_2, T = 298 K): δ (ppm) = 592.0 (br)

4.5.10 Gutmann Beckett Analysis of [4-2^{a}]$^{+}$

An experiment for the determination of a Gutmann-Beckett acceptor number was carried out according to a procedure outlined by Greb et al. [17] To a dichloromethane solution of [**4-2^{a}**][B(C_6F_5)$_4$] (0.095 mmol, 111.2 mg, 1.0 eq), triethylphosphine oxide was added (0.047 mmol, 6.4 mg, 0.5 eq) to ensure full saturation of the probe.

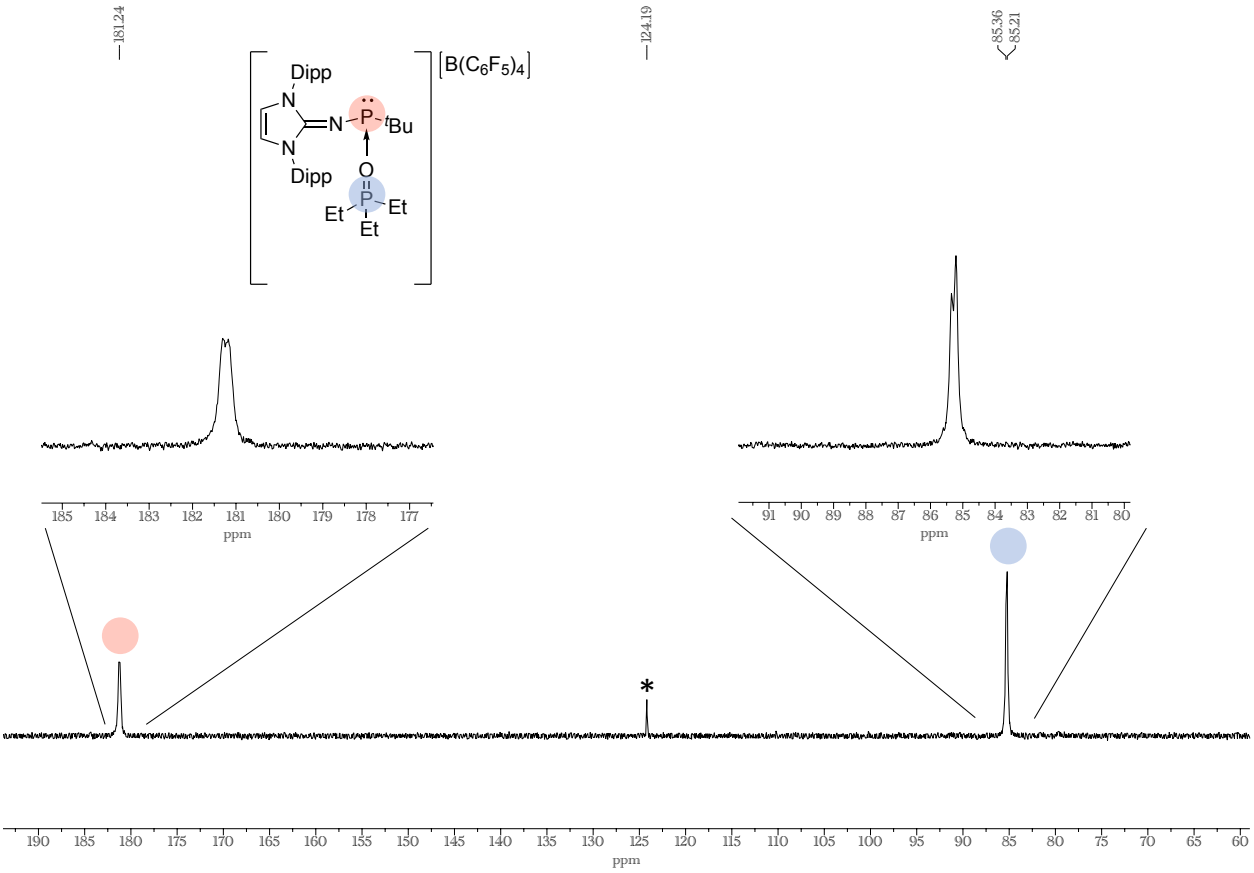

Figure 4-8: $^{31}P\{^{1}H\}$ NMR (162 MHz, 296 K) spectrum of the Gutmann-Beckett test for [**4-2^{a}**].$^{+}$ The asterisk denotes an unknown impurity.

Using the following formula and inputting a chemical shift of 85.3 ppm for [**4-2^{a}•Et$_3$PO**][B(C_6F_5)$_4$], an AN of 98 was determined.

$$AN = \frac{\delta_{interacting\ TEPO} - 41.0}{86.14 - 41.0}\ x\ 100$$

4.5.11 DMAP adduct formation with [4-2^{a}]$^{+}$

Phosphine **4-1^{a}** (50 mg, 0.095 mmol) was added to a suspension of K[B(C_6F_5)$_4$] (68.2 mg, 0.095) in 1,2-DFB and stirred for 1 hour. Subsequently, the solution was added to a solid portion of DMAP (0.1 mmol, 12.2 mg), and swirled, resulting in an immediate change in solution color from red to colorless. The product was dried to a residue, taken up in minimal amounts of CH_2Cl_2 and filtered through glass to remove KCl. Drying in vacuum resulted in a white solid. Complete conversion could be observed by NMR, however residual DMAP was detected.

^{1}H NMR (700 MHz, $CDCl_3$, T= 298 K): δ (ppm) = 7.42 (m, 5H, Dipp; *para* and C-H Ar DMAP overlapped), 7.30 (d, $^{3}J_{HH}$ = 7.7 Hz, 2H, Dipp; *meta*), 7.16 (d, $^{3}J_{HH}$ = 7.7 Hz, 2H, Dipp; *meta*), 6.67 (s, 2H, N-C<u>H</u>=C<u>H</u>-N), 6.24 (s, 2H, C-H Ar DMAP), 3.07 (s, 6H, N(CH_3)$_2$ of DMAP), 2.90 (sept, $^{3}J_{HH}$ = 6.9 Hz, 2H, C<u>H</u>(CH_3)$_2$), 2.70 (sept, $^{3}J_{HH}$ = 6.9 Hz, 2H, C<u>H</u>(CH_3)$_2$), 1.31 (d, $^{3}J_{HH}$ = 6.9 Hz, 6H, CH(C<u>H</u>$_3$)$_2$, 1.19 (m, 12H, CH(C<u>H</u>$_3$)$_2$), 1.04 (d, $^{3}J_{HH}$ = 6.9 Hz, 6H, CH(C<u>H</u>$_3$)$_2$), 0.35 (d, $^{3}J_{HP}$ = 13.4 Hz, 9H, P-C(C<u>H</u>$_3$)$_3$).

^{13}C{^{1}H} NMR (176 MHz, $CDCl_3$, T= 298 K): δ (ppm) = 156.9 (DMAP: *ipso*), 151.5 ($^{2}J_{CP}$ = 27.1 Hz,) 148.3 (dm, $^{1}J_{CF}$ = 243 Hz, B-(<u>C</u>$_6F_5$)$_4$; *ortho*), 147.4 (Dipp: *ortho*), 146.7 (Dipp: *ortho*) 140.4 (br, <u>C</u>-H Ar DMAP), 138.3 (dm, $^{1}J_{CF}$ = 246 Hz, B-(<u>C</u>$_6F_5$)$_4$; *para*), 136.4 (dm, $^{1}J_{CF}$ = 244 Hz, B-(<u>C</u>$_6F_5$)$_4$; *para*), 132.1 (Dipp: *ipso*), 130.9 (Dipp: *para*), 124.4 (Dipp; *meta*), 124.3 (Dipp; *meta*), 117.3 (N-<u>C</u>H=<u>C</u>H-N), 106.2 (<u>C</u>-H Ar DMAP), 39.8 (s, 6H, N(<u>C</u>H_3)$_2$ of DMAP), 35.3 ($^{1}J_{CP}$ =n14.7 Hz, P-<u>C</u>(CH_3)$_3$), 29.3 (Ph-<u>C</u>H(CH_3)$_2$), 29.1 (Ph-<u>C</u>H(CH_3)$_2$), 25.3 (Ph-CH(<u>C</u>H_3)$_2$), 24.7 (Ph-CH(<u>C</u>H_3)$_2$), 23.5 ($^{2}J_{CP}$ = 17 Hz, P-C(<u>C</u>H_3)$_3$), 22.4 (Ph-CH(<u>C</u>H_3)$_2$), 22.3 (Ph-CH(<u>C</u>H_3)$_2$).

^{31}P{^{1}H} NMR (121 MHz, $CDCl_3$, T= 298 K): δ (ppm) = 136.6 ppm

4.5.12 Synthesis of [4-4][$B(C_6F_5)_4$]

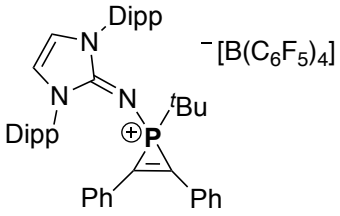

Following protocol **2**, the addition of diphenylacetylene/tolane (4.7 mg) led to an immediate color change in the reaction mixture from red to colorless. The product was isolated as a white powder.

Yield: 33 mg, 0.025 mmol, 98%)

^{1}H NMR (700 MHz, $CDCl_3$, T= 298 K): δ (ppm) = 7.52 (t, $^{3}J_{HH}$ = 7.5 Hz, 2H, tolane: *para*), 7.44 (t, $^{3}J_{HH}$ = 7.5 Hz, 4H, tolane; *meta*), 7.33 (d, $^{3}J_{HH}$ = 7.5 Hz, 4H, tolane; *ortho*), 7.11 (m, 6H, Dipp; *meta* and *para* overlapped) 6.73 (s, 2H, N-C<u>H</u>=C<u>H</u>-N), 2.65 (sept, $^{3}J_{HH}$ = 6.9 Hz, 4H, C<u>H</u>$(CH_3)_2$), 1.24 (d, $^{3}J_{HH}$ = 6.9 Hz, 12H, CH(C<u>H</u>$_3)_2$), 1.14 (d, $^{3}J_{HH}$ = 6.9 Hz, 12H, CH(C<u>H</u>$_3)_2$), 0.99 (d, $^{3}J_{HP}$ = 22.8 Hz, 9H, P-C(C<u>H</u>$_3)_3$).

^{11}B{^{1}H} NMR (96 MHz, $CDCl_3$, T= 298 K): δ (ppm) = -16.6.

^{13}C{^{1}H} NMR (176 MHz, $CDCl_3$, T= 298 K): δ (ppm) = 148.3 (dm, $^{1}J_{CF}$ = 241 Hz, B-(<u>C</u>$_6F_5)_4$; *ortho*), 145.6 (Dipp; *ortho*), 144.8, (phosphirenium <u>C</u>=<u>C</u>) 142.9 (d, $^{2}J_{CP}$= 7.3 Hz, N_2<u>C</u>=N-P), 138.3 (dm, $^{1}J_{CF}$ = 244 Hz, B-(<u>C</u>$_6F_5)_4$; *para*), 136.4 ($^{1}J_{CF}$ = 245 Hz, B-(<u>C</u>$_6F_5)_4$; *meta*), 132.4 (Ph tolane: *para*), 131.4 (Dipp: *para*), 130.8 (Dipp: *ipso*), 130.3 and 130.2 (Ph CH tolane; *ortho*),129.5 (Ph tolane: *meta*), 126.1 (Ph tolane; *ipso*), 124.8 (Dipp; *meta*), 124.1 (B-(<u>C</u>$_6F_5)_4$; *ipso*), 118.4 (N-<u>C</u>H=<u>C</u>H-N) 36.9 (d, $^{1}J_{CP}$ = 105 Hz, P-<u>C</u>$(CH_3)_3$), 29.2, (Ph-<u>C</u>H$(CH_3)_2$), 27.0 (P-C(<u>C</u>$H_3)_3$), 24.8 (Ph-CH(<u>C</u>$H_3)_2$), 22.9 (Ph-CH(<u>C</u>$H_3)_2$).

^{19}F NMR (282 MHz, $CDCl_3$, T= 298 K): δ (ppm) = -132.6 (m, 8F, B-(C$_6$<u>F</u>$_5)_4$; *ortho*), -163.4 (t, $^{3}J_{FF}$ = 20.6 Hz, 4F, B-(C$_6$<u>F</u>$_5)_4$; *para*), 167.0 (m, 8F, B-(C$_6$<u>F</u>$_5)_4$; *meta*).

[1]

^{31}P NMR (121 MHz, $CDCl_3$, 297 K) δ (ppm) = -82.5 (decet, $^{3}J_{HP}$ = 22.8 Hz).

DART-HRMS: Calculated for $[C_{45}H_{55}N_3P]^+$ ([**4-4**])$^+$: *m/z* = 668.4128, found: *m/z* = 668.4119

4.5.13 Synthesis of [4-5][$B(C_6F_5)_4$]

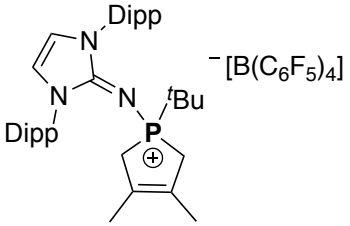

Following protocol **2**, the addition of 2,3-dimethylbutadiene (2.2 mg) led to an immediate color change in the reaction mixture from red to colorless. The product was isolated as a white powder.

Yield: 29 mg (0.023 mmol, 93 %).

^{1}H NMR (300 MHz, $CDCl_3$, T= 295 K): δ (ppm) = 7.54 (t, $^{3}J_{HH}$ = 7.7 Hz, 2H, Dipp; *para*), 7.33 (d, $^{3}J_{HH}$ = 7.7 Hz, 4H, Dipp; *meta*), 6.82 (s, 2H, N-C<u>H</u>=C<u>H</u>-N), 2.60 (sept, $^{3}J_{HH}$ = 6.9 Hz, 4H, C<u>H</u>(CH_3)$_2$), 2.21 (dd, $^{2}J_{HH}$ = 18.4 Hz, $^{2}J_{HP}$ = 9.2 Hz, 2H, P-C<u>H</u>$_2$), 1.44 (s, 6H, <u>H</u>$_3$C-C=C-C<u>H</u>$_3$)1.24 (2H, overlapped, P-C<u>H</u>$_2$) 1.24 (d, $^{3}J_{HH}$ = 6.9 Hz, 12H, CH(C<u>H</u>$_3$)$_2$), 1.21 (d, $^{3}J_{HH}$ = 6.8 Hz, 12H, CH(C<u>H</u>$_3$)$_2$), 0.65 (d, $^{3}J_{HP}$ = 17 Hz, 9H, P-C(C<u>H</u>$_3$)$_3$).

^{11}B{^{1}H} NMR (96 MHz, $CDCl_3$, T= 298 K): δ (ppm) = -16.6.

^{13}C{^{1}H} NMR (176 MHz, $CDCl_3$, T= 298 K): δ (ppm) = 148.3 (dm, $^{1}J_{CF}$ = 242 Hz, B-(<u>C</u>$_6$F$_5$)$_4$; *ortho*), 146.0 (Dipp; *ortho*), 145.1 (d, $^{2}J_{CP}$ = 3.9 Hz, N_2<u>C</u>=N-P), 138.3 (dm, $^{1}J_{CF}$ = 244 Hz, B-(<u>C</u>$_6$F$_5$)$_4$; *para*), 136.4 (dm, $^{1}J_{CF}$ = 246 Hz, B-(<u>C</u>$_6$F$_5$)4; *meta*), 131.7 (Dipp; *ipso*), 131.0 (Dipp; *para*), 128.7 (d, $^{2}J_{CP}$ = 9.1 Hz, <u>H</u>$_3$C-<u>C</u>=<u>C</u>-C<u>H</u>$_3$), 125.0 (Dipp; *meta*), 124.0 (B-(<u>C</u>$_6$F$_5$)$_4$; *ipso*), 118.1 (N-<u>C</u>H=<u>C</u>H-N), 33.3 (d, $^{1}J_{CP}$ = 54.8 Hz, H_2<u>C</u>-P-<u>C</u>H$_2$), 31.6 (d, $^{1}J_{CP}$ = 79.4 Hz, P-<u>C</u>(<u>C</u>H$_3$)$_3$, 29.2 (<u>C</u>H(CH$_3$)$_2$), 25.1 (CH(<u>C</u>H$_3$)$_2$), 22.4 (CH(<u>C</u>H$_3$)$_2$), 22.3 (P-C(<u>C</u>H$_3$)$_3$), 15.8 (d, $^{3}J_{CP}$ = 12.7 Hz, H$_3$<u>C</u>-C=C-<u>C</u>H$_3$).

^{19}F{^{1}H} NMR (282 MHz, $CDCl_3$, T= 298 K): δ (ppm) = -132.6 (br, 8F, B-(C$_6$<u>F</u>$_5$)$_4$; *ortho*), -163.4 (t, $^{3}J_{FF}$ = 20.6 Hz, 4F, B-(C$_6$<u>F</u>$_5$)$_4$; *para*), -167.00 (br, 8F, B-(C$_6$<u>F</u>$_5$)$_4$; *meta*).

^{31}P{^{1}H} NMR (121 MHz, $CDCl_3$, 296 K) δ (ppm) = 43.9.

DART-HRMS: Calculated for $[C_{45}H_{55}N_3P]^+$ ([**4-5**])$^+$: *m/z* = 572.4128, found: *m/z* = 572.4118.

4.5.14 Synthesis of [4-6][$B(C_6F_5)_4$]

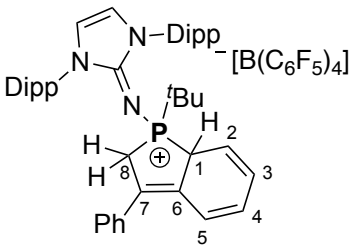

Following protocol **2**, the addition of 1,1-diphenylethylene (4.7 mg) led to an immediate color change in the reaction mixture from red to yellow. The product was isolated as a beige powder after washing with benzene.

Yield: Quantitative

^{1}H NMR (700 MHz, $CDCl_3$, T= 298 K): δ (ppm) = 7.56 (t, $^{3}J_{HH}$ = 7.8 Hz, 2H, Dipp; *para*), 7.42 – 7.29 (m, 7H, Dipp; *meta*, Ph; *meta and para*), 6.97 (d, $^{3}J_{HH}$ = 7.3 Hz, 2H Ph; *ortho*), 6.91 (s, 2H, N-C<u>H</u>=C<u>H</u>-N), 6.40 (d, $^{3}J_{HH}$ = 9.8 Hz, 1H, cyclohexadiene, position 5), 6.02 – 5.92 (m, 2H, cyclohexadiene, position 3 and 4), 5.52 (t, $^{3}J_{HH}$ = 7.8 Hz, 1H, cyclohexadiene), 3.06 (dm, $^{2}J_{HP}$ = 26.6 Hz, 1H, P-C<u>H</u> bridgehead), 2.75 – 2.63 (m, 4H, Ph-C<u>H</u>$(CH_3)_2$), 2.58 (dd, $^{3}J_{HH}$ = 17.7 Hz, $^{3}J_{HH}$ = 12.3 Hz, 1H, P-C<u>H</u>$_2$-R), 1.99 (ddt, $^{2}J_{HP}$ = 17.7 Hz, $^{2}J_{HH}$ = 5.9 Hz, 1H, P-C<u>H</u>$_2$-R), 1.34 (d, $^{3}J_{HH}$ = 6.9 Hz, 6H, Ph-CH(C<u>H</u>$_3$)$_2$), 1.31 (d, $^{3}J_{HH}$ = 6.9 Hz, 6H, Ph-CH(C<u>H</u>$_3$)$_2$), 1.24 (d, $^{3}J_{HH}$ = 6.9 Hz, 6H, Ph-CH(C<u>H</u>$_3$)$_2$), 1.22 (d, $^{3}J_{HH}$ = 6.9 Hz, 6H, Ph-CH(C<u>H</u>$_3$)$_2$), 0.78 ($^{3}J_{HP}$ = 16.3 Hz, 9H, P-C(C<u>H</u>$_3$)$_3$).

^{11}B{^{1}H} NMR (96 MHz, $CDCl_3$, T= 296 K): δ (ppm) = -16.7.

^{13}C{^{1}H} NMR (176 MHz, $CDCl_3$, T= 298 K): δ (ppm) = 148.4 (dm, $^{1}J_{CF}$ = 241 Hz, B-(<u>C</u>$_6F_5)_4$; *ortho*), 146.5 (Dipp; *ortho*), 146.4 (Dipp; *ortho*), 145.4 (N_2<u>C</u>=N-P), 138.3 (dm, $^{1}J_{CF}$ = 245 Hz, B-(<u>C</u>$_6F_5)_4$; *para*), 136.4 (dm, $^{1}J_{CF}$ = 245 Hz, B-(<u>C</u>$_6F_5)_4$; *meta*), 135.4 (d, $^{3}J_{CP}$ = 7.7 Hz, Ph; *ipso*) 132.1 (Dipp; *para*), 131.5 (d, $^{2}J_{CP}$ = 7.9 Hz, endocyclic C=C bridgehead, position 6), 131.0 (Dipp; *ipso*), 130.6 (d, $^{2}J_{CP}$ = 13.3 Hz, position 7),129.0 (Ph; *meta*) 128.9 (Ph; *para*), 127.7 (Ph; *ortho*), 126.2 (d, $^{4}J_{CP}$ = 3.8 Hz, cyclohexadiene <u>C</u>-H C4),125.7 (d, $^{3}J_{CP}$ = 10.6 Hz, cyclohexadiene <u>C</u>-H, position 3), 125.3 and 125.2 (Dipp; *meta*), 124.1 (br, B-(<u>C</u>$_6F_5)_4$; *ipso*),123.1 (d, $^{3}J_{CP}$ =10.9 Hz,

cyclohexadiene C-H, position 5), 120.8 (d, $^{2}J_{CP}$ = 9.1 Hz, cyclohexadiene C-H, position 2), 118.5 (N-CH=CH-N), 46.9 (d, $^{1}J_{CP}$ = 55.1 Hz, P-CH bridgehead, position 1), 34.1 (d, $^{1}J_{CP}$ = 71.3, P-$C(CH_3)_3$), 31.7 (d, $^{1}J_{CP}$ = 45.7 Hz, P-CH_2-R, position 8), 29.4 (Ph-$CH(CH_3)_2$), 25.5 (Ph-$CH(CH_3)_2$), 25.3 (Ph-$CH(CH_3)_2$), 24.8 (P-$C(CH_3)_3$), 22.7 (Ph-$CH(CH_3)_2$), 22.5 (Ph-$CH(CH_3)_2$).

$^{19}F\{^{1}H\}$ NMR (282 MHz, $CDCl_3$, T= 298 K): δ (ppm) = -132.6 (m, 8F, B-$(C_6F_5)_4$; *ortho*), -163.3 (t, $^{3}J_{FF}$ = 20.6 Hz, 4F, B-$(C_6F_5)_4$; *para*), -167.00 (m, 8F, B-$(C_6F_5)_4$; *meta*).

^{31}P NMR (121 MHz, $CDCl_3$, 296 K) δ (ppm) = 63.4 (br).

ESI-HRMS: Calculated for $[C_{45}H_{57}N_3P]^+$ ([**4-6**])$^+$: *m/z* = 670.4285, found: *m/z* = 670.4274.

4.5.15 Synthesis of [4-7][$B(C_6F_5)_4$]

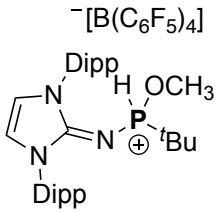

Following protocol **2**, the addition of methanol (0.8 mg, 1 uL) led to an immediate color change in the reaction mixture from red to colorless. The product was isolated as a white powder.

Yield: 70% (23.1 mg, 0.019 mmol)

^{1}H NMR (700 MHz, $CDCl_3$, T= 298 K): δ (ppm) = 7.55 (t, $^{3}J_{HH}$ = 7.8 Hz, 2H, Dipp; *para*), 7.37 (m, 4H, Dipp; *meta*,), 6.90 (s, 2H, N-C<u>H</u>=C<u>H</u>-N), 6.15 (d, $^{1}J_{HP}$ = 513.9 Hz, P-<u>H</u>), 3.03 (d, $^{3}J_{HP}$ = 12.8 Hz, 3H, P-OC<u>H</u>$_3$), 2.61 (sept, $^{3}J_{HH}$ = 6.8 Hz, 4H, Ph-C<u>H</u>$(CH_3)_2$), 1.32 – 1.13 (m, 24H, Ph-CH$(C\underline{H}_3)_2$), 0.75 (d, $^{3}J_{HP}$ = 20.2 Hz, P-C$(C\underline{H}_3)_3$).

^{11}B{^{1}H} NMR (96 MHz, $CDCl_3$, T= 296 K): δ (ppm) = -16.7.

^{13}C{^{1}H} NMR (176 MHz, $CDCl_3$, T= 298 K): δ (ppm) = 148.3 (dm, $^{1}J_{CF}$ = 242 Hz, B-(<u>C</u>$_6$F$_5$)$_4$; *ortho*), 146.5 and 146.5 (Dipp; *ortho*), 144.7 (N_2<u>C</u>=N-P), 138.3 (dm, $^{1}J_{CF}$ = 244 Hz, B-(<u>C</u>$_6$F$_5$)$_4$; *para*), 136.4 (dm, $^{1}J_{CF}$ = 247 Hz, B-(<u>C</u>$_6$F$_5$)$_4$; *meta*), 132.1 (Dipp; *para*), 130.2 (Dipp; *ipso*), 125.1 and 124.9 (Dipp; *meta*), 118.5 (N-<u>C</u>H=<u>C</u>H-N), 55.9 ($^{2}J_{CP}$ = 8.9 Hz, P-O<u>C</u>H$_3$), 32.6 ($^{2}J_{CP}$ = 106 Hz, P-<u>C</u>$(CH_3)_3$), 29.3 and 29.3 (Ph-<u>C</u>H$(CH_3)_2$, 22.8 and 22.8 (Ph-CH(<u>C</u>H$_3$)$_2$), 22.7, 22.6 and 22.6 (overlapped resonances of (Ph-CH(<u>C</u>H$_3$)$_2$ and P-C(<u>C</u>H$_3$)$_3$).

^{19}F{^{1}H} NMR (282 MHz, $CDCl_3$, T= 298 K): δ (ppm) = -132.6 (m, 8F, B-(C$_6$<u>F</u>$_5$)$_4$; *ortho*), -163.3 (t, $^{3}J_{FF}$ = 20.5 Hz, 4F, B-(C$_6$<u>F</u>$_5$)$_4$; *para*), -167.00 (m, 8F, B-(C$_6$<u>F</u>$_5$)$_4$; *meta*).

^{31}P NMR (121 MHz, $CDCl_3$, 296 K): δ (ppm) = 35.2.(m, $^{1}J_{HP}$ = 513.9 Hz, $^{3}J_{HP}$ = 12.8 Hz, $^{3}J_{HP}$ = 20.2 Hz, P-C(C<u>H</u>$_3$)$_3$.

DART-HRMS: Calculated for $[C_{32}H_{49}N_3OP]^+$ ([**4-7**])$^+$: *m/z* = 522.3608, found: *m/z* = 522.3601

4.5.16 Reaction of [4-2^{a}]$^{+}$ and phenol to [4-8]$^{+}$

Following protocol **2**, the addition of phenol led to an immediate color change in the reaction mixture from red to colorless and was monitored by 31P NMR spectroscopy. The large splitting ($^{1}J_{HP}$ = 522 Hz) indicates P–H bond formation.

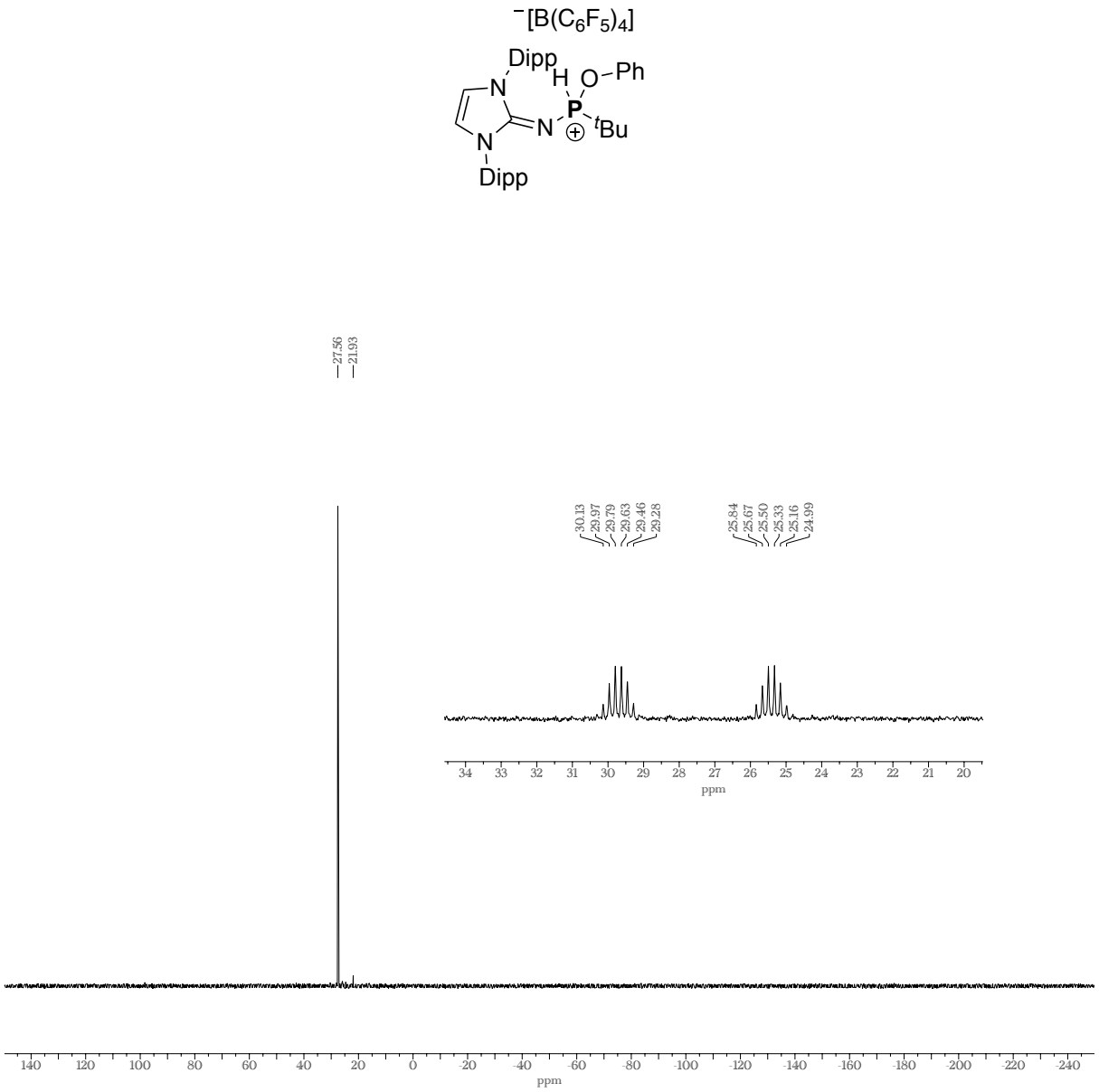

Figure 4-9: $^{31}P\{^{1}H\}$ NMR spectrum and ^{31}P NMR spectrum (zoom in) of the reaction of [**4-2^{a}**]$^{+}$ and phenol, in 1,2-DFB.

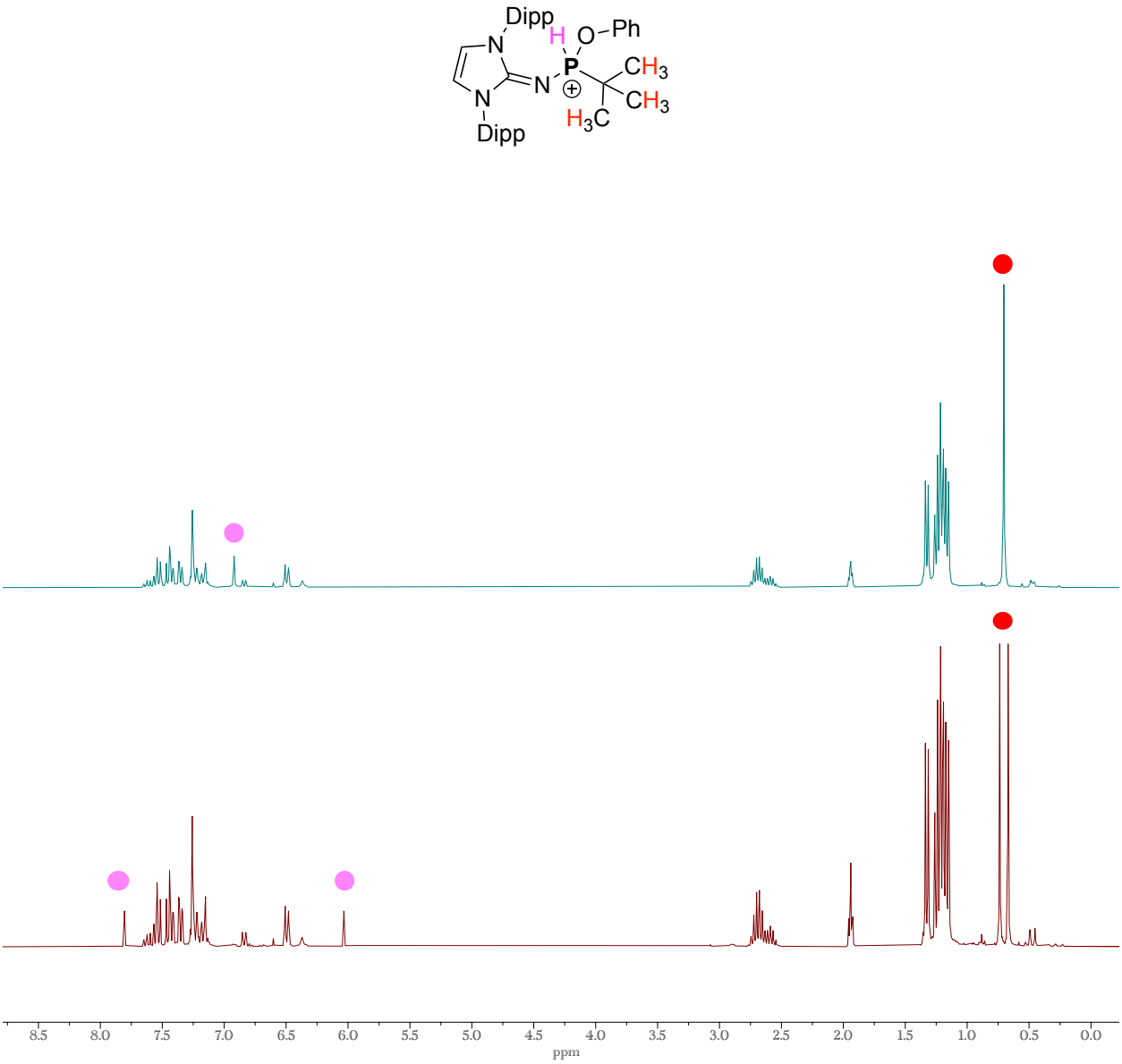

Figure 4-10: Stacked $^{1}H\{^{31}P\}$ NMR spectrum and ^{1}H NMR spectrum of the reaction of [**4-2**^{a}]$^{+}$ and phenol. After removing the reaction solvent (1,2-DFB) and washing with pentanes, the remaining residue was dissolved in CD_3CN and analyzed. The purple markers indicate the proton directly bound to phosphorus which collapses to a singlet upon decoupling. The red marker corresponds to the ^{t}Bu protons. The proton represented by the purple marker and protons represented by the red marker integrate in a 1:9 ratio.

4.5.17 Attempted Hydrolysis of [4-2a]$^+$

Adopting the same protocol in Chapter 3 used to hydrolyze the allenylidene phosphonium cation [**3-2**]$^+$, a suspension of approximately 10 mg of [**4-2^a**][$B(C_6F_5)_4$] in pentane was charged in a Schlenk tube. A single drop of degassed water was then added, then the vessel was periodically shaken and sonicated until complete dissipation of the red color of [**4-2^a**]$^+$. The pentane was decanted and the residue dried, then taken up in $CDCl_3$ for NMR analysis. The highest intensity peak in the ^{31}P {^1H} spectrum corresponds to the doublet of multiplets in the ^{31}P NMR spectrum.

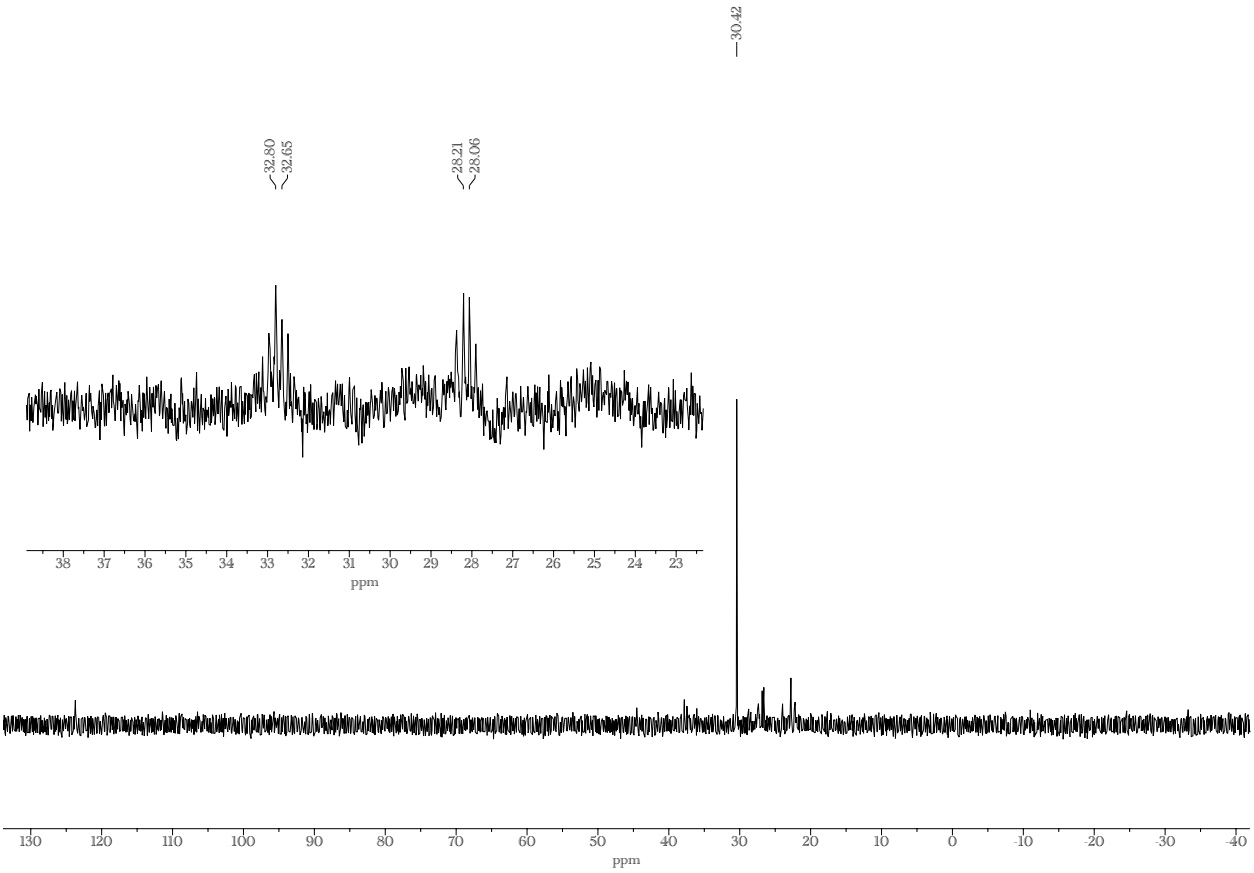

Figure 4-11: ^{31}P{^1H} spectrum and ^{31}P NMR spectrum (zoom in) in $CDCl_3$. Zoom in shows the most prominent peak.

4.5.18 Preparation of [4-9][B(C$_6$F$_5$)$_4$]

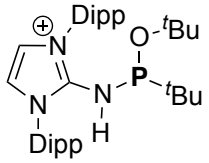

Following protocol **2**, the addition of *t*butanol (2 mg, 2.5 uL) led to an immediate color change in the reaction mixture from red to colorless. The product was isolated as a white powder.

Yield: 22.4 mg (72%, 0.018 mmol)

^{1}H NMR (700 MHz, $CDCl_3$, T= 298 K): δ (ppm) = 7.63 (t, $^{3}J_{HH}$ = 7.8 Hz, 2H, Dipp; *para*), 7.42 (m, 4H, Dipp; *meta*,), 6.96 (s, 2H, N-C<u>H</u>=C<u>H</u>-N), 5.09 (s, N-<u>H</u>), 2.55 (sept, $^{3}J_{HH}$ = 6.8 Hz, 2H, Ph-C<u>H</u>(CH$_3$)$_2$), 2.51 (sept, $^{3}J_{HH}$ = 6.8 Hz, 2H, Ph-C<u>H</u>(CH$_3$)$_2$), 1.38 (d, $^{3}J_{HH}$ = 6.8 Hz, 6H, Ph-CH(C<u>H</u>$_3$)$_2$), 1.37 (d, $^{3}J_{HH}$ = 6.8 Hz, 6H, Ph-CH(C<u>H</u>$_3$)$_2$), 1.21 (d, $^{3}J_{HH}$ = 6.8 Hz, 6H, Ph-CH(C<u>H</u>$_3$)$_2$), 1.17 (d, $^{3}J_{HH}$ = 6.8 Hz, 6H, Ph-CH(C<u>H</u>$_3$)$_2$), 0.98 (s, 9H, P-O-*t*Bu), 0.68 (d, $^{3}J_{HP}$ = 14.2 Hz, 9H, P-*t*Bu).

^{11}B{^{1}H} NMR (96 MHz, $CDCl_3$, T= 296 K): δ (ppm) = -16.7.

^{13}C{^{1}H} NMR (176 MHz, $CDCl_3$, T= 298 K): δ (ppm) = 148.3 (dm, $^{1}J_{CF}$ = 241 Hz, B-(<u>C</u>$_6$F$_5$)$_4$; *ortho*), 146.3 and 146.3 (Dipp; *ortho*), 145.9 (N$_2$<u>C</u>=N-P), 138.3 (dm, $^{1}J_{CF}$ = 245 Hz, B-(<u>C</u>$_6$F$_5$)$_4$; *para*), 136.4 (dm, $^{1}J_{CF}$ = 246 Hz, B-(<u>C</u>$_6$F$_5$)$_4$; *meta*),133.2 (Dipp; *para*), 128.5 (Dipp; *ipso*), 125.9 and 125.7 (Dipp; *meta*), 124.1 (br, B-(<u>C</u>$_6$F$_5$)$_4$; *ipso*), 120.1 (N-<u>C</u>H=<u>C</u>H-N), 79.1 (d, $^{2}J_{CP}$ = 9 Hz, P-O-<u>C</u>(CH$_3$)$_3$, 34.3 (d, $^{2}J_{CP}$ = 11 Hz, P-<u>C</u>(CH$_3$)$_3$), 30.2 ($^{3}J_{CP}$ = 7 Hz, P-O-C(<u>C</u>H$_3$)$_3$, 29.8, 29.7 and 29.6 (Ph-<u>C</u>H(CH$_3$)$_2$), 26.1 (Ph-CH(<u>C</u>H$_3$)$_2$), 25.7 (Ph-CH(<u>C</u>H$_3$)$_2$), 22.8 (d, $^{2}J_{CP}$ = 15 Hz, P-C(<u>C</u>H$_3$)$_3$), 22.5 (Ph-CH(<u>C</u>H$_3$)$_2$), 22.1 (Ph-CH(<u>C</u>H$_3$)$_2$),

^{19}F{^{1}H} NMR (282 MHz, $CDCl_3$, T= 298 K): δ (ppm) = -132.6 (m, 8F, B-(C$_6$<u>F</u>$_5$)$_4$; *ortho*), -163.3 (t, $^{3}J_{FF}$ = 20.6 Hz, 4F, B-(C$_6$<u>F</u>$_5$)$_4$; *para*), -167.00 (m, 8F, B-(C$_6$<u>F</u>$_5$)$_4$; *meta*).

^{31}P NMR (121 MHz, $CDCl_3$, 296 K): δ (ppm) = 125.4 (decet, $^{3}J_{HP}$ = 14.2 Hz, <u>P</u>-C(C<u>H</u>$_3$)$_3$)

DART-HRMS: Calculated for $[C_{35}H_{55}N_3OP]^+$ ([**4-9**])$^+$: calculated *m/z* =564.4083. Not found, largest molecular ion peak corresponded to the protonated guanidine $[H_2N{=}Dipp]^+$ ($[C_{27}H_{38}N_3]^+$)

4.5.19 Preparation of [4-10][B(C$_6$F$_5$)$_4$]

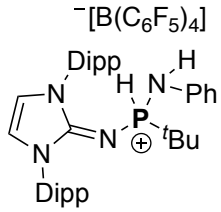

Following protocol **2**, the addition of aniline (2.5 mg, 2.4 uL) led to an immediate color change in the reaction mixture from red to colorless. The product was isolated as a white powder.

Yield: Quantitative

^{1}H NMR (700 MHz, $CDCl_3$, T= 298 K): δ (ppm) = 7.54 (t, $^3J_{HH}$ = 7.8 Hz, 2H, Dipp; *para*), 7.42 – 7.30 (m, 4H, Dipp; *meta*), 7.07 (dd, $^3J_{HH}$ = 7.7 Hz, 2H, P-HN-Ph; *meta*), 6.96 (t, $^3J_{HH}$ = 7.4 Hz, 1H, P-HN-Ph; *para*), 6.88 (s, 2H, N-C<u>H</u>=C<u>H</u>-N), 6.47 (dd, $^1J_{PH}$ = 490 Hz, $^2J_{HH}$ = 5.9 Hz, 1H, P-H), 6.39 (d, $^3J_{HH}$ = 7.7 Hz, 2H, P-HN-Ph; *ortho*), 4.47 (m, 1H, P-<u>H</u>N-Ph), 2.68 (m, 4H, C<u>H</u>(CH$_3$)$_2$), 1.27 (d, $^3J_{HH}$ = 6.9 Hz, 6H, CH(C<u>H</u>$_3$)$_2$), 1.25 – 1.12 (m, 18H, CH(C<u>H</u>$_3$)$_2$), 0.75 (d, $^3J_{PH}$ = 20.4 Hz, 9H, P-C(C<u>H</u>$_3$)$_3$).

^{11}B{^{1}H} NMR (96 MHz, $CDCl_3$, T= 296 K): δ (ppm) = -16.7.

^{13}C{^{1}H} NMR (176 MHz, $CDCl_3$, T= 298 K): δ (ppm) = 148.3 (dm, $^1J_{CF}$ = 242 Hz, B-(<u>C</u>$_6$F$_5$)$_4$; *ortho*), 146.5 (Dipp; *ortho*), 145.3 (N-<u>C</u>-N), 138.3 (dm, $^1J_{CF}$ = 243 Hz, B-(<u>C</u>$_6$F$_5$)$_4$; *para*), 138.2 (Aniline: *ipso*), 136.4 (dm, $^1J_{CF}$ = 246 Hz, B-(<u>C</u>$_6$F$_5$)$_4$; *meta*), 132.1 (Dipp; *para*), 130.5, (Dipp; *ipso*), 129.9 (Aniline; *meta*), 125.1 (Dipp; *meta*), 124.9 (Dipp; *meta*) 124.1 (Aniline; *para*), 124.0 (br, B-(<u>C</u>$_6$F$_5$)$_4$; *ipso*), 119.3 (d, $^3J_{CP}$ = 5.3 Hz, Aniline; *ortho*), 118.4 (N-<u>C</u>H=<u>C</u>H-N), 34.5 (d, $^1J_{CP}$ = 97.7 Hz, P-<u>C</u>(CH$_3$)$_3$), 29.4 (<u>C</u>H(CH$_3$)$_2$), 29.4 (<u>C</u>H(CH$_3$)$_2$), 25.1 (CH(<u>C</u>H$_3$)$_2$), 24.9 (CH(<u>C</u>H$_3$)$_2$), 23.6 (P-C(<u>C</u>H$_3$)$_3$), 22.6 (CH(<u>C</u>H$_3$)$_2$), 22.5(CH(<u>C</u>H$_3$)$_2$).

$^{19}F\{^{1}H\}$ NMR (282 MHz, $CDCl_3$, T= 296 K): δ (ppm) = -132.6 (m, 8F, B-($C_6\underline{F}_5$)$_4$; *ortho*), -163.3 (t, $^{3}J_{FF}$ = 20.6 Hz, 4F, B-($C_6\underline{F}_5$)$_4$; *para*), -166.9 (br, 8F, B-($C_6\underline{F}_5$)$_4$; *meta*).

^{31}P NMR (121 MHz, $CDCl_3$, 297 K); δ (ppm) = 13.8 (dd of decets, $^{1}J_{PH}$ = 490 Hz (P-H), $^{2}J_{HP}$ = 5.7 Hz (N-H), $^{3}J_{HP}$ = 20.4 Hz (P-C($C\underline{H}_3$)$_3$)).

DART-HRMS: Calculated for $[C_{37}H_{52}N_4P]^+$ ([**4-10**])$^+$: *m/z* =583.3924 , found: *m/z* = 583.3936

4.5.20 Observed reactivity of study [4-2^a]$^+$ to give [4-11][[B(C_6F_5)$_4$]

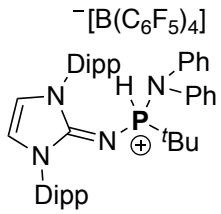

Following protocol **2**, the addition of *N,N*-diphenylamine (4.5 mg) led to a very slow color change in the reaction mixture from red to colorless. Initial ^{31}P NMR monitoring indicated a major resonance at 72 ppm, with no evidence of P–H bond formation. The reaction was split into two aliquots, one which heated between 60-70 °C, and one that was left to stand at room temperature. The heated solution (1,2-DFB) showed gradual conversion to the title compound over 18 days. A yellowish solid was recovered from the reaction as a yellow-white powder and subsequently characterized.

^{1}H NMR (700 MHz, $CDCl_3$, T= 295 K): δ (ppm) = 7.53 (t, $^{3}J_{HH}$ = 7.8 Hz, 2H, Dipp; *para*), 7.33 (d, $^{3}J_{HH}$ = 7.8 Hz, 2H, Dipp; *meta*), 7.29 (d, $^{3}J_{HH}$ = 7.8 Hz, 2H, Dipp; *meta*), 7.16 (m, 2H, P-N-Ph_2; *para*), 7.12 (m, 4H, P-N-Ph_2; *meta*), 6.86 (s, 2H, N-C$\underline{H}$=C$\underline{H}$-N) 6.72 (d, , $^{3}J_{HH}$ = 7.6 Hz, 4H, P-N-Ph_2; *ortho*), 6.67 (d, $^{1}J_{HP}$ = 504 Hz, 1H, P-H), 2.70 (sept, $^{3}J_{HH}$ = 6.8 Hz, 2H, C$\underline{H}$(CH_3)$_2$), 2.65 (sept, $^{3}J_{HH}$ = 6.8 Hz, 2H, C$\underline{H}$(CH_3)$_2$), 1.27 (d, $^{3}J_{HH}$ = 6.8 Hz, 6H, CH(C$\underline{H}_3$)$_2$), 1.22 (d, $^{3}J_{HH}$ = 6.8 Hz, 6H, CH(C$\underline{H}_3$)$_2$), 1.11 (d, $^{3}J_{HH}$ = 6.8 Hz, 6H, CH(C$\underline{H}_3$)$_2$), 0.98 (d, d, $^{3}J_{HH}$ = 6.8 Hz, 6H, CH(C$\underline{H}_3$)$_2$), 0.76 (d, $^{3}J_{PH}$ = 20.7 Hz, 9H, P-C(C$\underline{H}_3$)$_3$).

$^{11}B\{^{1}H\}$ NMR (96 MHz, $CDCl_3$, T= 298 K): δ (ppm) = -16.6

$^{13}C\{^{1}H\}$ NMR (176 MHz, $CDCl_3$, T= 298 K): δ (ppm) = 148.4 (dm, $^{1}J_{CF}$ = 243 Hz, B-($\underline{C}_6F_5)_4$; *ortho*), 146.5 and 146.3 (Dipp; *ortho*), 144.2 (N-$\underline{C}$-N), 143.1 (d, $^{2}J_{CP}$ = 3 Hz, P-N-Ph_2; *ipso*), 138.3 (dm, $^{1}J_{CF}$ = 246 Hz, B-($\underline{C}_6F_5)_4$; *para*), 136.4 (dm, $^{1}J_{CF}$ = 248 Hz, B-($\underline{C}_6F_5)_4$; *meta*), 132.0 (Dipp; *para*), 130.8 (Dipp; *ipso*), 130.2 (P-N-Ph_2; *meta*), 127.1 (P-N-Ph_2; *para*), 125.8 (P-N-Ph_2; *ortho*),125.3 (Dipp; *meta*), 124.9 (Dipp; *meta*), 118.8 (N-$\underline{C}$H=$\underline{C}$H-N), 34.4 (d, $^{1}J_{CP}$ = 99 Hz, P-$\underline{C}(CH_3)_3$), 29.6 ($\underline{C}H(CH_3)_2$), 29.3 ($\underline{C}H(CH_3)_2$), 25.6 ($CH(\underline{C}H_3)_2$), 25.3 ($CH(\underline{C}H_3)_2$), 25.2 (P-$C(\underline{C}H_3)_3$), 22.7 ($CH(\underline{C}H_3)_2$), 21.5 ($CH(\underline{C}H_3)_2$). B-($\underline{C}_6F_5)_4$; *ipso*: not observed.

$^{19}F\{^{1}H\}$ NMR (282 MHz, $CDCl_3$, T= 295 K): δ (ppm) = -132.6 (br, 8F, B-($C_6\underline{F}_5)_4$; *ortho*), -163.3 (t, $^{3}J_{FF}$ = 20.6 Hz, 4F, B-($C_6\underline{F}_5)_4$; *para*), -167.0 (br, 8F, B-($C_6\underline{F}_5)_4$; *meta*).

^{31}P NMR (121 MHz, $CDCl_3$, 295 K): δ (ppm) = 21.4 (d of decets $^{1}J_{HP}$ = 504 Hz (P-H), $^{3}J_{PH}$ = 20.7 Hz (P-$C(C\underline{H}_3)_3$).

4.5.21 Monitoring of the reaction of [4-2^{a}]$^{+}$ and *N,N*-methylphenyl amine to give [4-12]$^{+}$

Following protocol **2**, the addition of *N,N*-methylphenyl amine (2.8 mg) led to an immediate color change in the reaction mixture from red to colorless and was monitored by ^{31}P NMR spectroscopy. The large splitting constant ($^{1}J_{HP}$ = 500 Hz) measured from the center of each multiplet indicates P–H bond formation. The formation of the product was confirmed with HRMS, calculated m/z for $[C_{38}H_{54}N_4P]^+$ = 597.4081, found m/z =597.4072

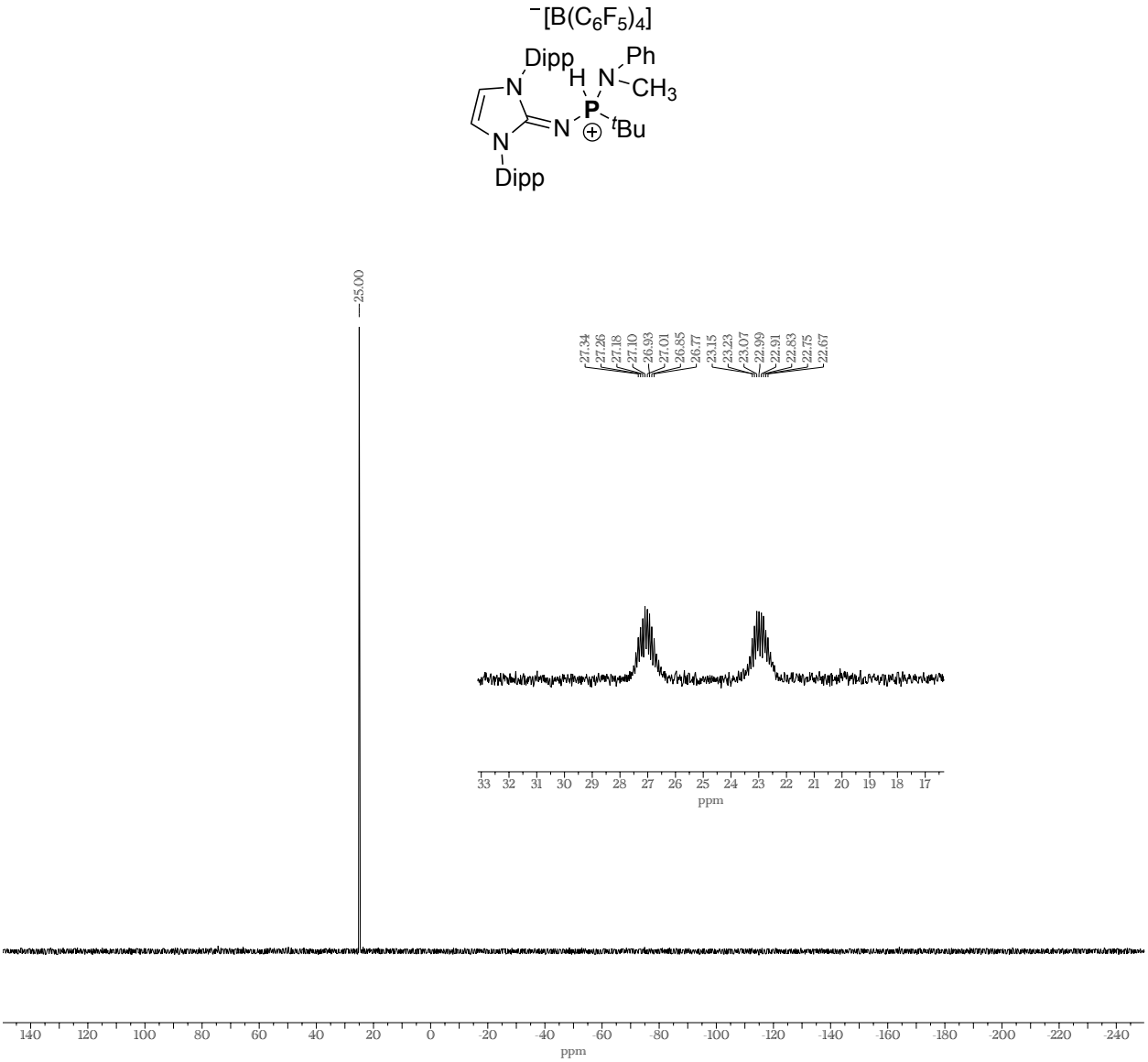

Figure 4-12: ^{31}P{^{1}H} NMR (121 MHz) spectrum and ^{31}P NMR spectrum (zoom in) in $CDCl_3$ for the reaction of [**4-2^{a}**]$^{+}$ and *N,N*-methylphenyl amine.

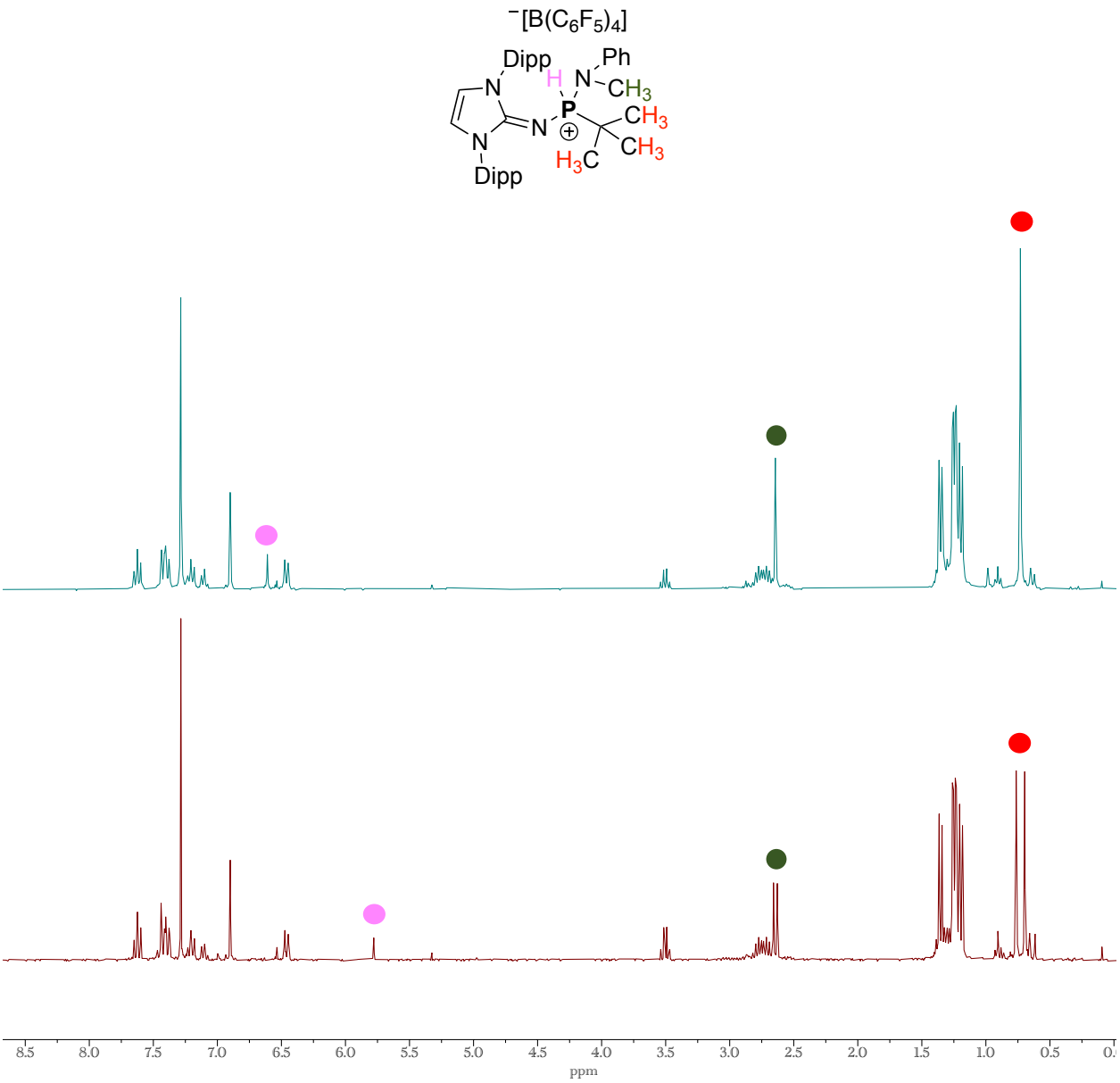

Figure 4-13: Stacked $^{1}H\{^{31}P\}$ NMR (300 MHz) spectrum (top) and ^{1}H NMR spectrum (bottom) of the reaction of [**4-2**^{a}]$^{+}$ and *N,N*-methylphenyl amine. After removing the reaction solvent (1,2-DFB) and washing with pentanes, the remaining residue was dissolved in $CDCl_3$ and analyzed. The purple markers indicate the proton directly bound to phosphorus which collapses to a singlet upon decoupling. Only one resonance for the split P-H doublet can be identified in the ^{1}H NMR spectrum. The red marker corresponds to the *t*Bu protons. The green protons represent the N-methyl group. The proton represented by the purple marker, and protons represented by the green and red markers integrate in a 1:3: 9 ratio.

4.5.22 Monitoring of the reaction of $[4\text{-}2a]^+$ and cyclohexyl isocyanide

Following protocol **2**, the addition of cyclohexyl isocyanide led to an immediate color change in the reaction mixture from red to colorless. After 15 minutes solvent was removed (1,2-DFB), leaving a white residue which was washed with pentane and dried. The solid was reconstituted in CD_2Cl_2 was monitored by ^1H and ^{31}P NMR spectroscopy.

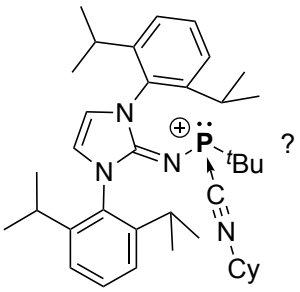

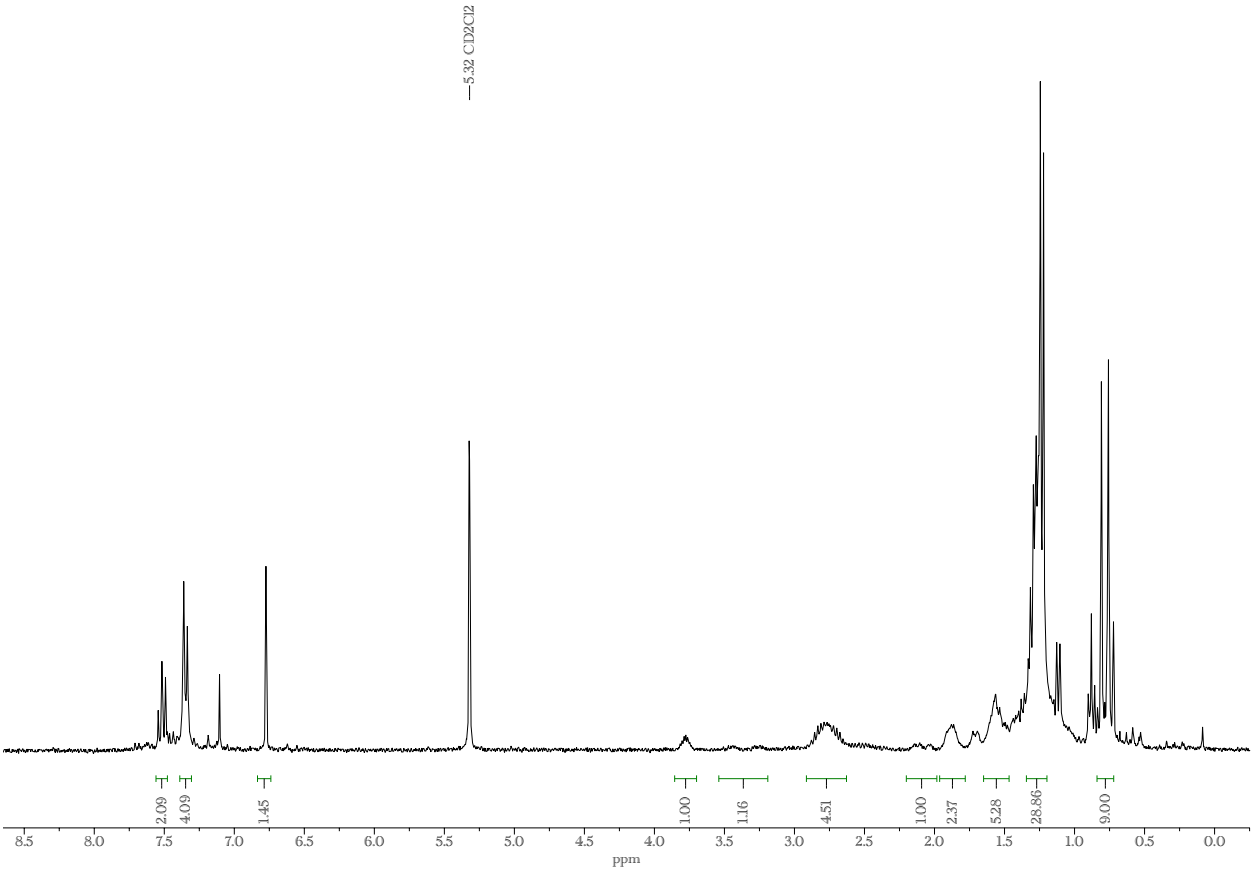

Figure 4-14:^1H NMR (300 MHz) spectrum in CD_2Cl_2 of the reaction between phosphenium cation $[\mathbf{4\text{-}2^a}]^+$ and cyclohexyl isocyanide.

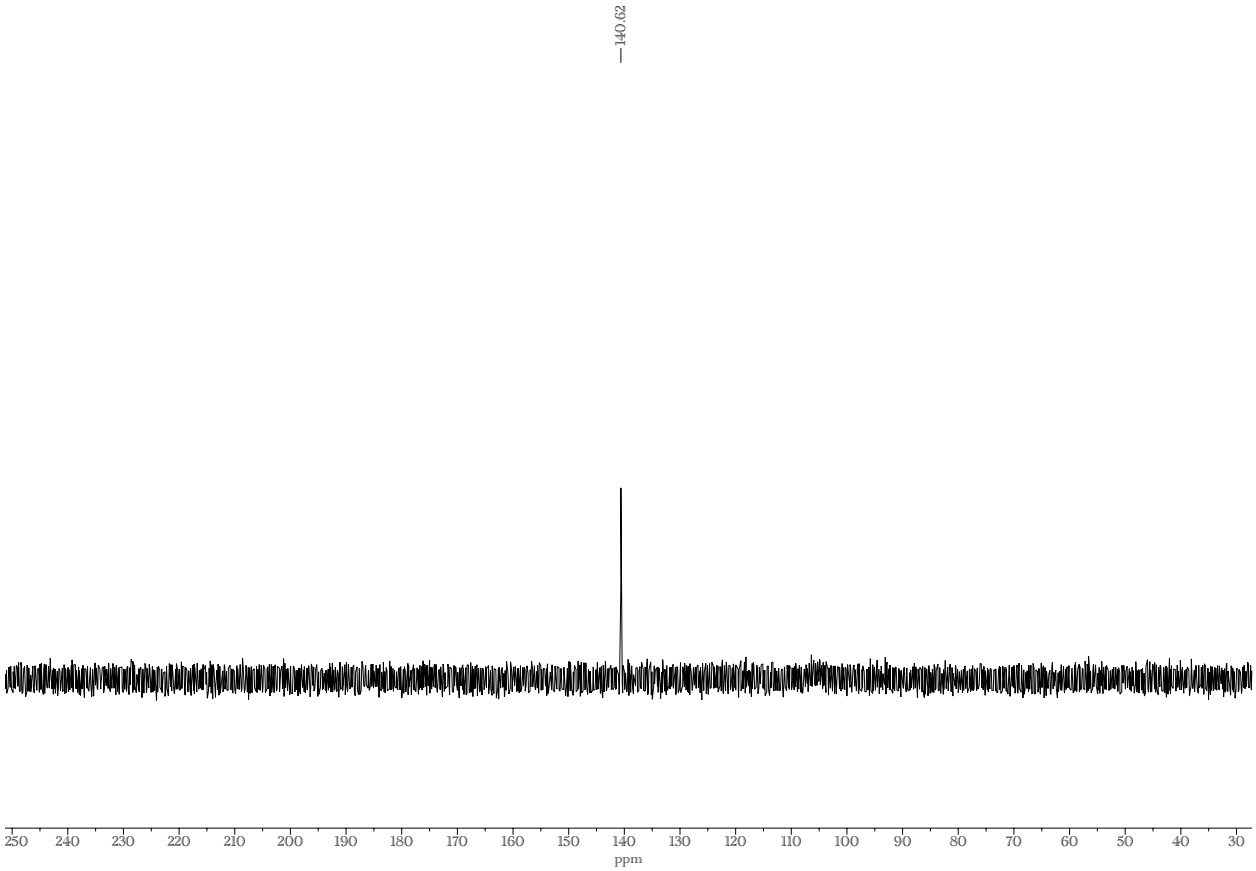

Figure 4-15: ^{31}P NMR (121 MHz) spectrum in CD_2Cl_2 of the reaction between phosphenium cation [**4-2^{a}**]$^{+}$ and cyclohexyl isocyanide.

4.5.23 The reaction of [4-2^{a}]$^{+}$ and ammonia borane

Following protocol **2**, **[4-2^{a}][B(C$_6$F$_5$)$_4$]** was generated *in situ* and added to a stirring suspension of ammonia borane in 1,2-DFB, resulting in an immediate change in color change. An aliquot of the mixture was filtered over glass directly into an NMR tube for analysis.

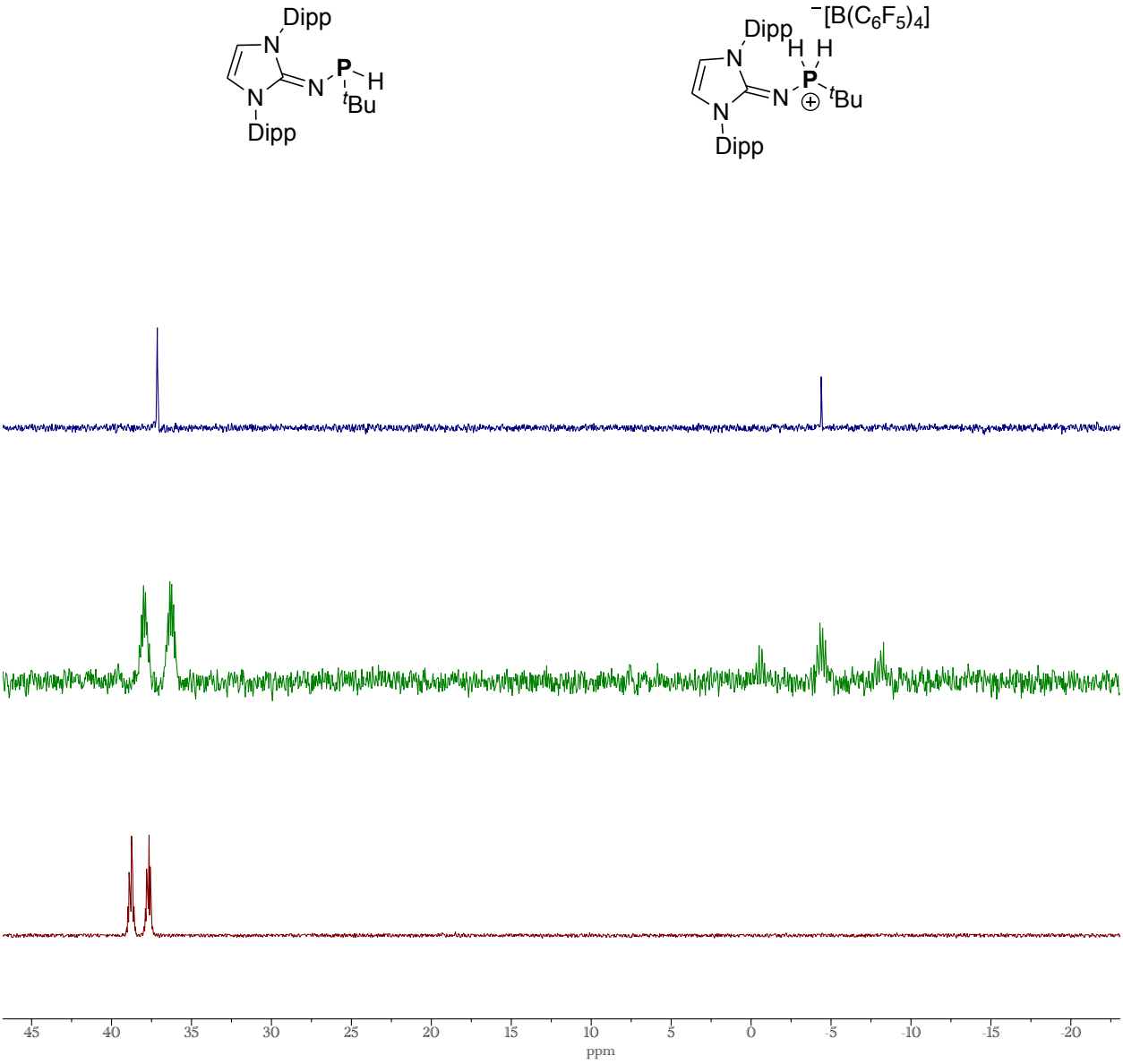

Figure 4-16: Stacked ^{31}P {^{1}H} NMR spectrum (top) and ^{31}P NMR spectrum (middle) of an aliquot of the reaction of [**4-2^{a}**]$^{+}$ with ammonia borane in 1,2-DFB. The bottom ^{31}P NMR spectrum (red) of the secondary phosphine prepared from **4-1^{a}** and N-Selectride ®, in C_6D_6.

4.5.24 Hydridophosphine prepared from 4-1[a] and N-Selectride ®

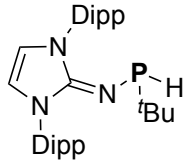

Phosphine **4-1[a]** (0.20 g, 0.38 mmol, 1 eq) was dissolved in THF (5 ml) and cooled to -78 °C with a dry ice/acetone cooling bath. N-Selectride ® (3M, 0.38 mmol, 390 ml 1.0 eq) was subsequently added dropwise *via* cannula transfer. The reaction mixture was stirred for 3 h while keeping it at -78 °C then allowed warm up to room temperature and stirred for an additional 10 h. All volatiles were removed *in vacuo,* and the residues were extracted with hexanes and filtered. The filtered solution was dried under reduced pressure to afford the title compound as a sticky beige powder. Note: The phosphine is extremely oily and difficult to dry. Once dried, the solid formed is sticky and troublesome to isolate. Several minor impurities were observed in the ^{31}P NMR spectrum so a ^{13}C{^{1}H} NMR spectrum was not obtained.

Yield: 62 mg (0.127 mmol, 34 %).

^{1}H NMR (400 MHz, C_6D_6, T= 298K): d (ppm) 7.25 (t, $^{3}J_{HH}$= 7.7 Hz, 2H, Dipp; *para*), 7.15 – 7.07 (m, 4H, Dipp; *meta*), 5.92 (s, 2H, N-C<u>H</u>=C<u>H</u>-N), 4.67 (d, $^{1}J_{HP}$ = 177 Hz, 1H , P-H), 3.32 (sept, $^{3}J_{HH}$ = 6.9 Hz, 2H, C<u>H</u>Me$_2$), 3.14 (sept, $^{3}J_{HH}$ = 6.9 Hz, 2H , C<u>H</u>Me$_2$), 1.50 (d, $^{3}J_{HH}$ = 6.9 Hz, 6H, CH(C<u>H</u>$_3$)$_2$), 1.41 (d, $^{3}J_{HH}$ = 6.9 Hz, 6H, CH(C<u>H</u>$_3$)$_2$), 1.24 – 1.18 (m, 12 H, CH(C<u>H</u>$_3$)$_2$), 0.85 (d, $^{3}J_{HP}$ = 12 Hz, 9H, P-C(C<u>H</u>$_3$)$_3$).

^{31}P NMR (162 MHz, C_6D_6, T = 298 K): δ (ppm) = 38.2 (doublet of decets,$^{1}J_{HP}$ = 177 Hz, $^{3}J_{HP}$ = 12 Hz)

3.5.25 SCXRD Analyses

Single-crystal X-ray diffraction data were collected on a Bruker APEX-II CCD detector or with a Bruker D8 QUEST PHOTON III C14, both using Mo-Ka radiation sources (l = 0.71073 Å). Crystals were selected under oil, mounted on either glass fibre or nylon loops and then immediately placed in a cold stream of N_2 on a diffractometer. The APEX2[S1] and APEX4[S2] software was used to operate the diffractometers. The data was integrated with SAINT15 [S3] and corrected for absorption effects based on Gaussian numerical integration and scaled with SADABS.[S4] Using Olex2,[S5] the structures were solved with the Superflip[S6] Olex2.solve [S7], ShelXS [S8], ShelXD [S8] or ShelXT[S9] using charge flipping, direct, or dual methods. The refinement was done with ShelXL[S8] using Least Squares minimization or Olex2.refine[S7] using Gauss-Newton minimization.

The crystallographic data for all compounds in this Chapter have yet to be deposited in the CCDC.

[4-2^a][AlCl$_4$]: Red block single crystals suitable for X-ray diffraction were obtained by layering a CH_2Cl_2 solution with hexane (1:2) and storing it at room temperature for a few days.

[4-3][B(C$_6$F$_5$)$_4$]: After concentrating **[4-2][B(C$_6$F$_5$)$_4$]** in a solution mixture of CH_2Cl_2 and PhCl for several weeks at room temperature, colorless crystals were extracted from an oily red residue.

4-1^a: Yellow single crystals suitable for X-ray diffraction were obtained by storing a concentrated n-hexane solution of the product at -40 °C.

4-1^c: Yellow single crystals suitable for X-ray diffraction were obtained by storing a concentrated n-hexane solution of the product at -40 °C.

4-1^d: Single crystals suitable for X-ray diffraction were obtained by storing a concentrated diethyl ether solution of the product at -40 °C.

Table 4-1: Crystal structure refinement data [**4-2**^{a}][$AlCl_4$], [**4-3**][$B(C_6F_5)_4$], and **4-1**^{a}.

Compound	**[4-2^{a}][$AlCl_4$]**	**[4-3][$B(C_6F_5)_4$]**	**4-1^{a}**
CCDC	*Not deposited*	*Not deposited*	*Not deposited*
Emp. formula	$C_{31}H_{45}N_3AlPCl_4$	$C_{86}H_{89.75}BClF_{20}N_6P_2$	$C_{31}H_{45}ClN_3P$
Formula weight	659.45	1695.58	526.12
Temperature/K	173.00	173.00	173.00
Crystal system	Monoclinic	Triclinic	Orthorhombic
Space group	$P2_1/c$	P-1	$P2_12_12_1$
a/Å	10.002(3)	14.2892(8)	11.4432(6)
b/Å	17.767(4)	15.6244(8)	13.8193(7)
c/Å	20.292(5)	19.6593(11)	19.8867(10)
α/°	90	90.264(2)	90
β/°	98.628(9)	107.595(2)	90
γ/°	90	96.022(2)	90
Volume/Å^3	3565.3(16)	4157.7(4)	3144.8(3)
Z	4	2	4
r_{calc}g/cm^3	1.229	1.354	1.111
μ/mm^{-1}	0.426	0.178	0.195
F(000)	1392.0	1760.0	1136.0
Crystal size/mm^3	0.2 × 0.1 × 0.1	0.5 x 0.2 x 0.02	0.16 × 0.06 × 0.03
Radiation	MoK_a (l = 0.71073)	MoK_a (l = 0.71073)	MoK_a (l = 0.71073)
2Θ range for data collection/°	4.06 to 61.286	4.206 to 56.762	4.106 to 56.66
Index ranges	-13 ≤ h ≤ 13, 0 ≤ k ≤ 25, 0 ≤ l ≤ 29	-19≤ h ≤ 18, -20 ≤ k ≤ 20, -26 ≤ l ≤ 26	-15 ≤ h ≤ 15, -18 ≤ k ≤ 16, -26 ≤ l ≤ 25
Reflections col.	4652	141769	40399
Independent ref.	4652 [R_{sigma} = 0.0885]	20793 [R_{int} = 0.0359, R_{sigma} = 0.0247]	7828 [R_{int} = 0.0843, R_{sigma} = 0.0698]
D/R/P	4652/306/373	20793/4/11	7828/226/474
Goodness-of-fit on F^2	1.251	1.035	1.035
Final R indexes [I>2s (I)]	R_1 = 0.1016, wR_2 = 0.1424	R_1 = 0.0749, wR_2 = 0.1822	R_1 = 0.0570, wR_2 = 0.0698
Final R indexes [all data]	R_1 = 0.1419, wR_2 = 0.1525	R_1 = 0.0917, wR_2 = 0.1948	R_1 = 0.0570, wR_2 = 0.1197
Largest diff. peak/hole/ eÅ^{-3}	0.34/-0.36	1.13/-2.12	0.18/-0.18

Table 4-2: Crystal structure refinement data **4-1c** and **4-1d**.

Compound	**4-1c**	**4-1d**
CCDC	*Not deposited*	*Not deposited*
Emp. formula	$C_{15}H_{31}ClN_3P$	$C_{27}H_{41}ClN_3P$
Formula weight	319.85	474.05
Temperature/K	173.00	153.00
Crystal system	Triclinic	Monoclinic
Space group	P-1	$P2_1/c$
a/Å	14.4339(8)	14.0675(10)
b/Å	16.0056(7)	11.3269(8)
c/Å	17.2606(10)	16.6605(12)
α/°	89.827(2)	90
β/°	67.057(2)	108.909(2)
γ/°	89.886(3)	90
Volume/Å^3	3672.1(3)	2511.4(3)
Z	8	4
r_{calc}g/cm^3	1.157	1.254
μ/mm^{-1}	0.292	0.236
F(000)	1392.0	1024.0
Crystal size/mm^3	0.31 × 0.21 × 0.17	0.16 x 0.06 x 0.03
Radiation	MoK_a (l = 0.71073)	MoK_a (l = 0.71073)
2Θ range for data collection/°	3.606 to 52.864	4.428 to 50.21
Index ranges	-18 ≤ h ≤ 18, 20 ≤ k ≤ 20, -21 ≤ l ≤ 21	-16≤ h ≤ 16, -13 ≤ k ≤ 13, -19 ≤ l ≤ 19
Reflections col.	94362	43767
Independent ref.	15058 [R_{int} = 0.0469, R_{sigma} = 0.0311]	4466 [R_{int} = 0.0577, R_{int} = 0.0364]
D/R/P	15058/0/858	4466/0/391
Goodness-of-fit on F^2	1.023	1.067
Final R indexes [I>2s (I)]	R_1 = 0.0476, wR_2 = 0.1275	R_1 = 0.0475, wR_2 = 0.1105
Final R indexes [all data]	R_1 = 0.0556, wR_2 = 0.1354	R_1 = 0.0618, wR_2 = 0.1167
Largest diff. peak/hole/ eÅ^{-3}	0.59/-0.38	0.21/-0.23

4.5.25 Computational Details

Density Functional Theory (DFT) calculations have been performed using the Gaussian 16 program package.[S10] All geometry optimizations were performed at B3LYP [S11] level of theory using Grimme's D3 dispersion model with Becke-Johnson Damping (D3-BJ) [S12] using def2-TZVP [S13] basis sets employing a conductor-like polorizable continuum model (cPCM) for dichloromethane.[S14] The absence of any imaginary frequencies confirmed that each optimized structure is at a local minimum. Natural bond orbital analyses was performed using NBO 3.1 module as implemented in the Gaussian 16 programs in B3LYP/Lanl2dz method. [S15] The Hirshfeld charges and the Mayer bond orders were calculated using Multiwfn 3.7 software package.[S16]. Molecular orbitals were visualized using GaussView 6 program. The fluoride ion affinity (FIA) of the truncated models $[^{sat}$NHI-P(*t*Bu)$]^+$ and $[^{unsat}$NHI-P(*t*Bu)$]^+$ was calculated in the gas phase. The FIAs were calculated according to the reported procedure by Christe [52] anchored to COF_2.

4.6.1 References

1. T. Chu, G. I. Nikonov, *Chem. Rev.* **2018**, *118*, 3608–3680.
2. M. He, C. Hu, R. Wei, X. F. Wang, L. L. Liu, *Chem. Soc. Rev.* **2024**, *53*, 3896–3951.
3. D. R. Tolentino, S. E. Neale, C. J. Isaac, S. A. Macgregor, M. K. Whittlesey, R. Jazzar, G. Bertrand, *J. Am. Chem. Soc.* **2019**, *141*, 9823–9826.
4. F. Vermersch, V. T. Wang, M. Abdellaoui, R. Jazzar, G. Bertrand, *Chem. Sci.* **2024**, *15*, 3707–3710.
5. D. Bourissou, O, Guerret, F. P. Gabbaï, G. Bertrand, Stable Carbenes. *Chem. Rev.* **2000**, *100*, 39–91.
6. A. H. Cowley, R. A. Kemp, *Chem. Rev.* **1985**, *85*, 367–382.
7. C. A. Caputo, J. T. Price, M. C. Jennings, R. McDonalds, N. D. Jones, *Dalton Trans.* **2008**, 3412–3421.
8. J. J. Weigand, M. Holthausen, R. Fröhlich, *Angew. Chem. Int. Ed.* **2009**, *48*, 295–298.
9. M. Q. Y. Tay, Y. Lu, R. Ganguly, D. Vidović, *Angew. Chem. Int. Ed.* **2013**, *52*, 3132–3135.
10. M. Q. Y. Tay, Y. Lu, R. Ganguly, D. Vidović, *Chem. Eur. J.* **2014**, *20*, 6628–6631.
11. M. Olaru, S. Mebs, J. Beckmann. *Angew. Chem. Int. Ed.* **2021**, *60*, 19133–19138.
12. N. Dordević, R. Ganguly, M. Petković, D. Vidović, *Inorg. Chem.* **2017**, *56*, 14671–14681.
13. T. J. Hannah, S. S. Chitnis, S. S. *Chem. Soc. Rev.* **2023**, *53*, 764–792.
14. L. M. Sigmund, R. Maier, L. Greb, *Chem. Sci.* **2022**, *13*, 510–521.
15. D. Bawari, D. Toami, R. Dobrovetsky, *Chem. Commun.* **2025**, *61*, 5871–5882.
16. W. Zhao, S, M. McCarthy, T. Y. Lai, H. P. Yennawar, A. T. Radosevich, *J. Am. Chem. Soc.* **2014**, *136*, 17634–17644.
17. D. Roth, A. T. Radosevich, L. Greb, *J. Am. Chem. Soc.* **2023**, *145*, 24184–24190.
18 S. Volodarsky, R. Dobrovetsky, *Chem. Commun.* **2018**, *54*, 6931–6934.

19. S. Volodarsky, D. Bawari, R. Dobrovetsky, *Angew. Chem. Int. Ed.* **2022**, *61*, e202208401

20. K. Chulsky, I. Malahov, D. Bawari, R. Dobrovetsky, *J. Am. Chem. Soc.* **2023**, *145*, 3786–3794.

21. D. Bawari, D. Toami, K. Jaiswal, R. Dobrovetsky, *Nat. Chem.* **2024**, *16*, 1261–1266.

22. P. Löwe, M. A. Wünsche, F. R. S. Purtscher, J. Gamper, T. S. Hofer, L. F. B. Wilm, M. B. Röthel, F. Dielmann, *Chem. Sci.* **2023**, *14*, 7928–7935.

23. M. D. Böhme, T. Eder, M. B. Röthel, P. D. Dutschke, L. F. B. Wilm, E. Hahn, F. Dielmann, *Angew. Chem. Int. Ed.* **2022**, *61*, e202202190.

24. H. Zhu, A. Kostenko, D. Franz, F. Hanusch, S. Inoue, *J. Am. Chem. Soc.* **2023**, *145*, 1011–1021.

25. V. Lavallo, Y. Canac, B. Donnadieu, W. W. Schoeller, G. Bertrand, *Angew. Chem. Int. Ed.* **2006**, *45*, 3488–3491.

26. C. Roques, M. R. Mazieres, J. P. Majoral, M. Sanchez, A. Foucaud, *J. Org. Chem*, **1989**, *54*, 5535–5539.

27. F. Dahcheh, D. Martin, D. W. Stephan, G. Bertrand, *Angew. Chemie - Int. Ed.* **2014**, *53*, 13159–13163.

28. C. Ganesamoorthy, J. Schoening, C. Wölper, L. Song, P. R. Schreiner, S. Schulz, *Nat. Chem.* **2020**, *12*, 608–614.

29. D. Reiter, R. Holzner, A. Porzelt, P. Frisch, S. Inoue, *Nat. Chem.* **2020**, *12*, 1131–1135.

30. N. Kuhn, R. Fawzi, M. Stiemann, J. Wiethoff, *Chem. Ber.* **1996**, *129*, 479–482.

31. M. A. Wünsche, T. Witteler, F. Dielmann, *Angew. Chem. Int. Ed.* **2018**, *57*, 7234–7239.

32. A. H. Cowley, M. Lattman, J. C. Wilburn, *Inorg. Chem.* **1981**, *20*, 2916–2919

33. J. Lortie, dissertation. Western University, **2024**.

34. A. D. Becke, *J. Chem. Phys.* **1993**, *98*, 1372–1377.

35. Weigend, R. Ahlrichs, *Phys. Chem. Chem. Phys*. **2005**, *7*, 3297–3305.

36. S. Grimme, S. Ehrlich, L. Goerigk, *J. Comput. Chem.* **2011**, *32*, 1456–1465.

37. U. Mayer, V. Gutmann, W. Gerger, *Monatsh. Chem.,* **1975***, 106*, 1235–1257.

38. M. A. Beckett, D. S. Brassington, S. J. Coles, M. B. Hursthouse, *Inorg. Chem. Commun.* **2000**, *3*, 530–533.

39. C. B. Caputo, L. J. Hounjet, R. Dobrovetsky, D. W. Stephan, *Science*, **2013**, *341*, 1374–1377.

40. C. Stoian, M. Olaru, S. Demeshko, M. Fischer, S. Mebs, E. Hupf, J. Beckmann, *Chem. Eur. J.* **2024**, 202403555.

41. P. Mehlmann, T. Witteler, L. F. B. Wilm, F. Dielmann, *Nat. Chem.* **2019**, *11*, 1139–1143.

42. C. K. SooHoo, S. G. Baxter, *J. Am. Chem. Soc.* **1983**, *105*, 7443-7444.

43. D. Gasperini, S. E. Neale, N. F. Mahon, S. A. MacGregor, R. L. Webster, *ACS Catal.* **2021**, *11*, 5452–5462.

44. L. N. Markovski, V. D. Romanenko, A. V. Ruban, A. B. Drapailo, *J. Chem. Soc., Chem. Commun.* **1984**, 1692.

45. Y. K. Loh, M. Melaimi, M. Gembicky, D. Munz, G. Bertrand, *Nature.* **2023**, *623*, 66–70.

46. G. D. Frey, V. Lavallo, B. Donnadieu, W. W. Schoeller, G. Bertrand, *Science.* **2007,** *316*, 439−441.

47. Y. Peng, J. D. Guo, B. D. Ellis, Z. Zhu, J. C. Fettinger, S. Nagase, P. P. Power, *J. Am. Chem. Soc.* **2009**, *131*, 16272–16282.

48. A. V. Protchenko, K. H. Birjkumar, D. Dange, A. D. Schwarz, D. Vidović, C. Jones, N. Kaltsoyannis, P. Mountford, S. Aldridge, *J. Am. Chem. Soc.* **2012**, *134*, 6500–6503.

49. T. Chu, I. Korobkov, G. I. Nikonov, *J. Am. Chem. Soc.* **2014**, *136*, 9195–9202.

50. A. V. Protchenko, J. I. Bates, L. M. A. Saleh, M. P. Blake, A. D. Schwarz, E. L. Kolychev, A. L. Thompson, C. Jones, P. Mountford, S. Aldridge, *J. Am. Chem. Soc.* **2016**, *138*, 4555–4564.

51. N. L. Dunn, M. Ha, A. T. Radosevich, *J. Am. Chem. Soc.* **2012**, *134*, 11330–11333.

52. K. O. Christe, D. A. Dixon, D. McLemore, W. W. Wilson, J. A. Sheehy, J. A. Boatz, *J. Fluor. Chem.* **2000**, *101*, 151–153.

53. J. F. Harrison, R. C. Liedtke, J. F. Liebman, *J. Am. Chem. Soc.* **1979**, *101*, 7162–7168.

54. J. M. Slattery, S. Hussein, *Dalton Trans.* **2012**, *41*, 1808–1815.

55. L. Liu, D. A. Ruiz, F. Dahcheh, G. Bertrand, *Chem. Commun.* **2015**, *51*, 12732–12735.

56. R. Nakano, R. Jazzar, G. Bertrand, *Nat. Chem.* **2018**, *10*, 1196–1200.

57. F. Ramirez, E. A. Tsolis, *J. Am. Chem. Soc.* **1970**, *92*, 7553–7558.

58. T. Matthias, B. Stephan, H. Eberhardt, Z. *Naturforsch. B*. **2004**, 59, 1497.

4.6.2 Crystallographic and Computational References

S1. APEX2 Version 2.1 – 0; Bruker AXS Inc. Madison, **2004**.

S2. APEX4; Bruker AXS Inc. Madison, **2021**.

S3. SAINT version 7.46a, Bruker AXS Inc. Madison **2004**.

S4. G. Sheldrick GM SADABS. University of Göttingen, Göttingen **1996**.

S5. O. V. Dolomanov, L. J. Bourhis, R. J. Gildea, J. A. K. Howard and H. Puschmann, *J. Appl. Crystallogr.* **2009**, *42*, 339–341.

S6. a) L. Palatinus, G. Chapuis, *J. Appl. Cryst.* **2007**, 40, 786-790; b) L. Palatinus, A. van der Lee, *J. Appl. Cryst.* **2008**, 41, 975-984; c) L. Palatinus, S. J. Prathapa, S. van Smaalen, *J. Appl. Cryst.* **2012**, *45*, 575-580.

S7. L. J. Bourhis; O. V. Dolomanov; R. J. Gildea; J. A. K. Howard; H. Puschmann, *Acta crystallogr. A*. **2015**, *71*, 59–75.

S8. G. M. Sheldrick, *Acta crystallogr. A*. **2008**, *64*, 112–122.

S9. G. M. Sheldrick, *Acta crystallogr. A*. **2015**, *71*, 3–8.

S10. Gaussian 16, Revision C.01, M. J. Frisch, G. W. Trucks, H. B. Schlegel, G. E. Scuseria, M. A. Robb, J. R. Cheeseman, G. Scalmani, V. Barone, G. A. Petersson, H. Nakatsuji, X. Li, M. Caricato, A. V. Marenich, J. Bloino, B. G. Janesko, R. Gomperts, B. Mennucci, H. P. Hratchian, J. V. Ortiz, A. F. Izmaylov, J. L. Sonnenberg, D. Williams-Young, F. Ding, F. Lipparini, F. Egidi, J. Goings, B. Peng, A. Petrone, T. Henderson, D. Ranasinghe, V. G. Zakrzewski, J. Gao, N. Rega, G. Zheng, W. Liang, M. Hada, M. Ehara, K. Toyota, R. Fukuda, J. Hasegawa, M. Ishida, T. Nakajima, Y. Honda, O. Kitao, H. Nakai, T. Vreven, K. Throssell, J. A. Montgomery, Jr., J. E. Peralta, F. Ogliaro, M. J. Bearpark, J. J. Heyd, E. N. Brothers, K. N. Kudin, V. N. Staroverov, T. A. Keith, R. Kobayashi, J. Normand, K. Raghavachari, A. P. Rendell, J. C. Burant, S. S. Iyengar, J. Tomasi, M. Cossi, J. M. Millam, M. Klene, C. Adamo, R. Cammi, J. W. Ochterski, R. L. Martin, K. Morokuma, O. Farkas, J. B. Foresman, and D. J. Fox, Gaussian, Inc., Wallingford CT, **2016**.

S11. A. D. Becke, *J. Chem. Phys*, **1993**, *98*, 5648–5652; b) C. Lee, W. Yang, R. G. Parr, *Phys. Rev. B.* **1998**, *37*, 785–789; c) S. H. Vosko, L. Wilk, M. Nusair, *Can. J. Phys*. **1980**, *58*, 1200-1211; d) P. J. Stephens, F. J. Devlin, C. F. Chabalowski, M. J. Frisch, *J. Phys. Chem*. **1994**, *98*, 11623–11627.

S12. a) L. Goerigk, S. Grimme, *J. Chem. Theory Comput.* **2011**, *7*, 291–309; b) L. Goerigk, A. Hansen, C. Bauer, S. Ehrlich, A. Najibi, S. Grimme, *Phys. Chem. Chem. Phys.* **2017**, *19*, 32184–32215; c) B. G. Johnson, M. J. Frisch, *J. Chem. Phys.* **1994**, *100*, 7429–7442.

S13. F. Weigend, R. Ahlrichs, *Phys. Chem. Chem. Phys.* **2005**, *7*, 3297–3305; b) F. Weigend, *Phys. Chem. Chem. Phys.* **2006**, *8*, 1057–1065.

S14. a) J. Tomasi, B. Mennucci, R. Cammi, *Chem. Rev*. **2005**, *105*, 2999-3093. b) V. Barone, M. Cossi, *J. Phys. Chem. A*. **1998**, 102, 1995-2001.

S15. a) F. Weinhold, C. R. Landis (Eds.) Discovering Chemistry with Natural Bond Orbitals, John Wiley & Sons, Inc, Hoboken, NJ, USA, **2012**; b) J. P. Foster, F. Weinhold, *J. Am. Chem. Soc.* **1980**, *102*, 7211–7218; c) A. E. Reed, R. B. Weinstock, F. Weinhold, *J. Chem. Phys.* **1985**, *83*, 735–746; d) J. E. Carpenter, F. Weinhold, *J. Mol. Struct.: THEOCHEM*.

1988, *169*, 41–62; e) F. Weinhold, J. E. Carpenter, *The Structure of Small Molecules and Ions*, R. Naaman and Z. Vager, Springer US, Boston, MA, **1988**, pp. 227–236.

S16. T. Lu, F. Chen, *J. Comput. Chem.* **2012**, *33*, 580–592.

S17. K. O. Christe, D. A. Dixon, D. McLemore, W. W. Wilson, J. A. Sheehy, J. A. Boatz, *J. Fluorine Chem*. **2000**, *101*, 151–153.

Chapter Five

5.1 Conclusions

This thesis served to uncover more parallels in the chemistry of low-coordinate phosphorus compounds and carbon compounds, a topic which has captivated main-group chemists for decades. Our initial interest was in preparing new types of trigonal planar phosphonium cations $[R_2P{=}E]^+$, analogs of unsaturated carbon compound ($R_2C{=}E$) that are ubiquitous in nearly all disciplines of chemistry. In this pursuit, we uncovered a new phosphorus Lewis acid, the allenylidene phosphonium cation $[R_2P{=}C{=}C{=}CR_2]^+$, which stands alongside several other recently reported main-group cumulene species. We would then transition our research direction to exploring the chemistry of phosphenium cations, phosphorus analog of carbenes. The main conclusions of each Chapter are briefly described below, as detailed conclusions and future directions for each research project have been discussed at length previously in this thesis.

In Chapter 2, we attempted to prepare the tetraphenyl allenylidene phosphonium cation $[Ph_2P{=}C{=}C{=}CPh_2]^+$, directly inspired from the first synthesized carbon cumulene, tetraphenylbutatriene ($Ph_2C{=}C{=}C{=}CPh_2$), published over 100 years ago. Our synthetic strategy to $[Ph_2P{=}C{=}C{=}CPh_2]^+$ was adopted from literature precedent for the preparation of transition metal allenylidenes $[L_xM{=}C{=}C{=}CR_2]^n$. Specifically, we explored a synthetic route where alkynyl phosphines of the form $R_2P{-}C{\equiv}C{-}C(OCH_3)R_2$ would serve as precursors to $[R_2P{=}C{=}C{=}CR_2]^+$, and the transformation would be mediated by CH_3O^- abstraction with a Lewis acid. While we were ultimately unsuccessful in our attempts to prepare $[Ph_2P{=}C{=}C{=}CPh_2]^+$, we were able to experimentally and computationally evaluate that our synthetic approach to an allenylidene phosphonium cation $[R_2P{=}C{=}C{=}CR_2]^+$ could potentially be realized if the correct substituent arrangement at carbon and phosphorus was implemented.

Subsequently, In Chapter 3 we accomplished our initial goal to prepare the cation $[R_2P{=}C{=}C{=}CR_2]^+$. To successfully stabilize $[R_2P{=}C{=}C{=}CR_2]^+$, three implementations were made. 1) Bulky π-electron rich substituents, known as N-heterocyclic imines were appended to phosphorus to tame the electrophilicity of the three-coordinate phosphonium center. 2) Secondly, at the terminal carbon, a fluorenylidene group was introduced to facilitate extensive π-conjugation

throughout the entire molecule. 3) Lastly, the Lewis acid reagent $B(OC_6F_5)_3$ which was used to generate $[R_2P{=}C{=}C{=}CR_2]^+$, was found to simultaneously produce a weakly coordinating anion $[B(OC_6F_5)_4]^-$. With the synthesis of $[R_2P{=}C{=}C{=}CR_2]^+$ realized, we investigated the electronic structure experimentally and computationally. We also provided preliminary exploration into its potentially rich cycloaddition chemistry.

Once again exploiting the properties of N-heterocyclic imines, we prepared a series of electrophilic alkyl-imino-phosphenium cations in Chapter 4. While these phosphenium cations were initially prepared to enable the synthesis of allenic trigonal planar phosphonium cations like $[R_2P{=}C{=}O]^+$ and $[R_2P{=}C{=}N{-}R]^+$, we ultimately found them competent towards a range of oxidative bond activation reactions.

5.2 Compiled List of References

Preface

1. N. N. Greenword, A. Earnshaw, Chemistry of The Elements. *Elsevier*, **2012**.
2. D. Mendeleev. *Z. Chem.* **1869**, *12*, 405-406.
3. J. M. Lipshultz, G. Li, A. T. Radosevich, *J. Am. Chem. Soc.* **2021**, *143*, 1699–1721.
4. A. Kuczkowski, S. Schulz, M. Nieger, P. R. Schreiner, *Organometallics* **2002**, *21*, 1408–1419.
5. R. L. Rich, *J. Chem. Educ.* **1986**, *63*, 828–829.
6. C. H. Cartledge, *J. Am. Chem. Soc.* **1928**, *50*, 2863-2872.
7. G. Rayner-Canham, *Found. Chem.* **2011**, *13*, 121–129.
8. A. J. Ihde, The Development of Modern Chemistry. *Dover*. **1984**
9. A. Paparo, C. D. Smith, C. Jones, C. *Angew. Chem. Int. Ed.* **2019**, *58*, 11459–11463.
10. S. Wang, J. D. Sears, C. E. Moore, A. L. Rheingold, M. L. Niedig, J. S. Figueroa, *Science.* **2022**, *375*, 1393–1397.
11. K. M. Marczenko, J. A. Zurakowski, K. L. Bamford, J. W. M. MacMillan, S. S. Chitnis, *Angew. Chem. Int. Ed.* **2019**, *58*, 18096–18101.
12. K. B. Dillon, F. Mathey, J. F. Nixon, *Phosphorus: The Carbon Copy. From Organophosphorus To Phospha-Organic Chemistry*; John Wiley & Sons: **1998**.
13. F. Mathey, *Acc. Chem. Res.* **1992**, *25*, 90–96.
14. F. Mathey, *Angew. Chem. Int. Ed.* **2003**, *42*, 1578–1604.
15. T. E. Gier, *J. Am. Chem. Soc.* **1961**, *83*, 1769–1770.
16. G. Becker, *Z. Anorg. Allg. Chemie* **1976**, *423*, 242–254.
17. G. Märkl, *Angew. Chem.* **1966**, *78*, 907–908.
18. O. J. Scherer, T. Brück, *Angew. Chem. Int. Ed.* **1987**, *26*, 59.
19. S. Fleming, M. K. Lupton, K. Jekot, *Inorg. Chem.* **1972**, *11,* 2534–2540.
20. M. Y. Riu, R. L. Jones, W. J. Transue, P. Müller, C. C. Cummins, *Sci. Adv.* **2020**, *6*, eaaz3168.
21. F. Dankert, S. P. Muhm, C. Nandi, S. Danés, S. Mullassery, P. Herbeck-Engel, B. Morgenstern, R. Weiss, P. Salvador, D. Munz, *J. Am. Chem. Soc.* **2025**. *147*, 15369-15376.

22. M. A. Wünsche, T. Witteler, F. Dielmann, *Angew. Chem. Int. Ed.* **2018**, *57*, 7234–7239.

Chapter 1

1. W. Schipper, *Eur. J. Inorg. Chem.* **2014**, 1567–1571.
2. K. A. Remick, J. D Helmann, *Adv. Microb. Physiol.* **2023**, *82*, 1–127.
3. F. Bachhuber, J. Von Appen, R. Dronskowski, P. Schmidt, T. Nilges, A. Pfitzner, R. Weihrich, *Angew. Chem. Int. Ed.* **2014**, *53*, 11629–11633.
4. X. Ye, M. Qi, M. Chen, L. Zhang, J. Zhang, *Adv. Mater. Interfaces* **2023**, *10*, 2201941.
5. J. Emslie, The 13th Element: The Sordid Tale of Murder, Fire, and Phosphorus, *Turner Publishing Company.* **2002**.
6, M. Donath, K. Schwedtmann, T. Schneider, F. Hennersdorf, A. Bauzá, A. Frontera, J. J. Weigand, *Nat. Chem.* **2022**, *14*, 384–391.
7. H. Grützmacher, *Nat. Chem.* **2022**, *14*, 361–364.
8. M. B. Geeson, C. C. Cummins, *ACS Cent. Sci.* **2020**, *6*, 848–860.
9. J. M. Bayne, D. W. Stephan, *Chem. Soc. Rev.* **2016**, *45*, 765–774.
10. J. M. Lipshultz, G. Li, A. T. Radosevich, *J. Am. Chem. Soc.* **2021**, *143*, 1699–1721.
11. H. Guo, Y. C. Fan, Z. Sun, Y. Wu, O. Kwon, *Chem. Rev.* **2018**, *118*, 10049–10293.
12. M. A. Wünsche, P. Mehlmann, T. Witteler, F. Buß, P. Rathmann, F. Dielmann, *Angew. Chem. Int. Ed.* **2015**, *54*, 11857–11860.
13. J. A. Gillespie, E. Zuidema, P. W. N. M. van Leeuwen, P. C. J. Kamer, Phosphorus (III) Ligands in Homogeneous Catalysis: Design and Synthesis (Eds.: P. C. J. Kamer, and P. W. N. M. van Leeuwen), John Wiley & Sons, Ltd, **2012**, 1-22
14. H. Shet, U. Parmar, S. Bhilare, A. R. Kapdi, *Org. Chem. Front.* **2021**, *8*, 1599–1656.
15. D. S. Surry, S. L. Buchwald, *Chem. Sci.* **2011**, *2*, 27–50.
16. A. L. Clevenger, R. M. Stolley, J. Aderibigbe, J. Louie, *Chem. Rev.* **2020**, *120*, 6124–6196.
17. O. Guerret, G. Bertrand, *Acc. Chem. Res.* **1997**, *30*, 486–493.
18. A. H. Cowley, R. A. Kemp, *Chem. Rev.* **1985**, *85*, 367–382.
19. D. Bawari, D. Toami, R. Dobrovetsky, *Chem. Commun.* **2025**, *61*, 5871–5882.
20 G. Wittig, G. Geissler, G. *Justus Liebigs Ann. Chem.* **1953**, *580*, 44–57.

21. P. A. Byrne, D. G. Gilheany, *Chem. Soc. Rev.* **2013**, *42*, 6670–6696.

22. R. L. Melen, *Science.* **2019**, *363*, 479–484.

23. P. P. Power, *Nature.* **2010**, *463*, 171–177.

24. D. W. Stephan, *J. Am. Chem. Soc.* **2015**, *137*, 10018–10032.

25. G. C. Welch, R. R. San Juan, J. D. Masuda, D. W. Stephan, *Science.* **2006**, *314*, 1124–1126.

26. P. A. Chase, G. C. Welch, T. Jurca, D. W. Stephan, *Angew. Chem. Int. Ed.* **2007**, *46*, 8050–8053.

27. J. Lam, K. M. Szkop, E. Mosaferi, D. W. Stephan, *Chem. Soc. Rev.* **2019**, *48*, 3592–3612.

28. J. Paradies, *Angew. Chem. Int. Ed.* **2014**, *53*, 3552–3557.

29. D. W. Stephan, G. Erker, *Angew. Chem. Int. Ed*. **2015**, *54*, 6400–6441.

30. C. B. Caputo, L. J. Hounjet, R. Dobrovetsky, D. W. Stephan, *Science*. **2013**, *341*, 1374–1377.

31 J. M. Bayne, D. W. Stephan, *Chem. Eur. J.* **2019**, *25*, 9350–9357.

32. D. Bawari, D. Toami, K. Jaiswal, R. Dobrovetsky, *Nat. Chem.* **2024**, *16*, 1261–1266.

33. T. Lundrigan, E. N. Welsh, T. Hynes, C. H. Tien, M. R. Adams, K. R. Roy, K. N. Robertson, A. W. H. Speed, *J. Am. Chem. Soc.* **2019**, *141*, 14083–14088.

34. M. Pérez, L. J. Hounjet, C. B. Caputo, R. Dobrovetsky, D. W. Stephan, *J. Am. Chem. Soc.* **2013**, *135*, 18308–18310.

35. M. Vogler, L. Süsse, J. H. W. Lafortune, D. W. Stephan, M. Oestreich, *Organometallics.* **2018**, *37*, 3303–3313.

36. M. Terada, M. Kouchi, *Tetrahedron.* **2006**, *62*, 401–409.

37. G. D. Frey, V. Lavallo, B. Donnadieu, W. W. Schoeller, G. Bertrand, *Science.* **2007**, *316*, 439–441.

38. V. Lavallo, J. Mafhouz, Y. Canac, B. Donnadieu, W. W. Schoeller, G. Bertrand, *J. Am. Chem. Soc.* **2004**, *126*, 8670–8671.

39. V. Lavallo, Y. Canac, C. Präsang, B. Donnadieu, G. Bertrand, *Angew. Chem. Int. Ed.* **2005**, *44*, 5705–5709.

40. A. J. Arduengo, R. L. Harlow, M. Kline, *J. Am. Chem. Soc.* **1991**, *113*, 361-363.

41. J. Vignolle, X. Cattoën, D. Bourissou, *Chem. Rev.* **2009**, *109*, 3333–3384.

42. M. Melaimi, M. Soleilhavoup, G. Bertrand, *Angew. Chem. Int. Ed*. **2010**, *49*, 8810–8849.

43. D. Bourissou, O. Guerret, F. P. Gabbaï, G. Bertrand, *Chem. Rev.* **2000**, *100*, 39–91.

44. S. K. Kushvaha, A. Mishra, H. W. Roesky, K. C. Mondal, *Chem. Asian J.* **2022**, *17*, e202101301.

45. V. Lavallo, Y. Canac, B. Donnadieu, W. W. Schoeller, G. Bertrand, *Angew. Chem. Int. Ed*. **2006**, *45*, 3488–3491.

46. F. Vermersch, V. T. Wang, M. Abdellaoui, R. Jazzar, G. Bertrand, *Chem. Sci.* **2024**, *15*, 3707–3710.

47. T. Chu, G. I. Nikonov, *Chem. Rev.* **2018**, *118*, 3608–3680.

48. M. He, C. Hu, R. Wei, X. F. Wang, L. L. Liu, *Chem. Soc. Rev.* **2024**, *53*, 3896–3951.

49. K. Dimroth and P. Hoffmann, *Angew. Chem. Int. Ed*. **1964**, *3*, 384

50. S. G. Baxter, R. L. Collins, A. H. Cowley, S. F. Sena, *J. Am. Chem. Soc*. **1981**, *103*, 714–715.

51. M. Olaru, A. Mischin, L. A. Malaspina, S. Mebs, J. Beckmann, *Angew. Chem. Int. Ed*. **2020**, *59*, 1581–1584.

52. S. Fleming, M. K. Lupton, K. Jekot, *Inorg. Chem.* **1972**, *11,* 2534–2540.

53. L. Rosenberg, *Coord. Chem. Rev.* **2012**, *256*, 606–626.

54. D. Gudat, A. Haghverdi, H. Hupfer, M. Nieger, *Chem. Eur. J.* **2000**, *6*, 3414–3425.

55. A. H. Cowley, R. A. Kemp, C. A. Stewart, *J. Am. Chem. Soc*. **1982**, *104*, 3239–3240.

56. S. K. Mehrotra, A. H. Cowley, *J. Am. Chem. Soc*. **1983**, *105*, 2074–2075.

57. C. K. SooHoo, S. G. Baxter, *J. Am. Chem. Soc.* **1983**, *105*, 7443-7444.

58. K. C. K. Swamy, N. S. Kumar, *Acc*. *Chem*. *Res*. **2006**, *39*, 324–333.

59. T. Mukaiyama, S. Matsui, K. Kashiwagi, *Chem. Lett.* **1989**, *18*, 993– 996,

60. R. Córdoba, J. Plumet, *Tetrahedron Lett.* **2003**, *44*, 6157– 6159.

61. C.-L. Zhu, F. -G. Zhang, W. Meng, J. Nie, D. Cahard, J. -A. Ma, *Angew. Chem. Int. Ed.* **2011**, *50*, 5869–5872.

62. J. P. Tan, K. Li, B. Shen, C. Zhuang, Z. Liu, K. Xiao, P. Yu, B. Yi, X. Ren, T. Wang, *Nat. Commun.* **2022**, *13*.

63. M. H. Holthausen, M. Mehta, D. W. Stephan, *Angew. Chem. Int. Ed.* **2014**, *53*, 6538–6541.

64. D. Roth, J. Stirn, D. W. Stephan, L. Greb, *J. Am. Chem. Soc.* **2021**, *143*, 15845–15851.

65. T. J. Hannah, S. S. Chitnis, *Chem. Soc. Rev.* **2023**, *53*, 764–792.

66. M. A. Wünsche, T. Witteler, F. Dielmann, *Angew. Chem. Int. Ed.* **2018**, *57*, 7234–7239.

67. P. Löwe, T. Witteler, F. Dielmann, *Chem. Commun.* **2021**, *57*, 5043–5046.

68. N. Burford, R. E. V. H. Spence, R. D. Rogers, Preparation, *J. Am. Chem. Soc.* **1989**, *111*, 5006–5008.

69. N. Burford, R. E. V. H. Spence, J. F. Richardson, *J. Chem. Soc. Dalton. Trans.* **1991**, 1615-1619.

70. A. D. Hendsbee, N. A. Giffin, Y. Zhang, C. C. Pye, J. D. Masuda, *Angew. Chem. Int. Ed.* **2012**, *51*, 10836–10840.

71. K. Huynh, A. J. Lough, M. A. M. Forgeron, M. Bendle, A. P. Soto, R. E. Wasylishen, I. Manners, *J. Am. Chem. Soc.* **2009**, *131*, 7905–7916.

72. A. Igau, H. Grützmacher, A. Baceiredo, G. Bertrand, *J. Am. Chem. Soc*. **1988**, *110*, 6463-6466.

73. A. Igau, A. Baceiredo, H. Grützmacher, H. Pritzkow, G. Bertrand, *J. Am. Chem. Soc.* **1989**, *111*, 6853–6854.

74. H. Grützmacher, H. Pritzkow, *Angew. Chem. Int. Ed.* **1991**, *30*, 709–710.

75. A. Schmidpeter, G. Jochem, K. Karaghiosoff, C. Robl, *Angew. Chem. Int. Ed.* **1992**, *31*, 1350–1352.

76. F. Dielmann, C. E. Moore, A. L. Rheingold, G. Bertrand, *J. Am. Chem. Soc.* **2013**, *135*, 14071–14703.

77. T. Ochiai, D. Franz, S. Inoue, *Chem. Soc. Rev.* **2016**, *45*, 6327–6344.

78. P. Löwe, M. A. Wünsche, F. R. S. Purtscher, J. Gamper, T. S. Hofer, L. F. B. Wilm, M. B. Röthel, F. Dielmann, *Chem. Sci.* **2023**, *14*, 7928–7935.

79. U. Heim, H. Pritzkow, U. Fleischer, H. Grützmacher, *Angew. Chem. Int. Ed*. **1993**, *32*, 1359–1361

80. P. Löwe, M. Feldt, M. A. Wünsche, L. F. B. Wilm, F. Dielmann, *J. Am. Chem. Soc.* **2020**, *142*, 9818–9826.

81. P. Löwe, M. Feldt, M. B. Röthel, L. F. B. Wilm, F. Dielmann, *Inorg. Chem.* **2021**, *60*, 14509–14514.

82. P. Löwe, dissertation, Westfälische Wilhelms-Universität Münster, **2022**.

83. P. Mehlmann, T. Witteler, L. F. B. Wilm, F. Dielmann, *Nat. Chem.* **2019**, *11*, 1139–1143.

84. Y. K. Loh, S. Aldridge, *Angew. Chem. Int. Ed.* **2021***, 60,* 8626 –8648

85 P. P. Power, *Organometallics.* **2020**, *39*, 4127–4138.

86. C. Weetman, *Chem. Eur. J.* **2021**, *27*, 1941–1954.

87. W. Kutzelnigg, *Angew. Chem. Int. Ed.* **1984**, *23*, 272–295.

88. K. B. Dillon, F. Mathey, J. F. Nixon, *Phosphorus: The Carbon Copy. From Organophosphorus To Phospha-Organic Chemistry*; John Wiley & Sons. **1998**.

89. F. Mathey, *Acc. Chem. Res.* **1992**, *25*, 90–96.

90. H. A. Bent. *J. Chem. Educ.* **1960**, 37, 616–624.

91. G. Becker, G. Gresser, W. Uhl, *Z. Naturforsch B.* **1981**, *36*, 16–19.

92. T. E. Gier, *J. Am. Chem. Soc.* **1961**, *83*, 1769–1770.

93. M. P. Duffy, W. Delaunay, P. A. Bouit, M. Hissler, *Chem. Soc. Rev.* **2016**, *45*, 5296–5310.

94. N. Asok, J. R. Gaffen, T. Baumgartner, *Acc. Chem. Res.* **2023**, *56*, 536–547.

95. C. Müller, L. E. E. Broeckx, I. De Krom, J. J. M. Weemers, *Eur. J. Inorg. Chem.* **2013**, 187–202.

96. J. M. Goicoechea, H. Grützmacher, *Angew. Chem. Int. Ed.* **2018**, *57*, 16968–16994.

97. T. Görlich, P. Coburger, E. S. Yang, J. M. Goicoechea, H. Grützmacher, C. Müller, C. *Angew. Chem. Int. Ed.* **2023**, *62*, e202217749.

98. J. C. T. R. Burckett-St. Laurent, P. B. Hitchcock, H. W. Kroto, F. Nixon, *J. Chem. Soc., Chem. Commun.* **1981**, 1141–1143.

99. J. F. Nixon, *Endeavour.* **1991**, *15*, 49–57.

100. W. Rösch, M. Regitz, *Z. Naturforsch B*. **1987**, *41*, 931-934.

101. W. Rösch, T. Facklam, M. Regitz, *Tetrahedron.* **1987**, *43*, 3247–3256.

102. R. Hoffman, *Angew. Chem. Int. Ed.* **1982**, *27*, 711–800.

103. F. Mathey, *Angew. Chem. Int. Ed.* **2003**, *42*, 1578–1604.

Chapter 2

1. F. Ahmad, A. Mahmood, T. Muhmood, *Heteroatom-Doped Carbon Allotropes: Progress*

*in Synthesis, Characterization and Applications.***2024***, 1*, 1-18.

2. X. Ye, M. Qi, M. Chen, L. Zhang, J. Zhang, *Adv. Mater. Interfaces.* **2023**, *10*, 2201941.

3. R. J. Lagow, J. J. Kampa, H. C. Wei, S. L. Battle, J. W. Genge, D. A. Laude, C. J. Harper, R. Bau, R. C. Stevens, J. F. Haw, E. Munson, *Science*. **1995**, *267*, 362–367.

4. R. H. Baughman, *Science.* **2006**, *312*, 1009–1010.

5. R.R. Tykwinski, *Chem. Rec.* **2015**, *15*, 1060–1074.

6. W. Xu, E. Leary, S. Hou, S. Sangtarash, M. T. González, G. Rubio-Bollinger, Q. Wu, H. Sadeghi, L. Tejerina, K. E. Christensen, N. Agraït, S. J. Higgins, C. J. Lambert, R. J. Nichols, H. L. Anderson, *Angew. Chem. Int. Ed.* **2019**, *131*, 8466–8470.

7. J. A. Januszewski, R. R. Tykwinksi, *Chem. Soc. Rev*. **2014**, *43*, 3184-3203

8. D. Wendinger, R. R. Tykwinksi, *Acc. Chem. Res*. **2017**, *50*, 1468-1479.

9. L. Leroyer, V. Maraval, R. Chauvin, *Chem. Rev.* **2012**, *112*, 1310–1343.

10 P. Pinter, D. Munz, *J. Phys. Chem. A.* **2020**, *124*, 10100–10110.

11. M. H. Garner, R. Hoffmann, S. Rettrup, G. C. Solomon, *ACS Cent. Sci.* **2018**, *4*, 688–700.

12. K. Brand, *Ber. Dtsch. Chem. Ges. B*. **1921**, *54*, 1987–2006.

13. Z. Berkovitch-Yellin, M. Lahav, L. Leiserowitz, *J. Am. Chem. Soc.* **1974**, *96*, 918–920.

14. P. H. Liu, L. Li, J. A. Webb, Y. Zhang, N. S. Goroff, Org Lett. **2004**, *6*, 2081–2083.

15. H. Irngartinger, W. Götzmann, *Angew. Chem. Int. Ed.* **1986**, *25*, 340–342.

16. E. Weber, W. Seichter, R-J. Wang, T. C. W. Mak, *Bull. Chem. Soc. Jpn.* **1991**, *64*, 659-66717.

17. B. Bildstein, M. Schweiger, H. Kopacka, K. H. Ongania, K. Wurst, *Organometallics* **1998**. *17*, 2414–2424.

18. D. Wu, Y. Li, R. Ganguly, R. Kinjo, *Chem. Commun.* **2014**, *50*, 12378–12381.

19. M. Franz, J. A. Januszewski, D. Wendinger, C. Neiss, L. D. Movsisyan, F. Hampel, H. L. Anderson, A. Görling, R. R. Tykwinski, *Angew. Chem. Int. Ed.* **2015**, *54*, 6645–6649.

20. Y. Li, K. C. Mondal, P. P. Samuel, H. Zhu, C. M. Orben, S. Panneerselvam, B. Dittrich, B. Schwederski, W. Kaim, T. Mondal, D. Koley, H. W. Roesky, *Angew. Chem. Int. Ed.* **2014**, *53*, 4168–4172.

21. L. Jin, M. Melaimi, A. Kostenko, M. Karni, Y. Apeloig, C. E. Moore, A. L. Rheingold, G. Bertrand, *Chem. Sci.* **2016**, *7*, 150–154.

22. R. L. Melen, *Science.* **2019**, *363*, 479–484.

23. P. P. Power, *Nature,* **2010**, *463*, 171–177.

24. M. He, C. Hu, R. Wei, X. F. Wang, L. L. Liu, *Chem. Soc. Rev.* **2024**, *53*, 3896–3951.

25. Y. K. Loh, S. Aldridge, *Angew. Chem. Int. Ed.* **2021***, 60 ,*8626 –8648

26. F. Dielmann, C. E. Moore, A. L. Rheingold, G. Bertrand, *J. Am. Chem. Soc.* **2013**, *135*, 14071–14703.

27. M. Fischer, M. M. D. Roy, L. L. Wales, M. A. Ellwanger, C. McManus, A. F. Roper, A. Heilmann, S. Aldridge, *Angew. Chem. Int. Ed.* **2022**, *61*, e202211616.

28. P. P. Power, *Organometallics*. **2020**, *39*, 4127–4138.

29. C. Weetman, *Chem. Eur. J.* **2021**, *27*, 1941–1954.

30. R. C. Fischer, P. P. Power, *Chem. Rev.* **2010**, *110*, 3877–3923.

31. B. C. Brodie, *Proc. Roy. Soc. (London)*. **1873***, 21*, 245–247.

32. L. H. Reyerson, K. Kobe, *Chem. Rev.* **1930**, *7*, 479–492.

33. O. Diels, B. Wolf, *Ber. Dtsch. Chem. Ges.* **1906**, *39*, 689-697.

34. P. Jensen, J. W. C. Johns, *J. Mol. Spectrosc.* **1986**, *118*, 248-266.

35. J. Koput, *Chem. Phys. Lett.* **2000**, *320*, 237.

36. R. Tonner, G. Frenking, *Chem. Eur. J.* **2008**, *14*, 3260–3272.

37. A. Ellern, T. Drews, K. Seppelt, *Z. anorg. allg. Chem.* **2001**, *627*, 73–76.

38. I. Bernhardi, T. Drews, K. Seppelt, *Angew. Chem. Int. Ed.* **1999**, *38*, 2232–2233.

39. F. Krischer, M. Jorges, T. F. Leung, H. Darmandeh, V. H. Gessner, *Angew. Chem. Int. Ed*.

2023, *62*, e202309629.

40. T. Wang, Z. Guo, L. E. English, D. W. Stephan, A. R. Jupp, M. Xu, *Angew. Chem. Int. Ed.* **2023**, *63, e202402728*.

41. Q. Le Dé, Y. Zhang, L. Zhao, F. Krischer, K. S. Feichtner, G. Frenking, V. H. Gessner, V. H. *Angew. Chem. Int. Ed.* **2025**, *64*, e202422496.

42. J. M. Goicoechea, H. Grützmacher, *Angew. Chem. Int. Ed.* **2018**, *57*, 16968–16994.

43. C. N. Matthews, G. H. Birum, *Tetrahedron Lett.* **1966**, *7*, 5707–5710.

44. C. N. Matthews, J. S. Driscoll, H.G. Birum, *Chem. Commun.(London).* **1966**, 736–737.

45. C. N. Matthews, G. H. Birum, G. H. *Acc. Chem. Res.* **1969**, *2*, 373-379.

46. R. Bertani, M. Casarin, L. Pandolfo, *Coord. Chem. Rev.* **2003**, *236*, 15–33.

47. L. T. Scharf, V. H. Gessner, *Inorg. Chem.* **2017**, *56*, 8599–8607.

48. H. J. Bestmann, *Angew. Chem. Int. Ed*. *Engl*., **1977**, *16*, 349–364.

49. G. Schmid, H. J. Bestmann, *Tetrahedron Letters*. **1975**, *46*. 4025–4026.

50. R. Schobert, C. Hölzel, *Topics in Heterocyclic Chemistry.* **2007**, *12*, 193-218.

51. A. Brar, D. K. Unruh, N. Ling, C. Krempner, C. *Org. Lett.* **2019**, *21*, 6305–6309.

52. M. Jörges, F. Krischer, V. H. Gessner, *Science.* **2022**, *378*, 1331– 1336.

53. T. Koike, J.-K. Yu, M. M. Hansmann, *Science.* **2024***, 385*, 305–311.

54. R. Wei, X.-F. Wang, D. A. Ruiz, L. L. Liu, *Angew. Chem. Int. Ed.* **2023**, *62*, *e202219211*.

55. X.-F. Wang, R. Wei, Q. Liang, C. Hu, L. L. Liu, *Chem*. **2025**. *11*, 102444.

56. H. -O. Berger, H. Nöth, B. Wrackmeyer B. *J. Organomet. Chem.* **1978**, *145*, 17-20.

57. K. Onuma, K. Suzuki, M. Yamashita, *Chem. Lett.* **2015**, *44*, 405–407.

58. M. J. D. Bosdet, W. E. Piers, *Can. J. Chem.* **2009**, *87*, 8–29.

59. R. Kitamura, K. Suzuki, M. Yamashita, *Chem. Commun.* **2018**, *54*, 5819, 5822.

60. H. Braunschweig, R. D. Dewhurst, K. Hammond, J. Mies, K. Radacki, A. Vargas, *Science.*

2012, *336*, 1420–1422.

61. J. Böhnke, H. Braunschweig, W. C. Ewing, C. Hörl, T. Kramer, I. Krummenacher, J. Mies, A. Vargas, *Angew. Chem. Int. Ed.* **2014**, *53*, 9082–9085.

62. V. Lavallo, Y. Canac, C. Präsang, B. Donnadieu, G. Bertrand, *Angew. Chem. Int. Ed.* **2005**, *44*, 5705–5709.

63. M. Michel, S. Kar, L. Endres, R. D. Dewhurst, B. Engels, H. Braunschweig, *Nat. Synth.* **2025**, *4*, https://doi.org/10.1038/s44160-025-00763-1.

64 A. K. Day, M. Abdellaoui, M. Soleilhavoup, G. Bertrand, *Chem Catal.* **2024**, *5*, 101159.

65. Y. K. Loh, M. Melaimi, M. Gembicky, D. Munz, G. Bertrand, *Nature.* **2023**, *623*, 66–70.

66. J. Tang, C. Hu, A. E. Crumpton, M. Dietz, D. Sarkar, L. P. Griffin, J. M. Goicoechea, S. Aldridge, *J. Am. Chem. Soc.* **2024**, *146*, 30778−30783.

67. J. Tang, C. Hu, A. E. Crumpton, L. P. Griffin, J. M. Goicoechea, S. Aldridge, *Chem. Sci.* **2024**, *16*, 2231–2237.

68. M. I. Bruce, *Chem. Rev*. **1991**, *91*, 197−257.

69. V. Cadierno, J. Gimeno, *Chem. Rev.* **2009**, *109*, 3512–3560.

70. M. Asay, B. Donnadieu, W. W. Schoeller, G. Bertrand, *Angew. Chem. Int. Ed.* **2009**, *48* 4796–4799.

71. E. O. Fischer, H. J. Kalder, A. Frank, F. H. Köhler, G. Huttner, *Angew. Chem. Int. Ed***. 1976**, *15*, 623–624.

72. H. Berke, *Angew. Chem. Int. Ed***. 1976**, *15*, 624.

73. J. P. Selegue, Organometallics. **1982**, *1,* 217–218.

74. M. H. Hansmann, F. Rominger, A. S. K. Hashmi, *Chem. Sci.* **2013**, *4*, 1552–1559.

75. L. Jin, M. Melaimi, A. Kostenko, M. Karni, Y. Apeloig, C. E. Moore, A. L. Rheingold, G. Bertrand, G. *Chem. Sci.* **2016**, *7*, 150–154.

76. N. Kim, R. A. Widenhoefer, *Angew. Chem. Int. Ed.* **2018**, *57*, 4722–4726.

77. X. S. Xiao, C. Zou, X. Guan, C. Yang, W. Lu, C. Che, *Chem. Commun.* **2016**, *52*, 4983–4986.

78. G. T. Kent, X. Yu, G. Wu, J. Autschbach, T. W. Hayton, *Chem. Sci.* **2021**, *12*, 14383–14388.

79. O. Ordoñez, X. Yu, M. A. Schuerlein, G. Wu, J. Autschbach, T. W. Hayton, *J. Am. Chem. Soc.* **2024**, *146*, 28306−28319

80. S. W. Roh, K. Choi, C. Lee, C. *Chem. Rev.* **2019**, *119*, 4293–4356.

81. H. Werner, R. Wiedemann, M. Laubender, B. Windmüller, P. Steinert, O. Gevert, J. Wolf, *J. Am. Chem. Soc.* **2002**, *124,* 6966–6980.

82. J. Díez, M. P. Gamasa, J. Gimeno, E. Lastra, A. Villar, *Organometallics* **2005**, *24*, 1410–1418.

83. M. Baya, M. L. Buil, M. A. Esteruelas, A. M. López, E. Oñate, J. Ramón Rodríguez, *Organometallics.* **2002**, *21*, 1841–1848.

84. J. Gimeno, V. Cadierno, J. Díez, S. E. García-Garrido, *Chem. Commun.* **2004**, 2716–1717.

85. Y. Nishibayashi, I. Wakiji, M. Hidai, *J. Am. Chem. Soc.* **2000**, *122*, 11019–11020.

86. R. J. Detz, M. M. E. Delville, H. Hiemstra, J. H. Maarseveen, *Angew. Chem. Int. Ed.* **2008**, *47*, 3777–3780.

87. G. Hattori, H. Matsuzawa, Y. Miyake, Y. Nishibayashi, *Angew. Chem. Int. Ed.* **2008**, *47* 3781–3783.

88. X. Sun, X. Duan, N. Zheng, W. Song, *Org. Lett.* **2023**, *25*, 2798–2805.

89. X. Duan, H. Shi, Y. Yue, W. Song, *Chem. Commun.* **2024**, *60*, 3926–3929.

90 Y. Wei, J. Jiang, Y. Jing, Z. Ke, L. Zhang, *Angew. Chem. Int. Ed.* **2024**, *136*, e202402286.

91. O. Guerret, G. Bertrand, *Acc. Chem. Res.* **1997**, *30*, 486–493.

92. P. Löwe, dissertation, Westfälische Wilhelms-Universität Münster, **2022**.

93. M. A. Wünsche, dissertation, Westfälische Wilhelms-Universität Münster, **2018**.

94. M. A. Wünsche, T. Witteler, F. Dielmann, *Angew. Chem. Int. Ed.* **2018**, *57*, 7234–7239.

95. L. Cabrera, G. C. Welch, J. D. Masuda, P. Wei, D. W. Stephan, *Inorganica Chim. Acta* **2006**, *359*, 3066–3071.

96. M. H Holthausen, T. Mahdi, C. Schlepphorst, L. J. Hounjet, J. J. Weigand, D. W. Stephan, *Chem. Commun.* **2014**, *50*, 10038–10040.

97. A. Brar, D. K. Unruh, A. J. Aquino, C. Krempner, *Chem. Commun.* **2019**, *55*, 3513–3516.

98. Q.S. Li, J. Zhang, S. Zhang, *Chem. Phys. Lett.* **2005**, *404*, 100–106.

99. S. Grimme, J. Antony, S. Ehrlich, H. Krieg, *J. Chem. Phys.* **2010**, *132*, 154104.

100. F. Weigend, R. Ahlrichs, *Phys. Chem. Chem. Phys.* **2005**, *7*, 3297–3305.

101. P. Löwe, M. A. Wünsche, F. R. S. Purtscher, J. Gamper, T. S. Hofer, L. F. B. Wilm, M. B. Röthel, F. Dielmann, *Chem. Sci.* **2023**, *14*, 7928–7935.

102. H. Grützmacher, H. Pritzkow, *Angew. Chem. Int. Ed.* **1991**, *30*, 709–710.

103. A. Igau, A. Baceiredo, H. Grützmacher, H. Pritzkow, G. Bertrand, *J. Am. Chem. Soc.* **1989**, *111*, 6853–6854.

104. F. Lavigne, E. Maerten, G. Alcaraz, N. Saffon-Merceron, C. Acosta-Silva, V. Branchadell, A. Baceiredo, *J. Am. Chem. Soc.* **2010**, *132*, 8864–8865.

105. S. K. Latypov, F. M. Polyancev, D. G. Yakhvarov, O. G. Sinyashin, *Phys. Chem. Chem. Phys.* **2015**, *17*, 6976–6987.

106. J. A. C. Clyburne, N. McMullen, *Coord. Chem. Rev.* **2000**, *210*, 73–99.

107. E. LaPierre, B. O. Patrick, I. Manners, *J. Am. Chem. Soc.* **2023**, *145*, 7107–7112.

108. M. Fischer, S. Nees, T. Kupfer, J. T. H. Braunschweig, C. Hering-Junghans, *J. Am. Chem. Soc.* **2021**, *143*, 4106–4111.

109. A. García-Romero, C. Hu, M. Pink, J. M. Goicoechea, *J. Am. Chem. Soc.* **2024**. *147*, 1231-1239

110. M. Olaru, D. Duvinage, Y. Naß, L. A. Malaspina, S. Mebs, J. Beckmann, *Angew. Chem. Int. Ed.* **2020**, *59*, 14414–14417.

111. G. Kehr, G. Erker, *Chem. Commun.* **2012**, *48*, 1839–1850.

112. B. Wrackmeyer, K. Horchler, R. Boese, *Angew. Chem. Int. Ed.* **1989**, *2*, 1500–1502.

113. A. Bismuto, G. S. Nichol, F. Duarte, M. J. Cowley, S. P. Thomas, *Angew. Chem. Int. Ed.*

2020, *59*, 12731–12735.

114. M. Dureen, D. W. Stephan, *J. Am. Chem. Soc.* **2009**, *131*, 8396–8397.

115. A. Fukazawa, H. Yamada, S. Yamaguchi, *Angew. Chem. Int. Ed.* **2008**, *47*, 5582–5585.

116. O. Ekkert, G. Kehr, R. Fröhlich, G. Erker, *J. Am. Chem. Soc.* **2011**, *133*, 4610–4616.

S1. O. V. Dolomanov, L. J. Bourhis, R. J. Gildea, J. A. K. Howard and H. Puschmann, *J. Appl. Crystallogr.* **2009**, 42, 339–341.

S2. G. Sheldrick GM SADABS. University of Göttingen, Göttingen **1996**.

S3. Gaussian 09, Revision D.01, M. J. Frisch, G. W. Trucks, H. B. Schlegel, G. E. Scuseria, M. A. Robb, J. R. Cheeseman, G. Scalmani, V. Barone, B. Mennucci, G. A. Petersson, H. Nakatsuji, M. Caricato, X. Li, H. P. Hratchian, A. F. Izmaylov, J. Bloino, G. Zheng, J. L. Sonnenberg, M. Hada, M. Ehara, K. Toyota, R. Fukuda, J. Hasegawa, M. Ishida, T. Nakajima, Y. Honda, O. Kitao, H. Nakai, T. Vreven, J. A. Montgomery, Jr., J. E. Peralta, F. Ogliaro, M. Bearpark, J. J. Heyd, E. Brothers, K. N. Kudin, V. N. Staroverov, T. Keith, R. Kobayashi, J. Normand, K. Raghavachari, A. Rendell, J. C. Burant, S. S. Iyengar, J. Tomasi, M. Cossi, N. Rega, J. M. Millam, M. Klene, J. E. Knox, J. B. Cross, V. Bakken, C. Adamo, J. Jaramillo, R. Gomperts, R. E. Stratmann, O. Yazyev, A. J. Austin, R. Cammi, C. Pomelli, J. W. Ochterski, R. L. Martin, K. Morokuma, V. G. Zakrzewski, G. A. Voth, P. Salvador, J. J. Dannenberg, S. Dapprich, A. D. Daniels, O. Farkas, J. B. Foresman, J. V. Ortiz, J. Cioslowski, and D. J. Fox, Gaussian, Inc., Wallingford CT, **2013**.

S4. Q. S. Li, J. Zhang, S. Zhang, Chem. Phys. Lett. **2005**, *404*, 100–106; (b) S. Grimme, J. Antony, S. Ehrlich, H. Krieg, J. Chem. Phys. **2010**, *132*, 154104.

S5. F. Weigend and R. Ahlrichs, Phys. Chem. Chem. Phys., **2005**, *7*, 3297–3305.

S6. S. K. Latypov, F. M. Polyancev, D. G. Yakhvarov, O. G. Sinyashin Phys. Chem. Chem. Phys., **2015**, *17*, 6976- 6987.

Chapter 3

1. T. Ochiai, D. Franz, S. Inoue, *Chem. Soc. Rev.* **2016**, *45*, 6327–6344.
2. M. D. Roy, E. Rivard, *Acc. Chem. Res.* **2017**, *50*, 2017–2025.
3. Y. K. Loh, L. Ying, M. Ángeles Fuentes, D. C. H. Do, S. Aldridge, *Angew. Chem. Int. Ed.* **2019**, *58*, 4847–4851.
4. M. Peters, A. Doddi, T. Bannenberg, M. Freytag, P.G. Jones, M. Tamm, *Inorg. Chem.* **2017**, *56*, 10785–10793.
5. A. Doddi, D. Bockfeld, T. Bannenberg, M. Tamm, *Chem. Eur. J.* **2020**, *26*, 14878–14887.
6. M. E. Doleschal, A. Espinosa Ferao, A. Kostenko, F. J. Kiefer, S. Inoue, *Angew. Chem. Int. Ed.* **2025**, *64, e202422186.*
7. P. Mehlmann, T. Witteler, L. F. B. Wilm, F. Dielmann, F. *Nat. Chem.* **2019**, *11*, 1139–1143.
8. L. F. B. Wilm, T. Eder, C. Mück-Lichtenfeld, P. Mehlmann, M. Wünsche, F. Buß, Dielmann, *Green Chem.* **2019**, *21*, 640–648.
9. M. Zhong, M. Yuan, *RSC Adv*. **2025**, *15*, 15052–15085.
10. N. Kuhn, R. Fawzi, M. Stiemann, J. Wiethoff, *Chem. Ber.* **1996**, *129*, 479–482.
11. P. Mehlmann, C. Mück-Lichtenfeld, T. T. Y. Tan, F. Dielmann, *Chem. Eur. J.* **2017**, *23*, 5929–5933.
12. O. Back, B. Donnadieu, M. von Hopffgarten, S. Klein, R. Tonner, G. Frenking, G. Bertrand, *Chem. Sci.* **2011**, *2*, 858–861.
13. F. Dielmann, O. Back, M. Henry-Ellinger, P. Jerabek, G. Frenking, G. Bertrand, *Science* **2012**, *337*, 1526–1528.
14. F. Dielmann, C. E. Moore, A. L. Rheingold, G. Bertrand, *J. Am. Chem. Soc.* **2013**, *135*, 14071–14703.
15. M. A. Wünsche, T. Witteler, F. Dielmann, *Angew. Chem. Int. Ed.* **2018**, *57*, 7234–7239.
16. P. Löwe, T. Witteler, F. Dielmann, *Chem. Comm.* **2021**, *57*, 5043–5046.

17. P. Löwe, M. A. Wünsche, F. R. S. Purtscher, J. Gamper, T. S. Hofer, L. F. B. Wilm, M. B. Röthel, F. Dielmann, *Chem. Sci.* **2023**, *14*, 7928–7935.
18. M. A. Wünsche, dissertation, Westfälische Wilhelms-Universität Münster, **2018**.
19. P. Löwe, dissertation, Westfälische Wilhelms-Universität Münster, **2022**.
20. D. Sarkar, P. Vasko, L. Ying, J. J. C. Struijs, L. P. Griffin, S. Aldridge, *Angew. Chem. Int. Ed.* **2025**, *64*, e202502326.
21. D. Sarkar, P. Vasko, A. F. Roper, A. E. Crumpton, M. D. Roy, L. P. Griffin, C. Bogle, S. Aldridge, *J. Am. Chem. Soc.* **2024**, *146*, 11792–11800.
22. J. T. Boronski, A. E. Crumpton, A. F. Roper, S. Aldridge, *Nat. Chem.* **2024**, *16*, 1295–1300.
23. D. Sarkar, P. Vasko, T. Gluharev, L. P. Griffin, C. Bogle, J. J. C. Struijs, J. Tang, A. F. Roper, A. E. Crumpton, S. Aldridge, *Angew. Chem. Int. Ed.* **2024**, *63*, e202407427.
24. M. Balmer, Y. J. Franzke, F. Weigend, C. von Hänisch, *Chem. Eur. J.* **2020**, *26*, 192–197.
25. M. Doleschal, A. Kostenko, J. Y. Liu, S. Inoue, *Nat. Chem.* **2024**, *16*, 2009–2016.
26. V. Nesterov, R. Baierl, F. Hanusch, A. E. Ferao, S. Inoue, *J. Am. Chem. Soc.* **2019**, *141*, 14576–14580.
27. T. F. Leung, D. Jiang, M-C. Wu, D. Xiao, W-M. Ching, G. P. A. Yap, T. Yang, L. Zhao, T-G. Ong, G. Frenking, *Nat. Chem.* **2021**, *13*, 89–93.
28. L. C. Torres, R. Dobrovetsky, C. B. Caputo, *Chem. Comm.* **2021**, *57*, 8272–8275.
29. L. C. Torres, A. Brar, J. LeBlanc, C B. Ameyaw, C. B. Caputo, *Z. Anorg. Allg. Chem.* **2023**, *649*, e202200383.
30. O. Ekkert, G. Kehr, R. Fröhlich, G. Erker, *Chem. Commun*. **2011**, *47*, 10482–10484.
31. M. D. Böhme, T. Eder, M. B. Röthel, P. D. Dutschke, L. F. B. Wilm, E. Hahn, F. Dielmann, *Angew. Chem. Int. Ed.* **2022**, *61*, e202202190.
32. D. Naumann, H. Butler, R. Gnann, *Z. Anorg. Allg. Chem.* **1992**, *618*, 74–76.
33. A. D. Hendsbee, N. A. Giffin, Y. Zhang, C.C. Pye, J. D. Masuda, *Angew. Chem. Int. Ed.*

2012, *51*, 10836–10840.

34. R. Heyes, J. C. Lockhart, *J. Chem. Soc. A*. **1968**, 326–328.

35. H. C. Brown, S. K. Gupta, *J. Am. Chem. Soc*. **1970**, *93*, 6983–6984.

36. D. J. Pasto, V. Balasubramaniyan, P. W. Wojtkowski, *Inorg. Chem*. 1969, *8*, 594–598.

37. Y. Hasegawa, G. Kehr, S. Ehrlich, S. Grimme, C. G. Daniliuc, G. Erker, *Chem. Sci*. **2014**, *5*, 797–803.

38. F. Lavigne, E. Maerten, G. Alcaraz, N. Saffon-Merceron, C. Acosta-Silva, V. Branchadell, A. Baceiredo, *J. Am. Chem. Soc.* **2010**, *132*, 8864–8865.

39. U. Heim, H. Pritzkow, H. Schönberg, H. Grützmacher, *J. Chem. Soc. Chem. Commun.* **1993**, 673–674.

40. J. A. Januszewski, R. R. Tykwinksi, *Chem. Soc. Rev*. **2014**, *43*, 3184–3203.

41. D. Wendinger, R. R. Tykwinksi, *Acc. Chem. Res*. **2017**, *50*, 1468−1479.

42. E. Weber, W. Seichter, R-J. Wang, T. C. W. Mak, *Bull. Chem. Soc. Jpn.* **1991**, *64*, 659−667.

43. M. Franz, J. A. Januszewski, D. Wendinger, C. Neiss, L. D. Movsisyan, F. Hampel, H. L. Anderson, A. Görling, R. R. Tykwinski, *Angew. Chem. Int. Ed.* **2015**, *54*, 6645–6649.

44. Y. Li, K. C. Mondal, P. P. Samuel, H. Zhu, C. M. Orben, S. Panneerselvam, B. Dittrich, B. Schwederski, W. Kaim, T. Mondal, D. Koley, H. W. Roesky, *Angew. Chem. Int. Ed.* **2014**, *53*, 4168–4172.

45. L. Jin, M. Melaimi, L. L. Liu, G. Bertrand, *Org. Chem. Front.* **2014**, *1*, 351–354.

46. A. D. Becke, *J. Chem. Phys.* **1993**, *98*,1372–1377.

47. F. Weigend, R. Ahlrichs, *Phys. Chem. Chem. Phys*. **2005**, *7*, 3297–3305.

48. S. Grimme, S. Ehrlich, L. Goerigk, *J. Comput. Chem.* **2011**, *32*,1456–1465.

49. N. E. Kolobova, L. L. Ivanov, O. S. Zhvanko, O. M. Khitrova, A. S. Batsanov, Y. T. Struchkov, *J. Organomet. Chem.* **1984**, *262*, 39−47.

50. M. I. Bruce, *Chem. Rev*. **1991**, *91*, 197−257.

51. O. Ordoñez, X. Yu, M. A. Schuerlein, G. Wu, J. Autschbach, T. W. Hayton, *J. Am. Chem. Soc.* **2024**, *146*, 28306−28319.

52. K. O. Christe, D. A. Dixon, D. McLemore, W. W. Wilson, J. A. Sheehy, J. A. Boatz, *J. Fluor. Chem.* **2000**, *101*, 151–153.

53. C. B. Caputo, L. J. Hounjet, R. Dobrovetsky, D. W. Stephan, *Science*. **2013**, *341*, 1374–1377.

54. D. Roth, J. Stirn, D. W. Stephan, L. Greb, *J. Am. Chem. Soc.* **2021**, *143*, 15845–15851.

55. U. Mayer, V. Gutmann, W. Gerger, *Monatsh. Chem.* **1975***, 106*, 1235–1257.

56. M. A. Beckett, D. S. Brassington, S. J. Coles, M. B. Hursthouse, *Inorg. Chem. Commun.* **2000**, *3*, 530–533.

57. H. J. Bestmann, *Angew. Chem. Int. Ed*. *Engl*. **1977**, *16*, 349–364.

58. R. Wei, X-F. Wang, D. A. Ruiz, L. L. Liu, *Angew. Chem. Int. Ed*. **2023**, *62*, e202219211.

59. A. Brar, D. K, Unruh, A. J. Aquino, C. Krempner, *Chem. Comm.* **2019**, *55*, 3513–3516.

60. H. Burzlaff, R. Hagg, E. Wilhelm, H. J. Bestmann, *Chem. Ber.* **1985**, *118*, 1720–1723.

61. U. Heim, H. Pritzkow, U. Fleischer, H. Grützmacher, *Angew. Chem. Int. Ed*. **1993**, *32*, 1359–1361.

62. E. Buchner, T. Curtius, *Ber. Dtsch. Chem. Ges.* **1885**, *18*, 2377–2379. b) E. Buchner, T. Curtius, *Ber. Dtsch. Chem. Ges.* **1885**, *18*, 2371–2377.

63. T. Ye and M. A. McKervey, *Chem. Rev.* **1994**, *94*, 1091–1160.

64. Y. Chen, P. Su, D. Wang, Z. Ke, G. Tan, *Nat. Commun.* **2024**, *15*, 4579.

65. L. L. Liu, J. Zhou, R. Andrews, D. W. Stephan, *J. Am. Chem. Soc.* **2018**, *140*, 7466–7470.

66. L. L. Liu, J. Zhou, L.L. Cao, R. Andrews, R. L. Falconer, C. A. Russell, D. W. Stephan, *J. Am. Chem. Soc.* **2018**, *140*, 147–150.

67. M. Kira, S. Ishida, T. Iwamoto, C. Kabuto, *J. Am. Chem. Soc.* **2002**, *124*, 3830–3831.

68. T. Kosai, S. Ishida, T. Iwamoto, *Angew. Chem. Int. Ed.* **2016**, *55*, 15554–15558.

69. T. Kosai, S. Ishida, T. Iwamoto, *Chem. Commun.* **2015**, *51*, 10707–10709.

70. H. Suzuki, N. Tokitoh, R. Okazaki, *J. Am. Chem. Soc.* **1994**, *116*, 11572–11573.

71. D. Wendel, A. Porzelt, F. A. D. Herz, D. Sarkar, C. Jandl, S. Inoue, B. Rieger, *J. Am. Chem. Soc.* **2017**, *139*, 8134–8137.

72. C. Xu, Z. Ye, L. Xiang, S. Yang, Q. Peng, X. Leng, Y. Chen, *Angew. Chem. Int. Ed.* **2021**, *60*, 3189–3195.

73. H. Zhu, A. Kostenko, D. Franz, F. Hanusch, S. Inoue. *J. Am. Chem. Soc.* **2023**, *145*, 1011–1021.

74. X. Zhang, L. L. Liu, *Angew. Chem. Int. Ed.* **2022**, *134*, e202116658.

75. L. L. Liu, J. Zhou, L.L. Cao, Y. Kim, D. W. Stephan, *J. Am. Chem. Soc*. **2019**, *141*, 8083–8087.

76. D. Raiser, C. P. Sindlinger, H. Schubert, L. Wesemann, *Angew. Chem. Int. Ed.* **2020**, *59*, 3151–3155.

77. Y. K. Loh, M. Melaimi, D. Munz, G. Bertrand, *J. Am. Chem. Soc.* **2023**, *145*, 2064–2069.

78. H. D. Hartzler, *J. Am. Chem. Soc.* **1966**, *88*, 3155–3156.

79. H. D. Hartzler, *J. Am. Chem. Soc.* **1971**, *93*, 4527–4531.

80. B. Bildstein, M. Schweiger, H. Angleitner, H. Kopacha, K. Wurst, K. H. Ongania, M. Fontani, P. Zanello, *Organometallics.* **1999**, *18*, 4286–4295.

81. J. A. Januszewski, F. Hampel, C. Neiss, A. Görling, R. R. Tykwinksi, *Angew. Chem. Int. Ed. Engl.* **2014**, *53*, 3743–3747.

82. C. Ehm, D. Lentz, *Chem. Commun.* **2010**, *46*, 2399–2401.

83. K. Brand, *Ber. Dtsch. Chem. Ges. B*. **1921**, *54*, 1987–2006.

84. A. Igau, A. Baceiredo, H. Grützmacher, H. Pritzkow, G. Bertrand, *J. Am. Chem. Soc.* **1989**, *111*, 6853–6854.

85. J. B. Farahi, K. M. Doxsee, *J. Am. Chem. Soc.* **1988**, *110*, 7240–7242.

86. P. Löwe, M. Feldt, M. A. Wünsche, L. F. B. Wilm, F. Dielmann, *J. Am. Chem. Soc.* **2020**, *142*, 9818–9826.

S1. APEX2 Version 2.1 – 0; Bruker AXS Inc. Madison, **2004**.

S2. APEX4; Bruker AXS Inc. Madison, **2021**.

S3. SAINT version 7.46a, Bruker AXS Inc. Madison **2004**.

S4. G. Sheldrick GM SADABS. University of Göttingen, Göttingen **1996**.

S5. O. V. Dolomanov, L. J. Bourhis, R. J. Gildea, J. A. K. Howard and H. Puschmann, *J. Appl. Crystallogr.* **2009**, *42*, 339–341.

S6. a) L. Palatinus, G. Chapuis, *J. Appl. Cryst.* **2007**, 40, 786-790; b) L. Palatinus, A. van der Lee, *J. Appl. Cryst.* **2008**, 41, 975-984; c) L. Palatinus, S. J. Prathapa, S. van Smaalen, *J. Appl. Cryst.* **2012**, *45*, 575-580.

S7. L. J. Bourhis; O. V. Dolomanov; R. J. Gildea; J. A. K. Howard; H. Puschmann, *Acta crystallogr. A*. **2015**, *71*, 59–75.

S8. G. M. Sheldrick, *Acta crystallogr. A*. **2008**, *64*, 112–122.

S9. G. M. Sheldrick, *Acta crystallogr. A*. **2015**, *71*, 3–8.

S10. Gaussian 16, Revision C.01, M. J. Frisch, G. W. Trucks, H. B. Schlegel, G. E. Scuseria, M. A. Robb, J. R. Cheeseman, G. Scalmani, V. Barone, G. A. Petersson, H. Nakatsuji, X. Li, M. Caricato, A. V. Marenich, J. Bloino, B. G. Janesko, R. Gomperts, B. Mennucci, H. P. Hratchian, J. V. Ortiz, A. F. Izmaylov, J. L. Sonnenberg, D. Williams-Young, F. Ding, F. Lipparini, F. Egidi, J. Goings, B. Peng, A. Petrone, T. Henderson, D. Ranasinghe, V. G. Zakrzewski, J. Gao, N. Rega, G. Zheng, W. Liang, M. Hada, M. Ehara, K. Toyota, R. Fukuda, J. Hasegawa, M. Ishida, T. Nakajima, Y. Honda, O. Kitao, H. Nakai, T. Vreven, K. Throssell, J. A. Montgomery, Jr., J. E. Peralta, F. Ogliaro, M. J. Bearpark, J. J. Heyd, E. N. Brothers, K. N. Kudin, V. N. Staroverov, T. A. Keith, R. Kobayashi, J. Normand, K. Raghavachari, A. P. Rendell, J. C. Burant, S. S. Iyengar, J. Tomasi, M. Cossi, J. M. Millam,

M. Klene, C. Adamo, R. Cammi, J. W. Ochterski, R. L. Martin, K. Morokuma, O. Farkas, J. B. Foresman, and D. J. Fox, Gaussian, Inc., Wallingford CT, **2016**.

S11. A. D. Becke, *J. Chem. Phys*, **1993**, *98*, 5648–5652; b) C. Lee, W. Yang, R. G. Parr, *Phys. Rev. B.* **1998**, *37*, 785–789; c) S. H. Vosko, L. Wilk, M. Nusair, *Can. J. Phys*. **1980**, *58*, 1200-1211; d) P. J. Stephens, F. J. Devlin, C. F. Chabalowski, M. J. Frisch, *J. Phys. Chem*. **1994**, *98*, 11623–11627.

S12. a) L. Goerigk, S. Grimme, *J. Chem. Theory Comput.* **2011**, *7*, 291–309; b) L. Goerigk, A. Hansen, C. Bauer, S. Ehrlich, A. Najibi, S. Grimme, *Phys. Chem. Chem. Phys.* **2017**, *19*, 32184–32215; c) B. G. Johnson, M. J. Frisch, *J. Chem. Phys.* **1994**, *100*, 7429–7442.

S13. F. Weigend, R. Ahlrichs, *Phys. Chem. Chem. Phys.* **2005**, *7*, 3297–3305; b) F. Weigend, *Phys. Chem. Chem. Phys.* **2006**, *8*, 1057–1065.

S14. A. V. Marenich, C. J. Cramer, D. G. Truhlar, *Phys. Chem. B*. **2009**, *113*, 6378–6396.

S15. a) F. Weinhold, C. R. Landis (Eds.) Discovering Chemistry with Natural Bond Orbitals, John Wiley & Sons, Inc, Hoboken, NJ, USA, **2012**; b) J. P. Foster, F. Weinhold, *J. Am. Chem. Soc.* **1980**, 102, 7211–7218; c) A. E. Reed, R. B. Weinstock, F. Weinhold, *J. Chem. Phys.* **1985**, 83, 735–746; d) J. E. Carpenter, F. Weinhold, *J. Mol. Struct.: THEOCHEM*. **1988**, 169, 41–62; e) F. Weinhold, J. E. Carpenter, *The Structure of Small Molecules and Ions*, R. Naaman and Z. Vager, Springer US, Boston, MA, **1988**, 227–236.

S16. T. Lu, F. Chen, *J. Comput. Chem.* **2012**, *33*, 580–592.

S17. K. O. Christe, D. A. Dixon, D. McLemore, W. W. Wilson, J. A. Sheehy, J. A. Boatz, *J. Fluorine Chem*. **2000**, *101*, 151–153.

Chapter 4

1. T. Chu, G. I. Nikonov, *Chem. Rev.* **2018**, *118*, 3608–3680.

2. M. He, C. Hu, R. Wei, X. F. Wang, L. L. Liu, *Chem. Soc. Rev.* **2024**, *53*, 3896–3951.

3. D. R. Tolentino, S. E. Neale, C. J. Isaac, S. A. Macgregor, M. K. Whittlesey, R. Jazzar, G.

Bertrand, *J. Am. Chem. Soc.* **2019**, *141*, 9823–9826.

4. F. Vermersch, V. T. Wang, M. Abdellaoui, R. Jazzar, G. Bertrand, *Chem. Sci.* **2024**, *15*, 3707–3710.

5. D. Bourissou, O, Guerret, F. P. Gabbaï, G. Bertrand, Stable Carbenes. *Chem. Rev.* **2000**, *100*, 39–91.

6. A. H. Cowley, R. A. Kemp, *Chem. Rev.* **1985**, *85*, 367–382.

7. C. A. Caputo, J. T. Price, M. C. Jennings, R. McDonalds, N. D. Jones, *Dalton Trans.* **2008**, 3412–3421.

8. J. J. Weigand, M. Holthausen, R. Fröhlich, *Angew. Chem. Int. Ed.* **2009**, *48*, 295–298.

9. M. Q. Y. Tay, Y. Lu, R. Ganguly, D. Vidović, *Angew. Chem. Int. Ed.* **2013**, *52*, 3132–3135.

10. M. Q. Y. Tay, Y. Lu, R. Ganguly, D. Vidović, *Chem. Eur. J.* **2014**, *20*, 6628–6631.

11. M. Olaru, S. Mebs, J. Beckmann. *Angew. Chem. Int. Ed.* **2021**, *60*, 19133–19138.

12. N. Dordević, R. Ganguly, M. Petković, D. Vidović, *Inorg. Chem.* **2017**, *56*, 14671–14681.

13. T. J. Hannah, S. S. Chitnis, S. S. *Chem. Soc. Rev.* **2023**, *53*, 764–792.

14. L. M. Sigmund, R. Maier, L. Greb, *Chem. Sci.* **2022**, *13*, 510–521.

15. D. Bawari, D. Toami, R. Dobrovetsky, *Chem. Commun.* **2025**, *61*, 5871–5882.

16. W. Zhao, S, M. McCarthy, T. Y. Lai, H. P. Yennawar, A. T. Radosevich, *J. Am. Chem. Soc.* **2014**, *136*, 17634–17644.

17. D. Roth, A. T. Radosevich, L. Greb, *J. Am. Chem. Soc.* **2023**, *145*, 24184–24190.

18 S. Volodarsky, R. Dobrovetsky, *Chem. Commun.* **2018**, *54*, 6931–6934.

19. S. Volodarsky, D. Bawari, R. Dobrovetsky, *Angew. Chem. Int. Ed.* **2022**, *61*, e202208401

20. K. Chulsky, I. Malahov, D. Bawari, R. Dobrovetsky, *J. Am. Chem. Soc.* **2023**, *145*, 3786–3794.

21. D. Bawari, D. Toami, K. Jaiswal, R. Dobrovetsky, *Nat. Chem.* **2024**, *16*, 1261–1266.

22. P. Löwe, M. A. Wünsche, F. R. S. Purtscher, J. Gamper, T. S. Hofer, L. F. B. Wilm, M. B. Röthel, F. Dielmann, *Chem. Sci.* **2023**, *14*, 7928–7935.

23. M. D. Böhme, T. Eder, M. B. Röthel, P. D. Dutschke, L. F. B. Wilm, E. Hahn, F. Dielmann, *Angew. Chem. Int. Ed.* **2022**, *61*, e202202190.

24. H. Zhu, A. Kostenko, D. Franz, F. Hanusch, S. Inoue, *J. Am. Chem. Soc.* **2023**, *145*, 1011–1021.

25. V. Lavallo, Y. Canac, B. Donnadieu, W. W. Schoeller, G. Bertrand, *Angew. Chem. Int. Ed.* **2006**, *45*, 3488–3491.

26. C. Roques, M. R. Mazieres, J. P. Majoral, M. Sanchez, A. Foucaud, *J. Org. Chem*, **1989**, *54*, 5535–5539.

27. F. Dahcheh, D. Martin, D. W. Stephan, G. Bertrand, *Angew. Chemie - Int. Ed.* **2014**, *53*, 13159–13163.

28. C. Ganesamoorthy, J. Schoening, C. Wölper, L. Song, P. R. Schreiner, S. Schulz, *Nat. Chem.* **2020**, *12*, 608–614.

29. D. Reiter, R. Holzner, A. Porzelt, P. Frisch, S. Inoue, *Nat. Chem.* **2020**, *12*, 1131–1135.

30. N. Kuhn, R. Fawzi, M. Stiemann, J. Wiethoff, *Chem. Ber.* **1996**, *129*, 479–482.

31. M. A. Wünsche, T. Witteler, F. Dielmann, *Angew. Chem. Int. Ed.* **2018**, *57*, 7234–7239.

32. A. H. Cowley, M. Lattman, J. C. Wilburn, *Inorg. Chem.* **1981**, *20*, 2916–2919

33. J. Lortie, dissertation. Western University, **2024**.

34. A. D. Becke, *J. Chem. Phys.* **1993**, *98*, 1372–1377.

35. Weigend, R. Ahlrichs, *Phys. Chem. Chem. Phys*. **2005**, *7*, 3297–3305.

36. S. Grimme, S. Ehrlich, L. Goerigk, *J. Comput. Chem.* **2011**, *32*, 1456–1465.

37. U. Mayer, V. Gutmann, W. Gerger, *Monatsh. Chem.,* **1975***, 106*, 1235–1257.

38. M. A. Beckett, D. S. Brassington, S. J. Coles, M. B. Hursthouse, *Inorg. Chem. Commun.* **2000**, *3*, 530–533.

39. C. B. Caputo, L. J. Hounjet, R. Dobrovetsky, D. W. Stephan, *Science*, **2013**, *341*, 1374–1377.

40. C. Stoian, M. Olaru, S. Demeshko, M. Fischer, S. Mebs, E. Hupf, J. Beckmann, *Chem. Eur. J.* **2024**, 202403555.

41. P. Mehlmann, T. Witteler, L. F. B. Wilm, F. Dielmann, *Nat. Chem.* **2019**, *11*, 1139–1143.

42. C. K. SooHoo, S. G. Baxter, *J. Am. Chem. Soc.* **1983**, *105*, 7443-7444.

43. D. Gasperini, S. E. Neale, N. F. Mahon, S. A. MacGregor, R. L. Webster, *ACS Catal.* **2021**, *11*, 5452–5462.

44. L. N. Markovski, V. D. Romanenko, A. V. Ruban, A. B. Drapailo, *J. Chem. Soc., Chem. Commun.* **1984**, 1692.

45. Y. K. Loh, M. Melaimi, M. Gembicky, D. Munz, G. Bertrand, *Nature.* **2023**, *623*, 66–70.

46. G. D. Frey, V. Lavallo, B. Donnadieu, W. W. Schoeller, G. Bertrand, *Science.* **2007,** *316*, 439−441.

47. Y. Peng, J. D. Guo, B. D. Ellis, Z. Zhu, J. C. Fettinger, S. Nagase, P. P. Power, *J. Am. Chem. Soc.* **2009**, *131*, 16272–16282.

48. A. V. Protchenko, K. H. Birjkumar, D. Dange, A. D. Schwarz, D. Vidović, C. Jones, N. Kaltsoyannis, P. Mountford, S. Aldridge, *J. Am. Chem. Soc.* **2012**, *134*, 6500–6503.

49. T. Chu, I. Korobkov, G. I. Nikonov, *J. Am. Chem. Soc.* **2014**, *136*, 9195–9202.

50. A. V. Protchenko, J. I. Bates, L. M. A. Saleh, M. P. Blake, A. D. Schwarz, E. L. Kolychev, A. L. Thompson, C. Jones, P. Mountford, S. Aldridge, *J. Am. Chem. Soc.* **2016**, *138*, 4555–4564.

51. N. L. Dunn, M. Ha, A. T. Radosevich, *J. Am. Chem. Soc.* **2012**, *134*, 11330–11333.

52. K. O. Christe, D. A. Dixon, D. McLemore, W. W. Wilson, J. A. Sheehy, J. A. Boatz, *J. Fluor. Chem.* **2000**, *101*, 151–153.

53. J. F. Harrison, R. C. Liedtke, J. F. Liebman, *J. Am. Chem. Soc.* **1979**, *101*, 7162–7168.

54. J. M. Slattery, S. Hussein, *Dalton Trans.* **2012**, *41*, 1808–1815.

55. L. Liu, D. A. Ruiz, F. Dahcheh, G. Bertrand, *Chem. Commun.* **2015**, *51*, 12732–12735.

56. R. Nakano, R. Jazzar, G. Bertrand, *Nat. Chem.* **2018**, *10*, 1196–1200.

57. F. Ramirez, E. A. Tsolis, *J. Am. Chem. Soc.* **1970**, *92*, 7553–7558.

58. T. Matthias, B. Stephan, H. Eberhardt, Z. *Naturforsch*. *B*. **2004**, 59, 1497.

S1. APEX2 Version 2.1 – 0; Bruker AXS Inc. Madison, **2004**.

S2. APEX4; Bruker AXS Inc. Madison, **2021**.

S3. SAINT version 7.46a, Bruker AXS Inc. Madison **2004**.

S4. G. Sheldrick GM SADABS. University of Göttingen, Göttingen **1996**.

S5. O. V. Dolomanov, L. J. Bourhis, R. J. Gildea, J. A. K. Howard and H. Puschmann, *J. Appl. Crystallogr.* **2009**, *42*, 339–341.

S6. a) L. Palatinus, G. Chapuis, *J. Appl. Cryst.* **2007**, 40, 786-790; b) L. Palatinus, A. van der Lee, *J. Appl. Cryst.* **2008**, 41, 975-984; c) L. Palatinus, S. J. Prathapa, S. van Smaalen, *J. Appl. Cryst.* **2012**, *45*, 575-580.

S7. L. J. Bourhis; O. V. Dolomanov; R. J. Gildea; J. A. K. Howard; H. Puschmann, *Acta crystallogr. A*. **2015**, *71*, 59–75.

S8. G. M. Sheldrick, *Acta crystallogr. A*. **2008**, *64*, 112–122.

S9. G. M. Sheldrick, *Acta crystallogr. A*. **2015**, *71*, 3–8.

S10. Gaussian 16, Revision C.01, M. J. Frisch, G. W. Trucks, H. B. Schlegel, G. E. Scuseria, M. A. Robb, J. R. Cheeseman, G. Scalmani, V. Barone, G. A. Petersson, H. Nakatsuji, X. Li, M. Caricato, A. V. Marenich, J. Bloino, B. G. Janesko, R. Gomperts, B. Mennucci, H. P. Hratchian, J. V. Ortiz, A. F. Izmaylov, J. L. Sonnenberg, D. Williams-Young, F. Ding, F. Lipparini, F. Egidi, J. Goings, B. Peng, A. Petrone, T. Henderson, D. Ranasinghe, V. G. Zakrzewski, J. Gao, N. Rega, G. Zheng, W. Liang, M. Hada, M. Ehara, K. Toyota, R. Fukuda, J. Hasegawa, M. Ishida, T. Nakajima, Y. Honda, O. Kitao, H. Nakai, T. Vreven, K. Throssell, J. A. Montgomery, Jr., J. E. Peralta, F. Ogliaro, M. J. Bearpark, J. J. Heyd,

E. N. Brothers, K. N. Kudin, V. N. Staroverov, T. A. Keith, R. Kobayashi, J. Normand, K. Raghavachari, A. P. Rendell, J. C. Burant, S. S. Iyengar, J. Tomasi, M. Cossi, J. M. Millam, M. Klene, C. Adamo, R. Cammi, J. W. Ochterski, R. L. Martin, K. Morokuma, O. Farkas, J. B. Foresman, and D. J. Fox, Gaussian, Inc., Wallingford CT, **2016**.

S11. A. D. Becke, *J. Chem. Phys*, **1993**, *98*, 5648–5652; b) C. Lee, W. Yang, R. G. Parr, *Phys. Rev. B.* **1998**, *37*, 785–789; c) S. H. Vosko, L. Wilk, M. Nusair, *Can. J. Phys*. **1980**, *58*, 1200-1211; d) P. J. Stephens, F. J. Devlin, C. F. Chabalowski, M. J. Frisch, *J. Phys. Chem*. **1994**, *98*, 11623–11627.

S12. a) L. Goerigk, S. Grimme, *J. Chem. Theory Comput.* **2011**, *7*, 291–309; b) L. Goerigk, A. Hansen, C. Bauer, S. Ehrlich, A. Najibi, S. Grimme, *Phys. Chem. Chem. Phys.* **2017**, *19*, 32184–32215; c) B. G. Johnson, M. J. Frisch, *J. Chem. Phys.* **1994**, *100*, 7429–7442.

S13. F. Weigend, R. Ahlrichs, *Phys. Chem. Chem. Phys.* **2005**, *7*, 3297–3305; b) F. Weigend, *Phys. Chem. Chem. Phys.* **2006**, *8*, 1057–1065.

S14. a) J. Tomasi, B. Mennucci, R. Cammi, *Chem. Rev*. **2005**, *105*, 2999-3093. b) V. Barone, M. Cossi, *J. Phys. Chem. A*. **1998**, 102, 1995-2001.

S15. a) F. Weinhold, C. R. Landis (Eds.) Discovering Chemistry with Natural Bond Orbitals, John Wiley & Sons, Inc, Hoboken, NJ, USA, **2012**; b) J. P. Foster, F. Weinhold, *J. Am. Chem. Soc.* **1980**, *102*, 7211–7218; c) A. E. Reed, R. B. Weinstock, F. Weinhold, *J. Chem. Phys.* **1985**, *83*, 735–746; d) J. E. Carpenter, F. Weinhold, *J. Mol. Struct.: THEOCHEM*. **1988**, *169*, 41–62; e) F. Weinhold, J. E. Carpenter, *The Structure of Small Molecules and Ions*, R. Naaman and Z. Vager, Springer US, Boston, MA, **1988**, pp. 227–236.

S16. T. Lu, F. Chen, *J. Comput. Chem.* **2012**, *33*, 580–592.

S17. K. O. Christe, D. A. Dixon, D. McLemore, W. W. Wilson, J. A. Sheehy, J. A. Boatz, *J. Fluorine Chem*. **2000**, *101*, 151–153.